Patrick Grid

Line 0E – 2D UBC Smooth DC Resistivity Model

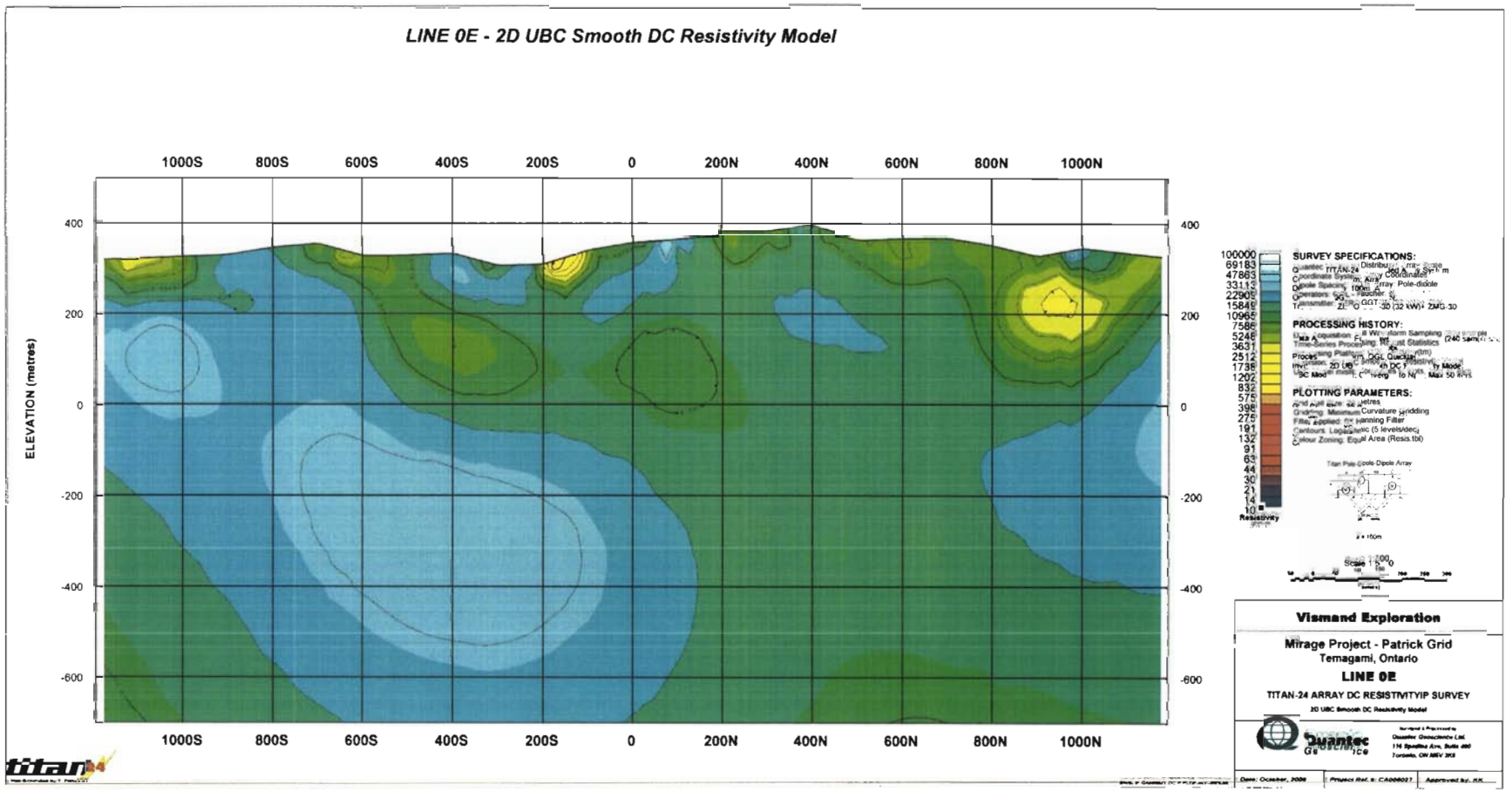

Line 0E – 2D UBC Smooth IP Chargeability Model

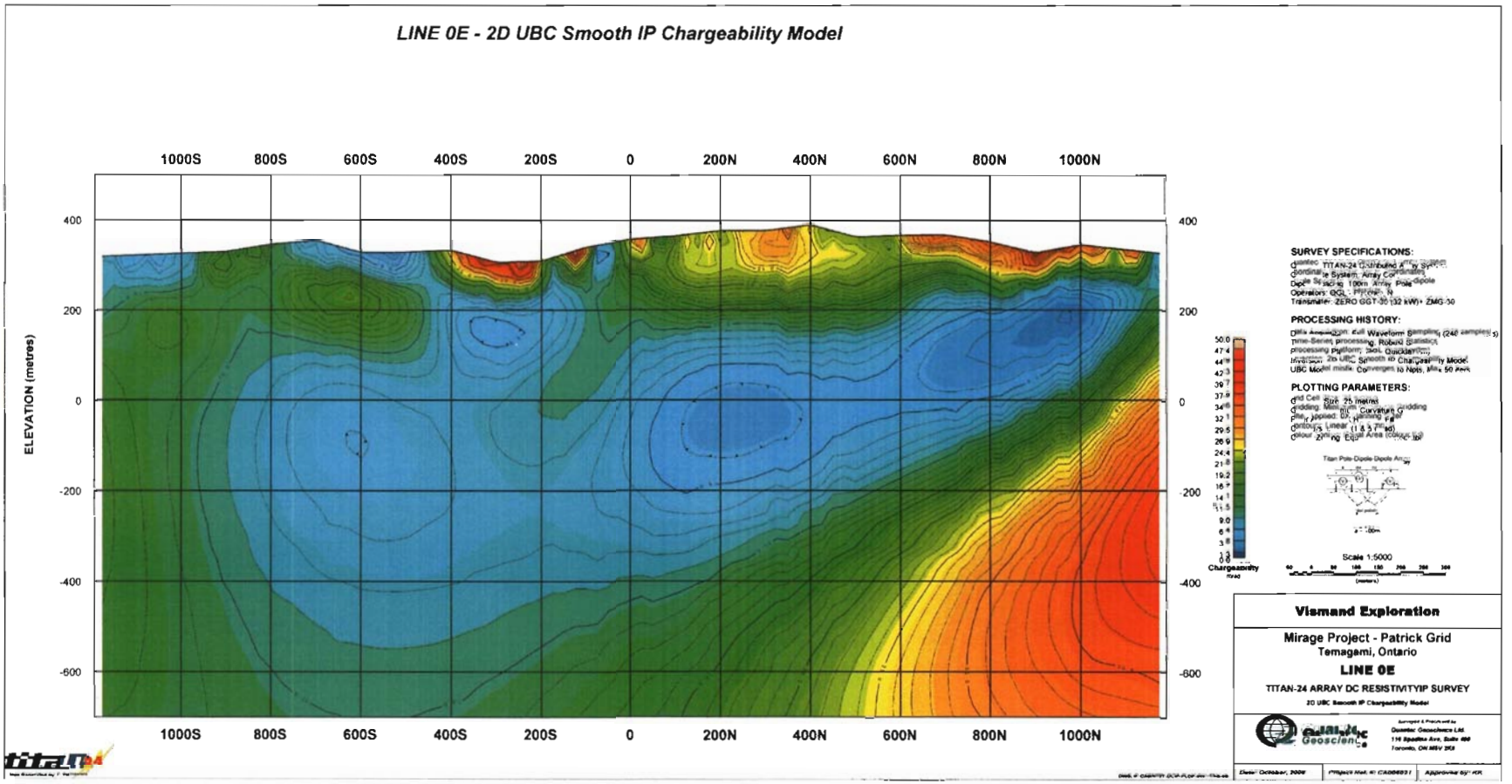

Line 0E – 2D UBC Null Con IP Chargeability Model

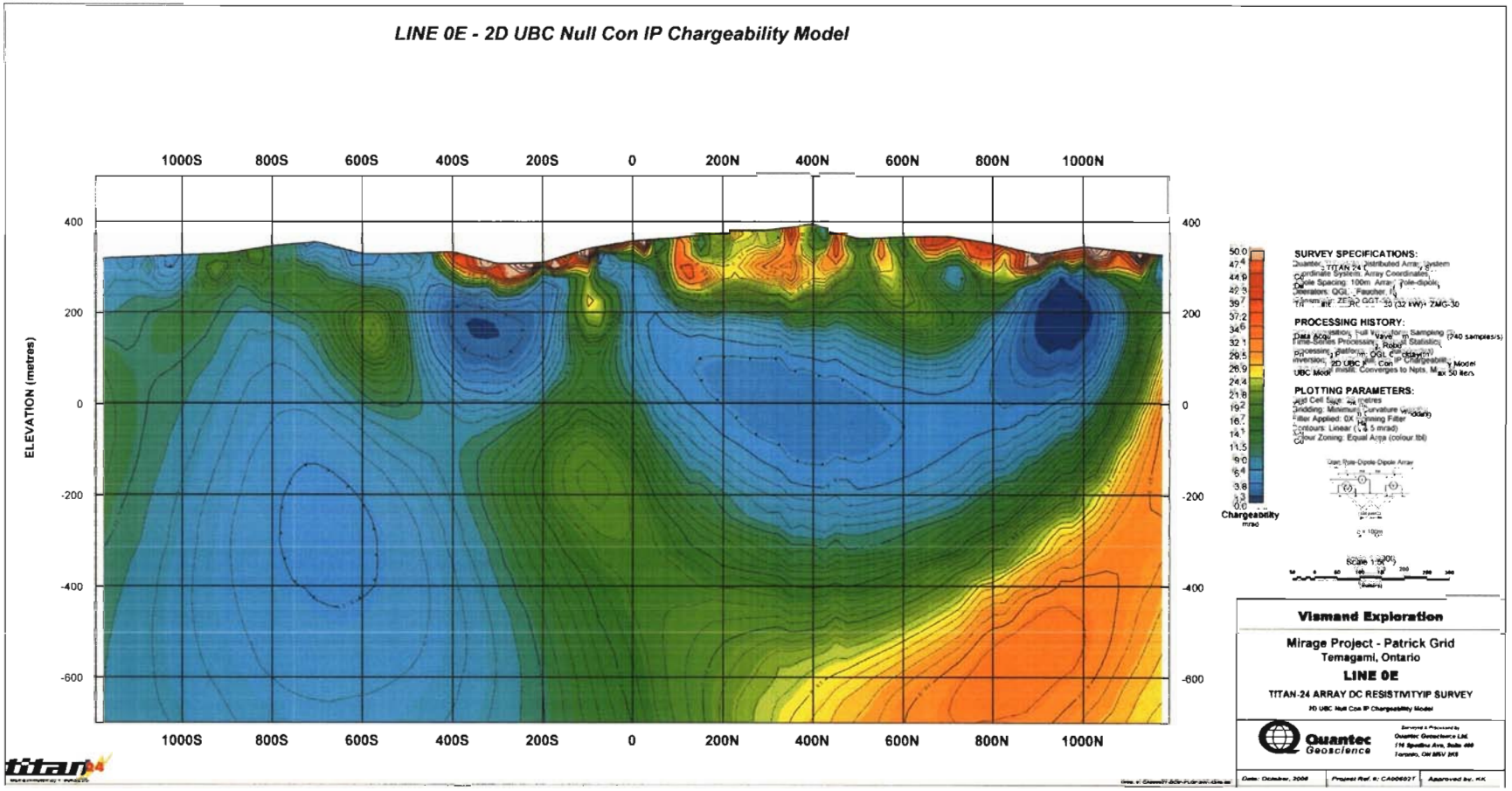

Line 0E – 2D MT PW TM+TE(phs) Sharp Inversion (starting from smooth 1D PW model)

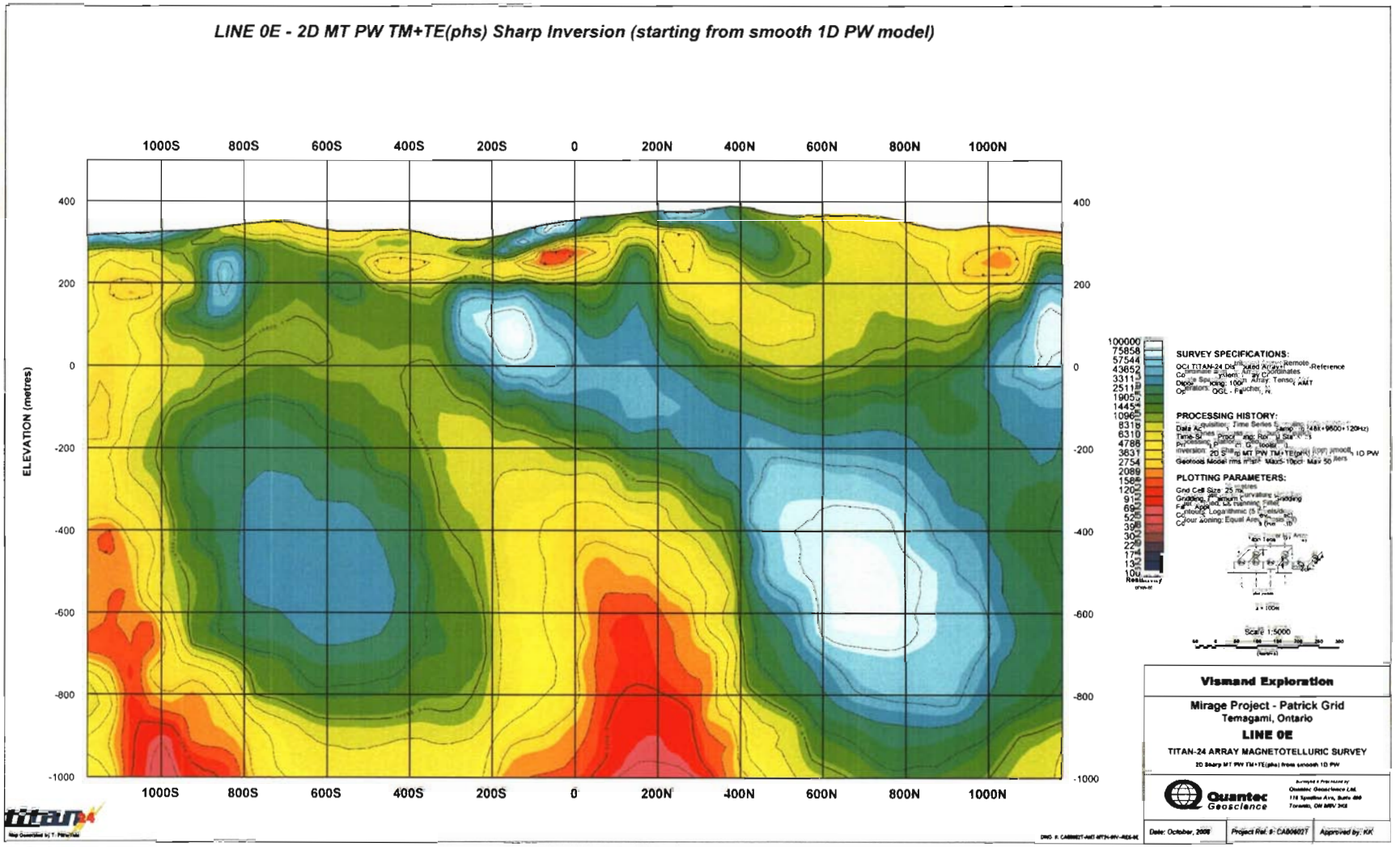

Line 0E – 2D MT PW TM+TE Sharp Inversion (starting from smooth 1D PW model)

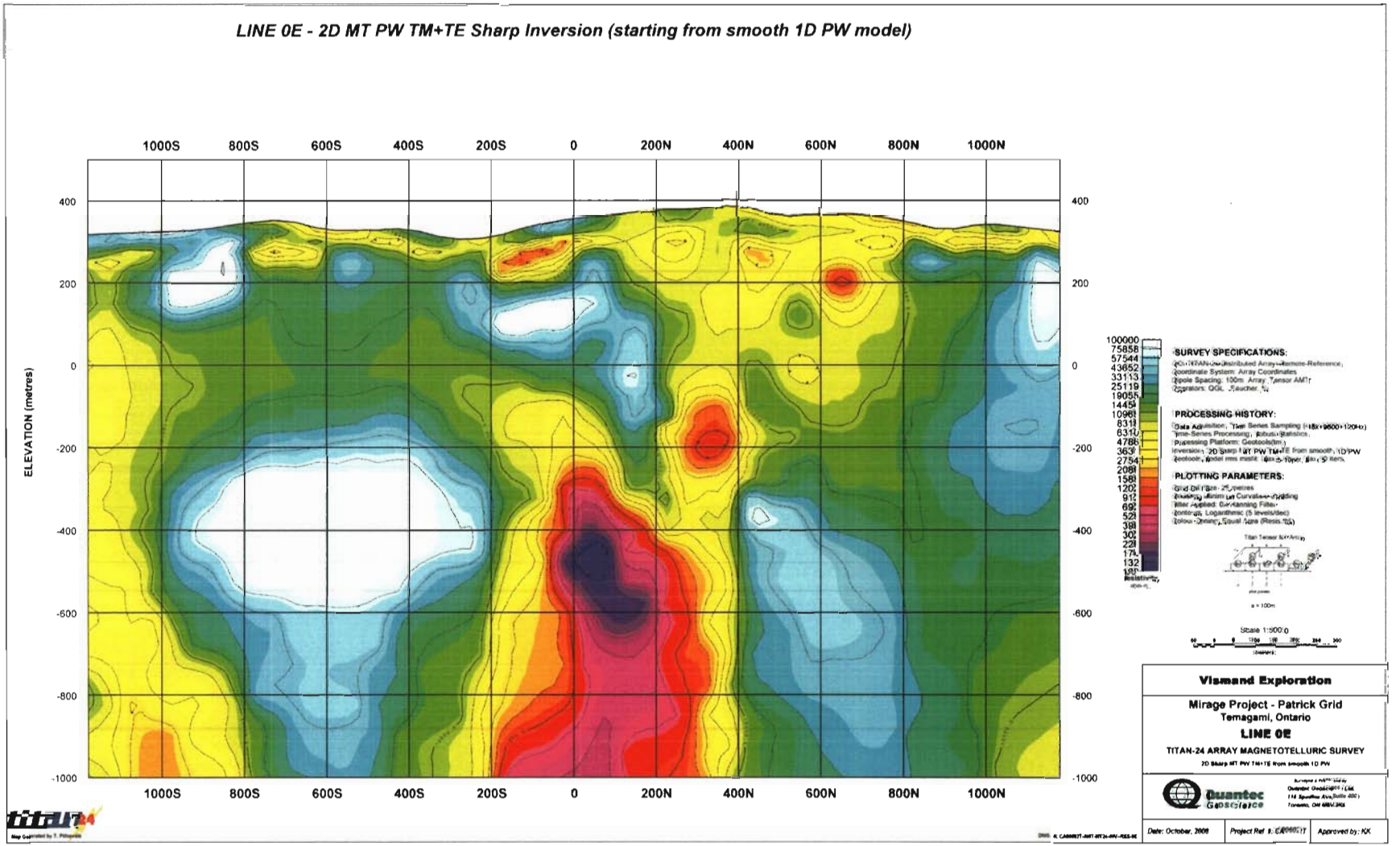

Line 0E – 2D MT PW TM+TE(phs) Inversion (starting from 1000 ohm-m halfspace)

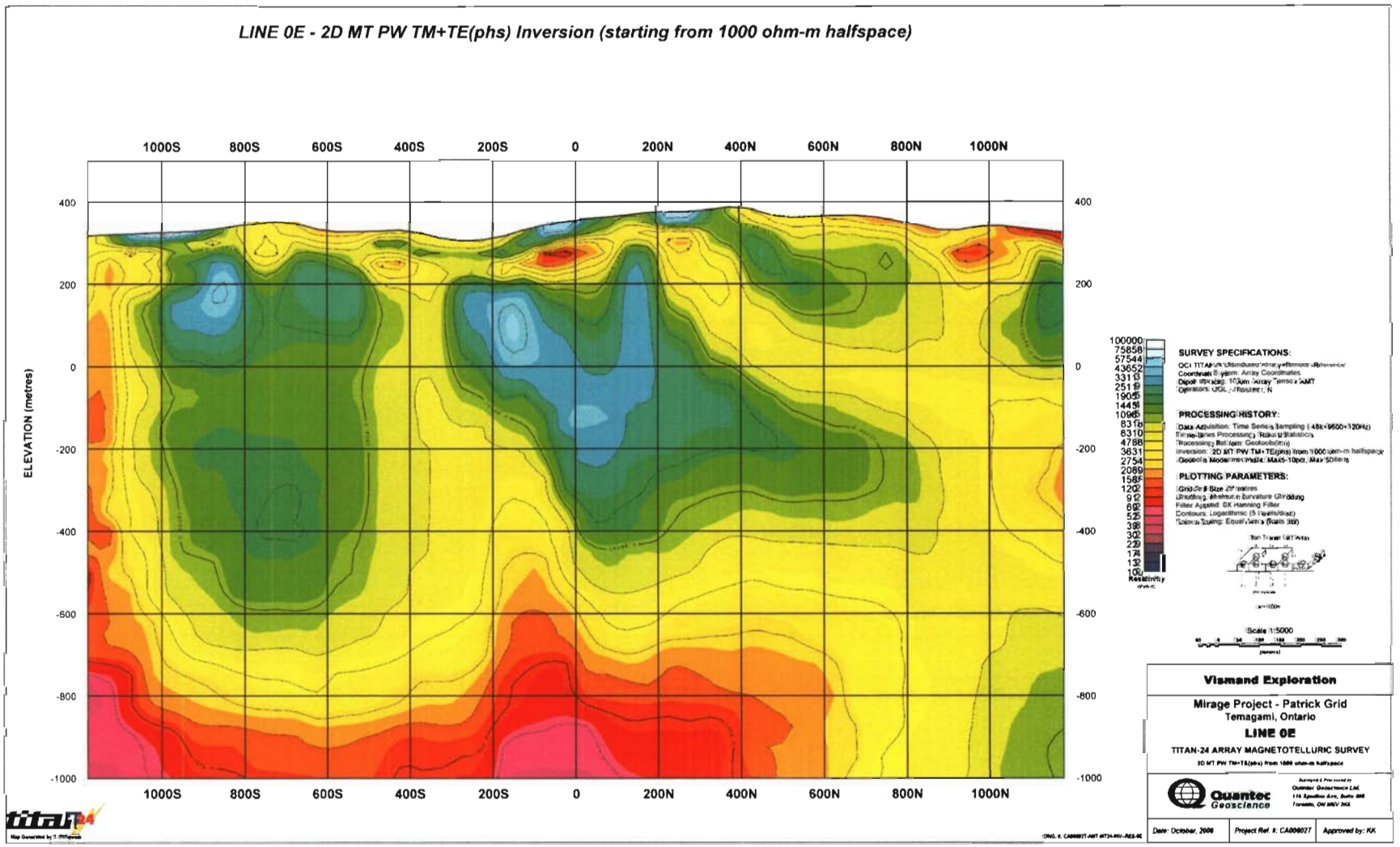

Line 0E – 2D MT PW TM+TE Inversion (starting from 1000 ohm-m halfspace)

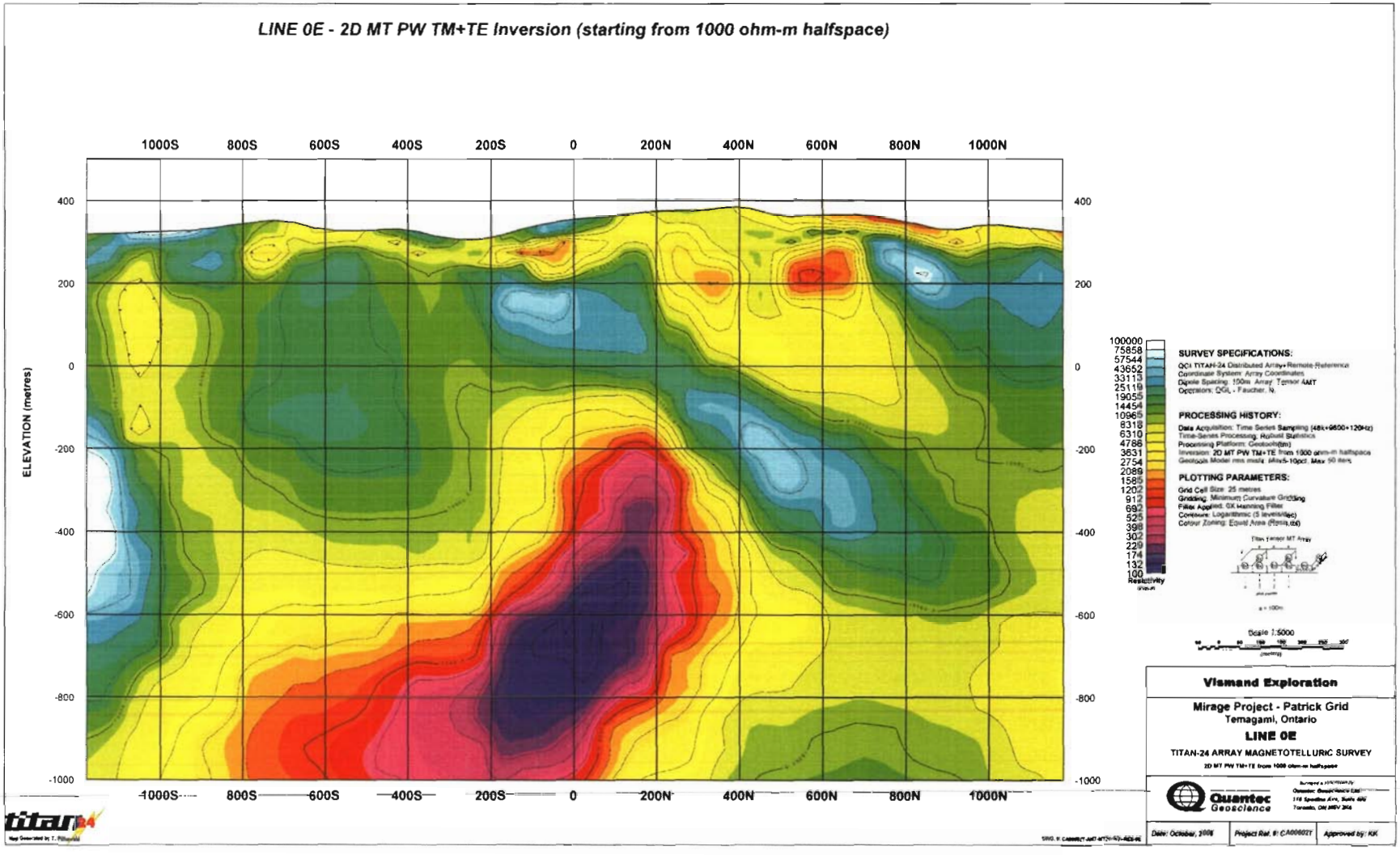

Line 0E – 2D MT RLM TM+TE(phs) Inversion (starting from 1D Det model)

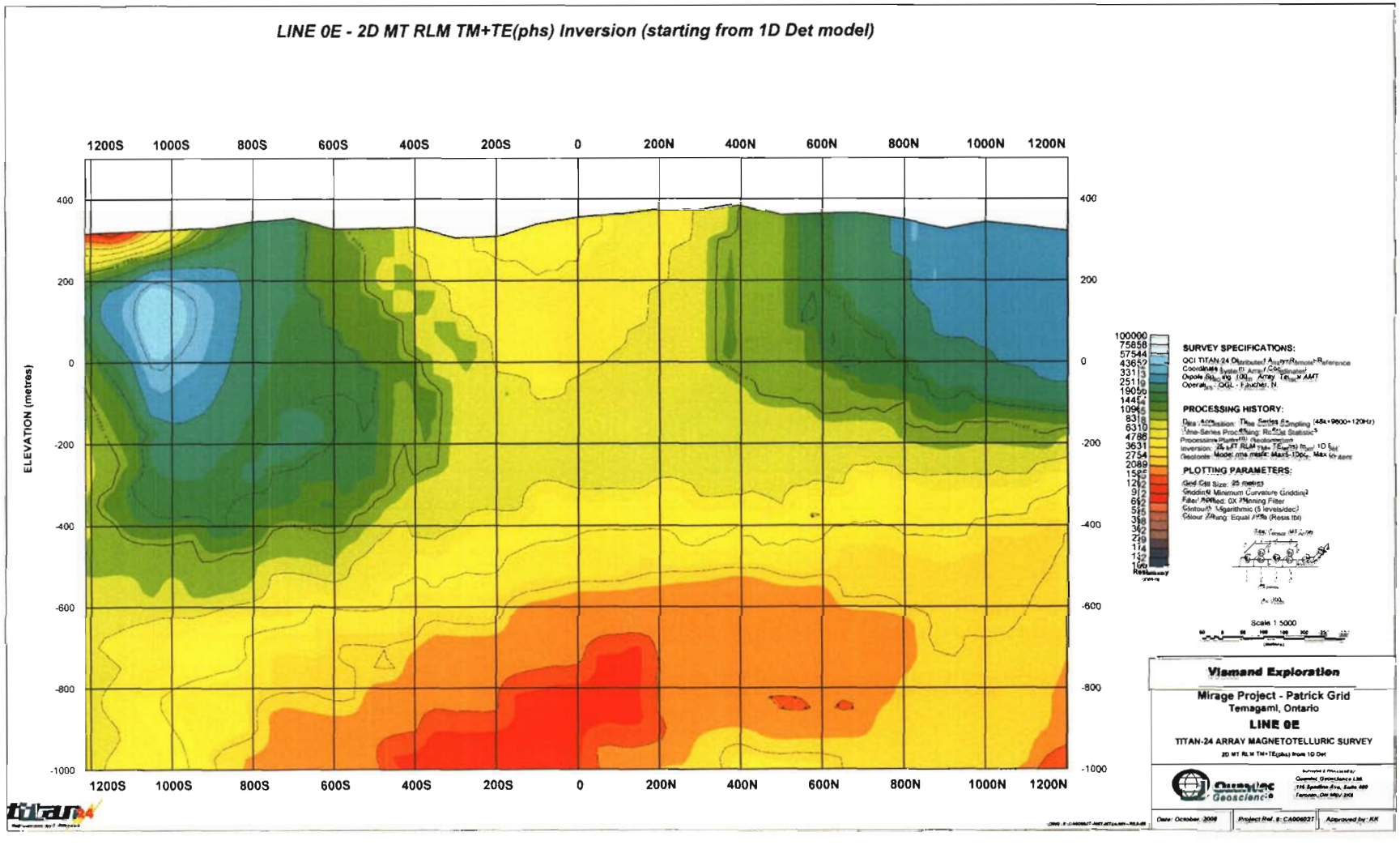

Line 0E – 2D MT RLM TM+TE Inversion (starting from 1D Det model)

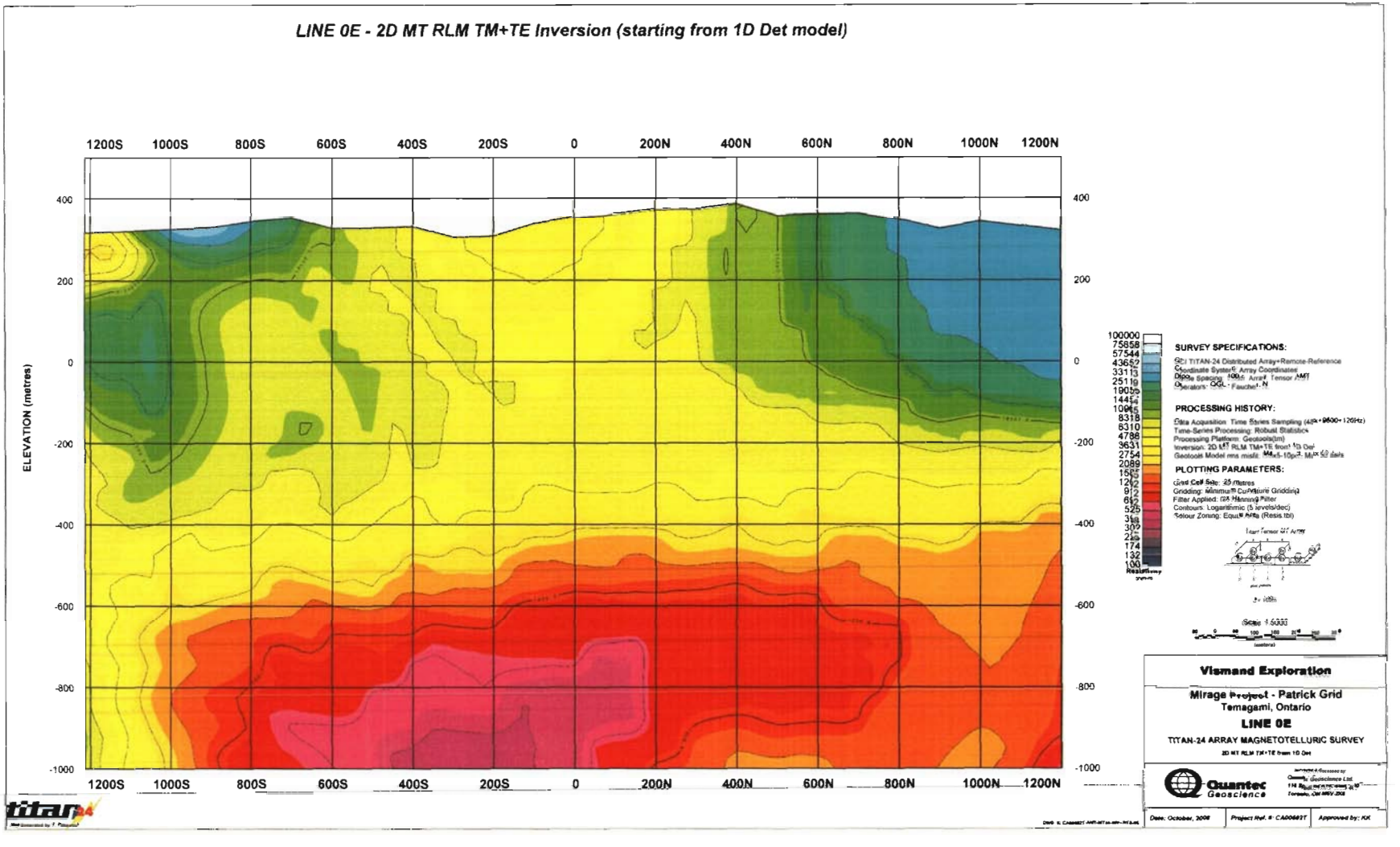

Line 0E – 2D MT RLM TM+TE(phs) Inversion (starting from 1000 ohm-m halfspace)

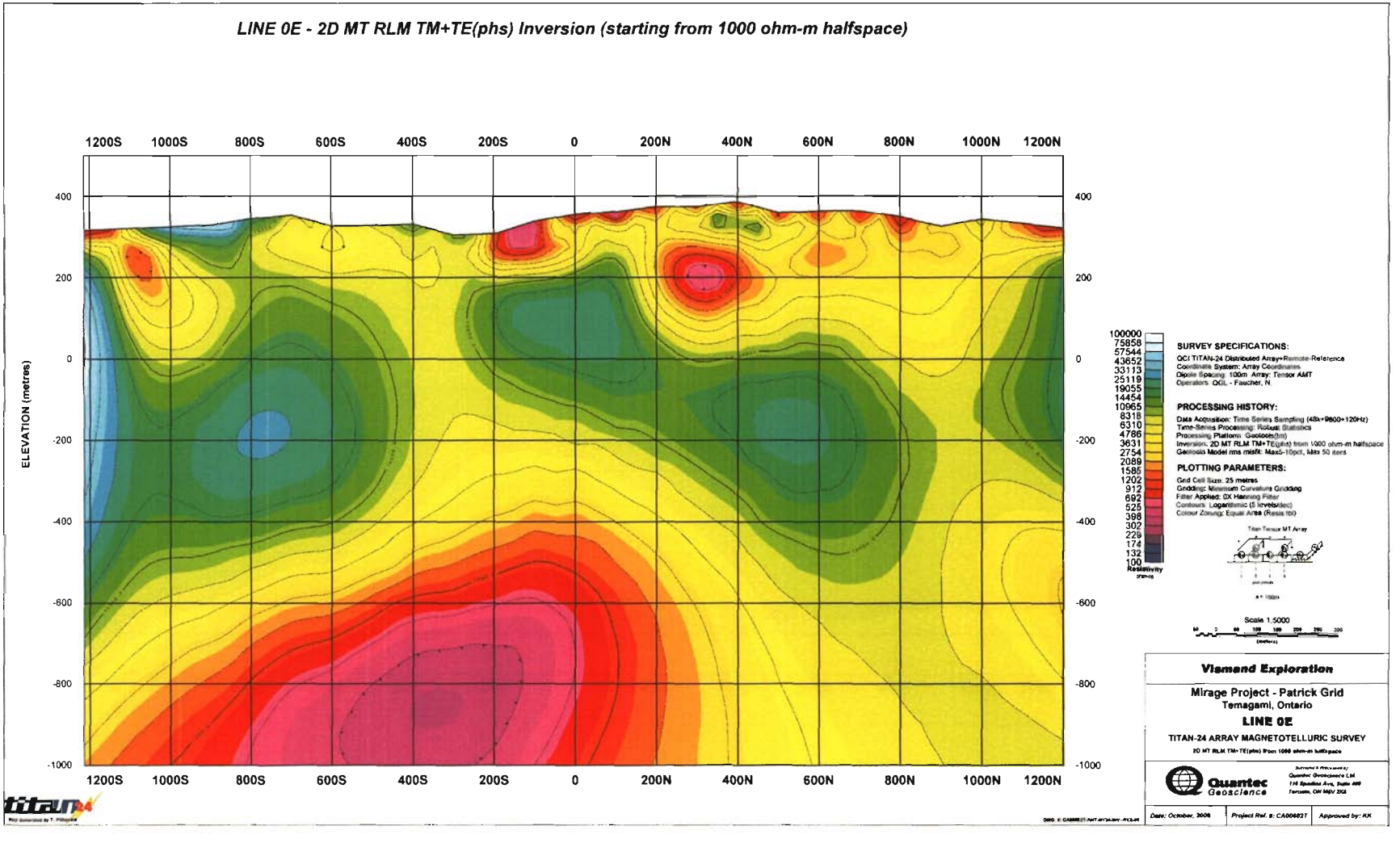

Line 0E – 2D MT RLM TM+TE Inversion (starting from 1000 ohm-m halfspace)

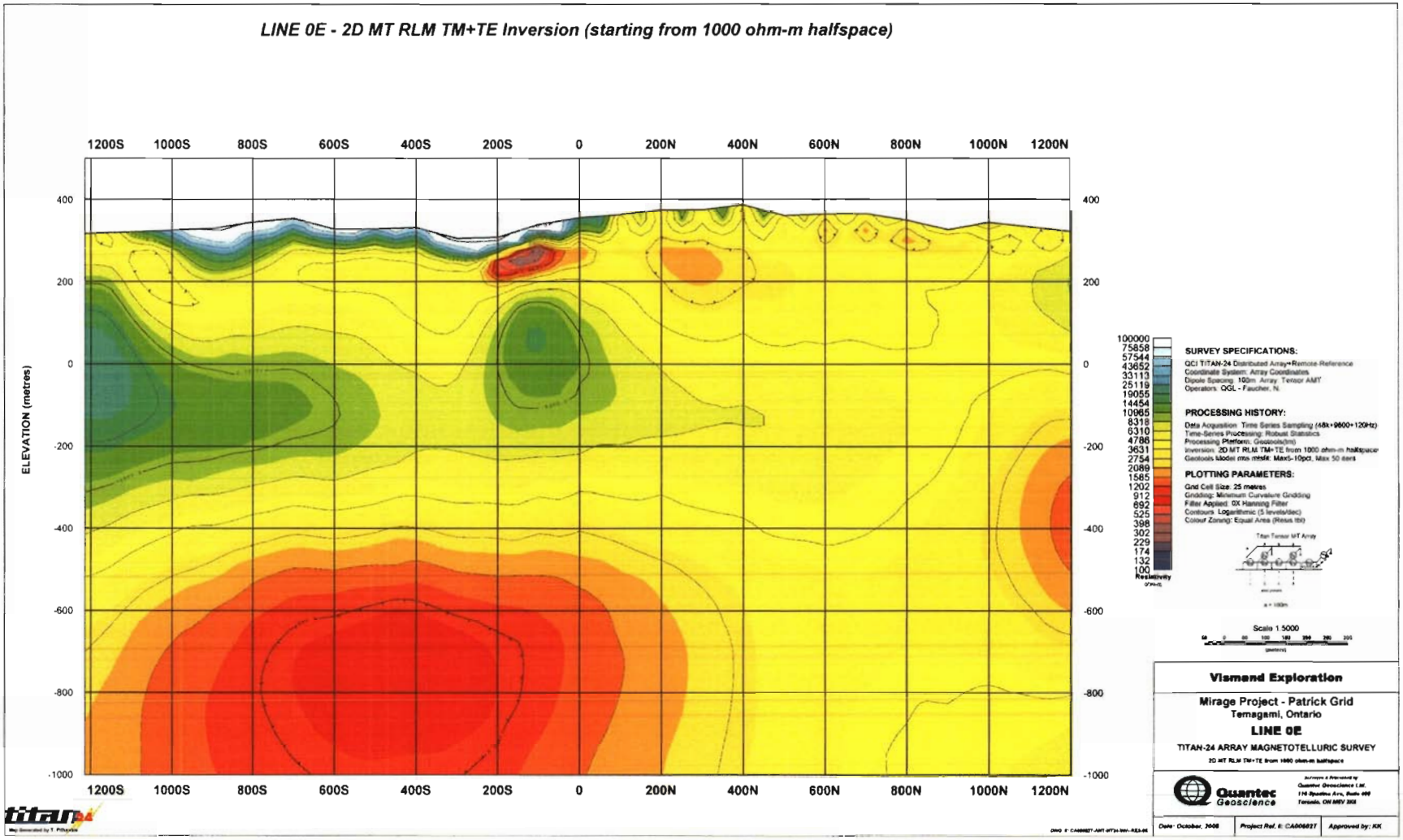

Line 400E – 2D UBC Smooth DC Resistivity Model

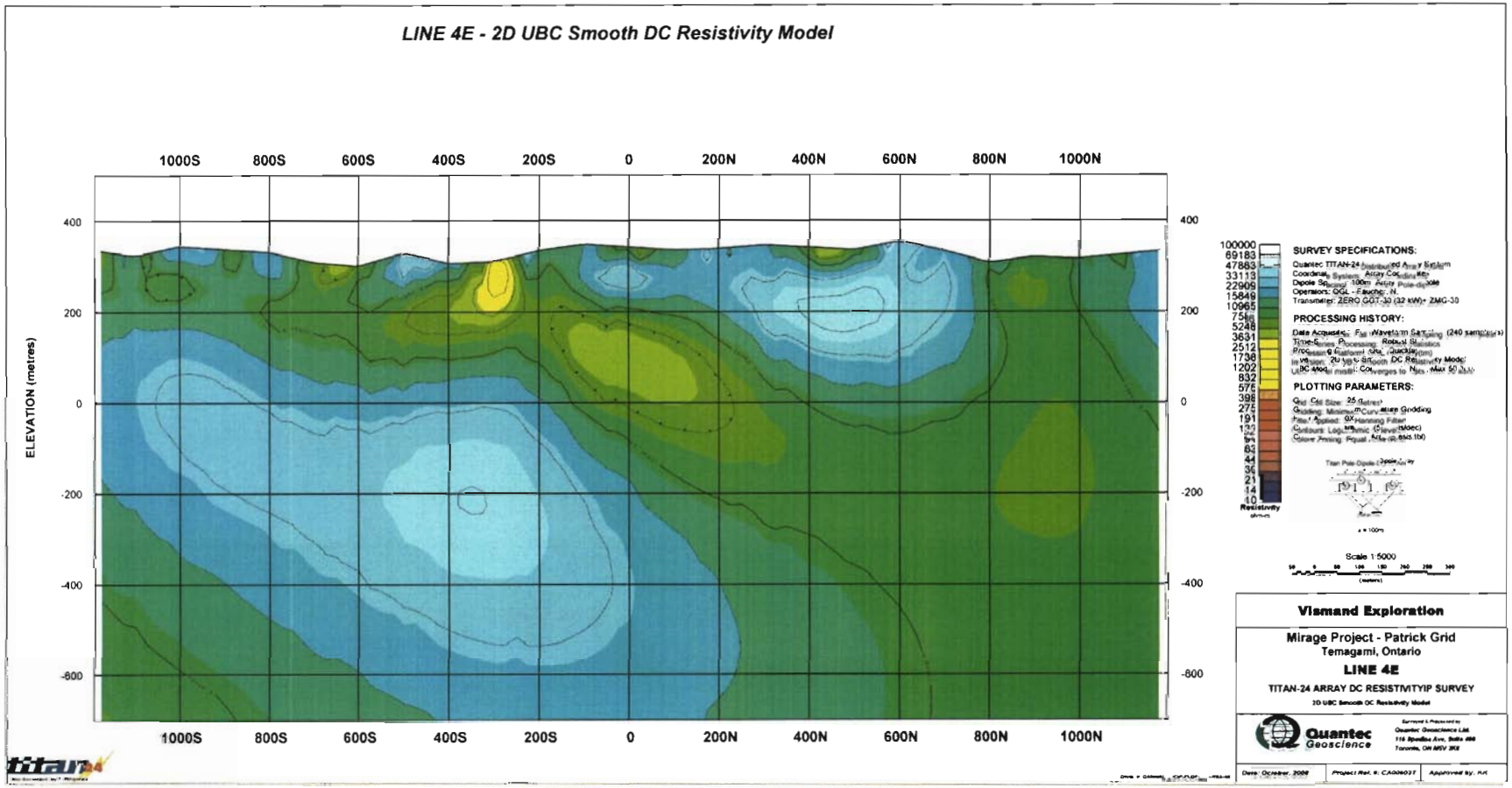

Line 400E – 2D UBC Smooth IP Chargeability Model

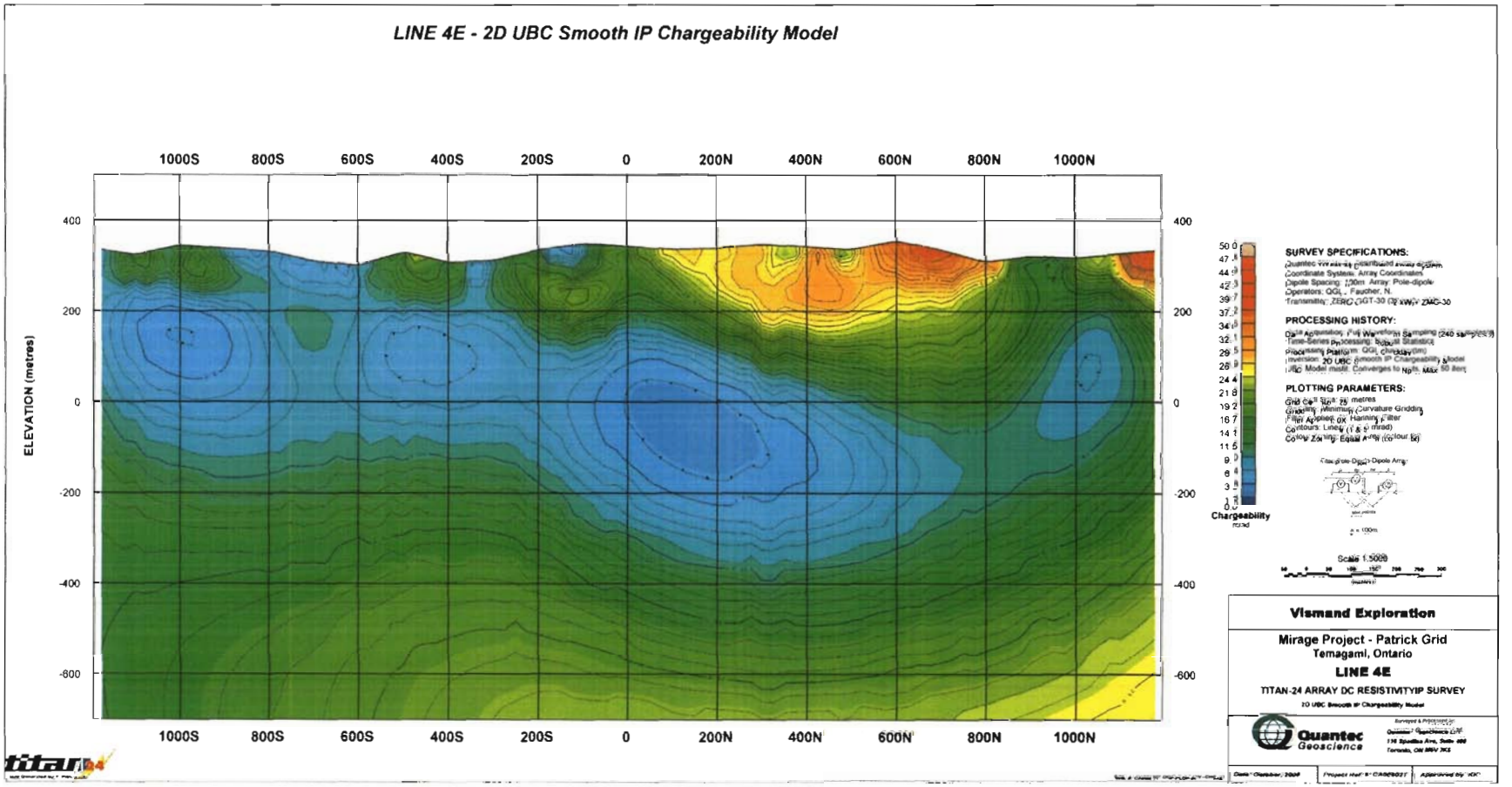

Line 400E – 2D UBC Null Con IP Chargeability Model

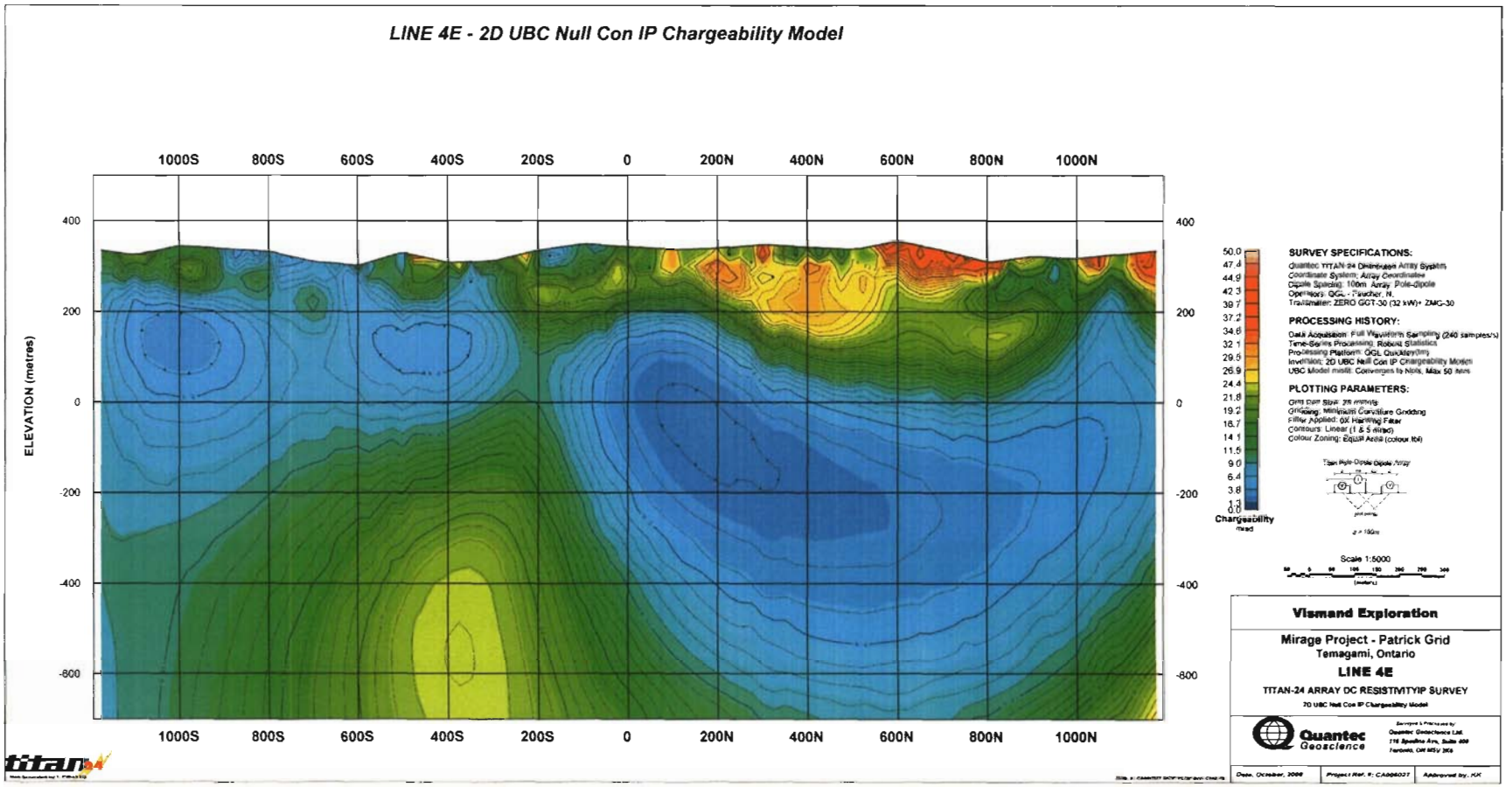

Line 400E – 2D MT PW TM+TE(phs) Sharp Inversion (starting from smooth 1D PW model)

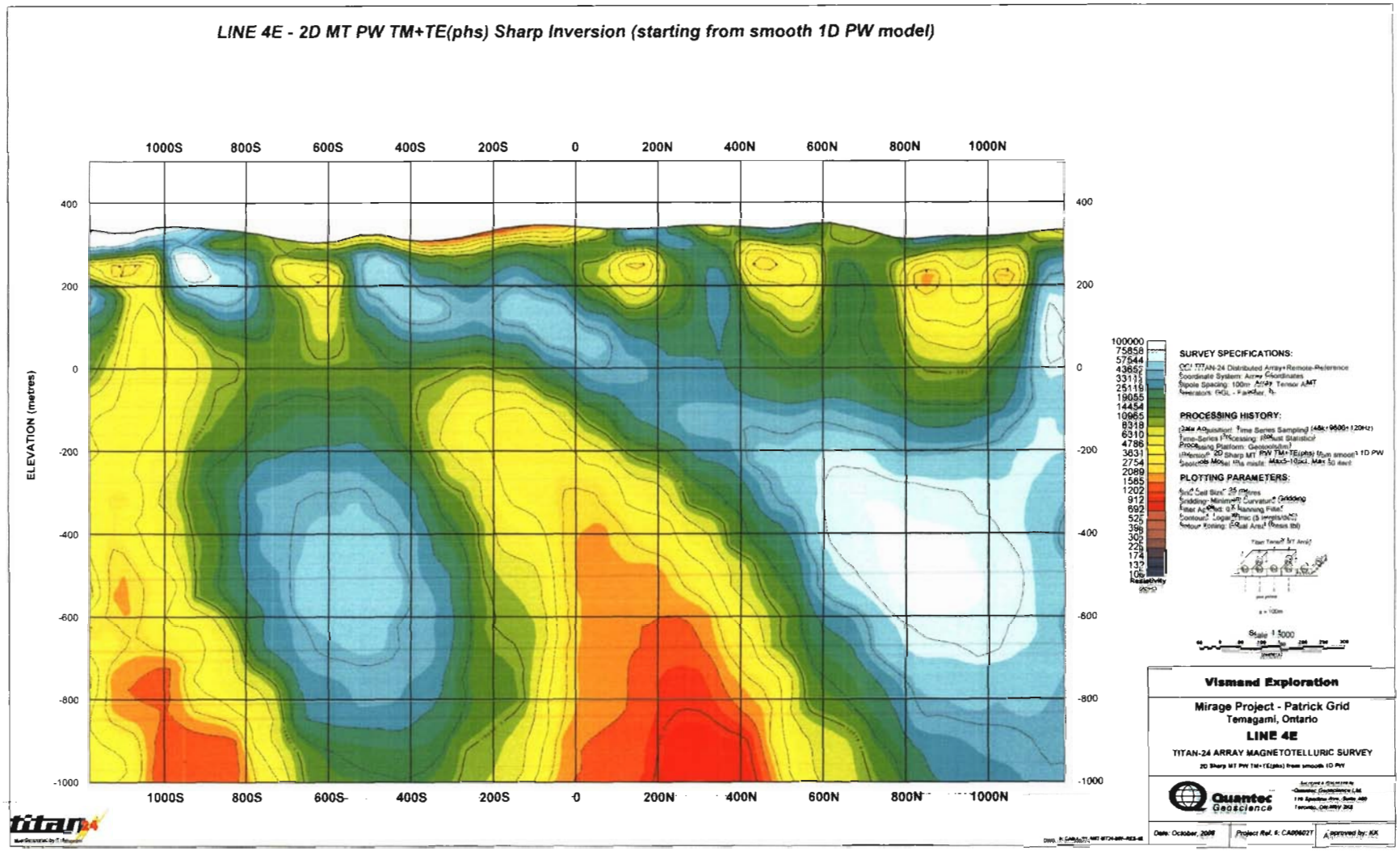

Line 400E – 2D MT PW TM+TE Sharp Inversion (starting from smooth 1D PW model)

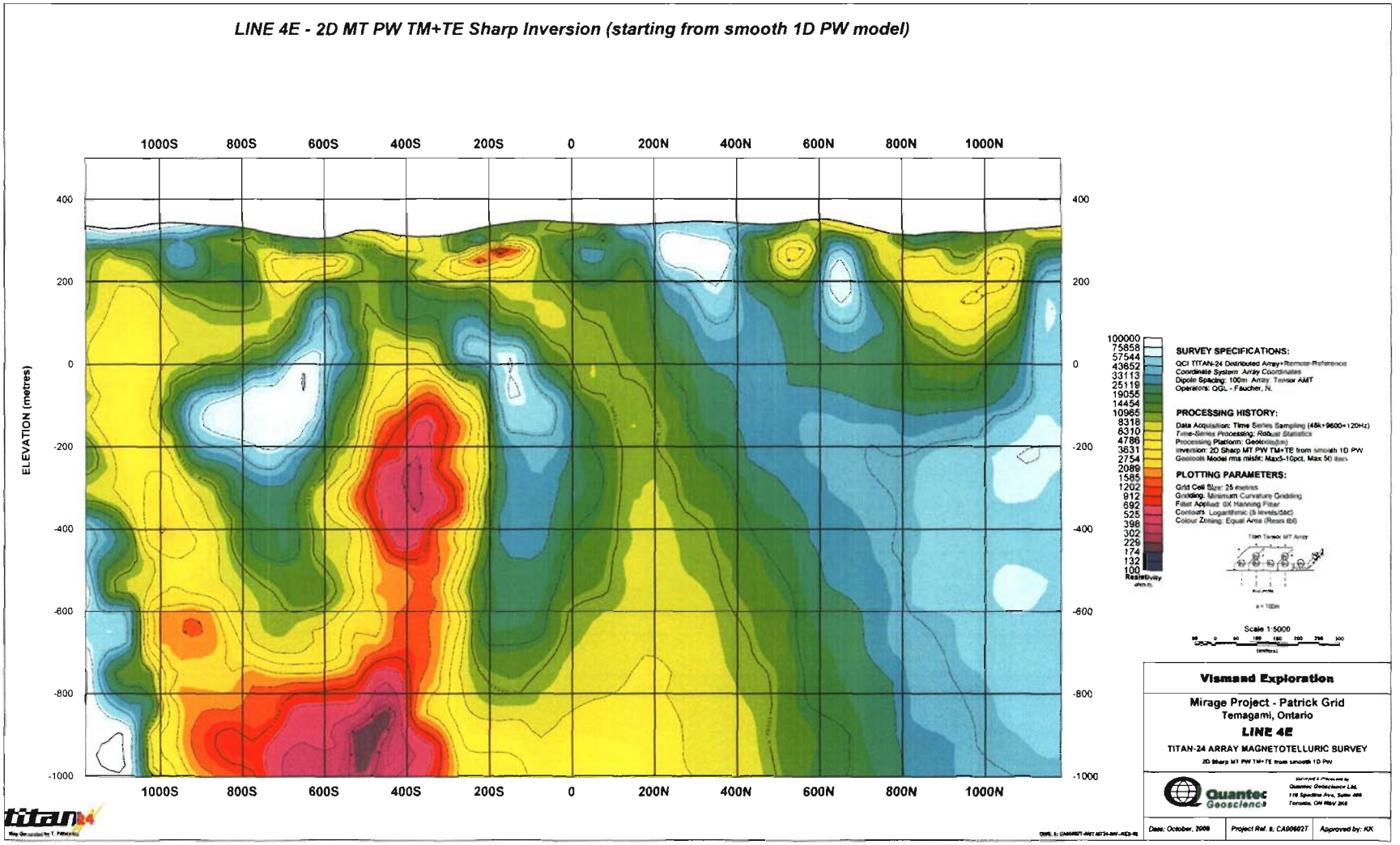

Line 400E – 2D MT PW TM+TE(phs) Inversion (starting from 1000 ohm-m halfspace)

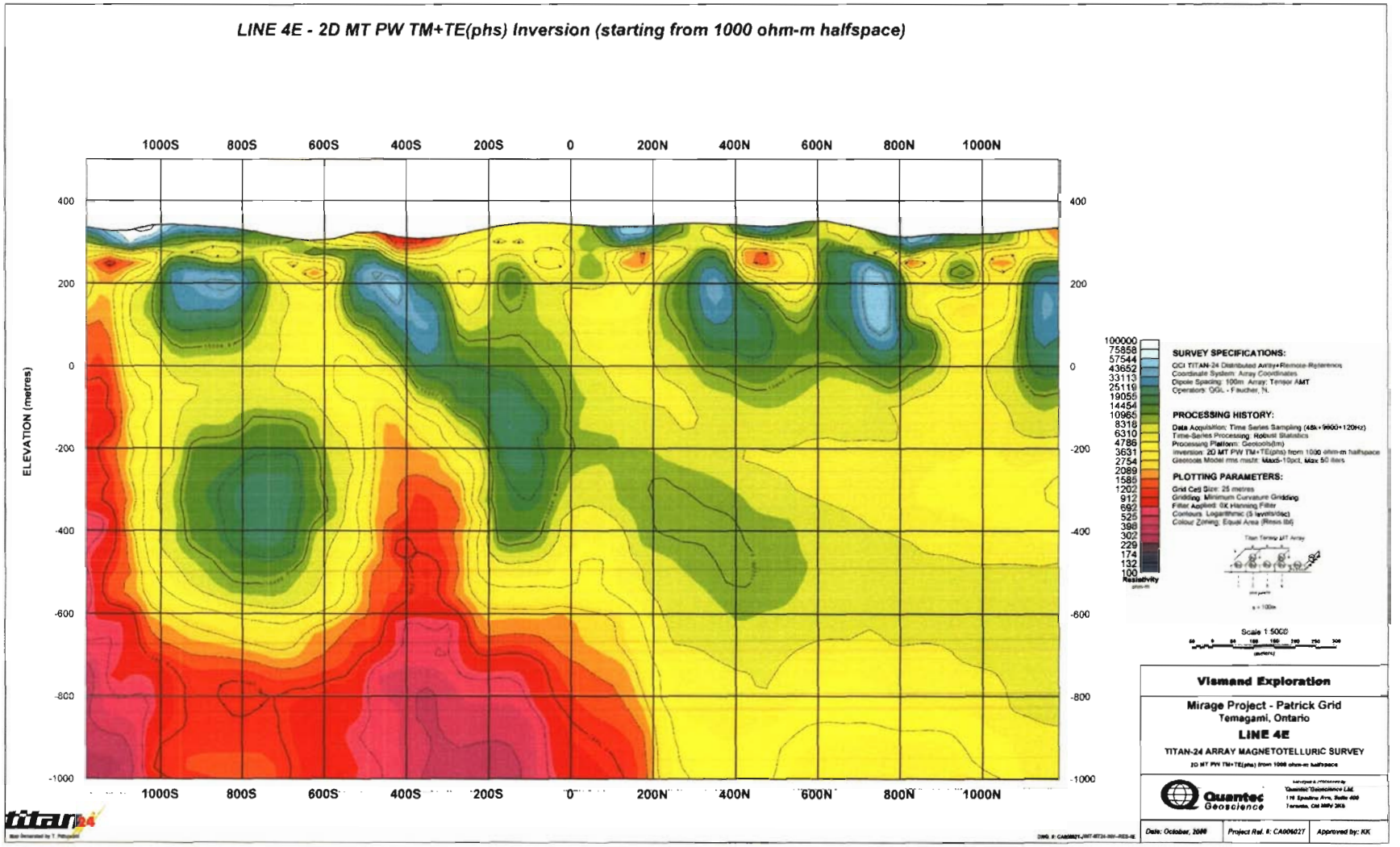

Line 400E – 2D MT PW TM+TE Inversion (starting from 1000 ohm-m halfspace)

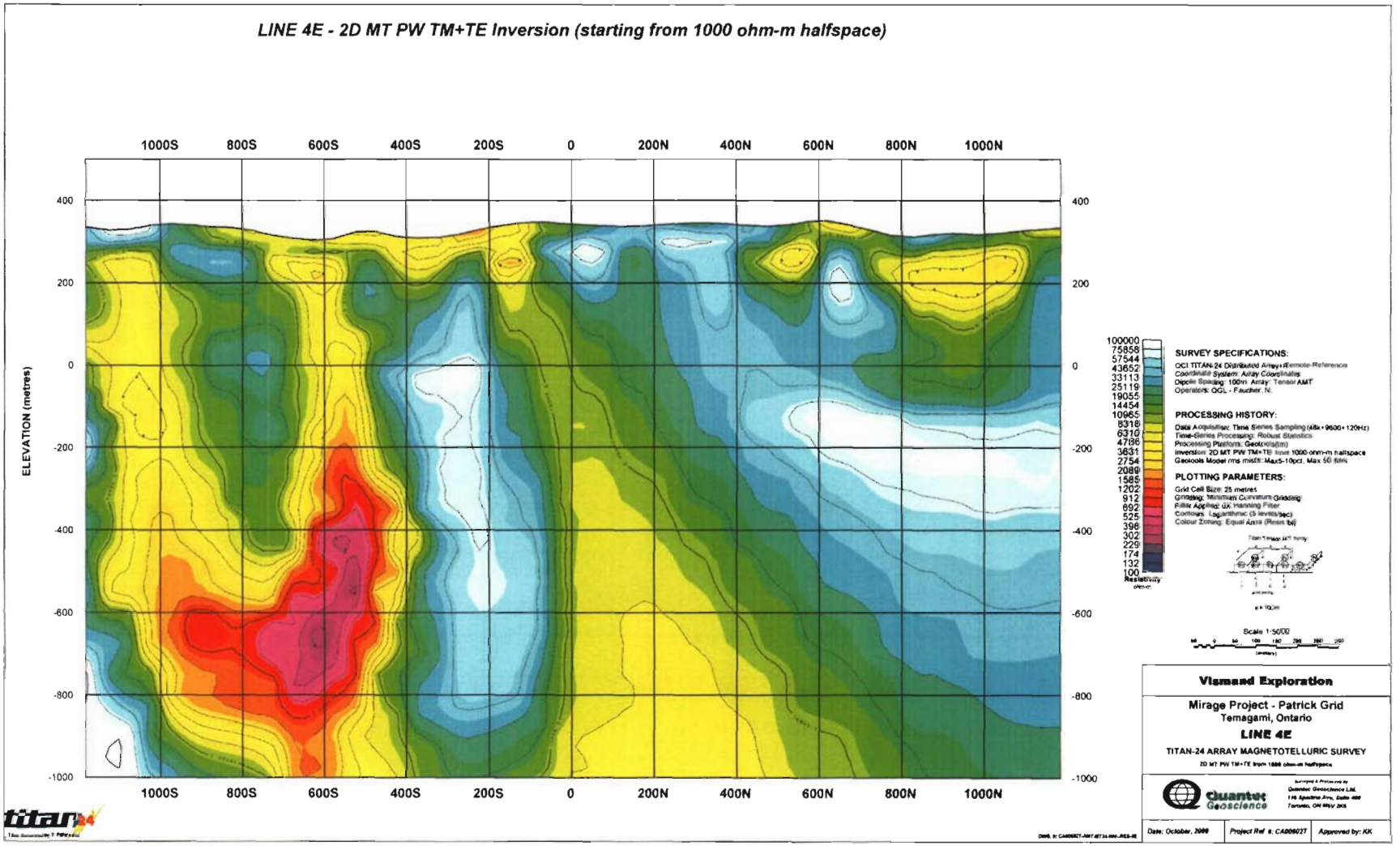

Line 400E – 2D MT RLM TM+TE(phs) Inversion (starting from 1D Det model)

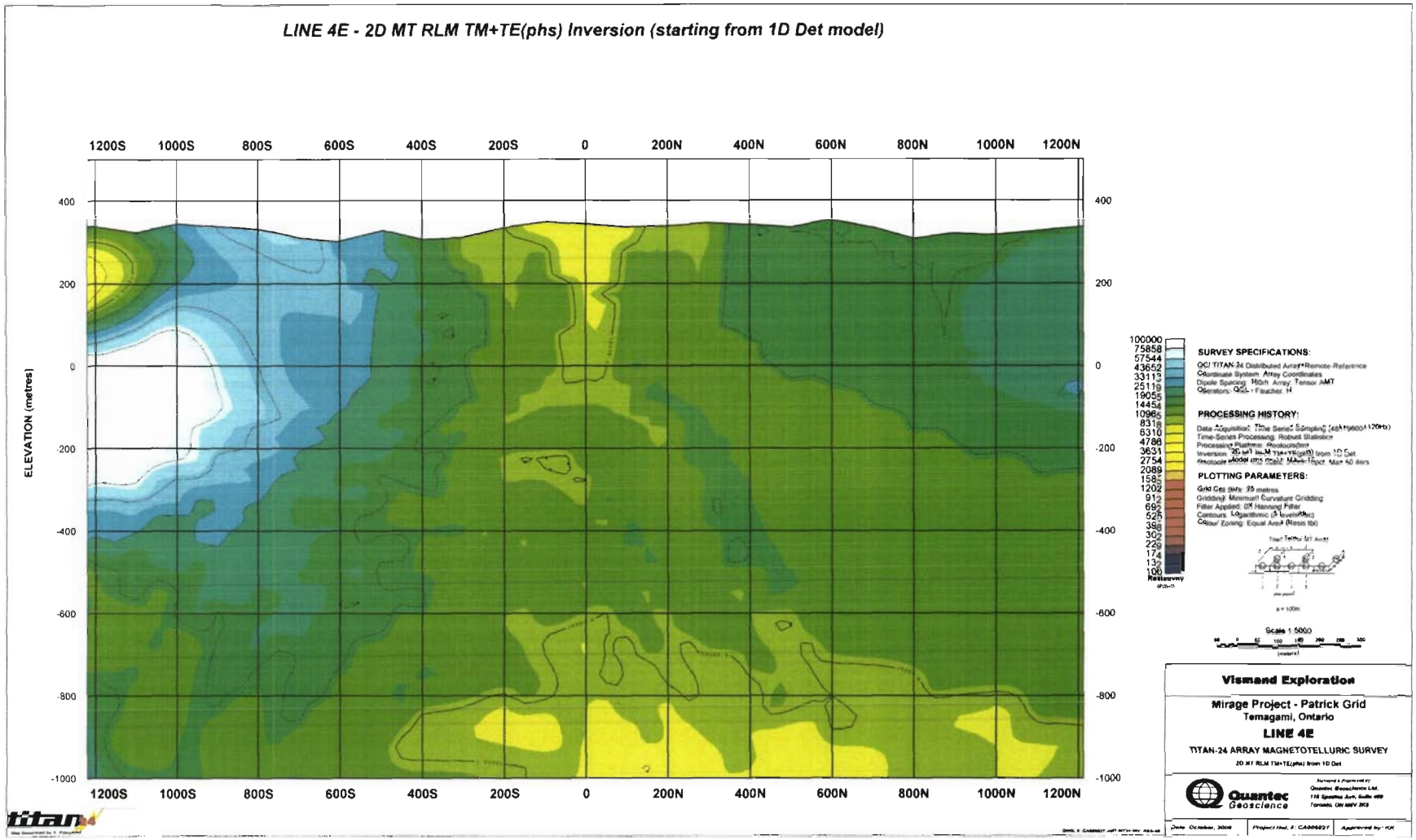

Line 400E – 2D MT RLM TM+TE Inversion (starting from 1000 ohm-m halfspace)

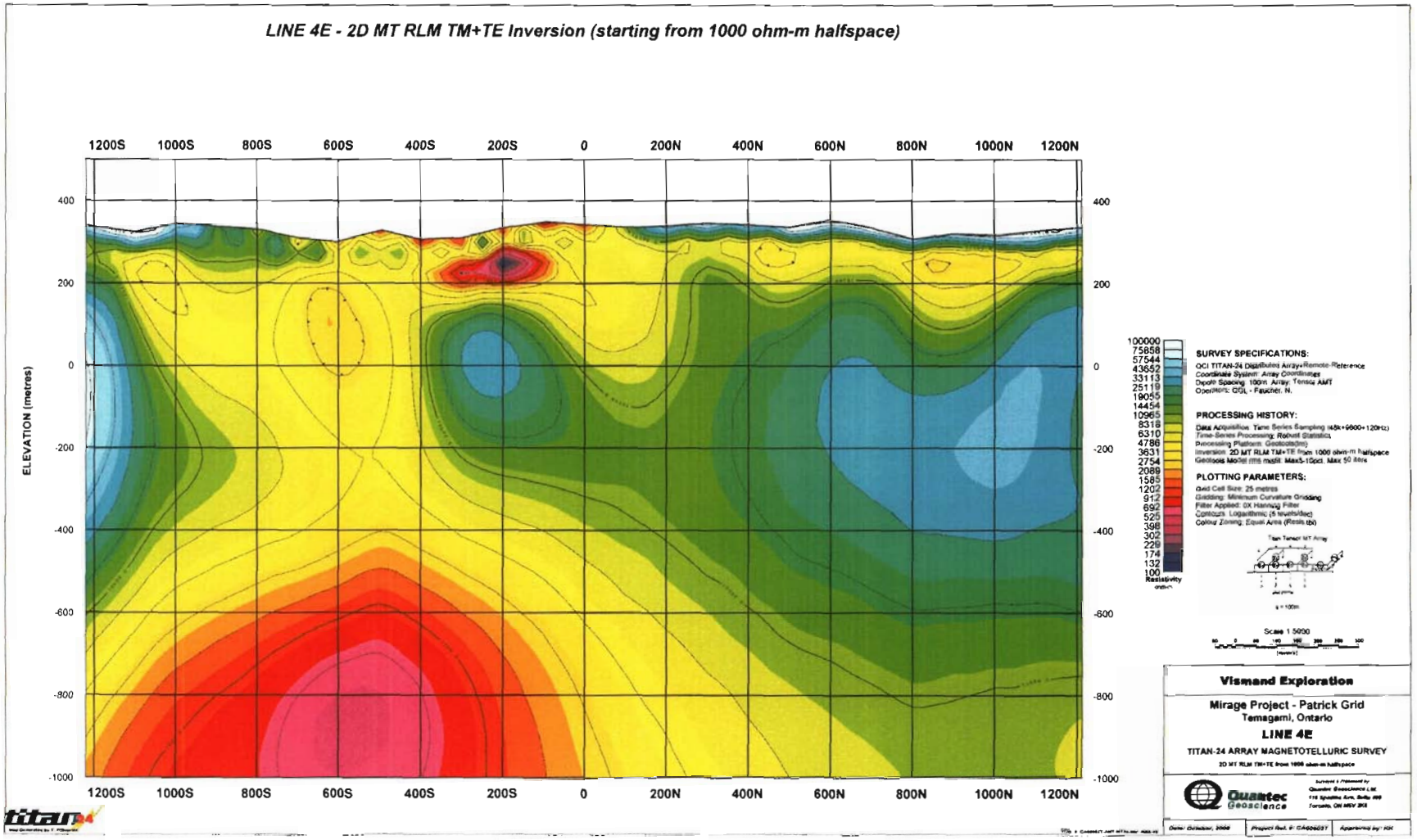

Line 800E – 2D UBC Smooth DC Resistivity Model

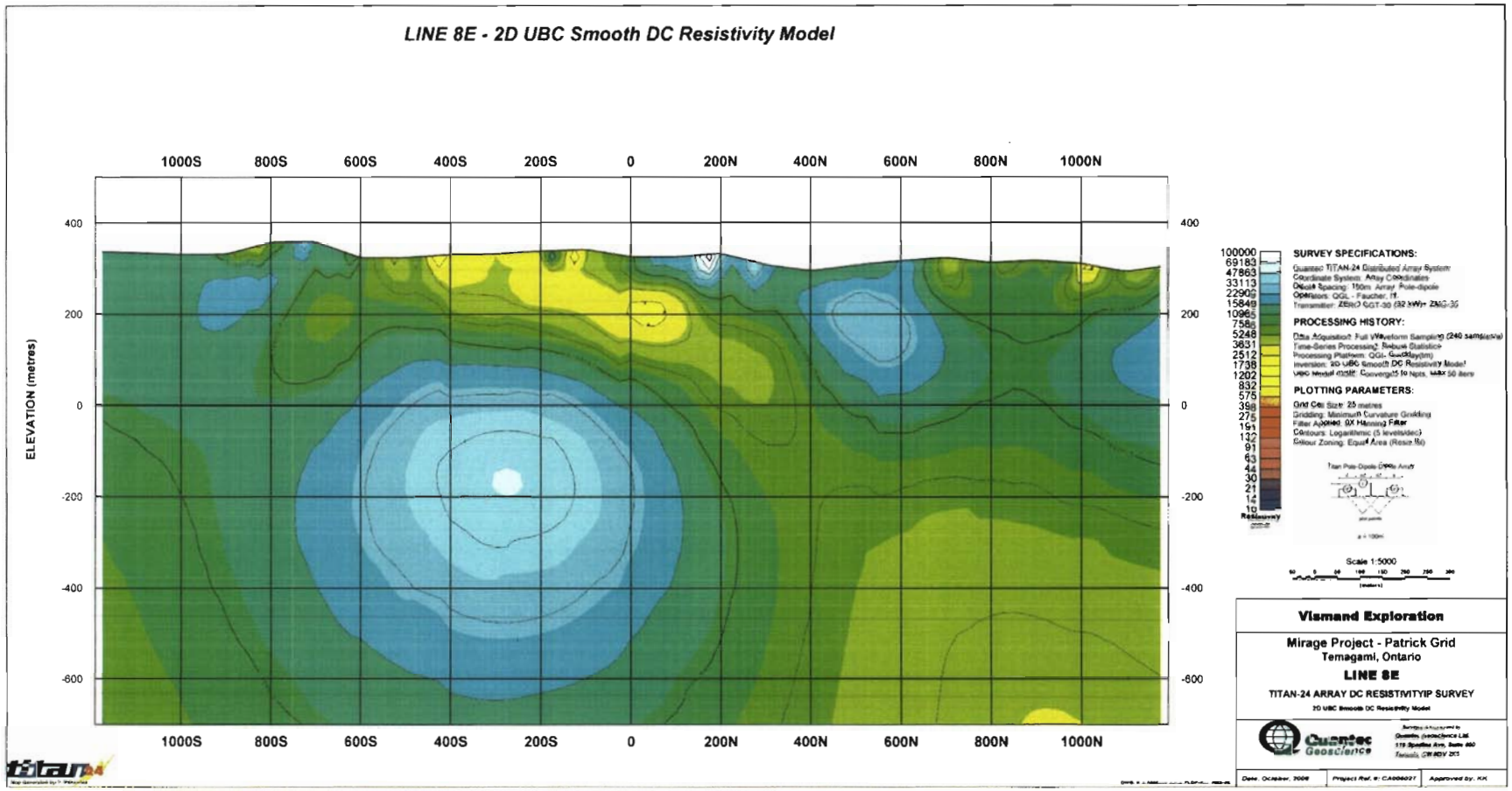

Line 800E – 2D UBC Smooth IP Chargeability Model

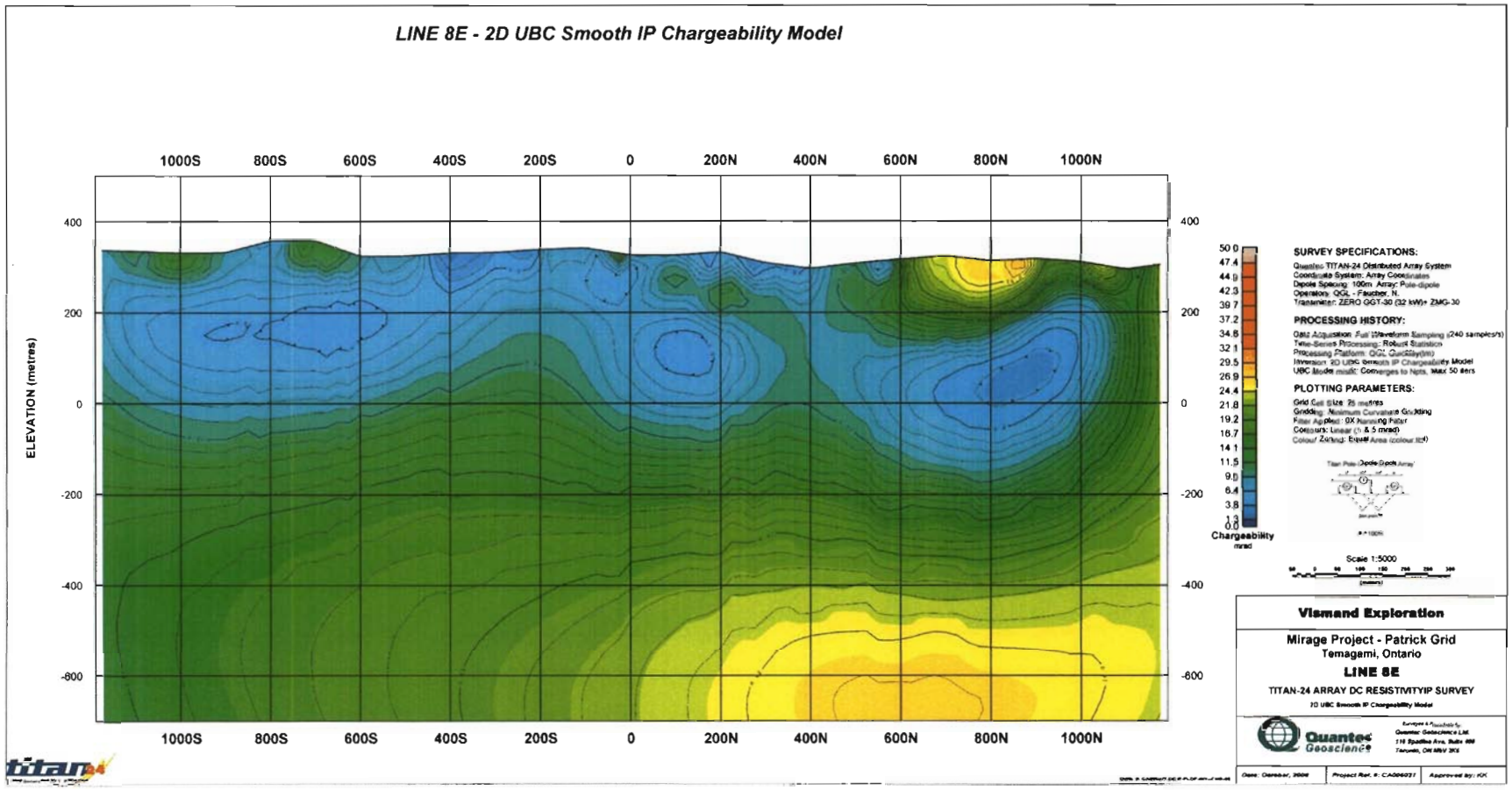

Line 800E – 2D UBC Null Con IP Chargeability Model

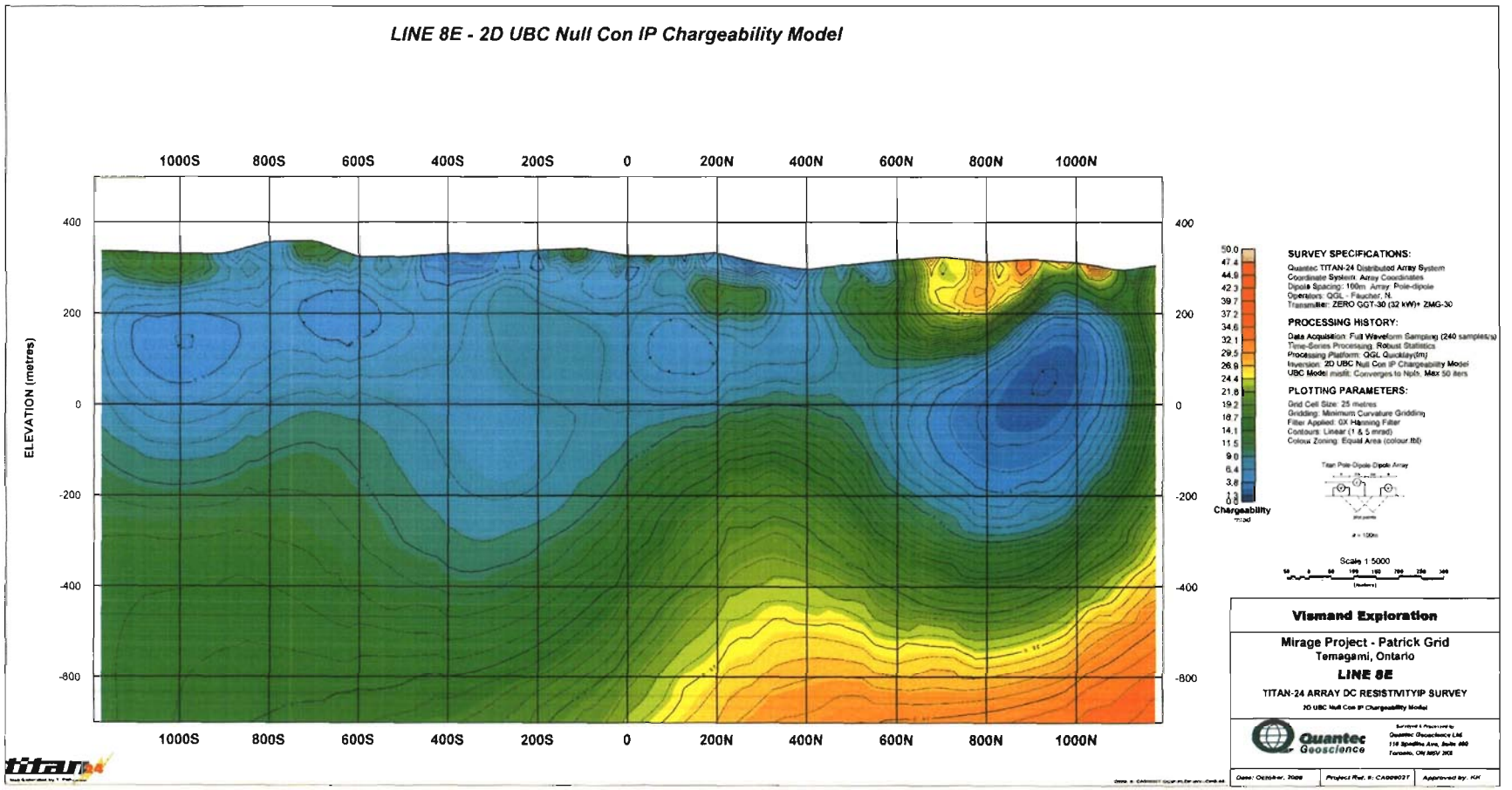

Line 800E – 2D MT PW TM+TE(phs) Sharp Inversion (starting from smooth 1D PW model)

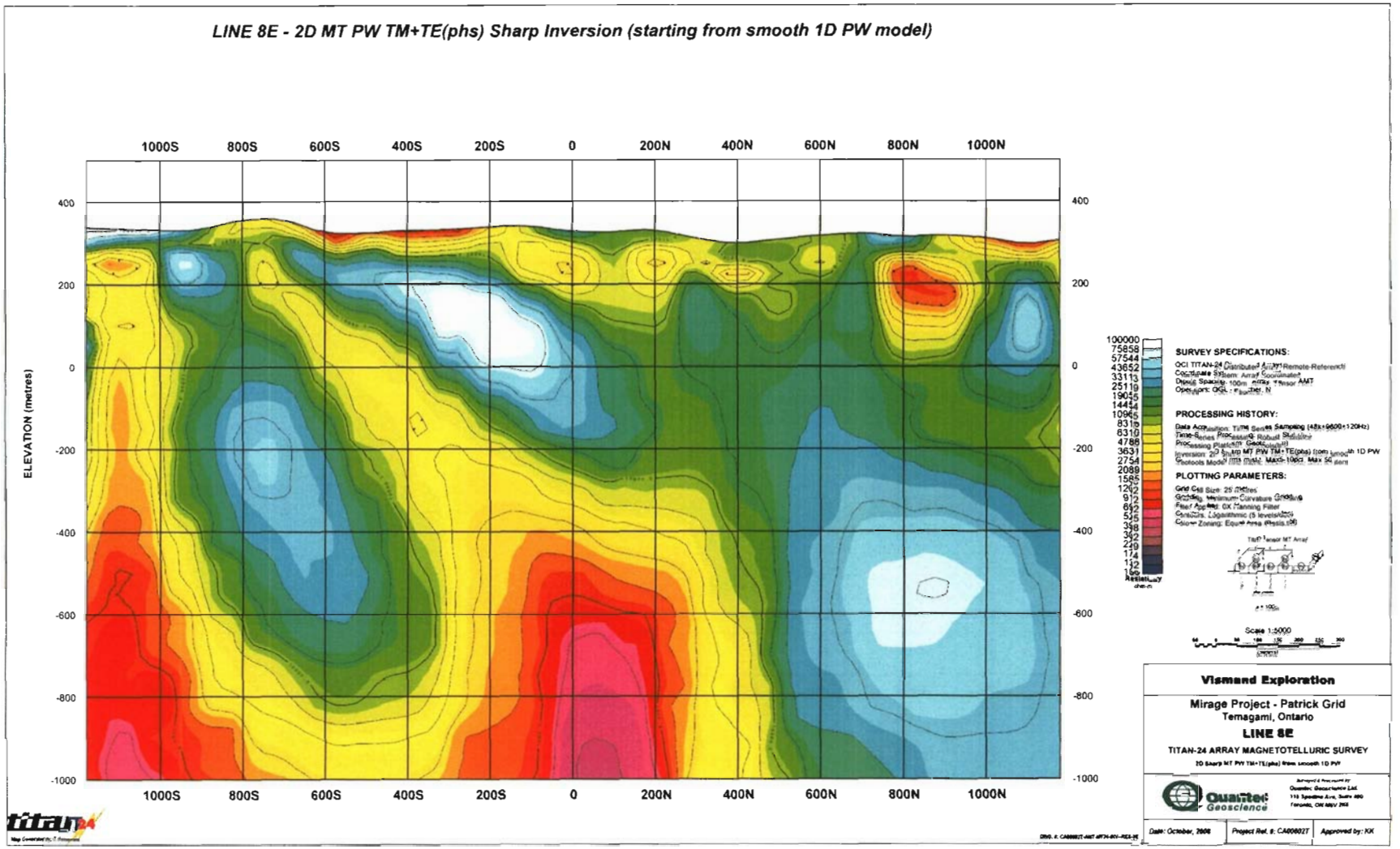

Line 800E – 2D MT PW TM+TE Sharp Inversion (starting from smooth 1D PW model)

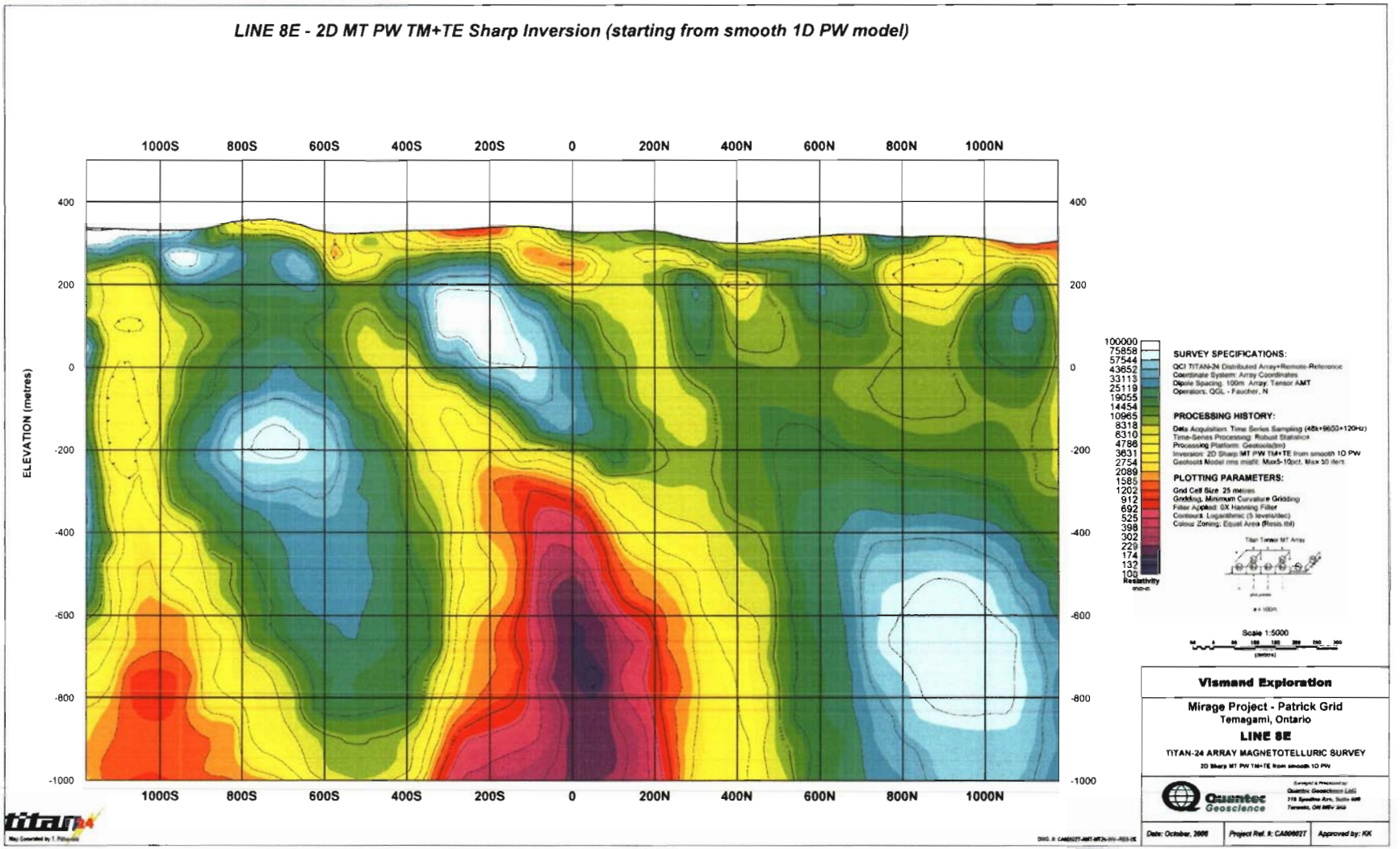

Line 800E – 2D MT PW TM+TE(phs) Inversion (starting from 1000 ohm-m halfspace)

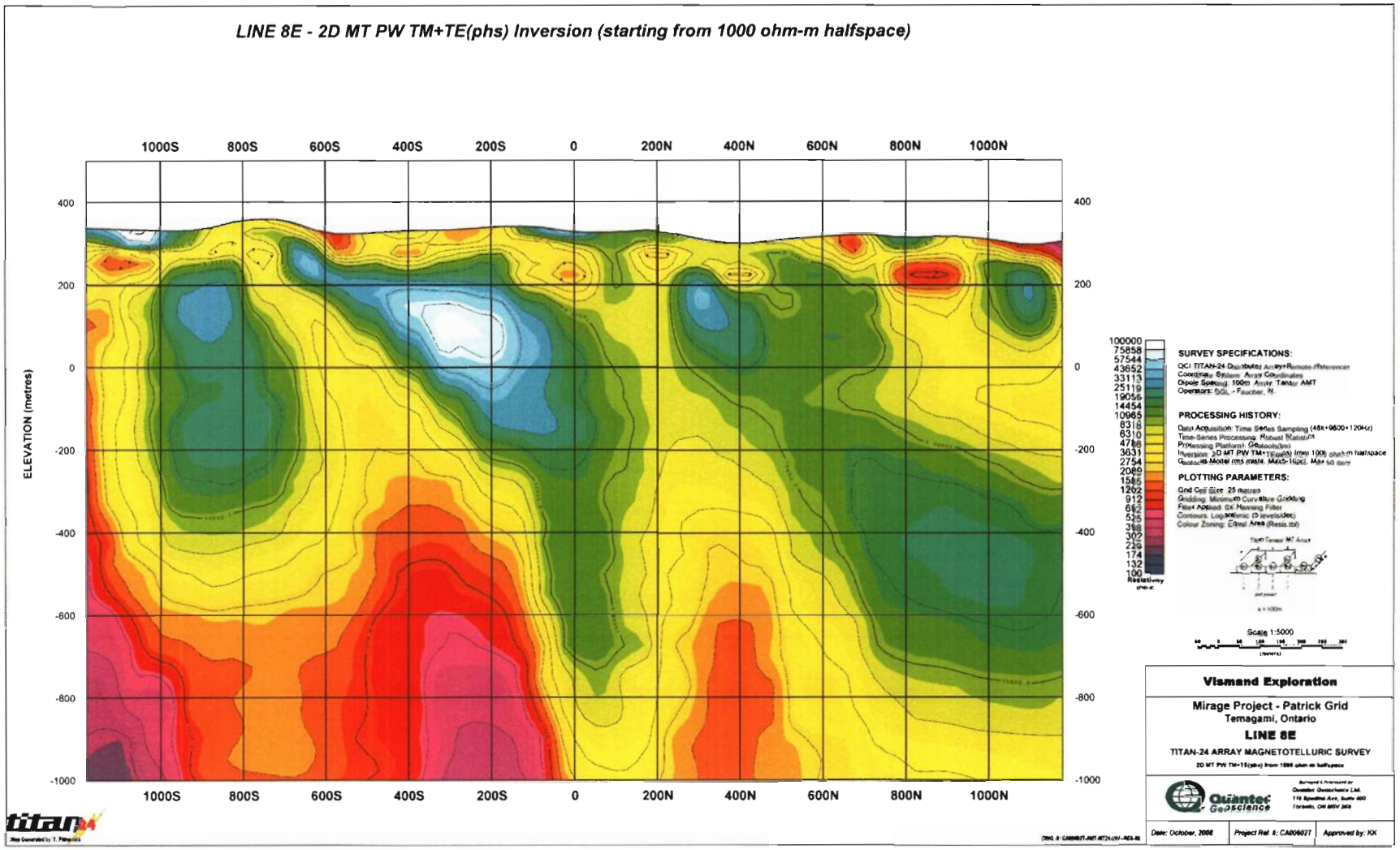

Line 800E – 2D MT PW TM+TE Sharp Inversion (starting from smooth 1D PW model)

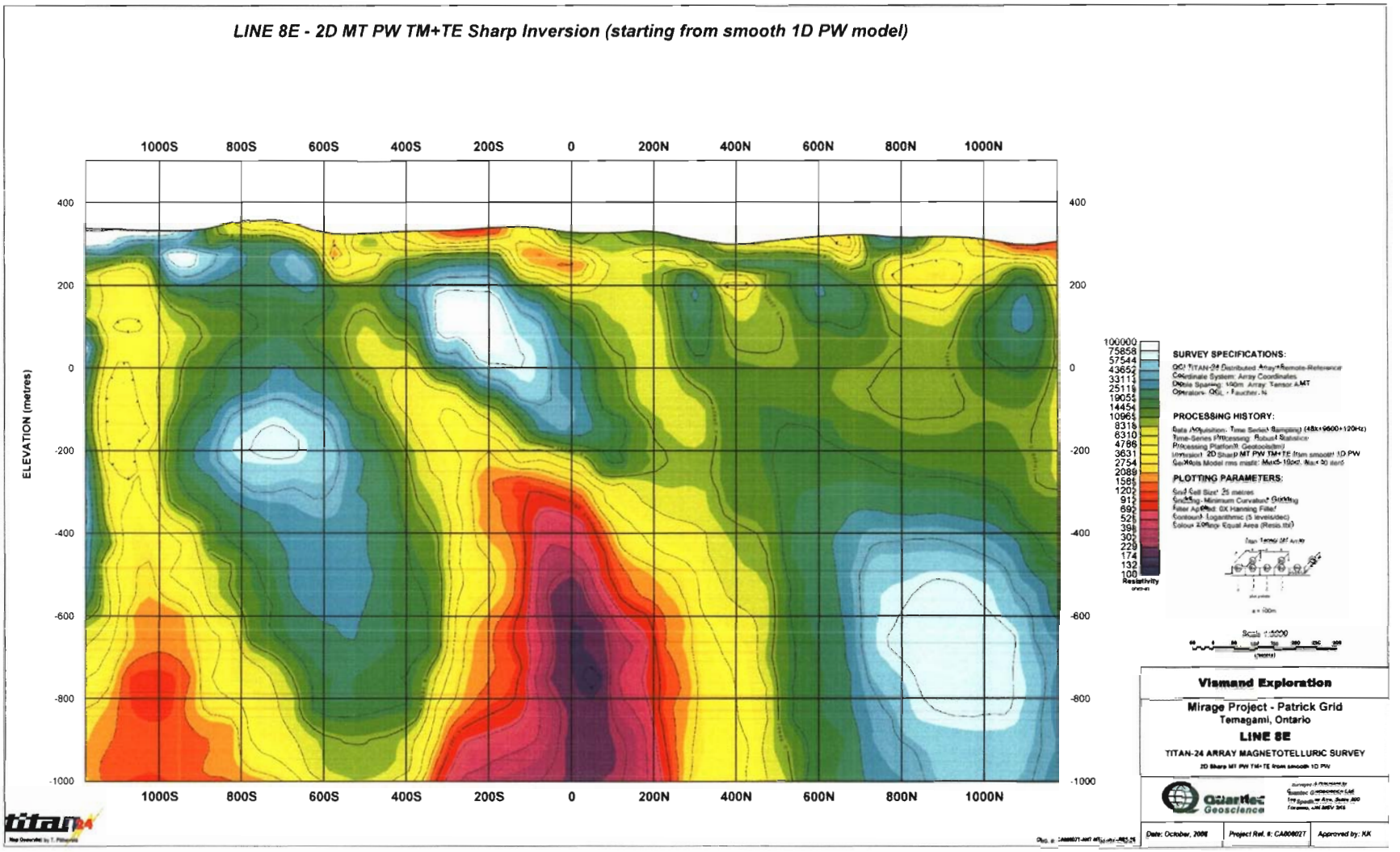

Line 800E – 2D MT PW TM+TE(phs) Inversion (starting from 1000 ohm-m halfspace)

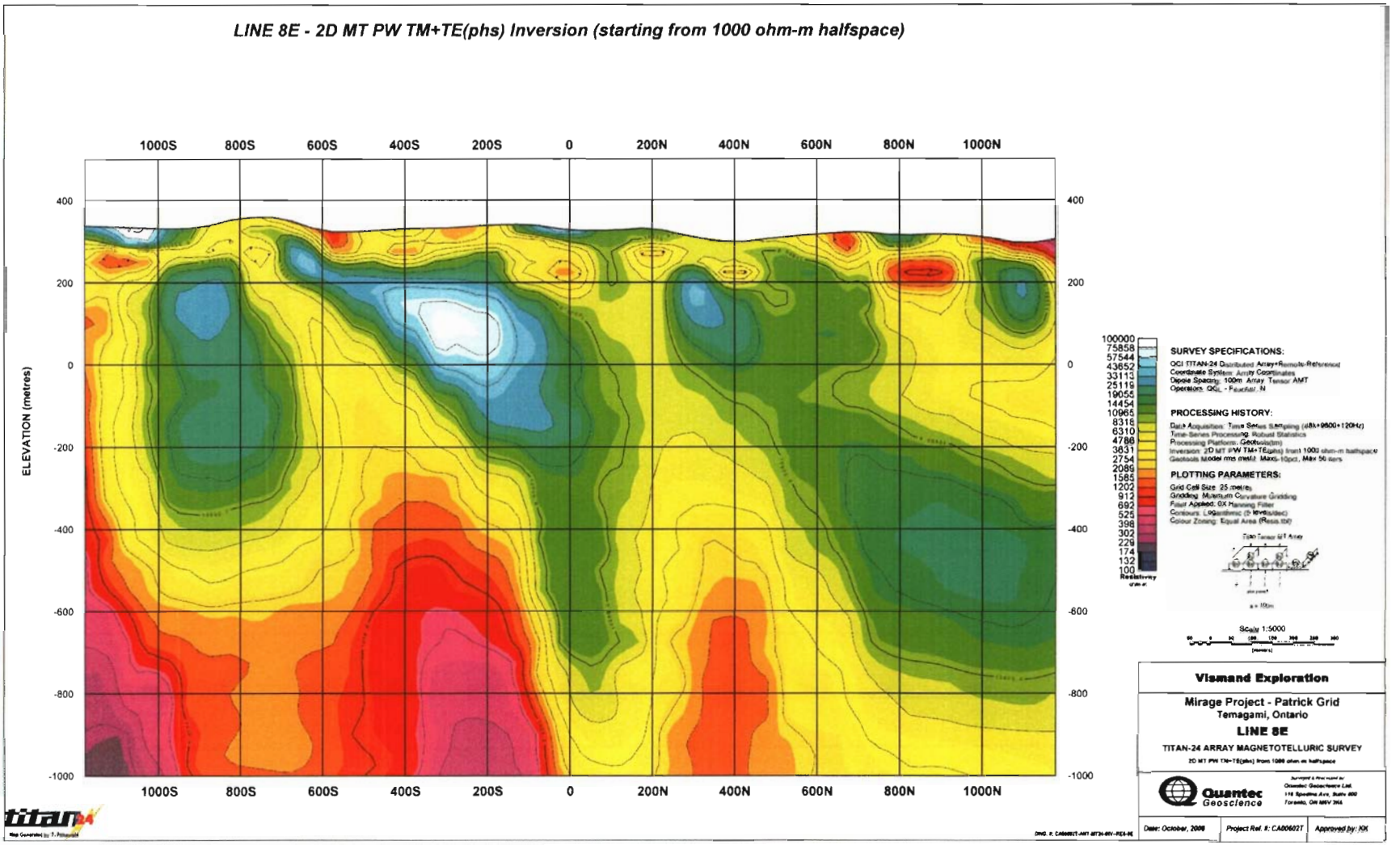

Line 800E – 2D MT PW TM+TE Inversion (starting from 1000 ohm-m halfspace)

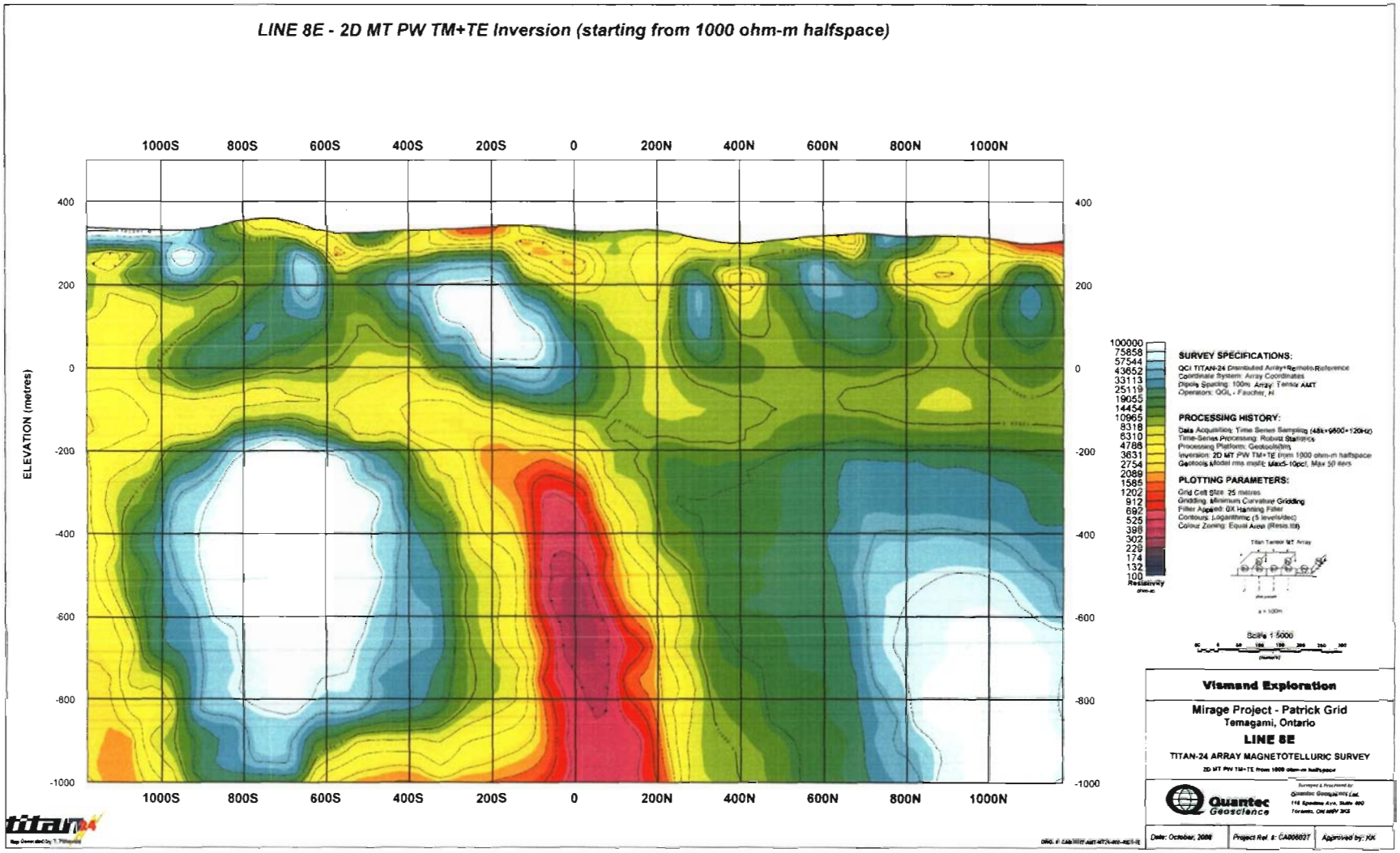

Line 800E – 2D MT RLM TM+TE(phs) Inversion (starting from 1D Det model)

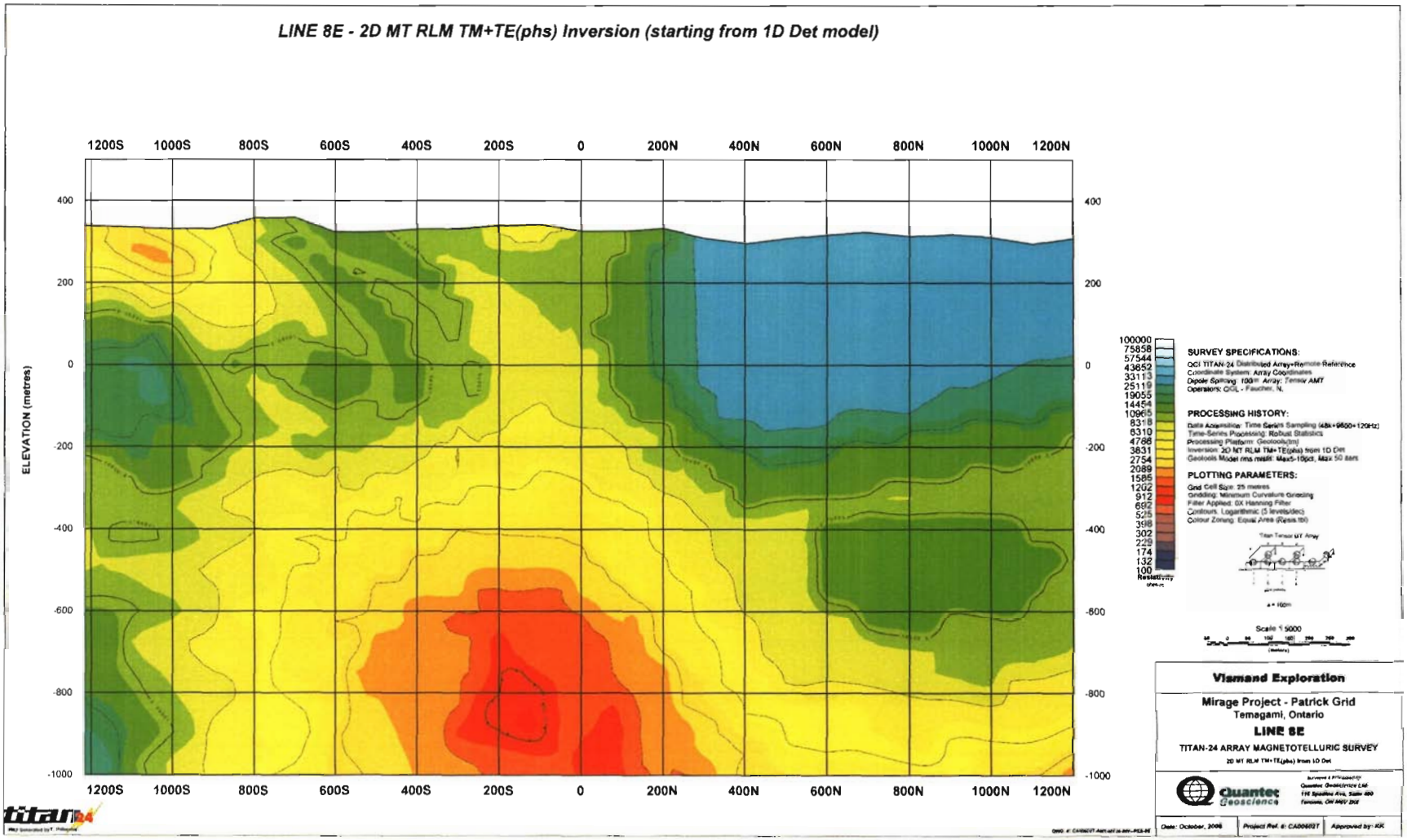

Line 800E – 2D MT RLM TM+TE Inversion (starting from 1D Det model)

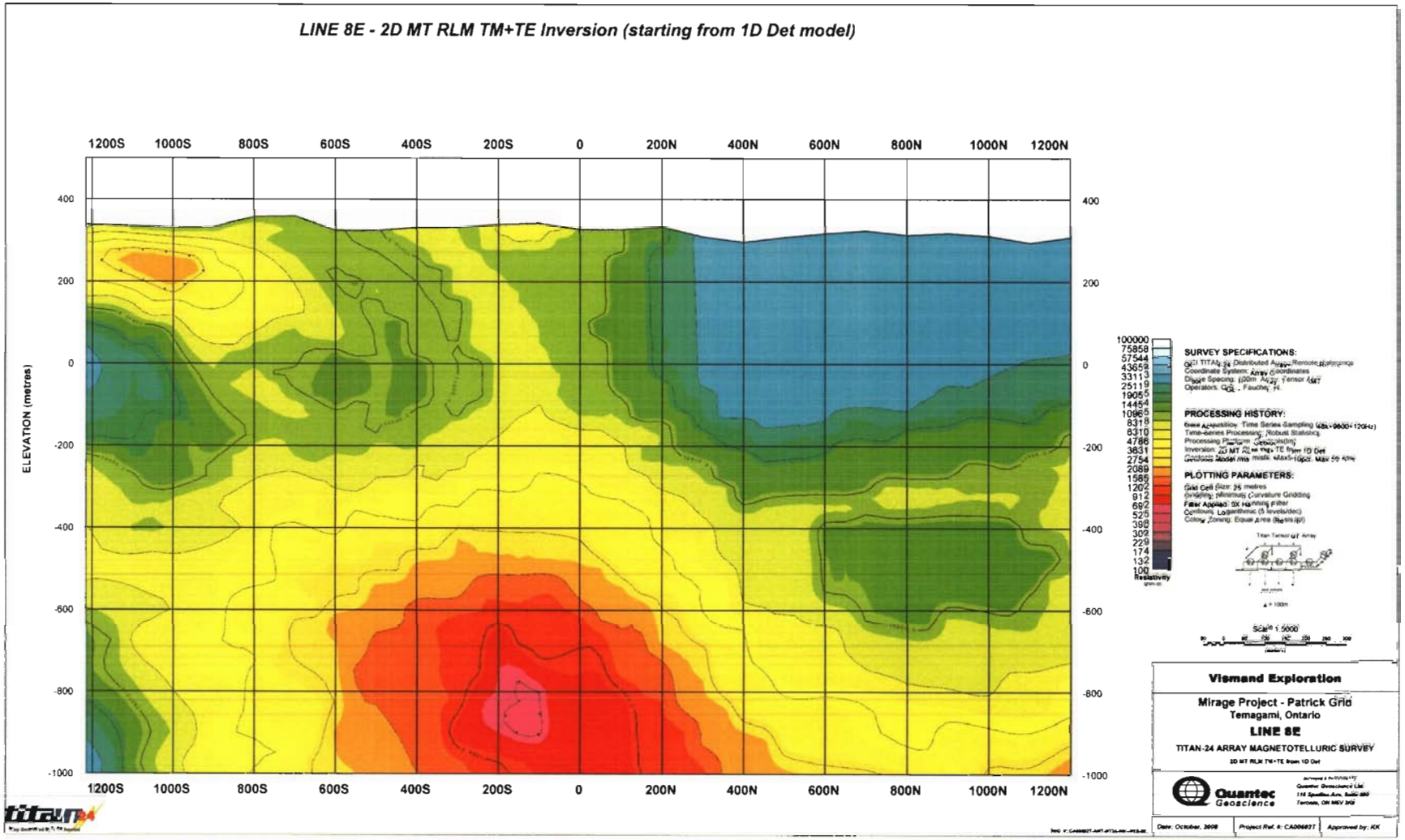

Line 800E – 2D MT RLM TM+TE(phs) Inversion (starting from 1000 ohm-m halfspace)

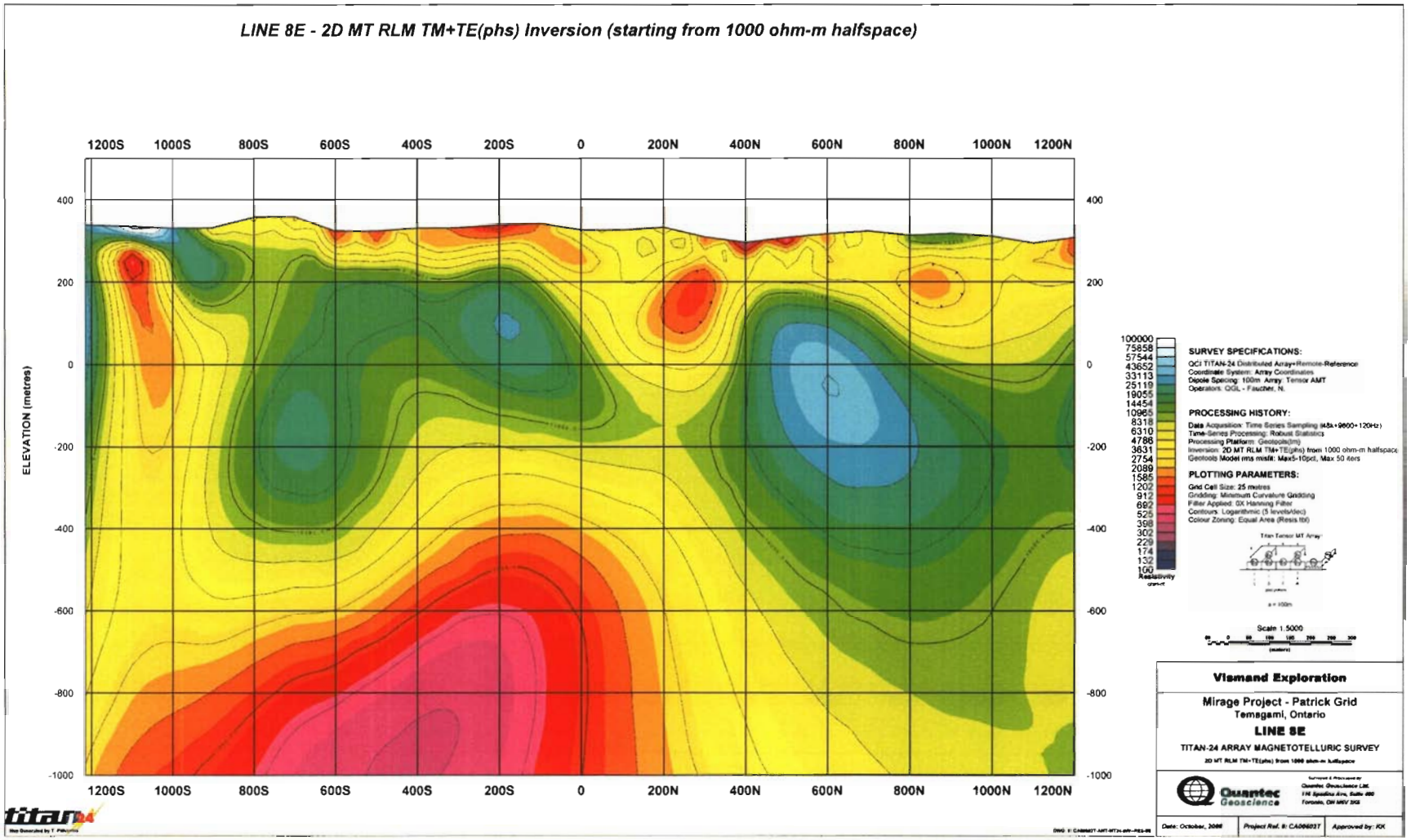

Line 800E – 2D MT RLM TM+TE Inversion (starting from 1000 ohm-m halfspace)

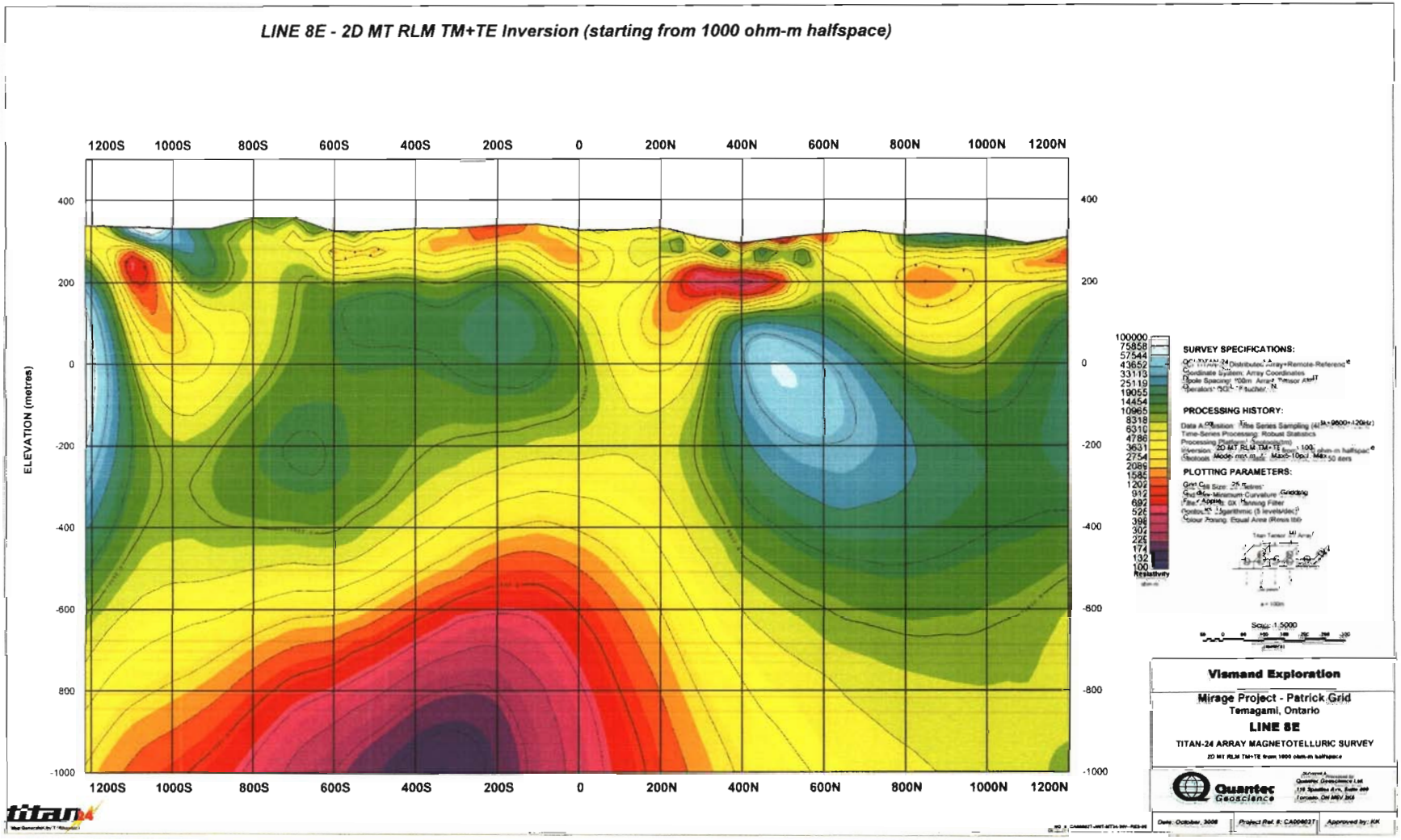

2D Resistivity (Z=50m) – 2D UBC Smooth DC Resistivity Model

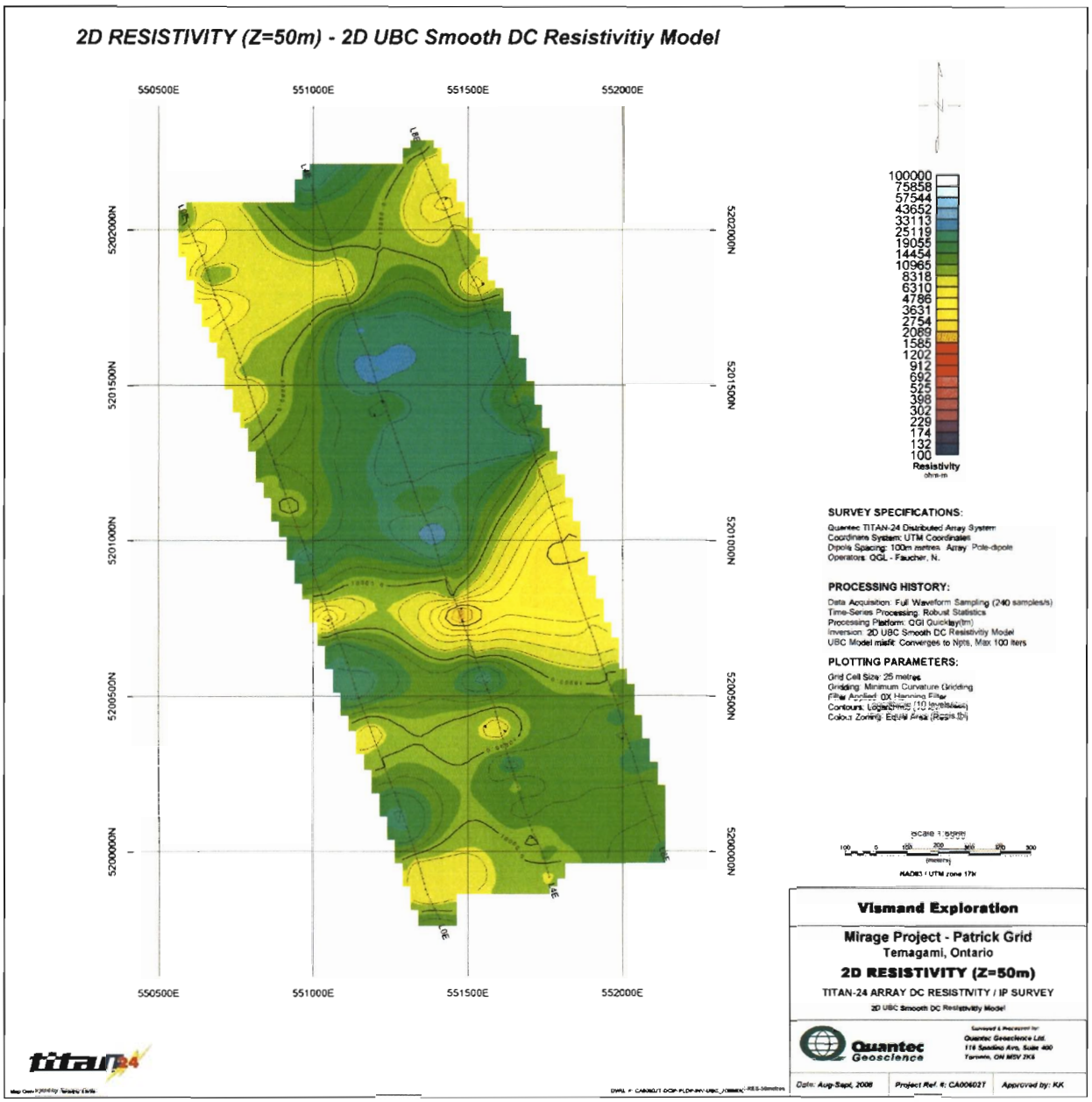

2D Resistivity (Z=100m) – 2D UBC Smooth DC Resistivity Model

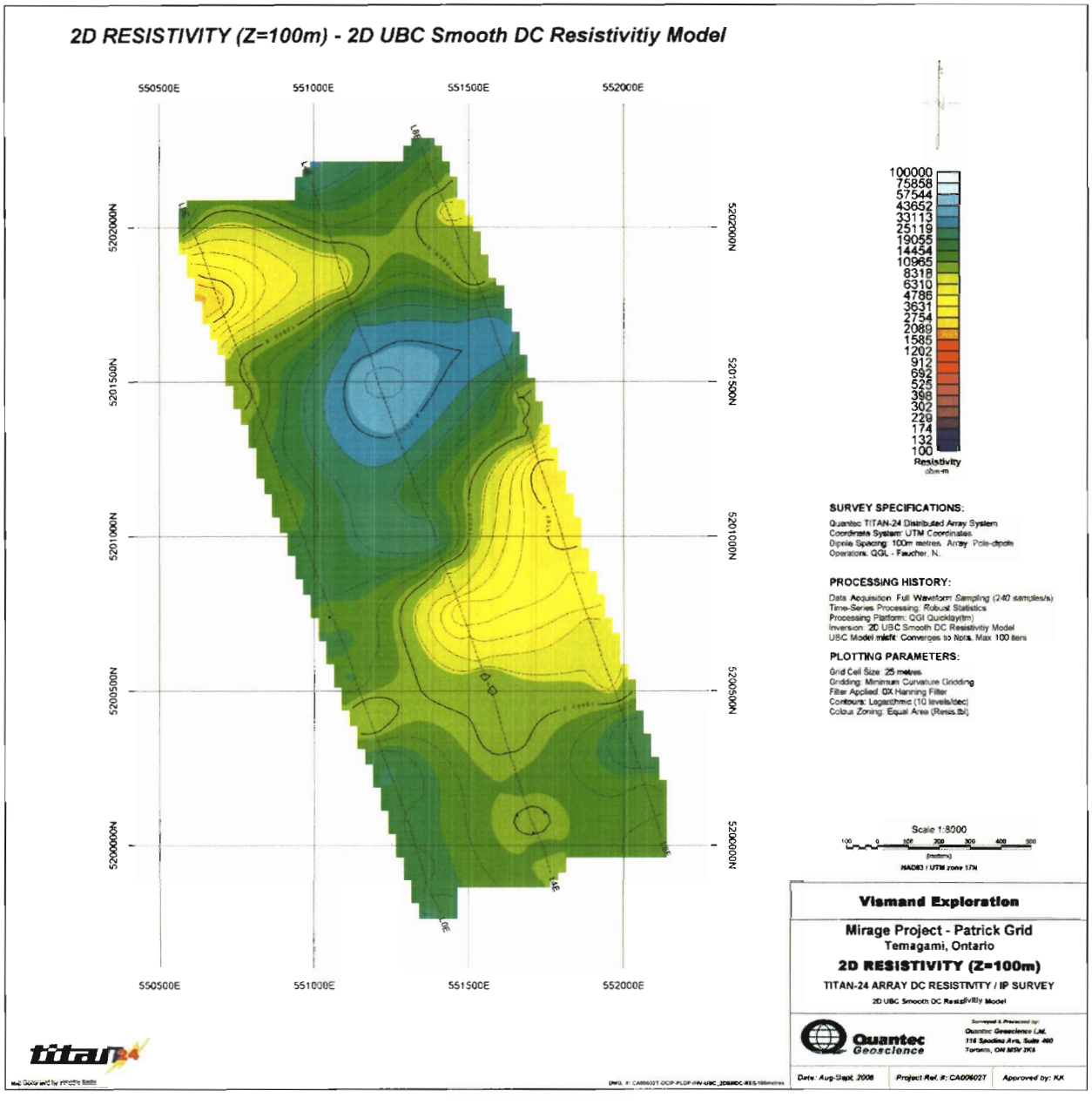

2D Resistivity (Z=200m) – 2D UBC Smooth DC Resistivity Model

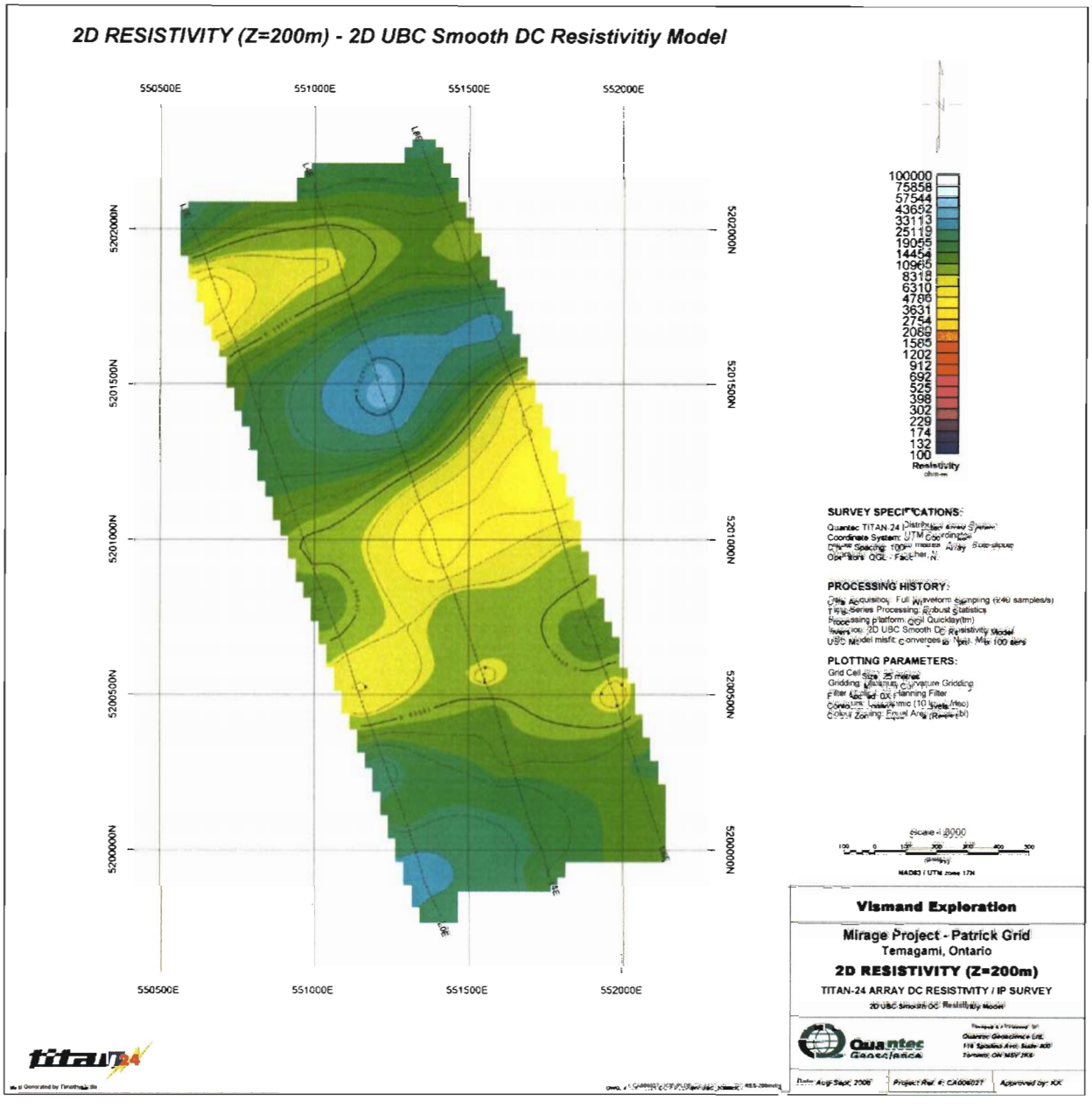

2D Resistivity (Z=400m) – 2D UBC Smooth DC Resistivity Model

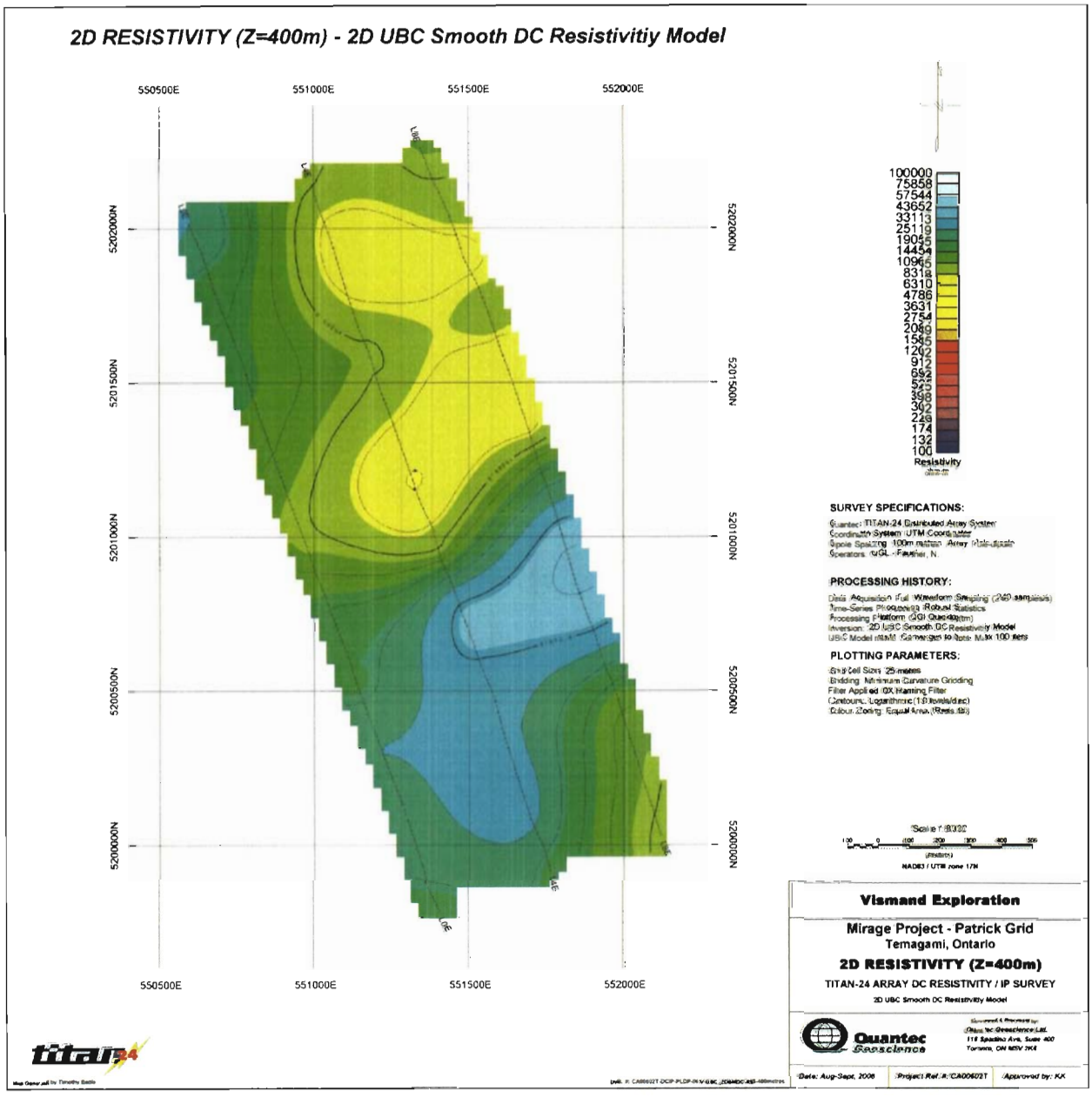

2D Chargeability (Z=50m) – 2D UBC Smooth IP Chargeability Model

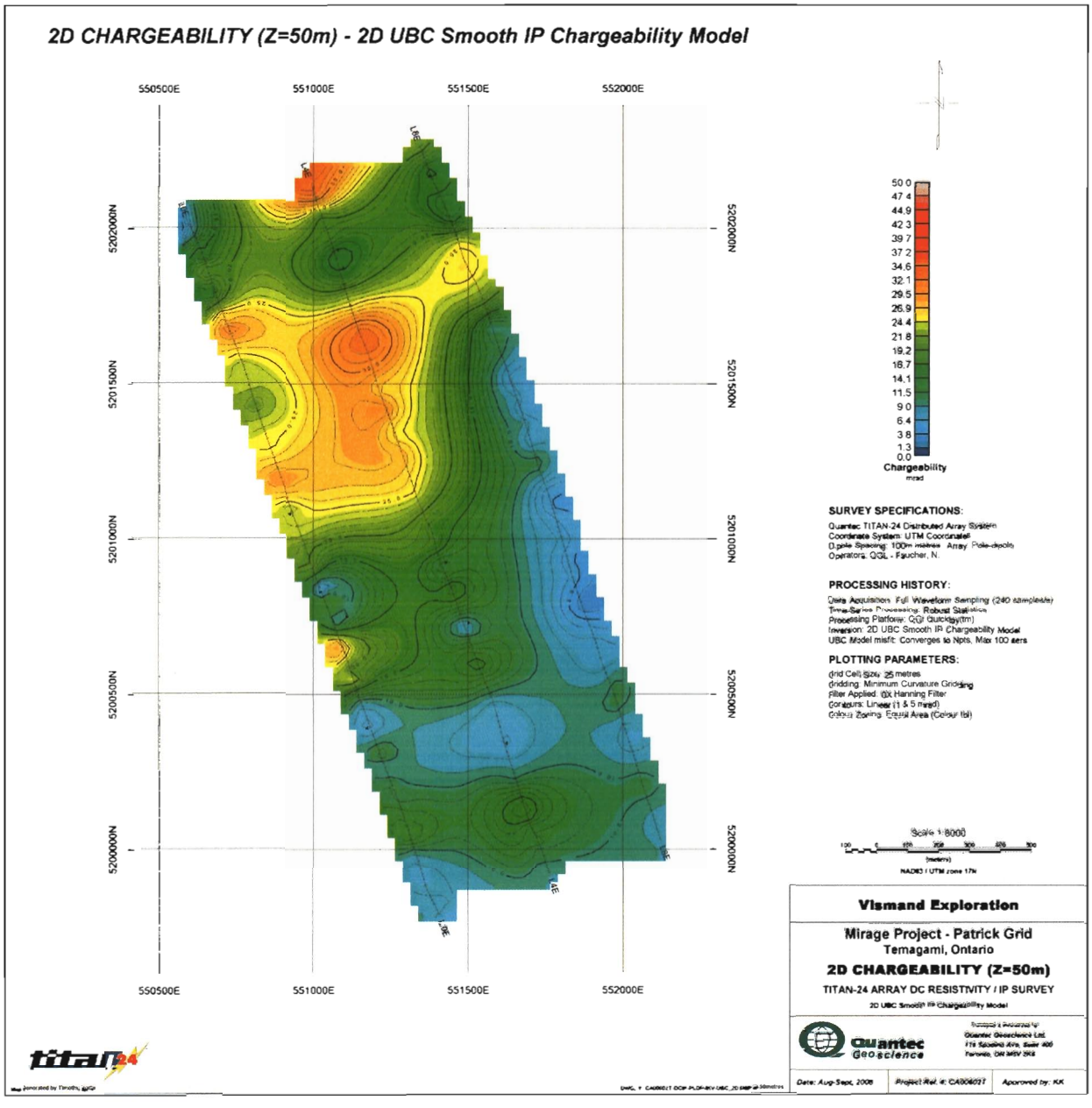

2D Chargeability (Z=100m) – 2D UBC Smooth IP Chargeability Model

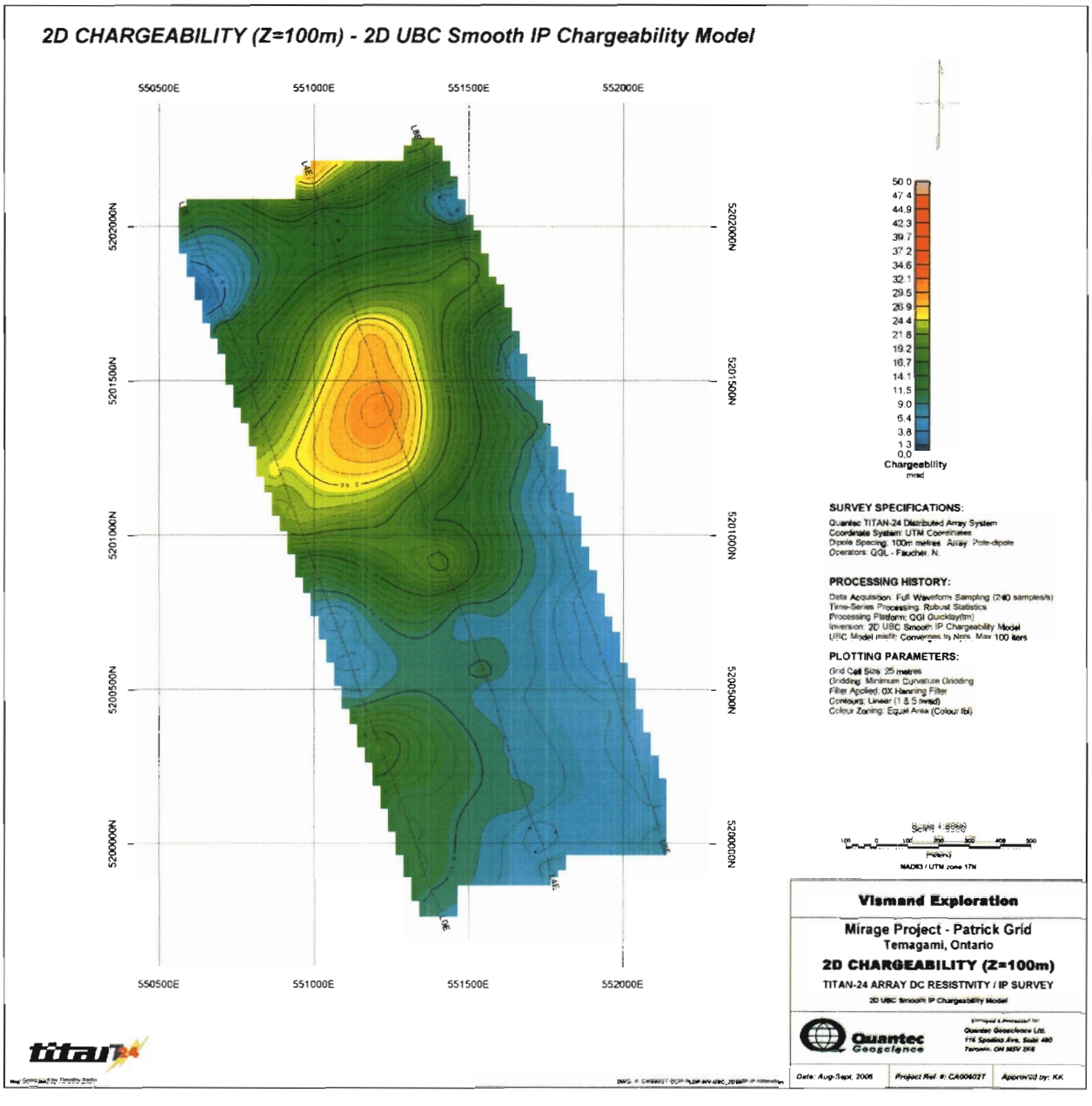

2D Chargeability (Z=200m) – 2D UBC Smooth IP Chargeability Model

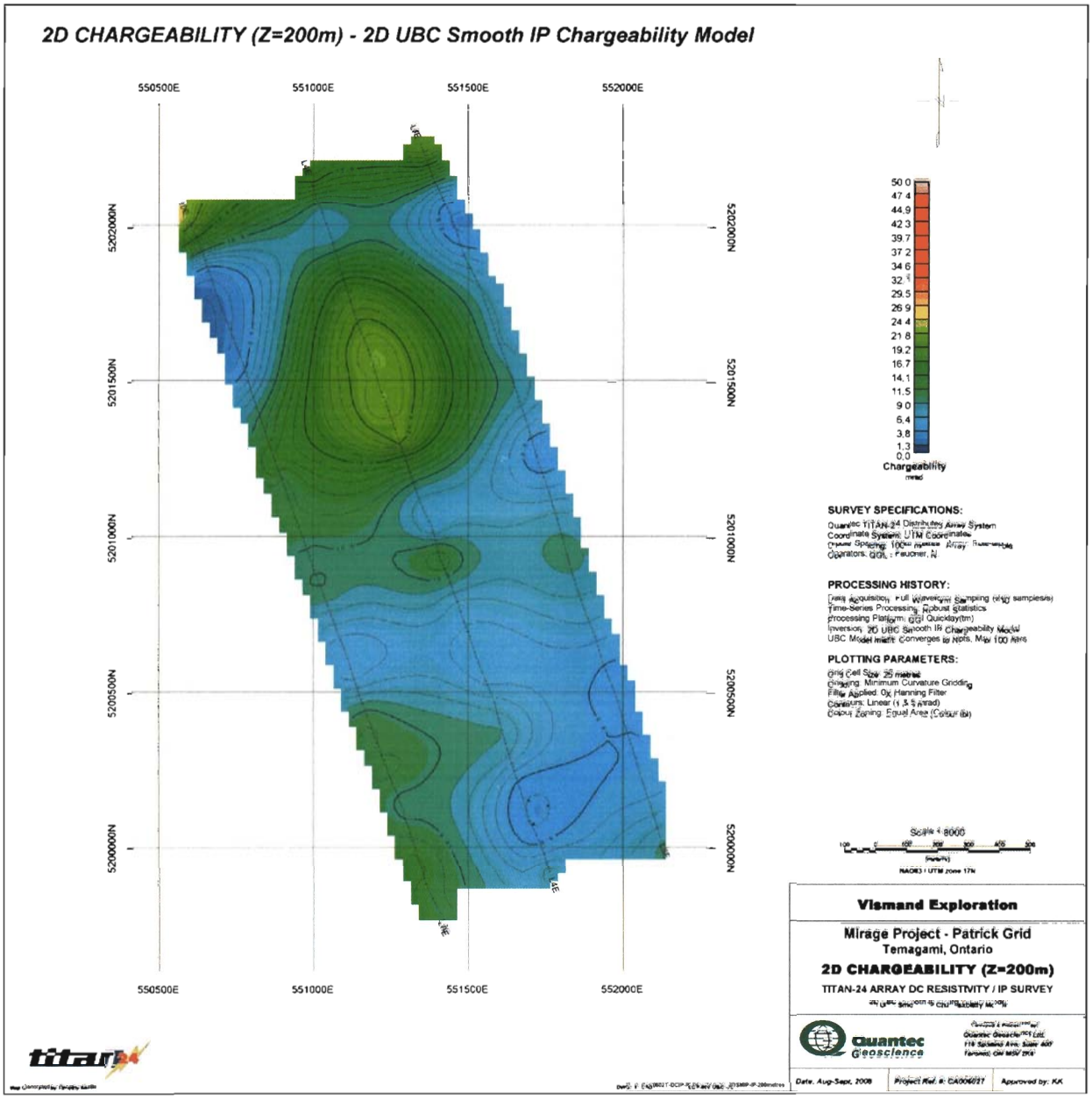

2D Chargeability (Z=400m) – 2D UBC Smooth IP Chargeability Model

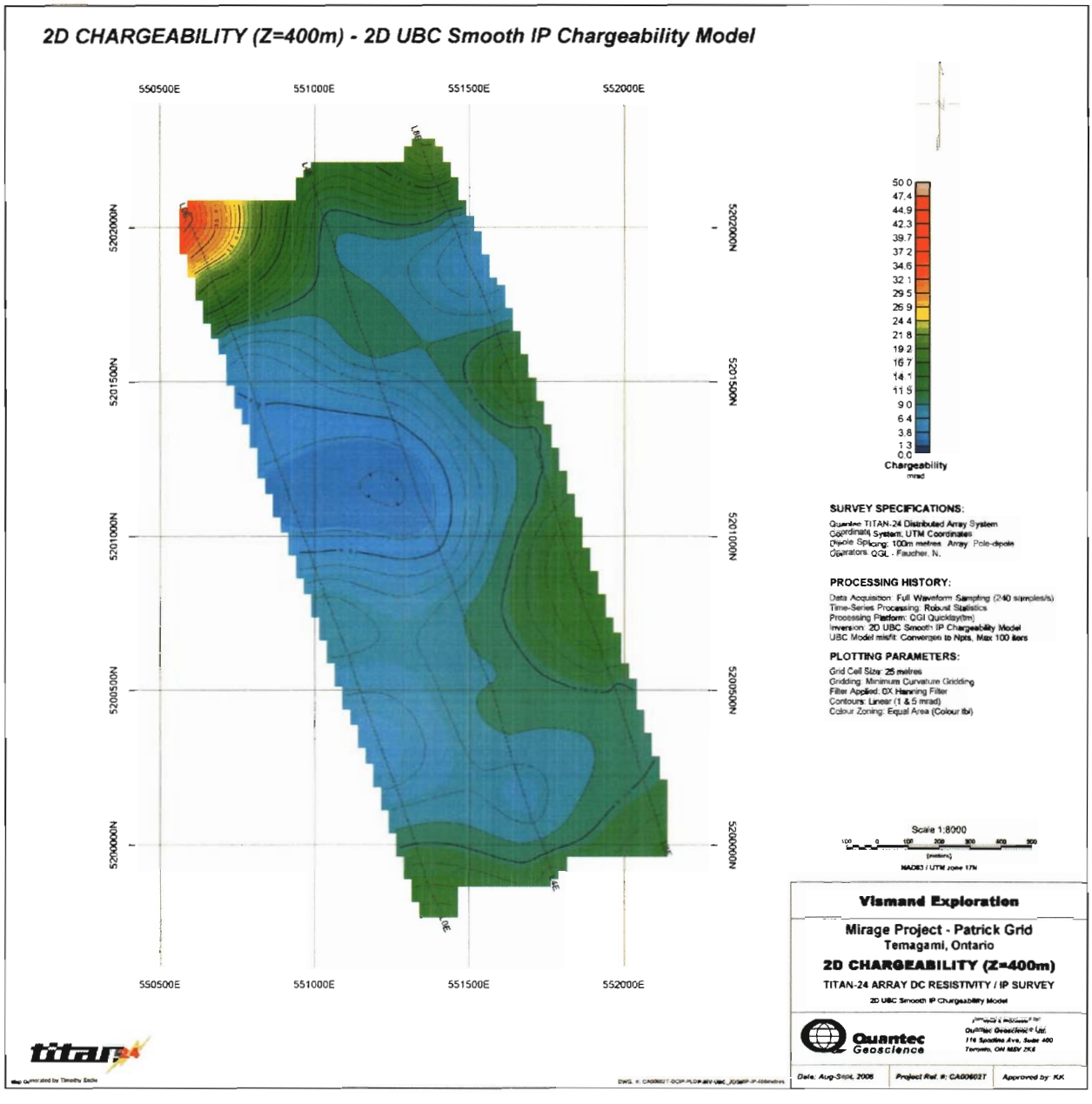

2D Chargeability (Z=50m) – 2D UBC Null Con IP Chargeability Model

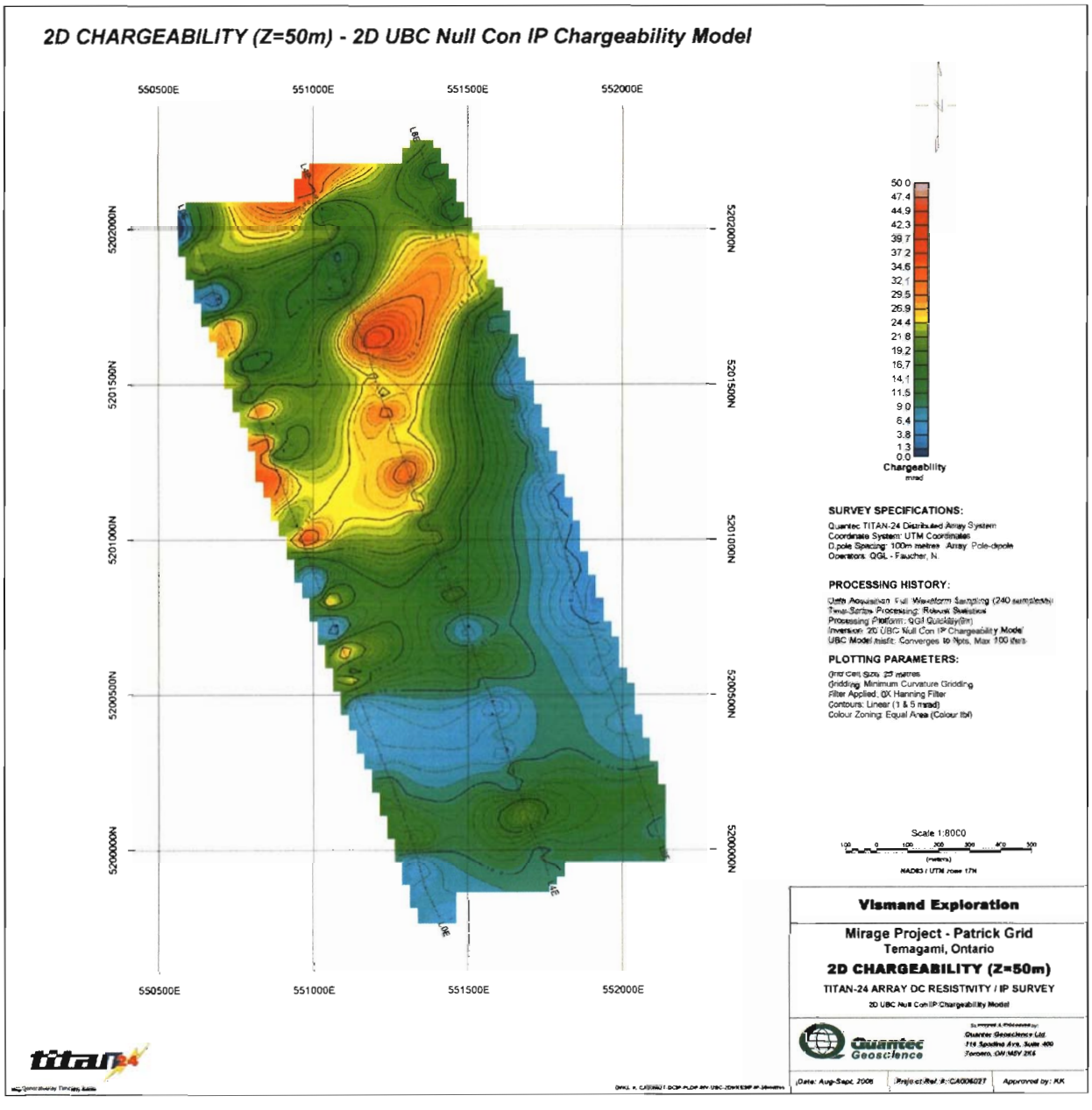

2D Chargeability (Z=100m) – 2D UBC Null Con IP Chargeability Model

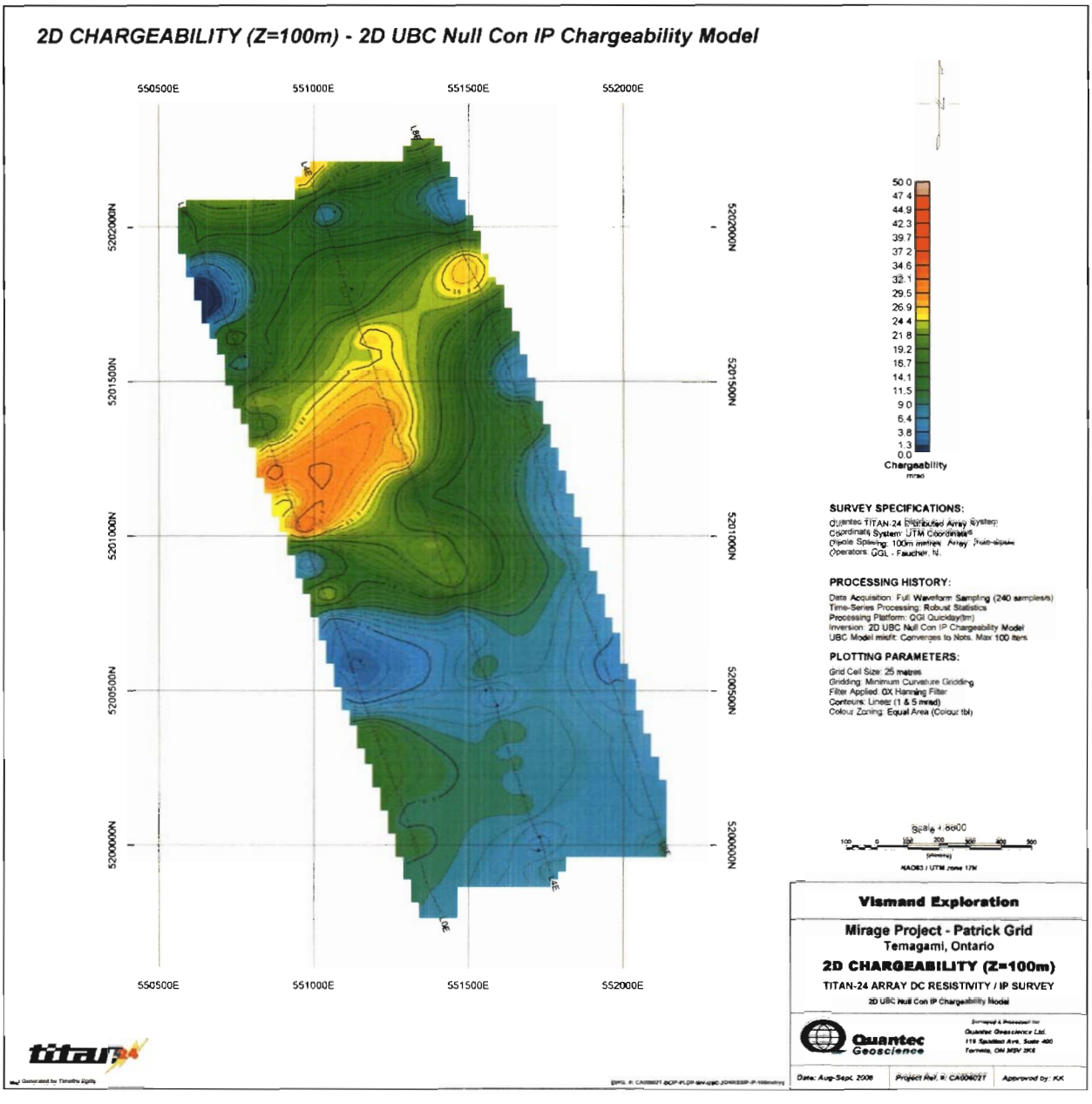

2D Chargeability (Z=200m) – 2D UBC Null Con IP Chargeability Model

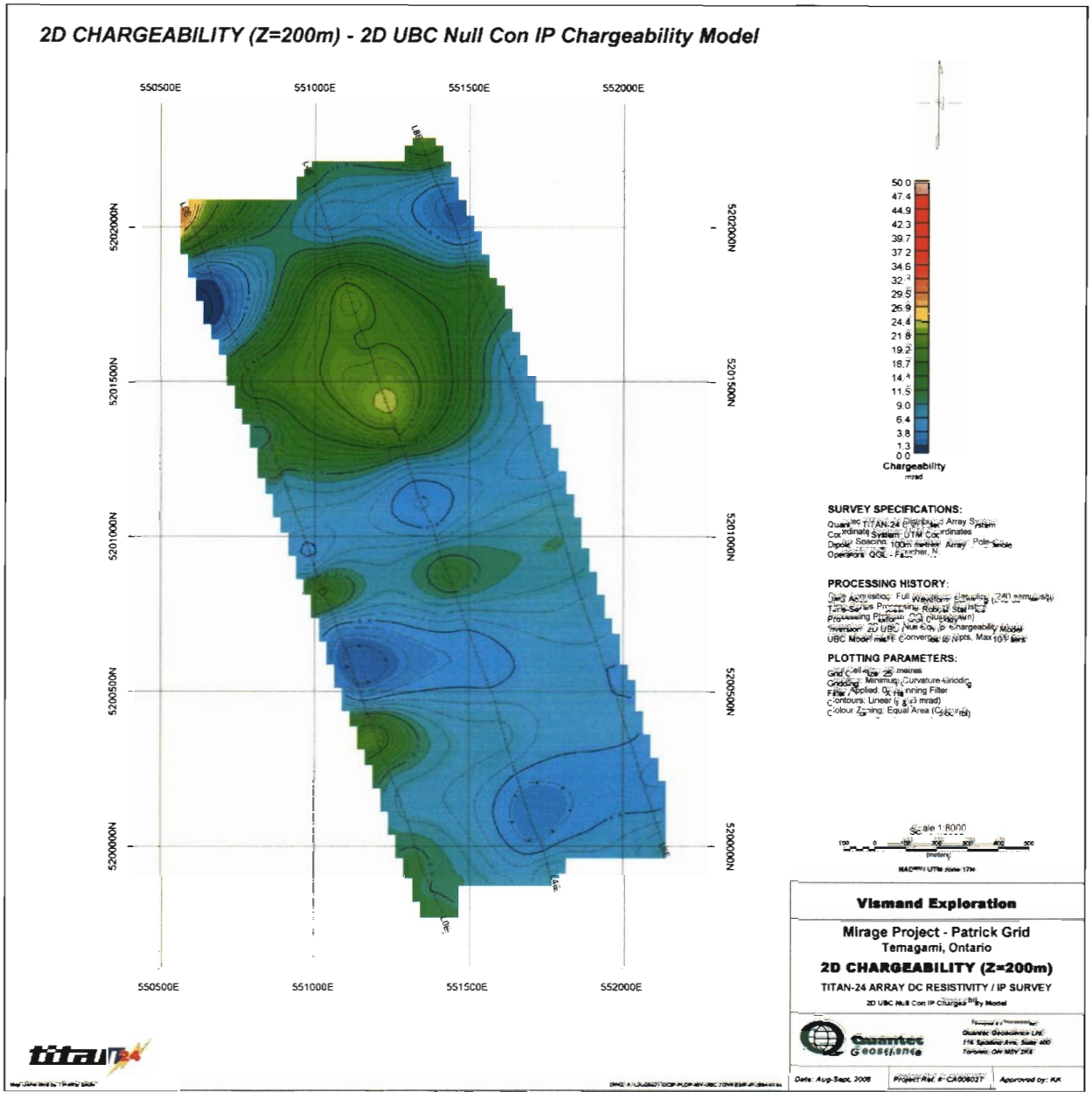

2D Chargeability (Z=400m) – 2D UBC Null Con IP Chargeability Model

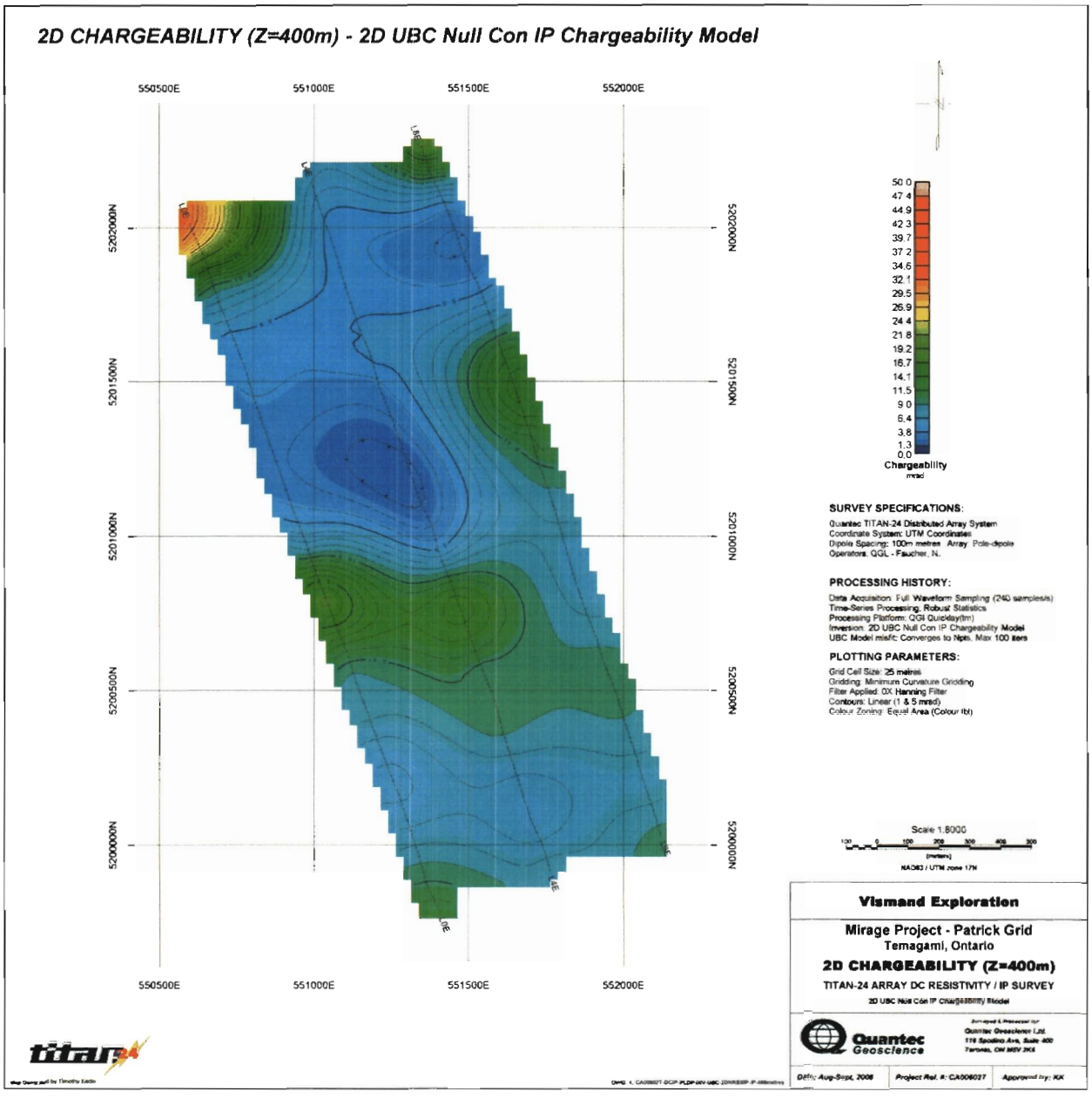

2D Resistivity (Z=50m) – 2D MT PW TM+TE(phs) Inversion (starting from 1000 ohm-m halfspace)

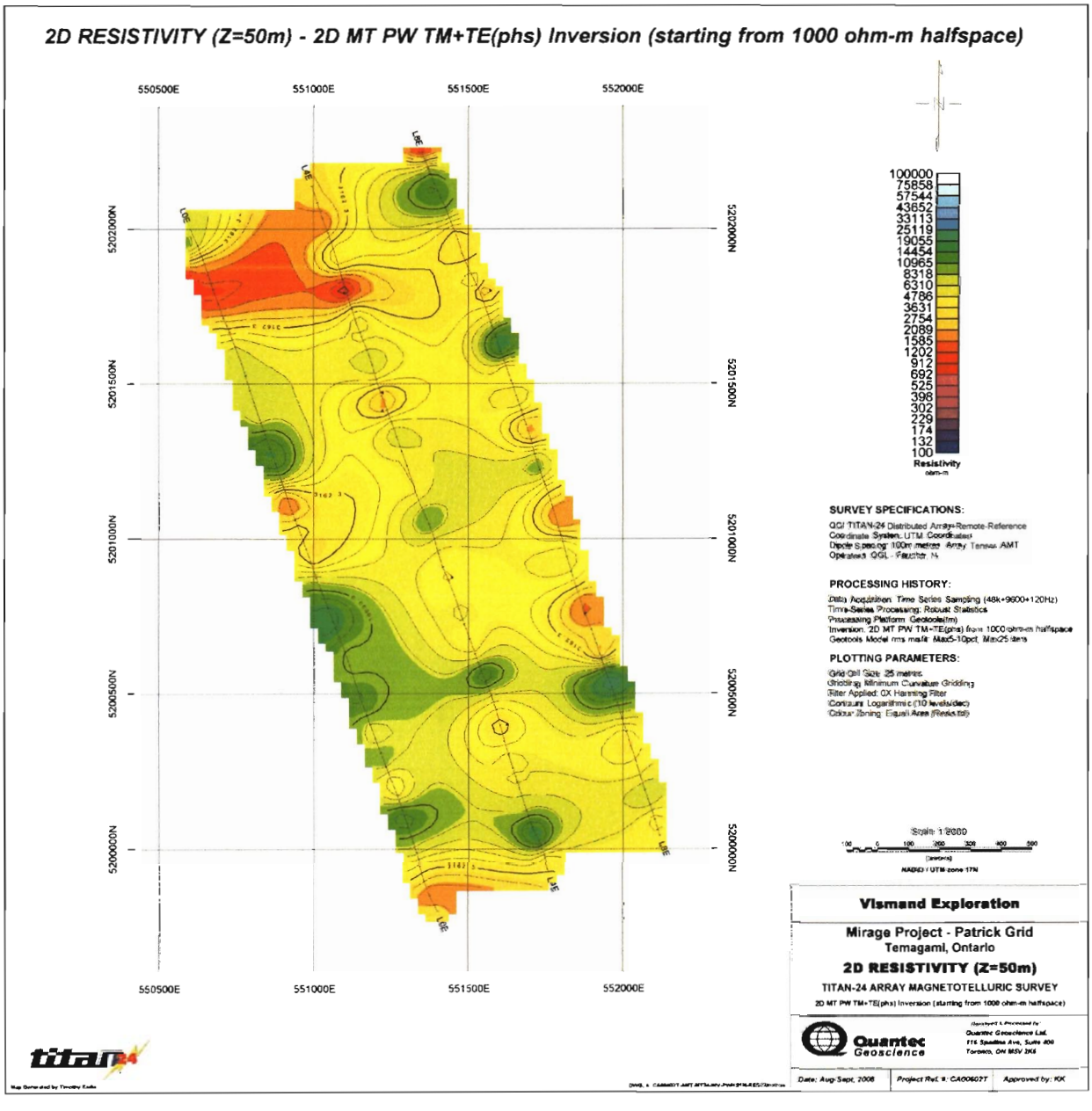

2D Resistivity (Z=100m) – 2D MT PW TM+TE(phs) Inversion (starting from 1000 ohm-m halfspace)

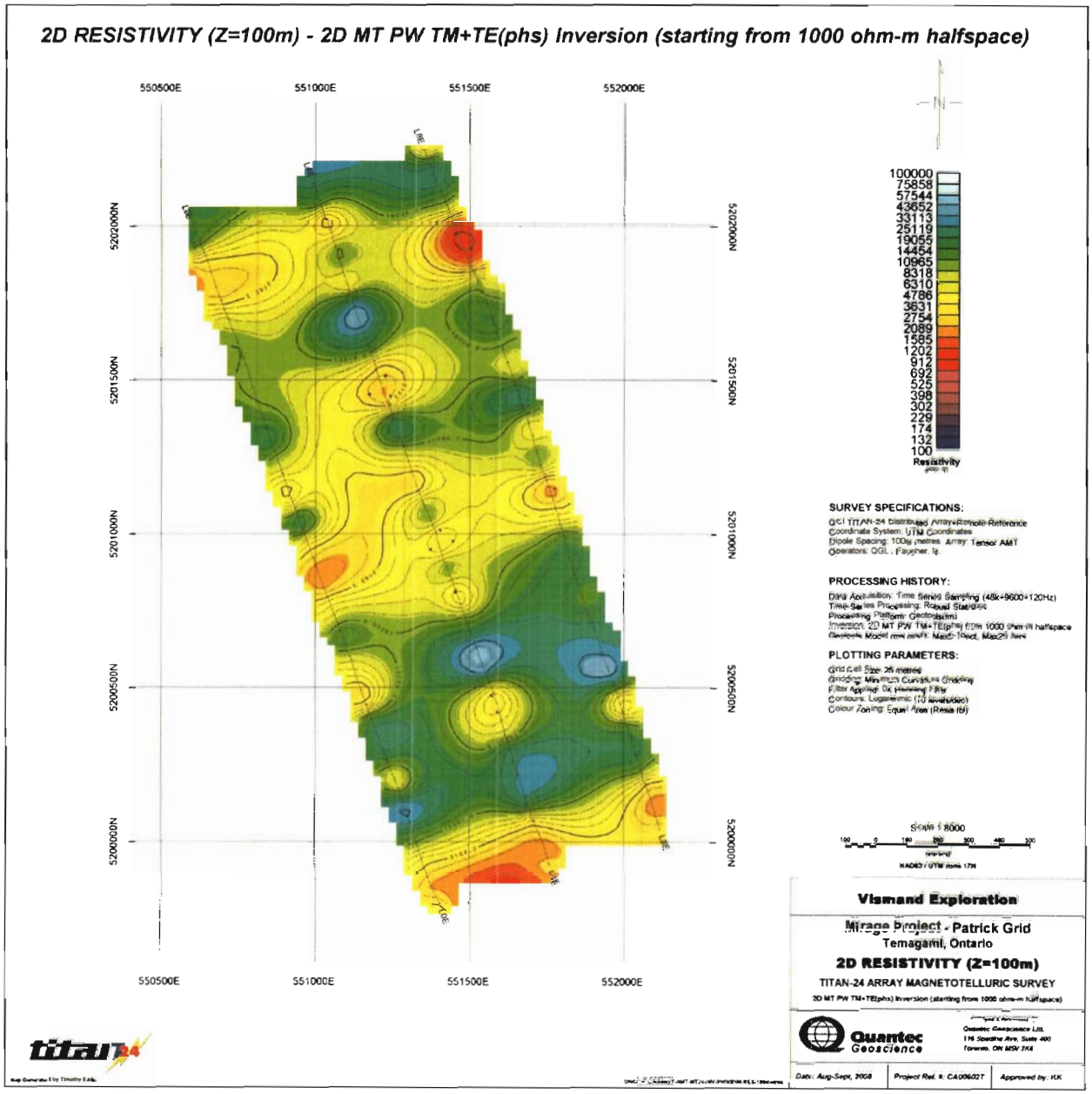

2D Resistivity (Z=200m) – 2D MT PW TM+TE(phs) Inversion (starting from 1000 ohm-m halfspace)

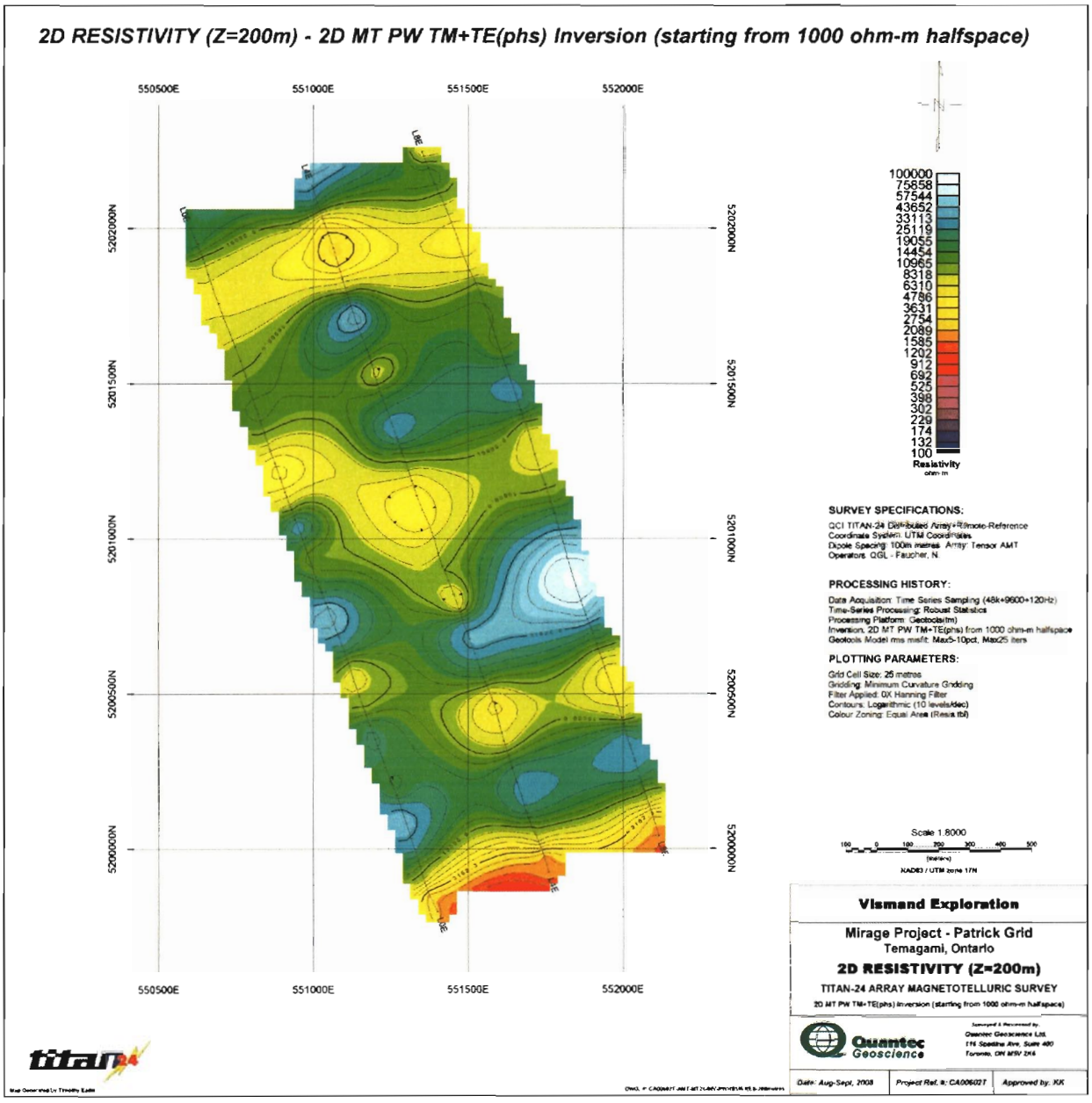

2D Resistivity (Z=400m) – 2D MT PW TM+TE(phs) Inversion (starting from 1000 ohm-m halfspace)

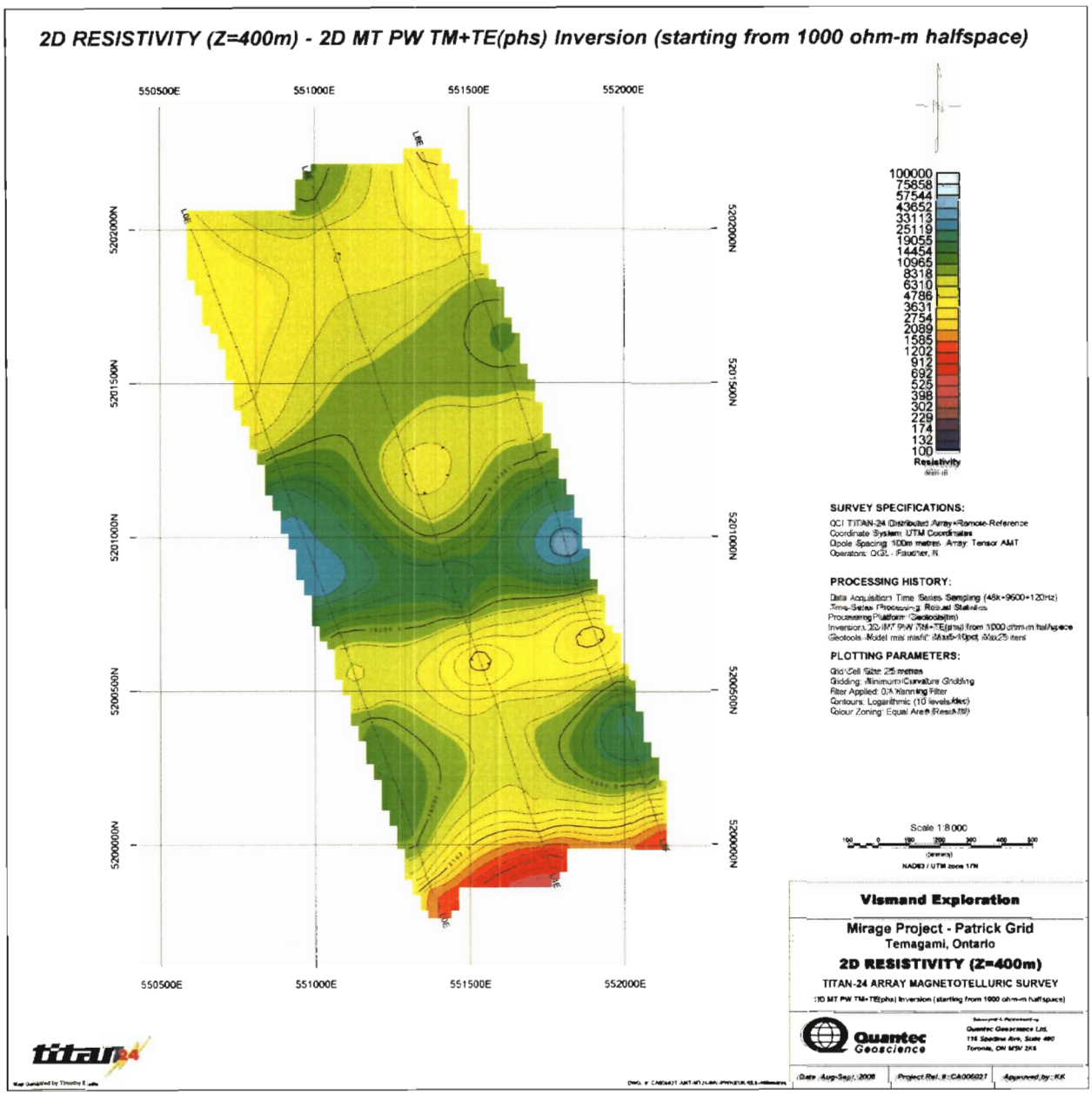

2D Resistivity (Z=1000m) – 2D MT PW TM+TE(phs) Inversion (starting from 1000 ohm-m halfspace)

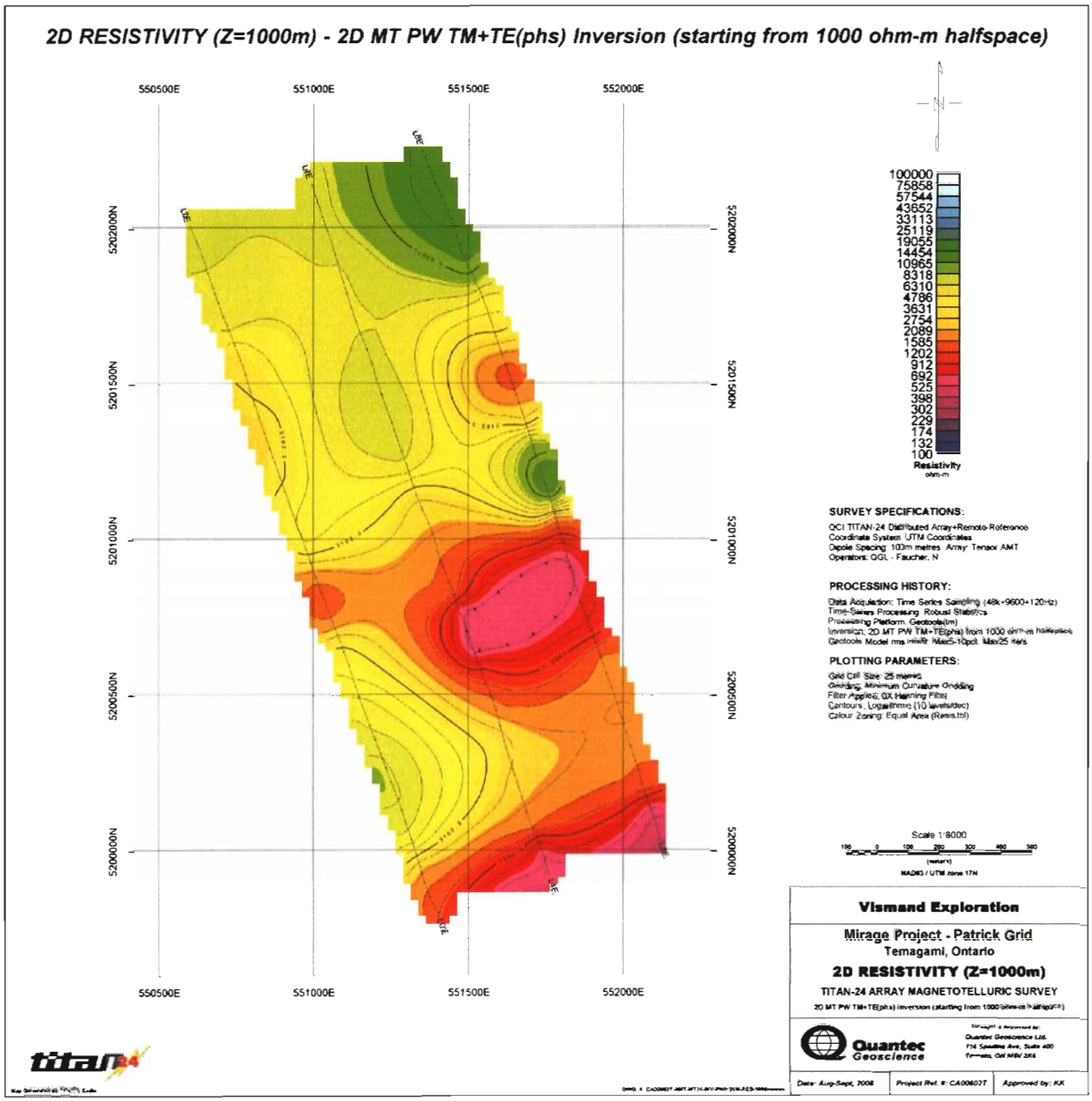

Sudnip Grid

Line 0N – 2D UBC Smooth DC Resistivity Model

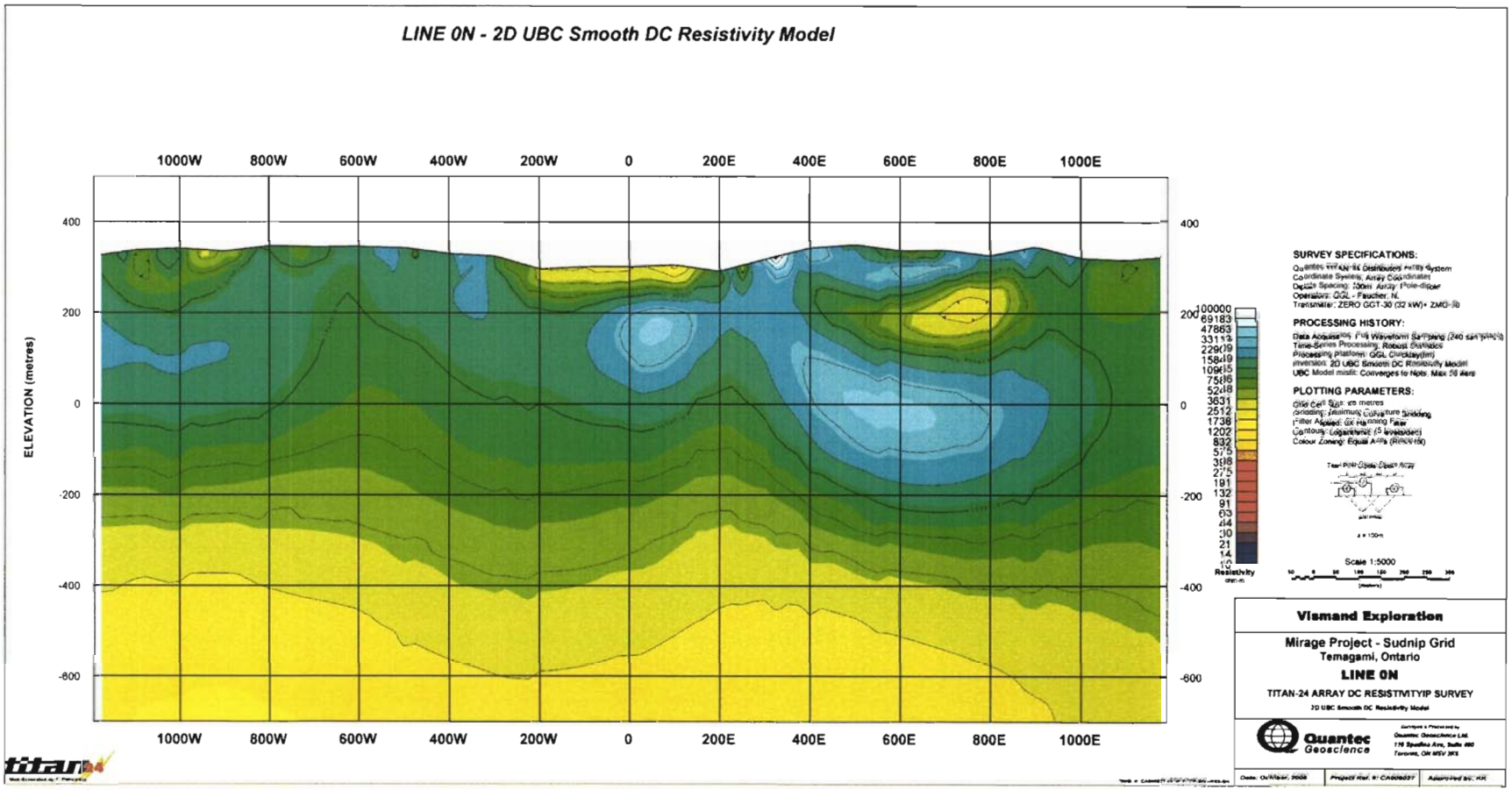

Line 0N – 2D UBC Smooth IP Chargeability Model

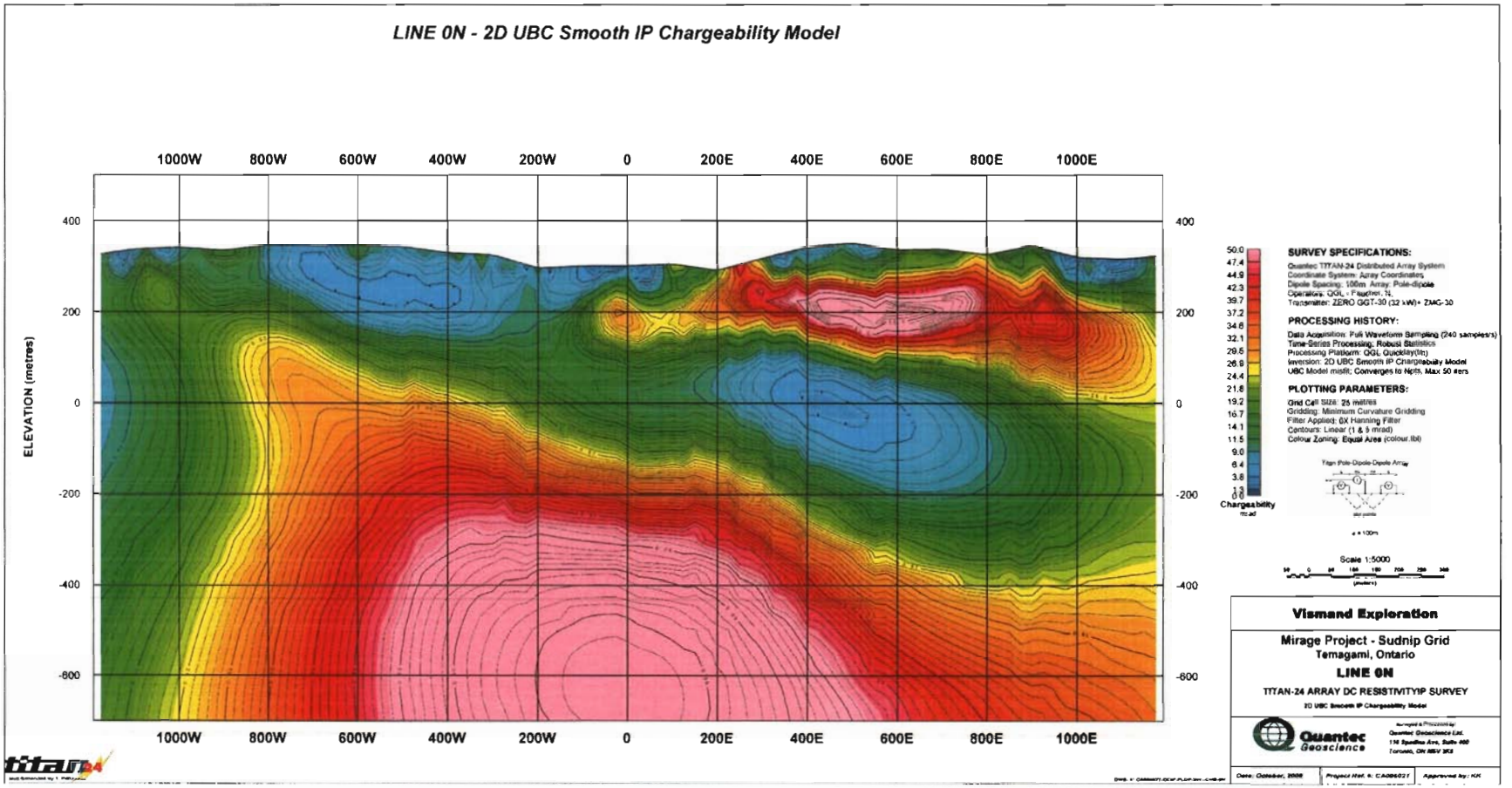

Line 0N – 2D UBC Null Con IP Chargeability Model

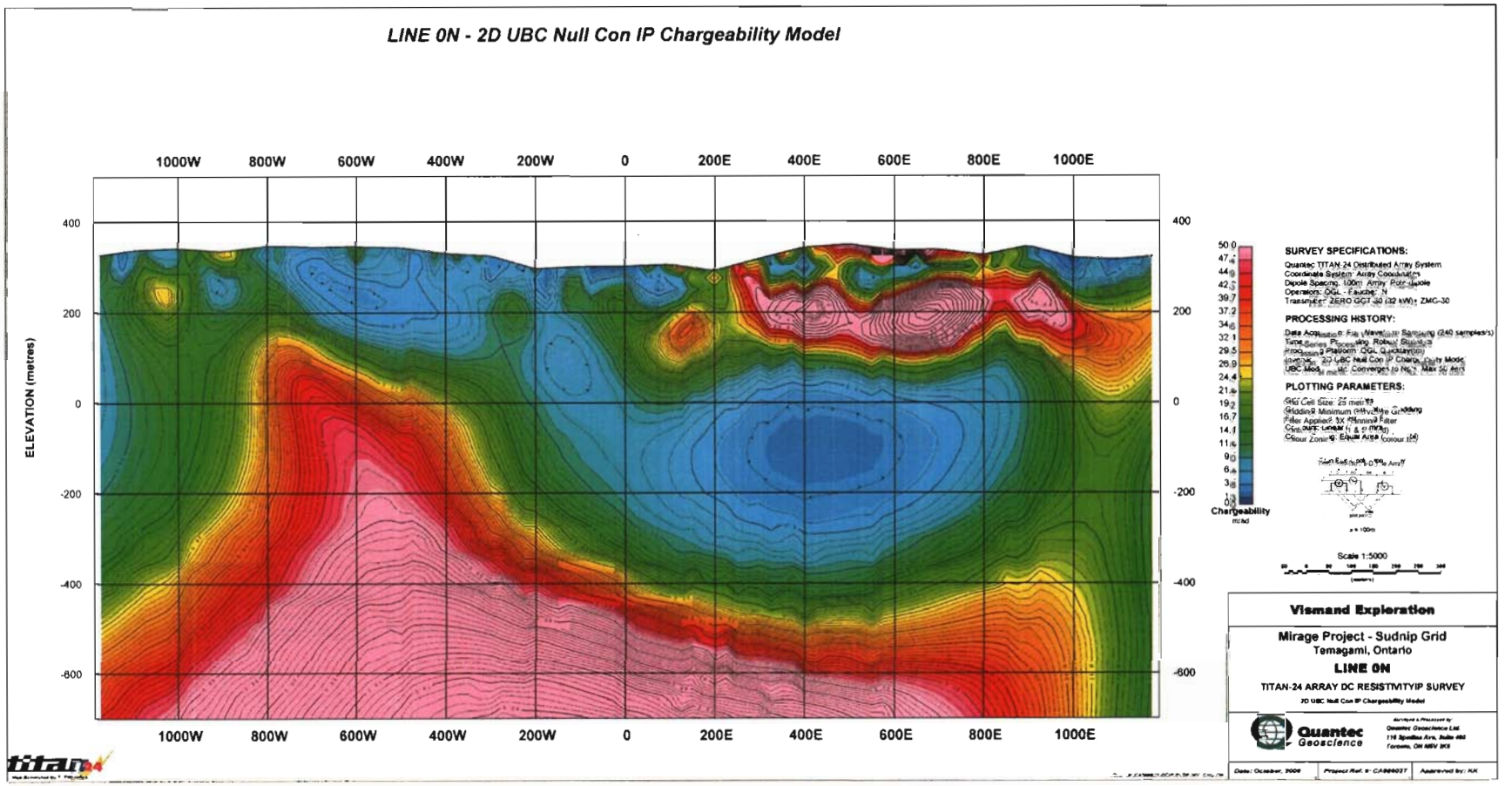

Line 0N – 2D MT PW TM+TE(phs) Sharp Inversion (starting from smooth 1D PW model)

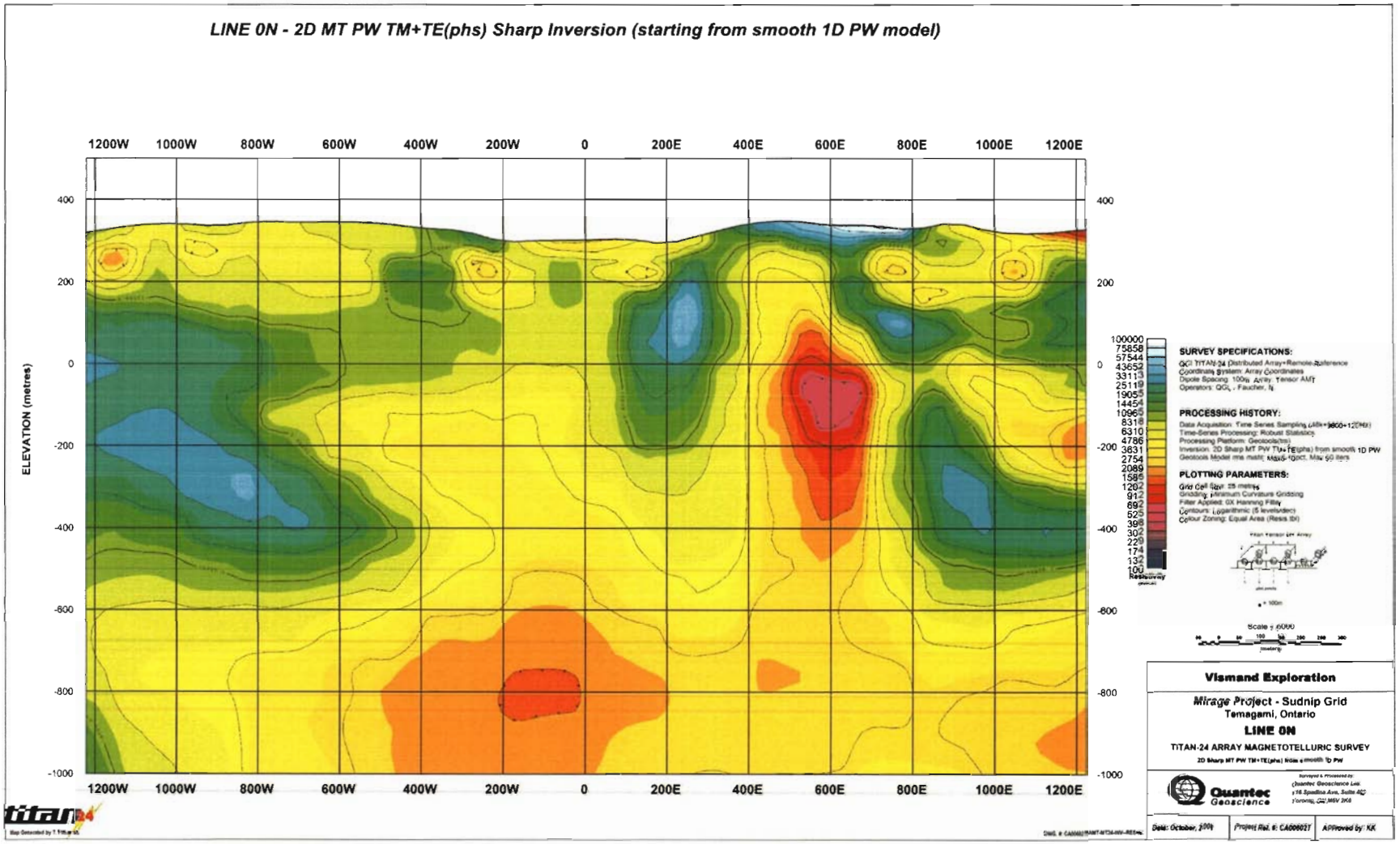

Line 0N – 2D MT PW TM+TE Sharp Inversion (starting from smooth 1D PW model)

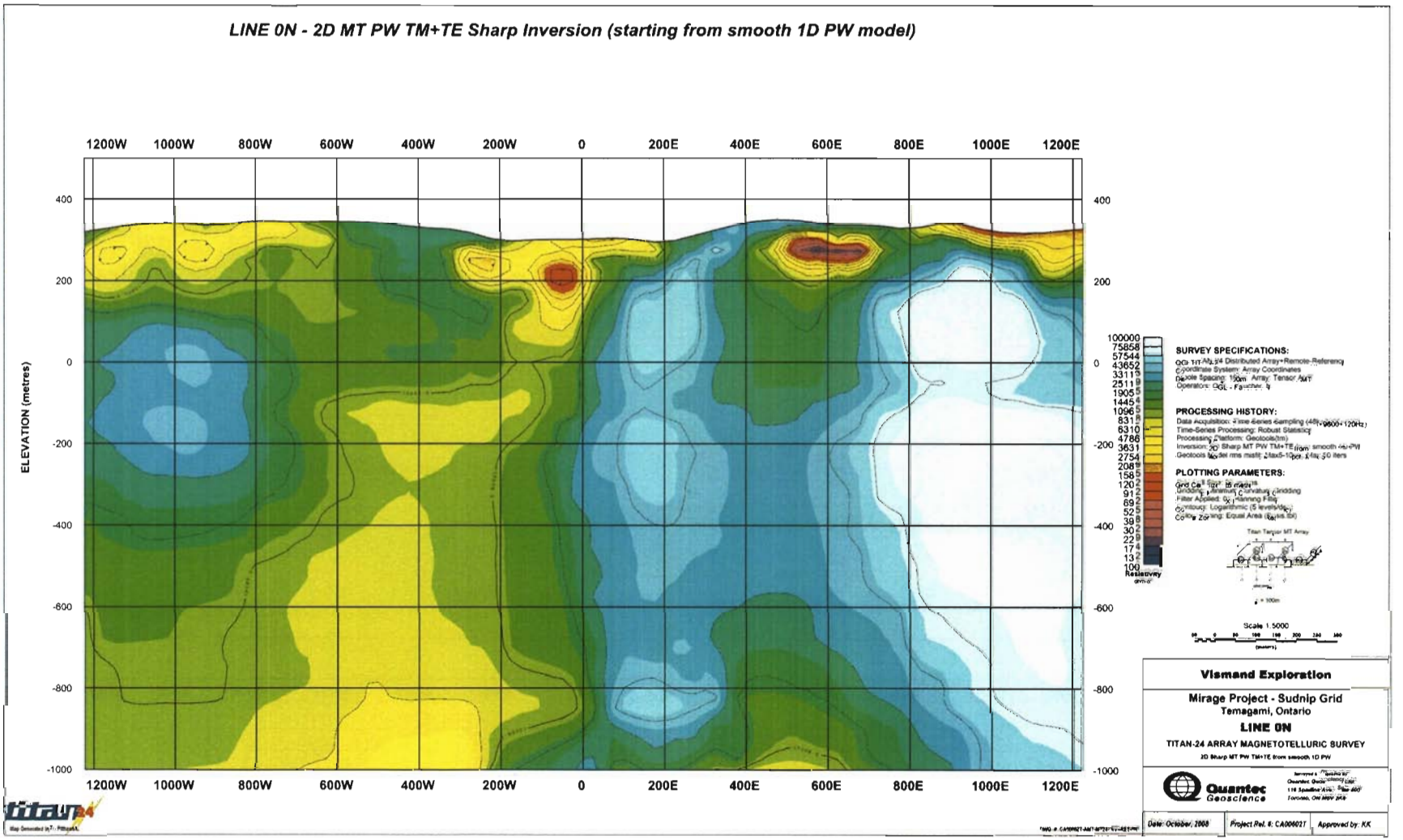

Line 0N – 2D MT PW TM+TE(phs) Inversion (starting from 1000 ohm-m halfspace)

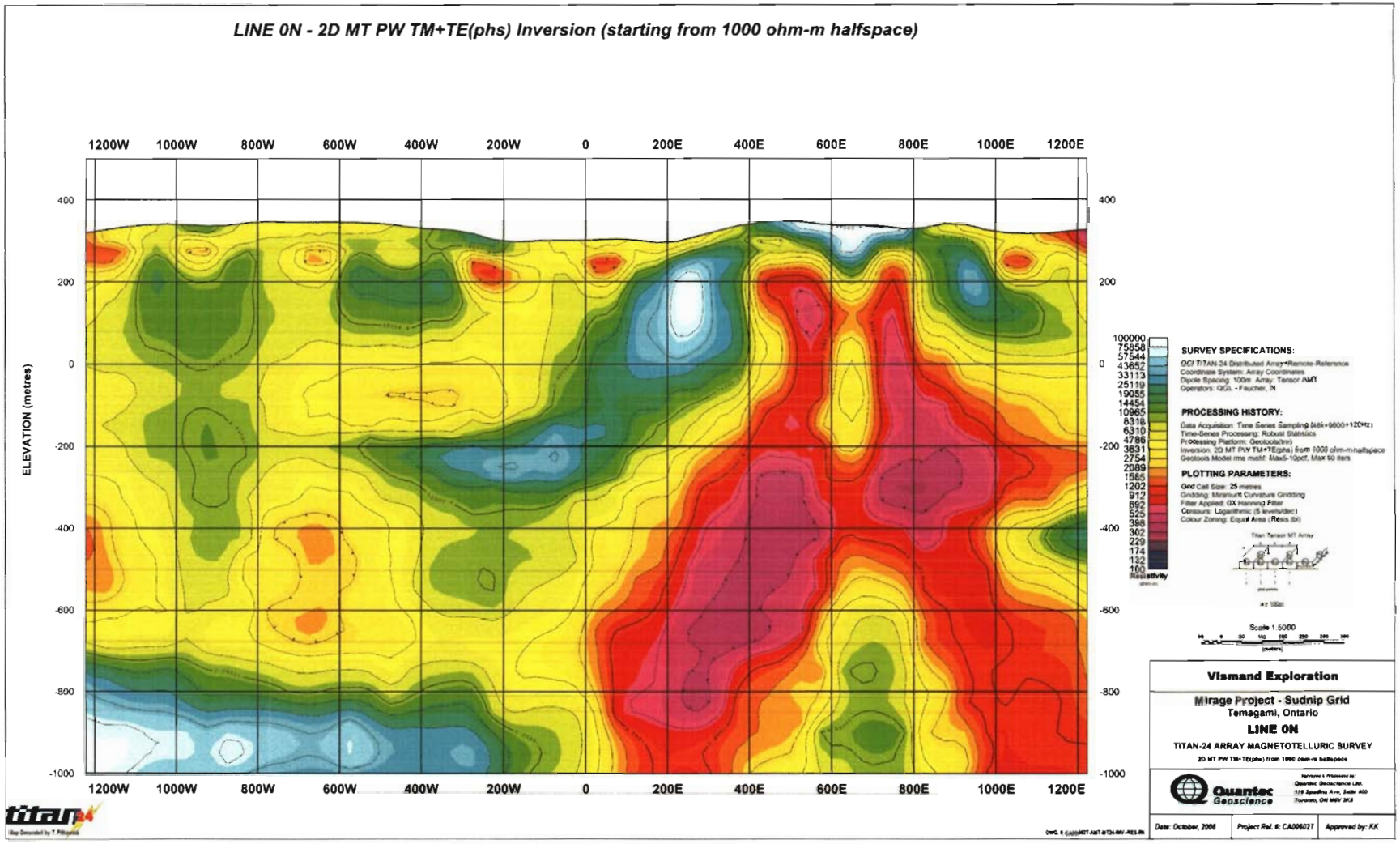

Line 0N – 2D MT PW TM+TE Inversion (starting from 1000 ohm-m halfspace)

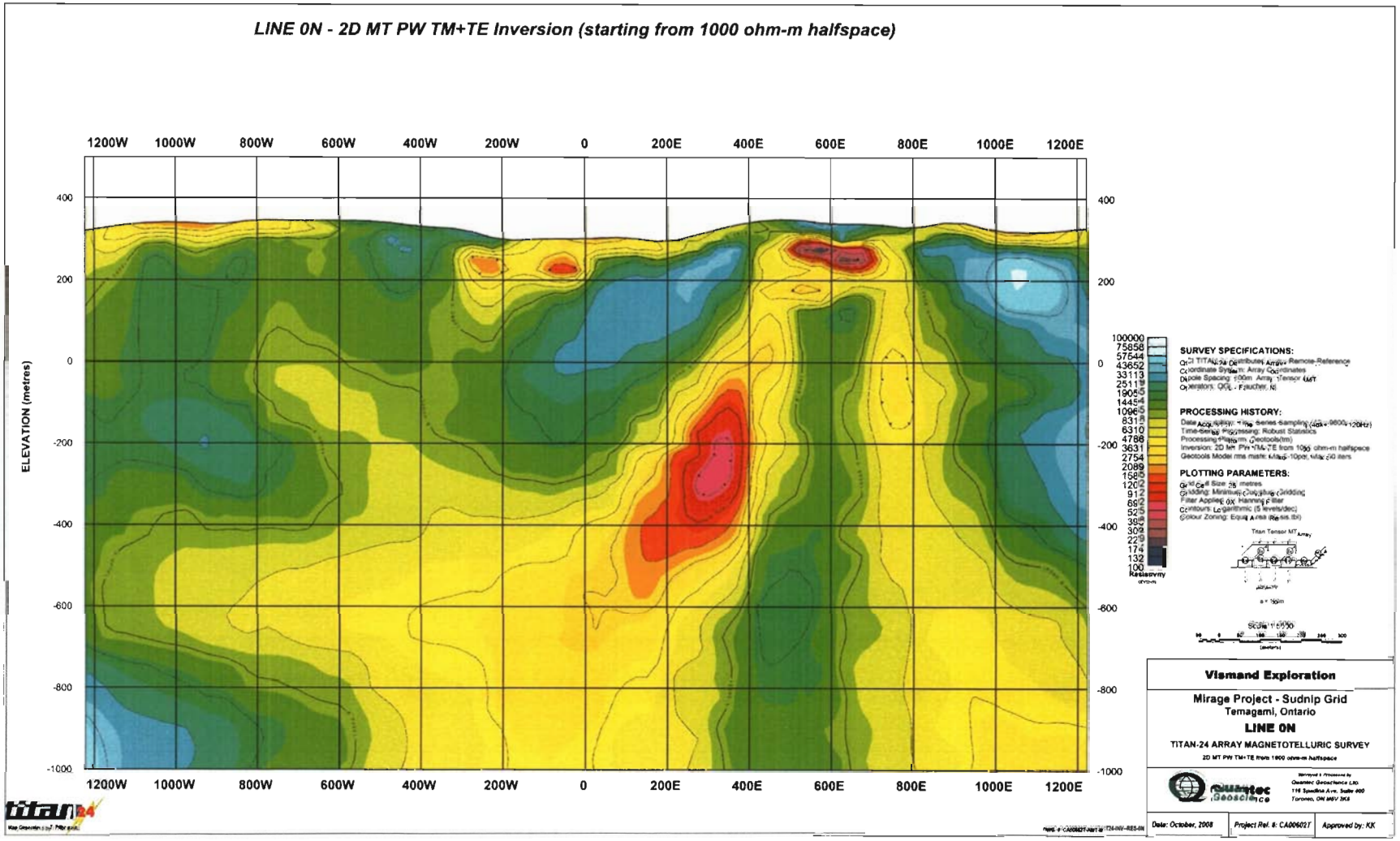

Line 0N – 2D MT RLM TM+TE(phs) Inversion (starting from 1D Det model)

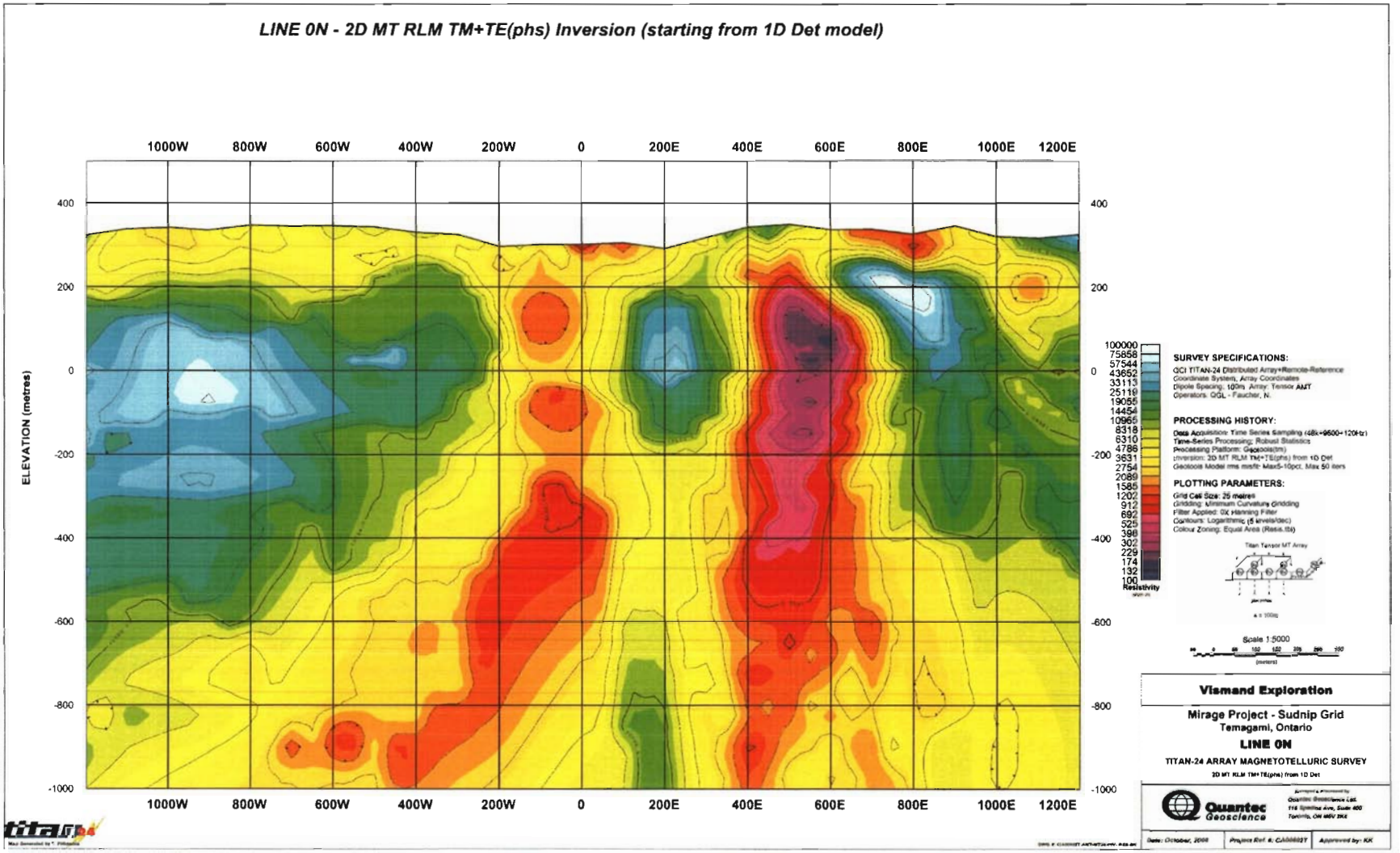

Line 0N – 2D MT RLM TM+TE Inversion (starting from 1D Det model)

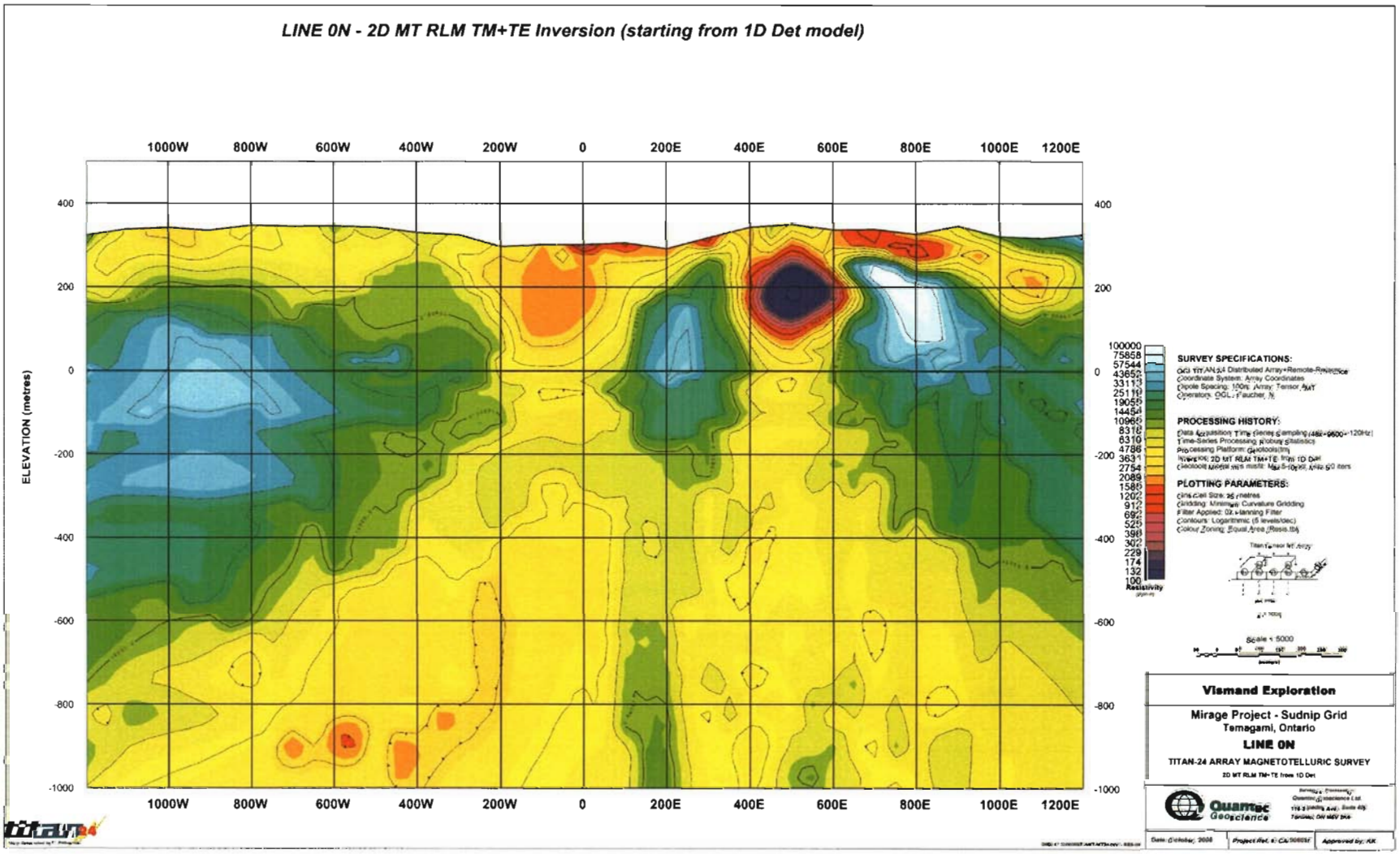

Line 0N – 2D MT RLM TM+TE(phs) Inversion (starting from 1000 ohm-m halfspace)

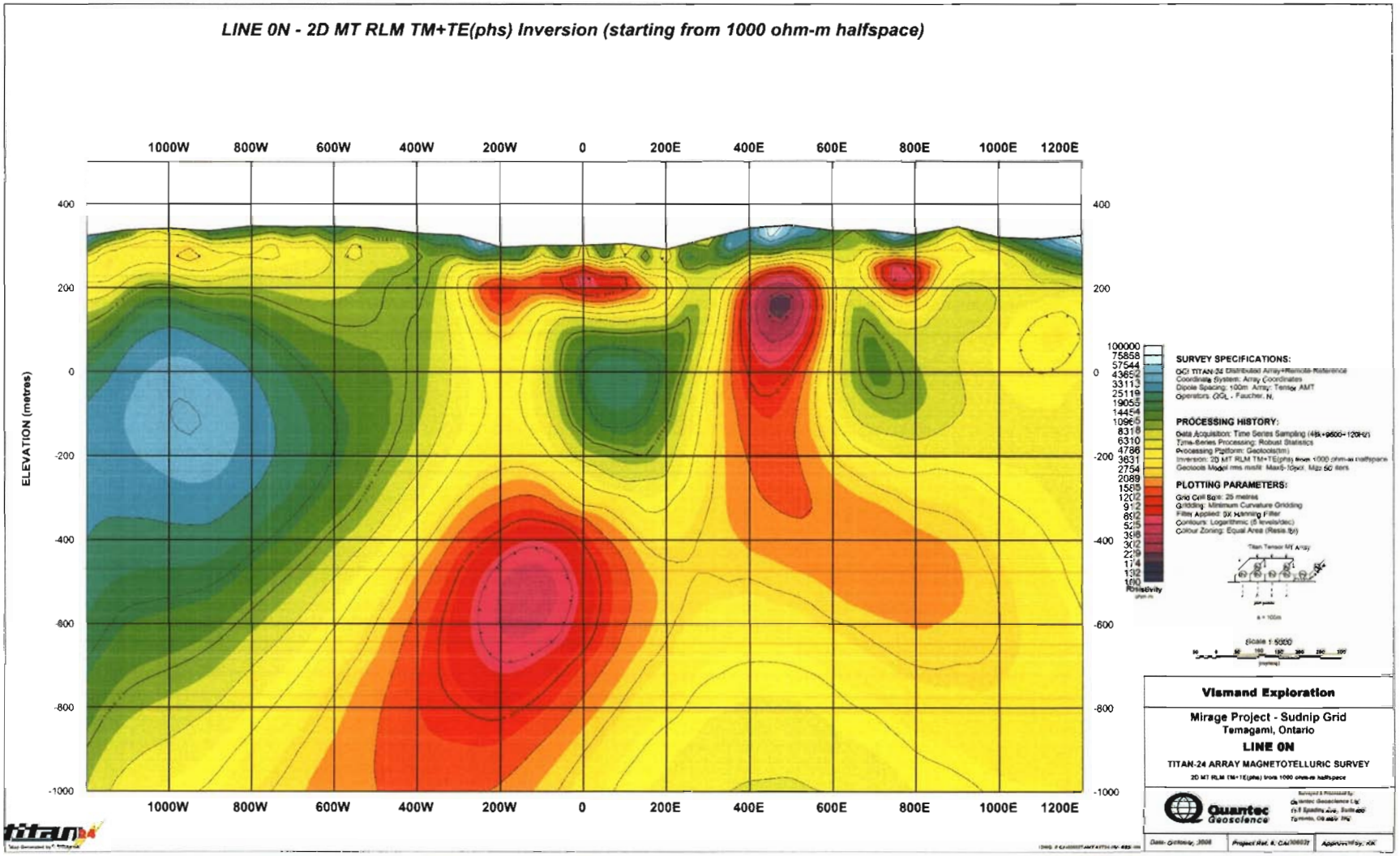

Line 0N – 2D MT RLM TM+TE Inversion (starting from 1000 ohm-m halfspace)

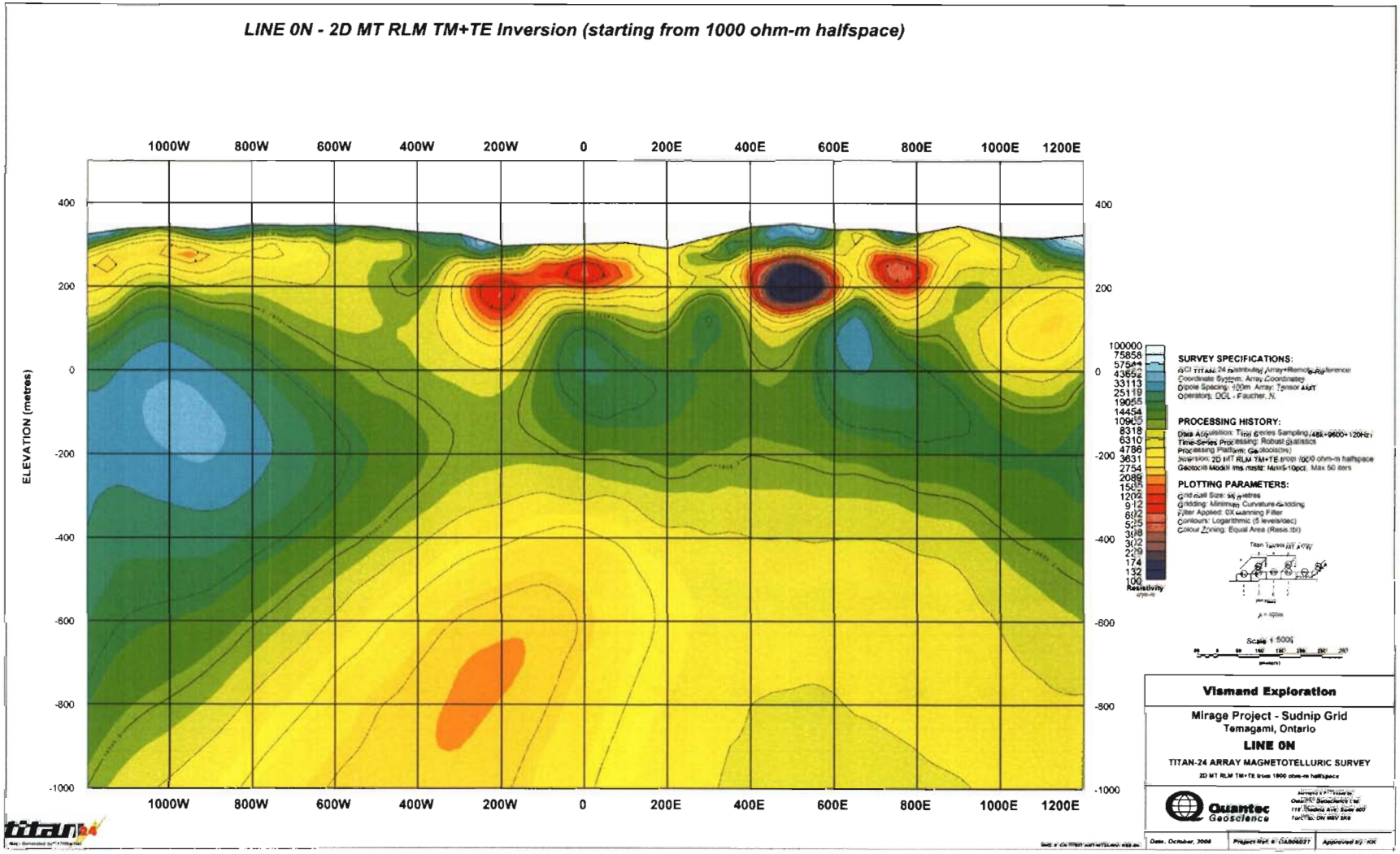

Line 400N – 2D UBC Smooth DC Resistivity Model

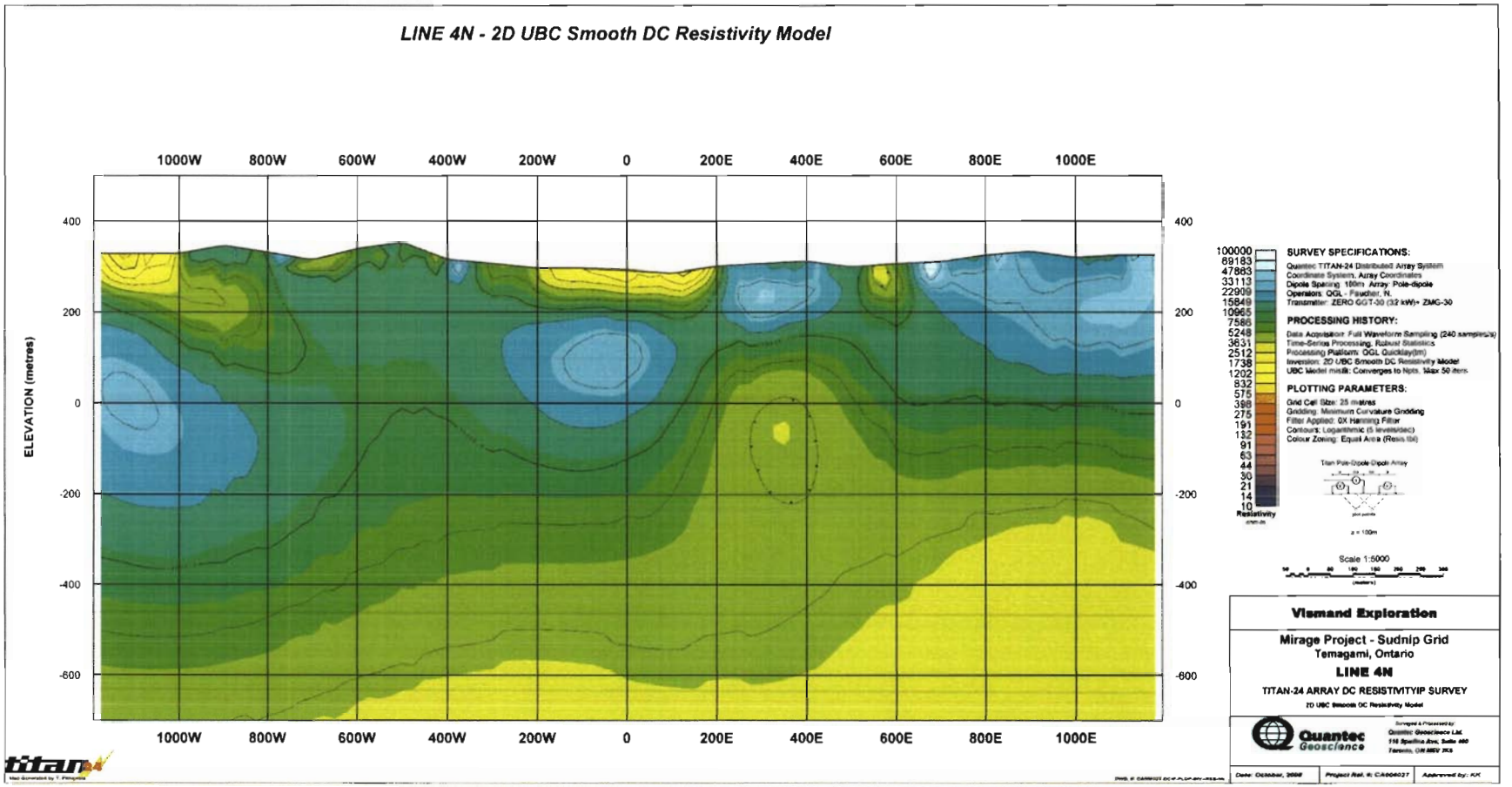

Line 400N – 2D UBC Smooth IP Chargeability Model

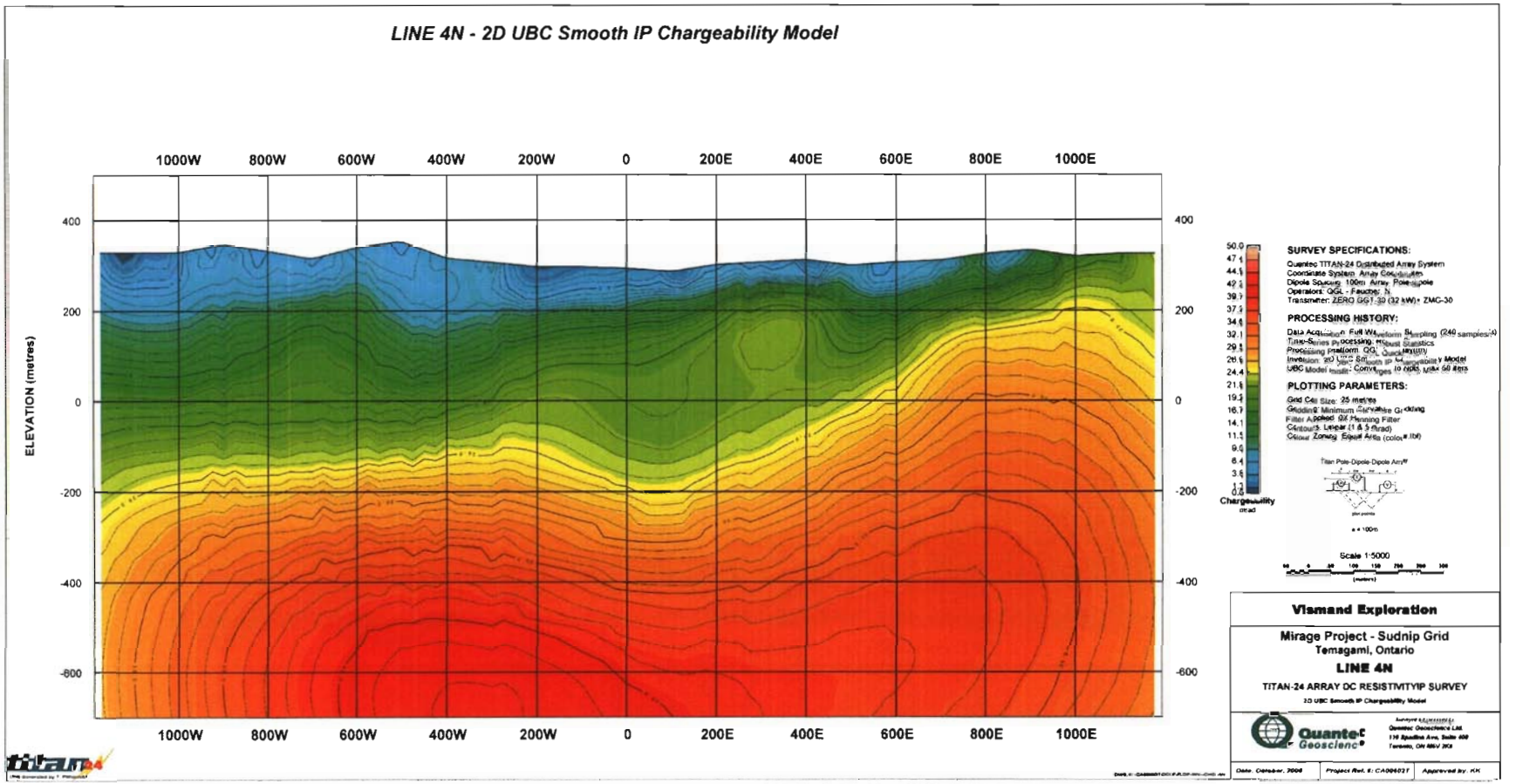

Line 400N – 2D UBC Null Con IP Chargeability Model

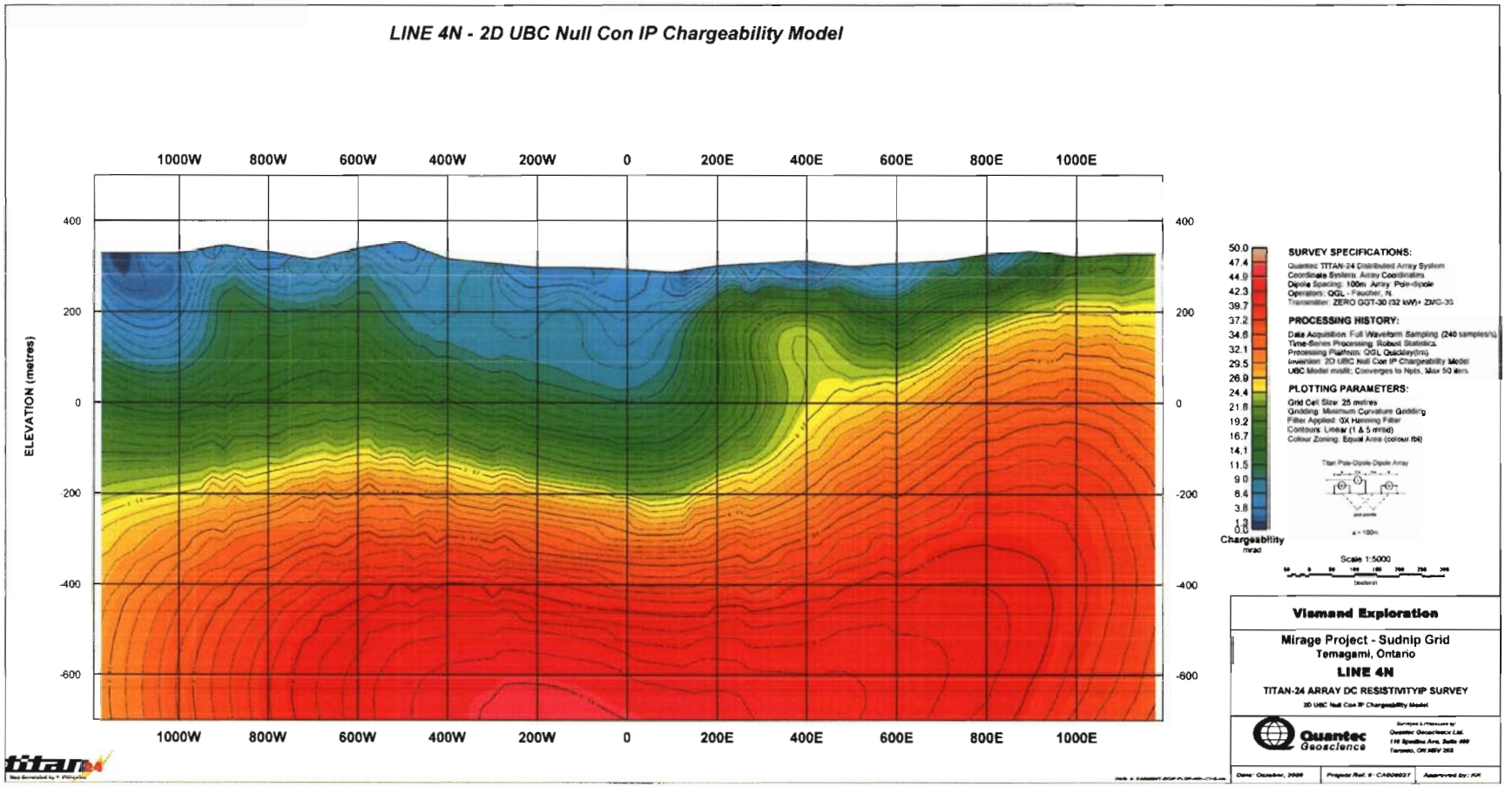

Line 400N – 2D MT PW TM+TE(phs) Sharp Inversion (starting from smooth 1D PW model)

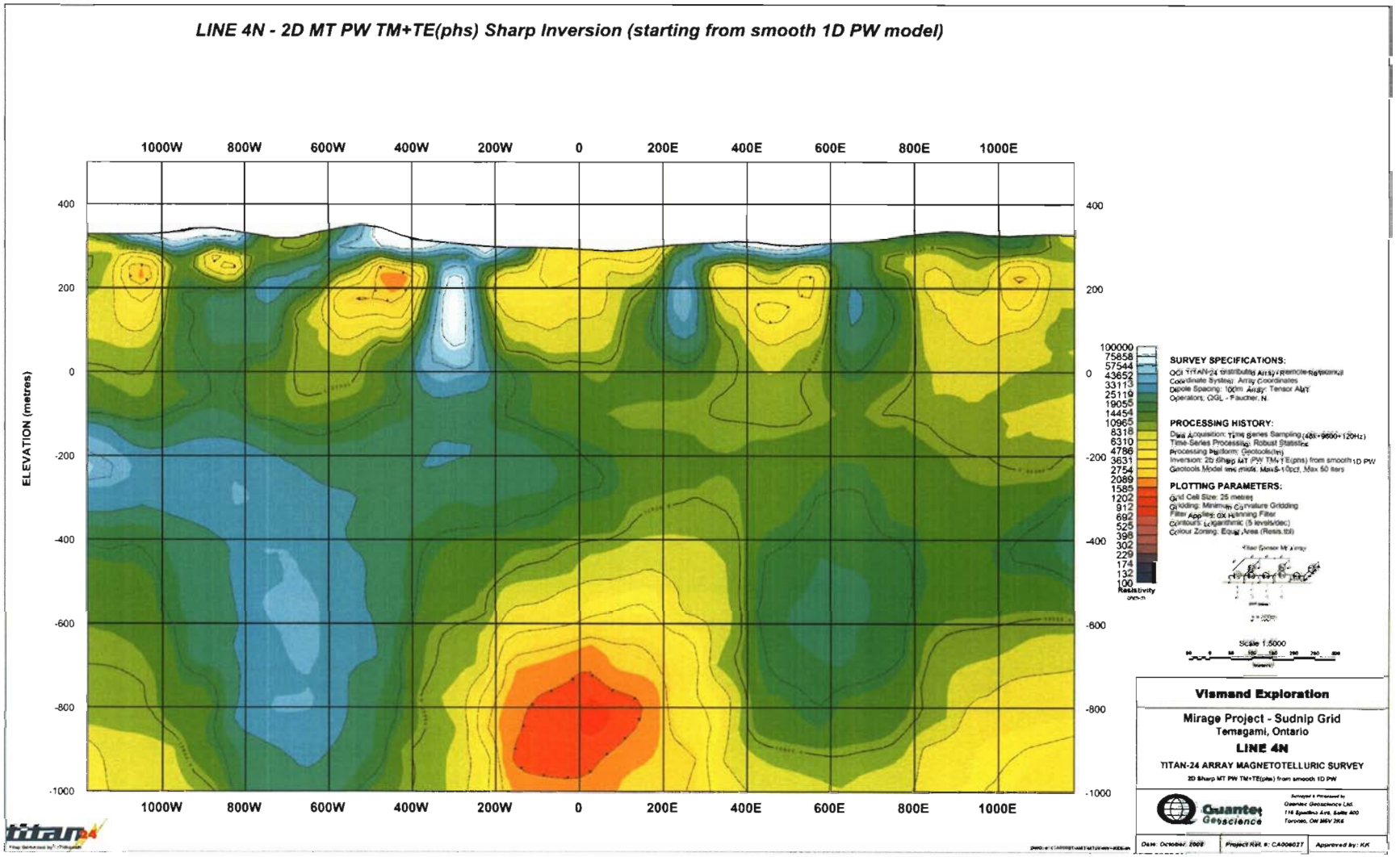

Line 400N – 2D MT PW TM+TE Sharp Inversion (starting from smooth 1D PW model)

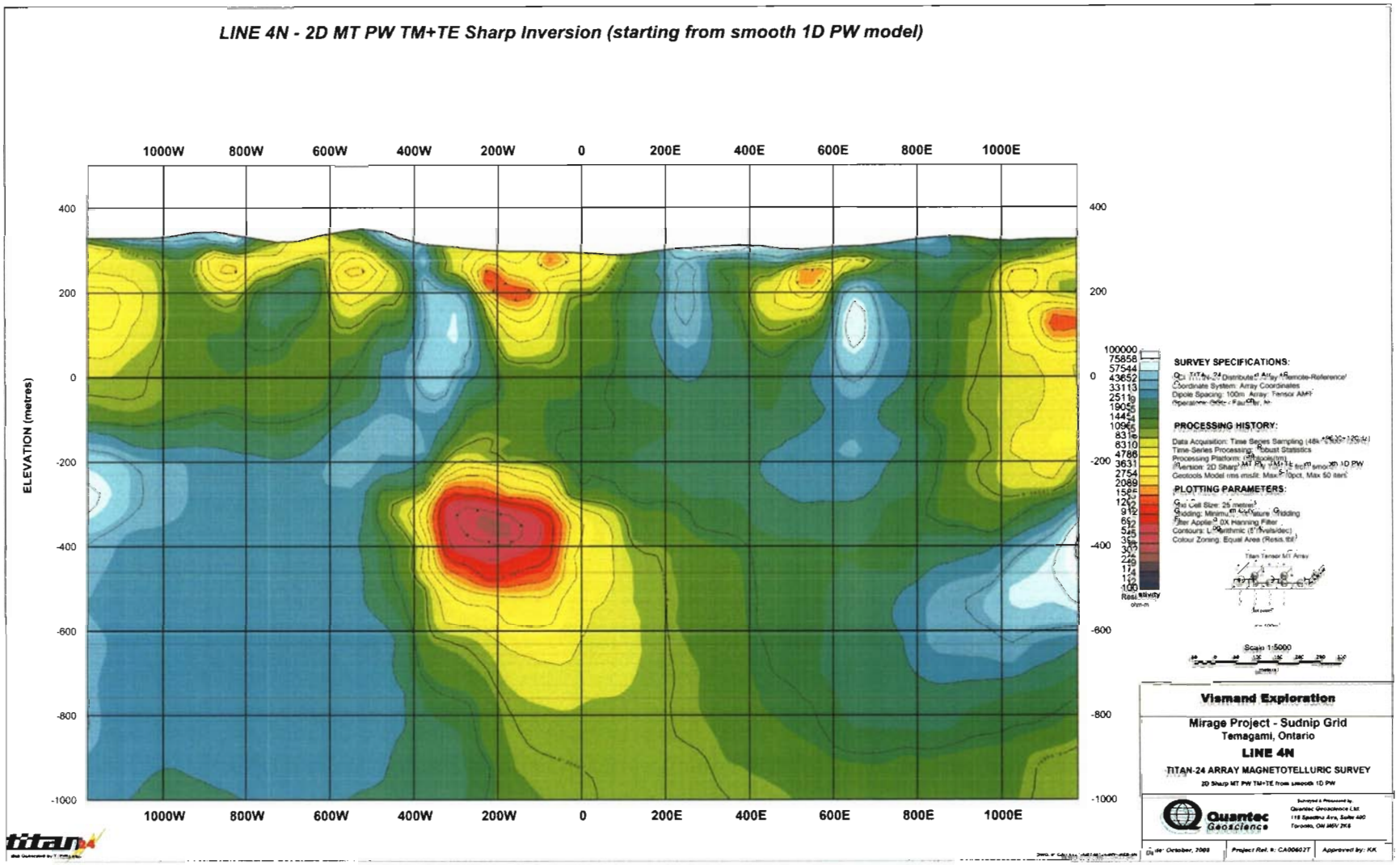

Line 400N – 2D MT PW TM+TE(phs) Inversion (starting from 1000 ohm-m halfspace)

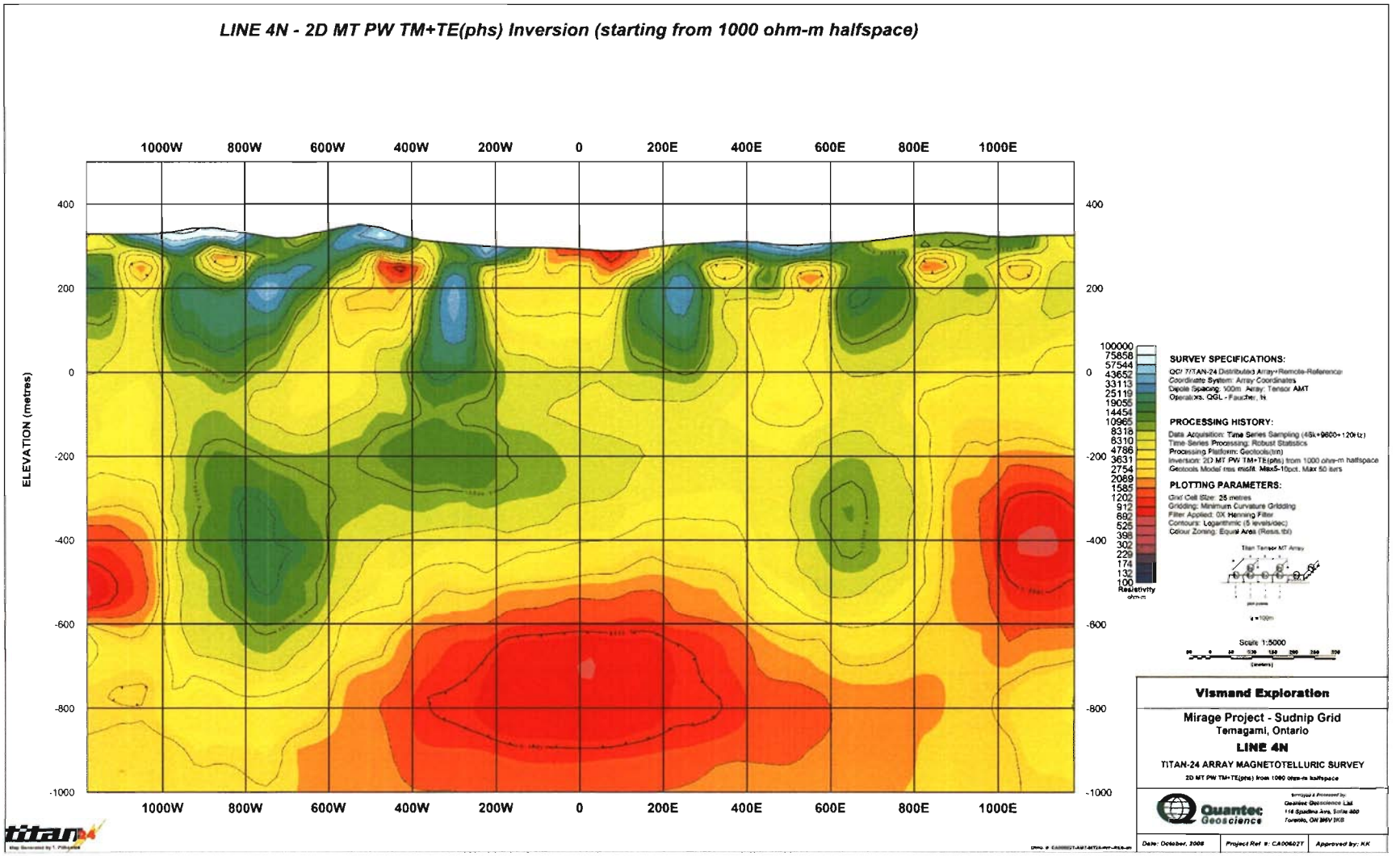

Line 400N – 2D MT PW TM+TE Inversion (starting from 1000 ohm-m halfspace)

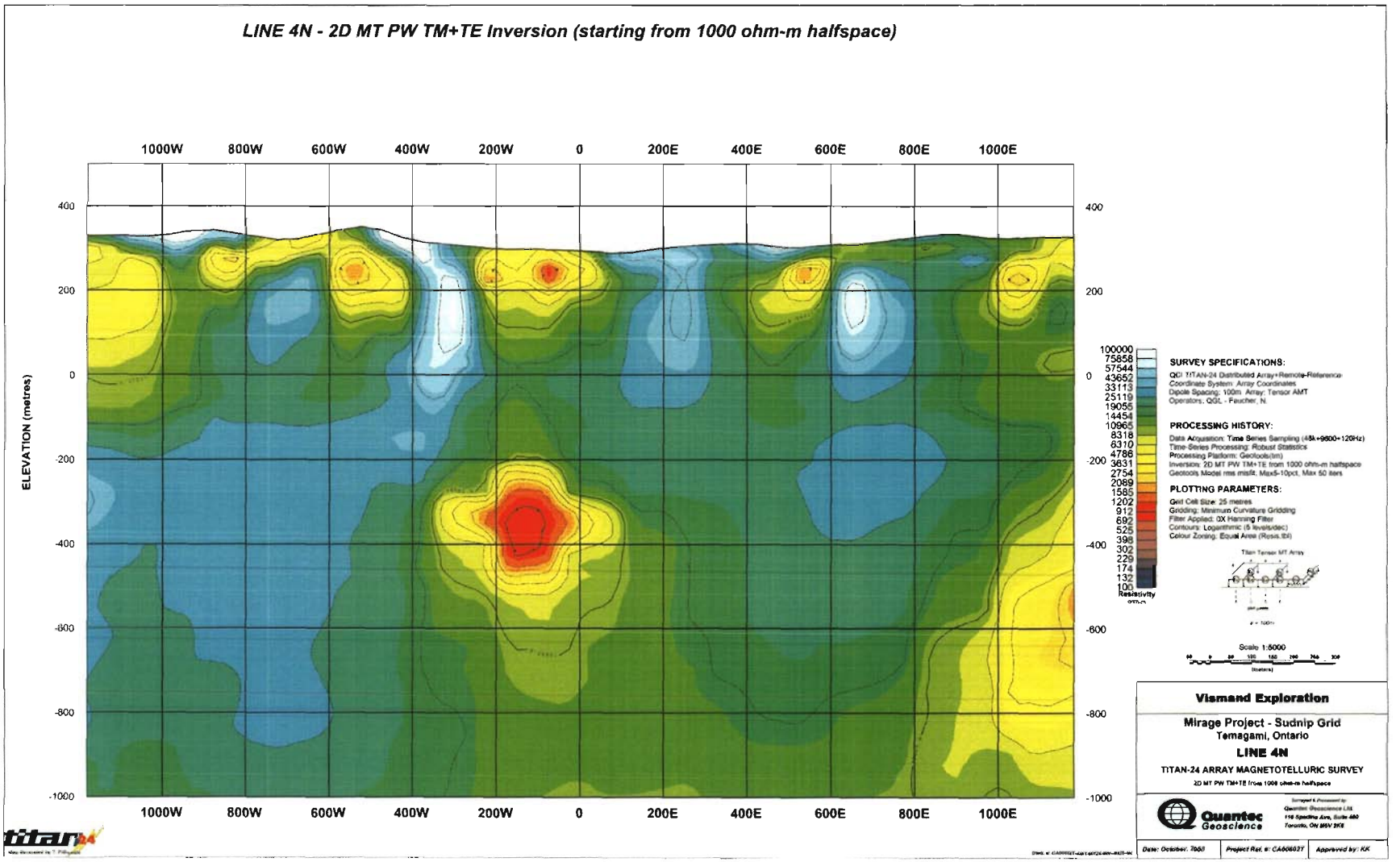

Line 400N – 2D MT RLM TM+TE(phs) Inversion (starting from 1D Det model)

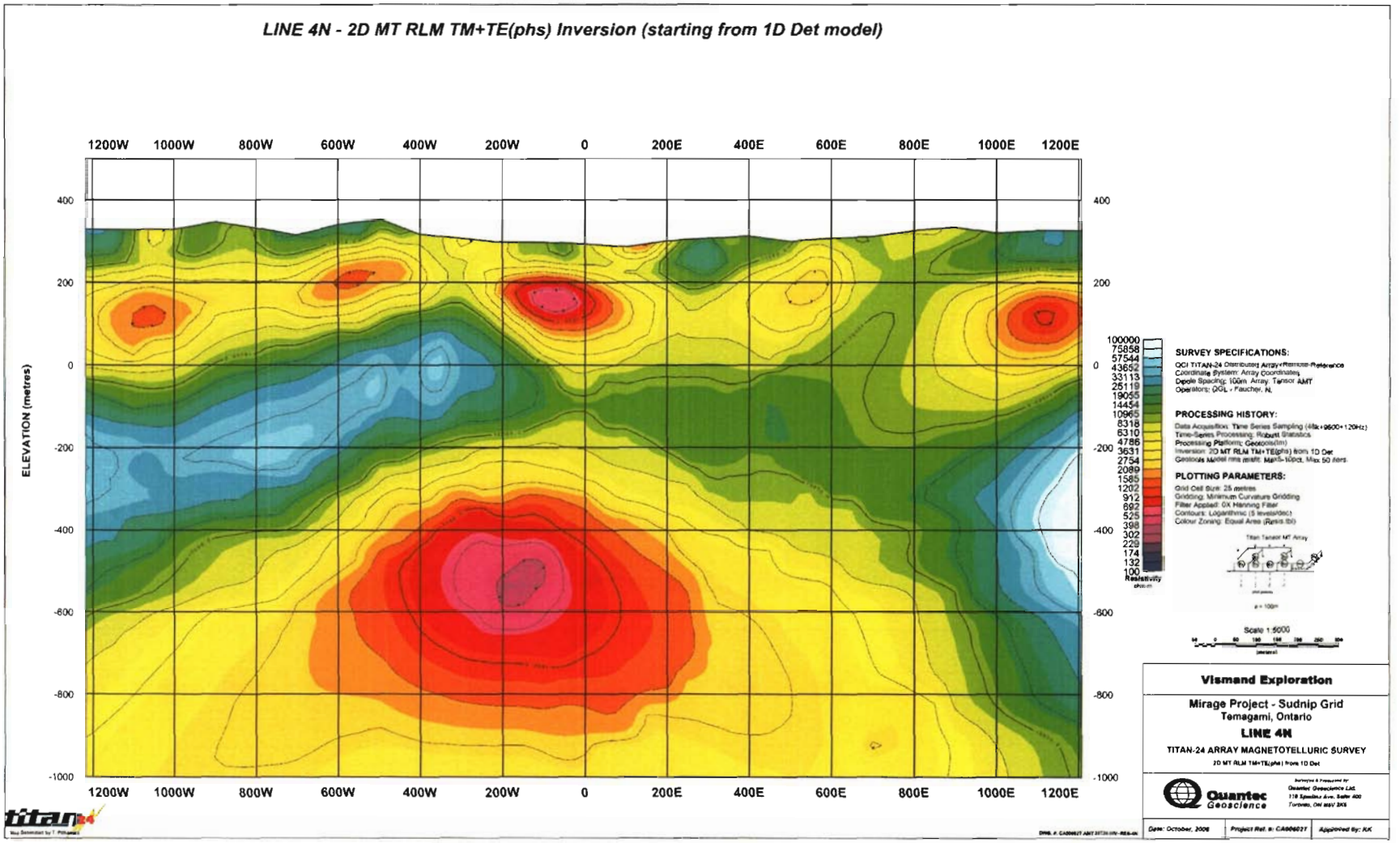

Line 400N – 2D MT RLM TM+TE Inversion (starting from 1D Det model)

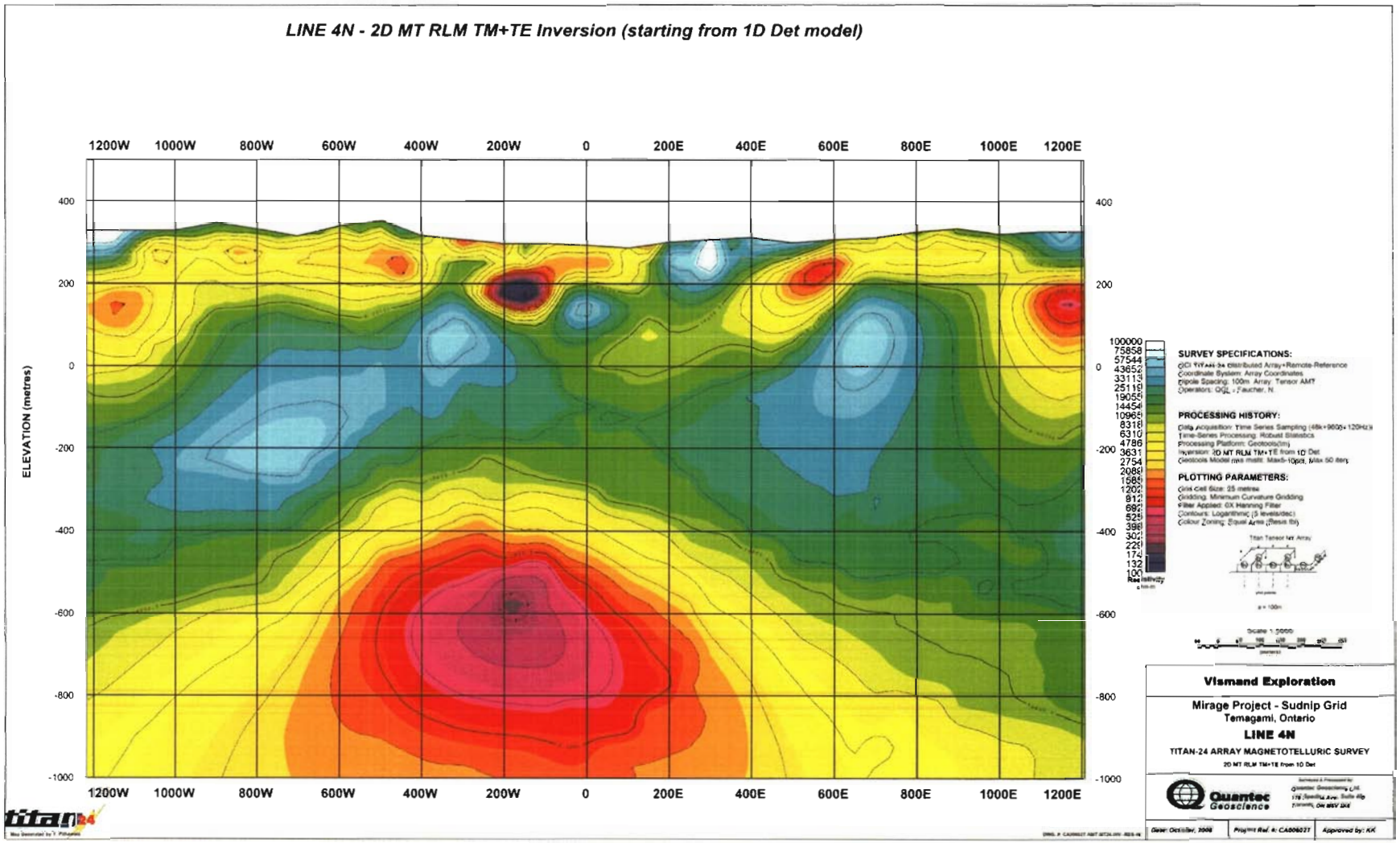

Line 800N – 2D UBC Smooth DC Resistivity Model

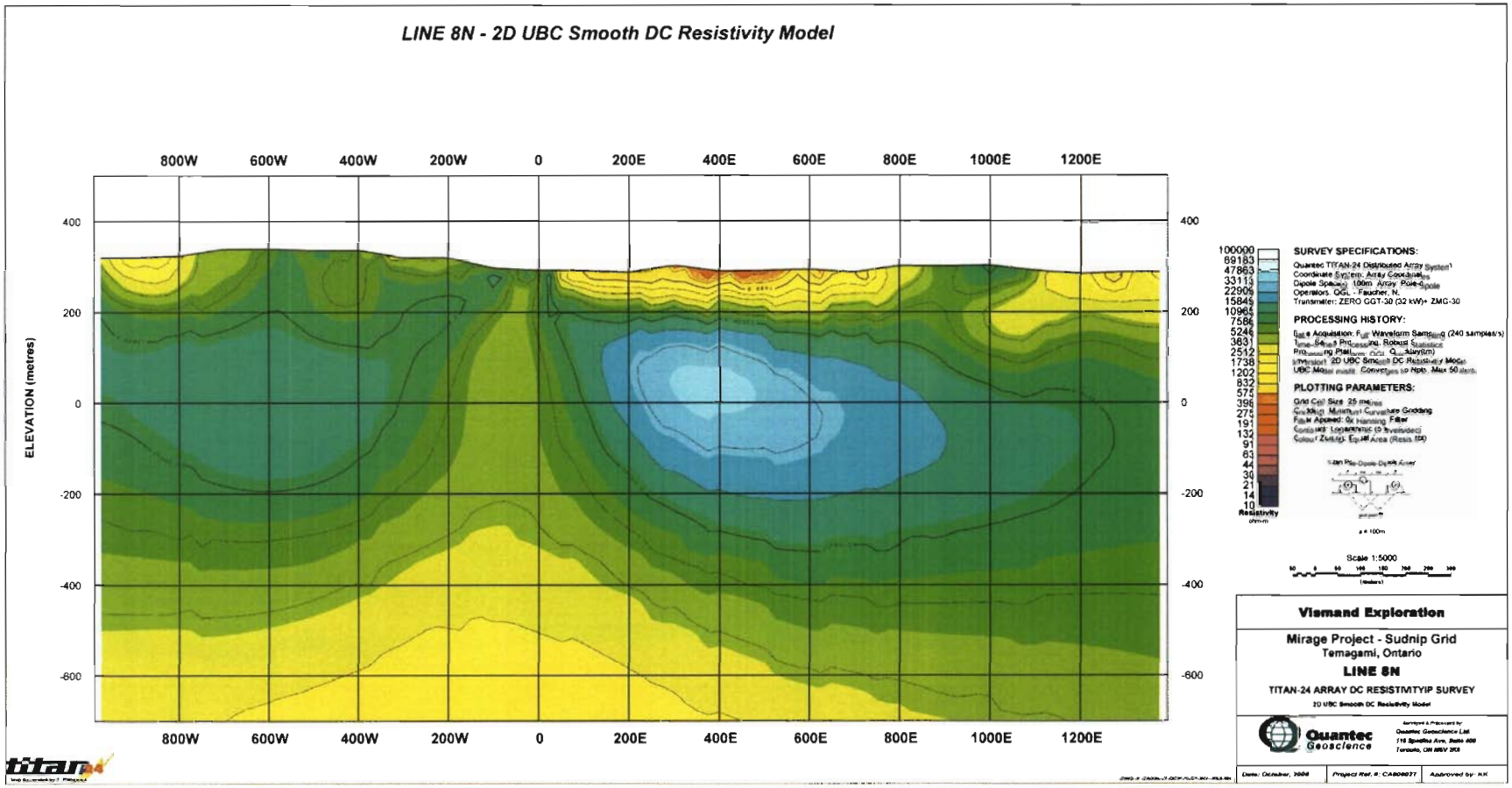

Line 800N – 2D UBC Smooth IP Chargeability Model

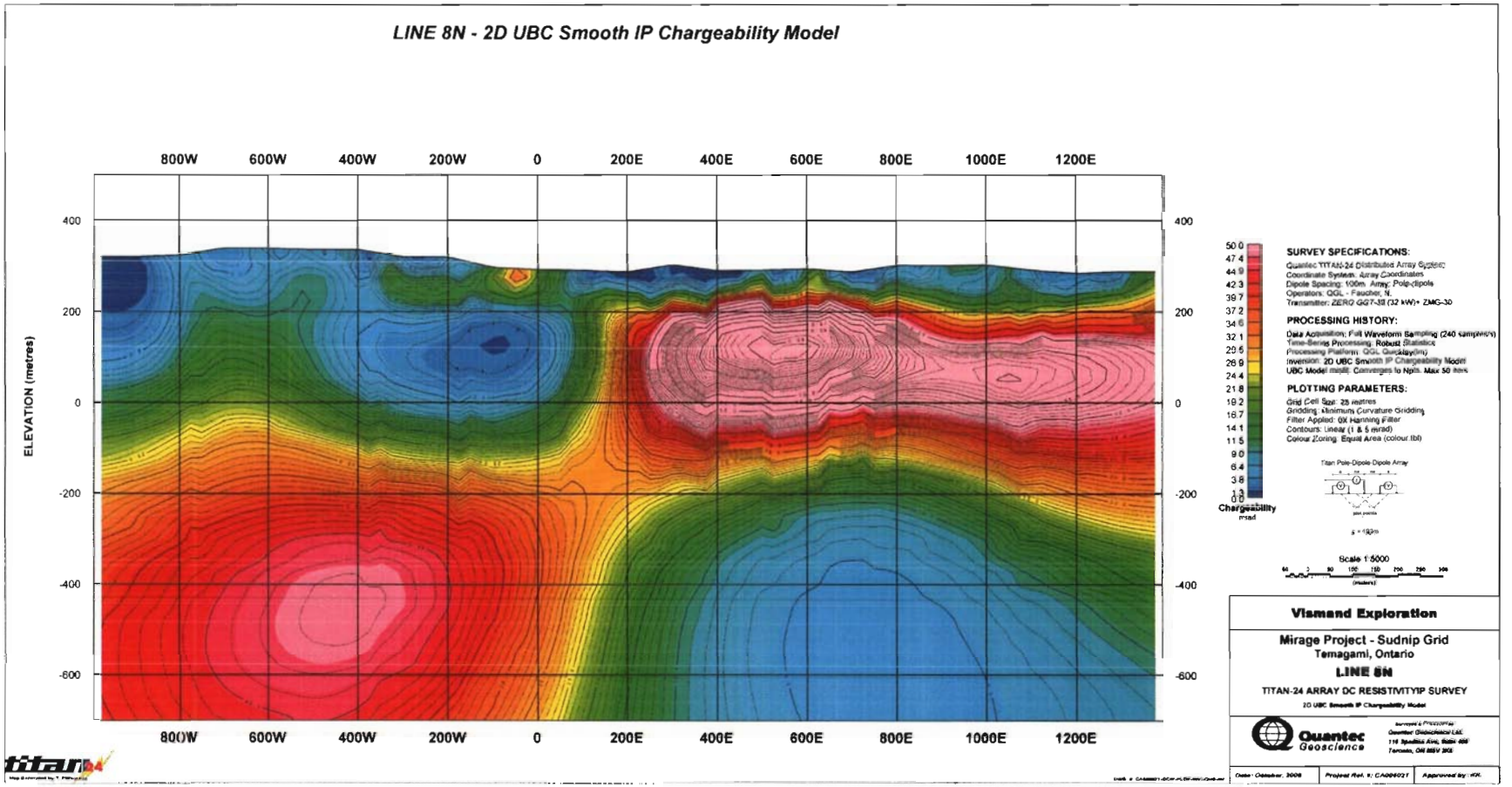

Line 800N – 2D UBC Null Con IP Chargeability Model

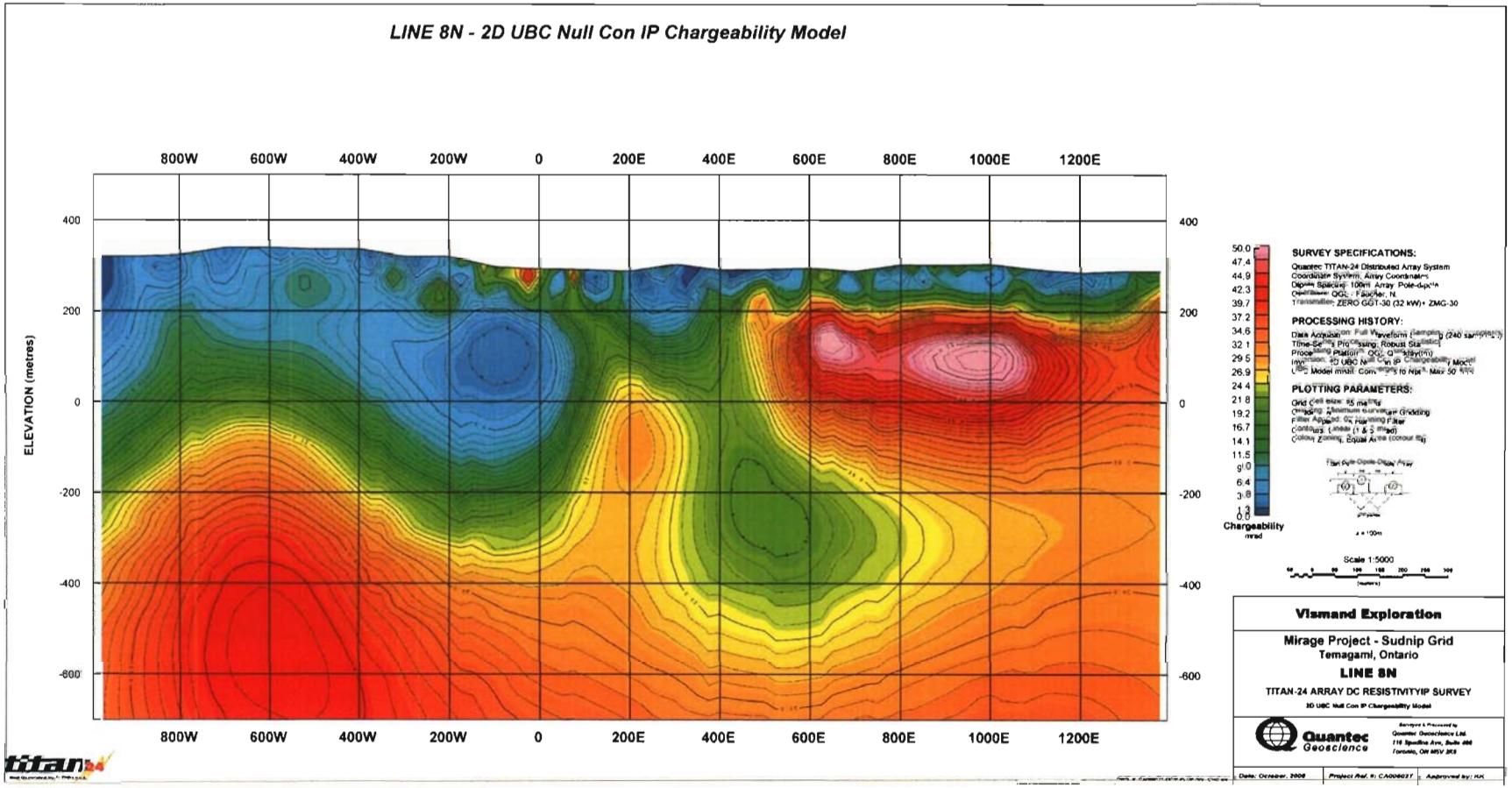

Line 800N – 2D MT PW TM+TE(phs) Sharp Inversion (starting from smooth 1D PW model)

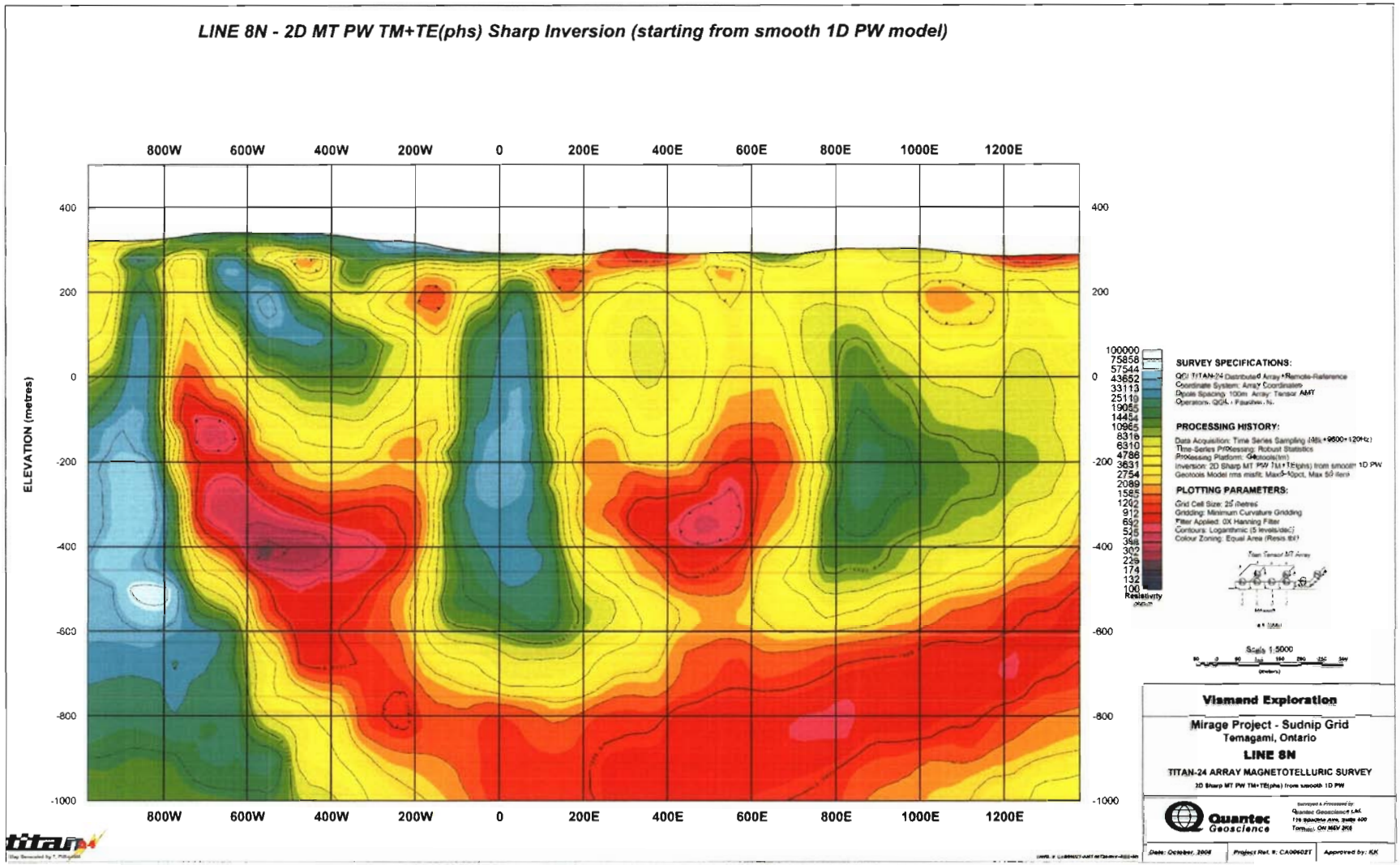

Line 800N – 2D MT PW TM+TE Sharp Inversion (starting from smooth 1D PW model)

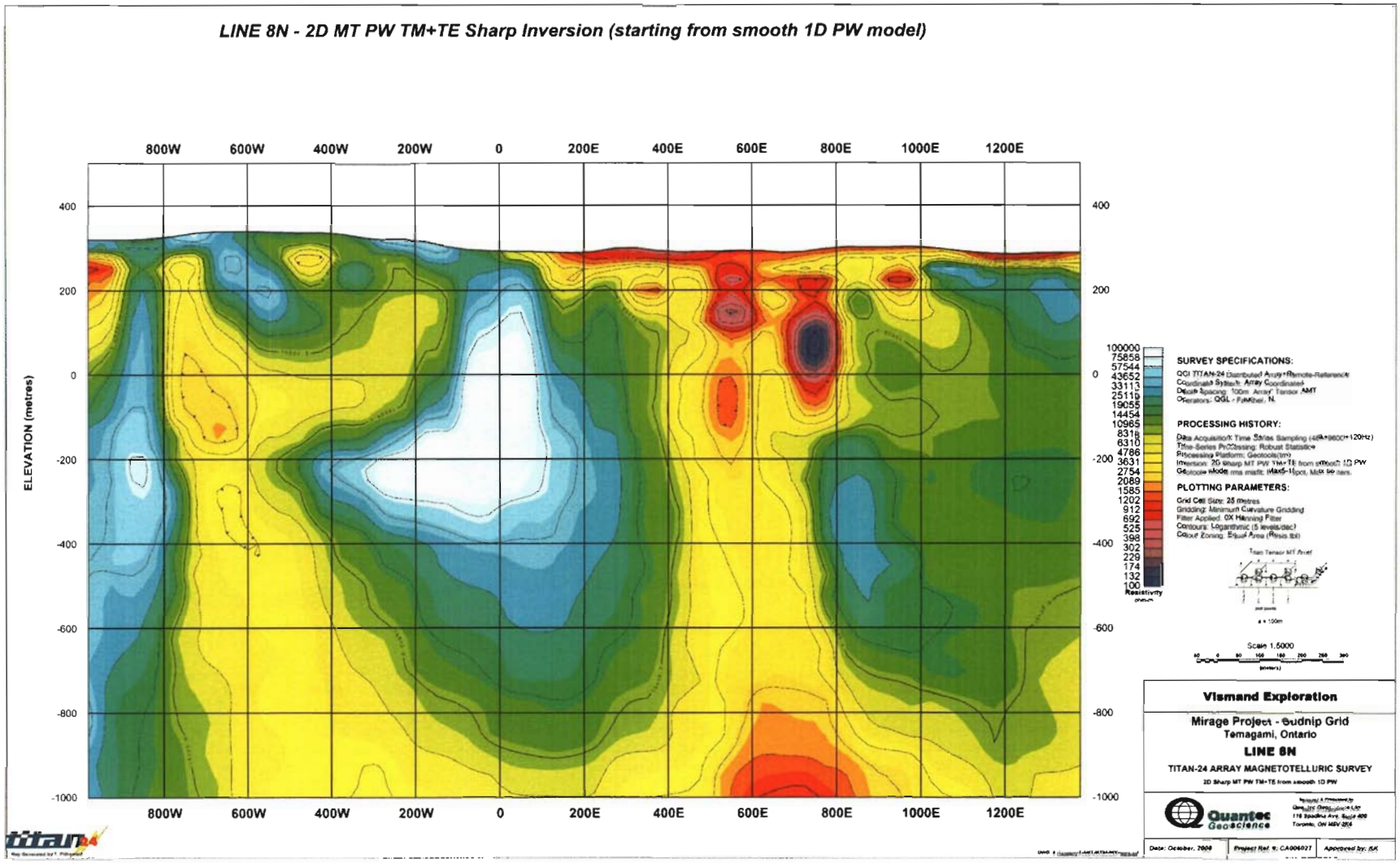

Line 800N – 2D MT PW TM+TE(phs) Inversion (starting from 1000 ohm-m halfspace)

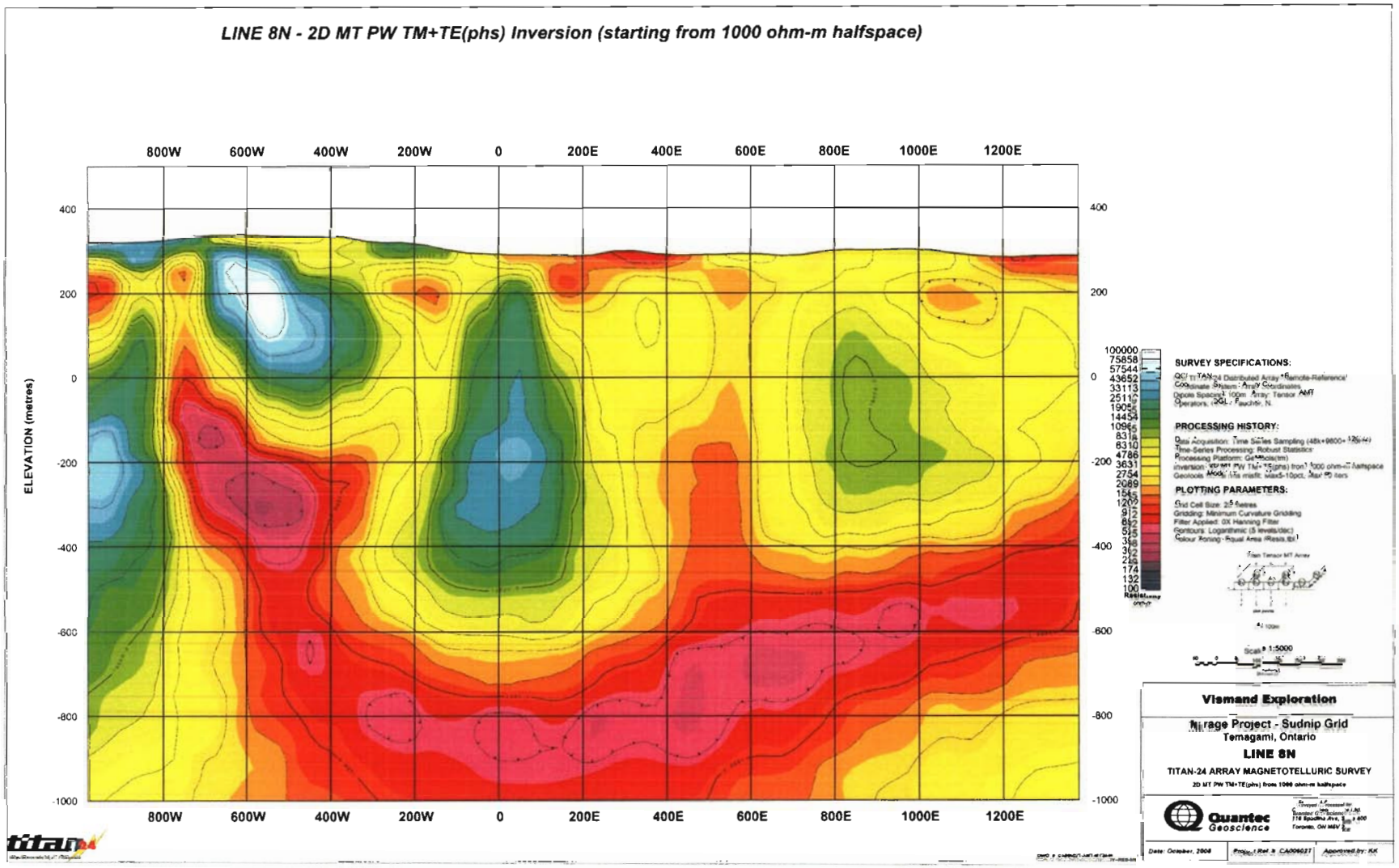

Line 800N – 2D MT PW TM+TE Inversion (starting from 1000 ohm-m halfspace)

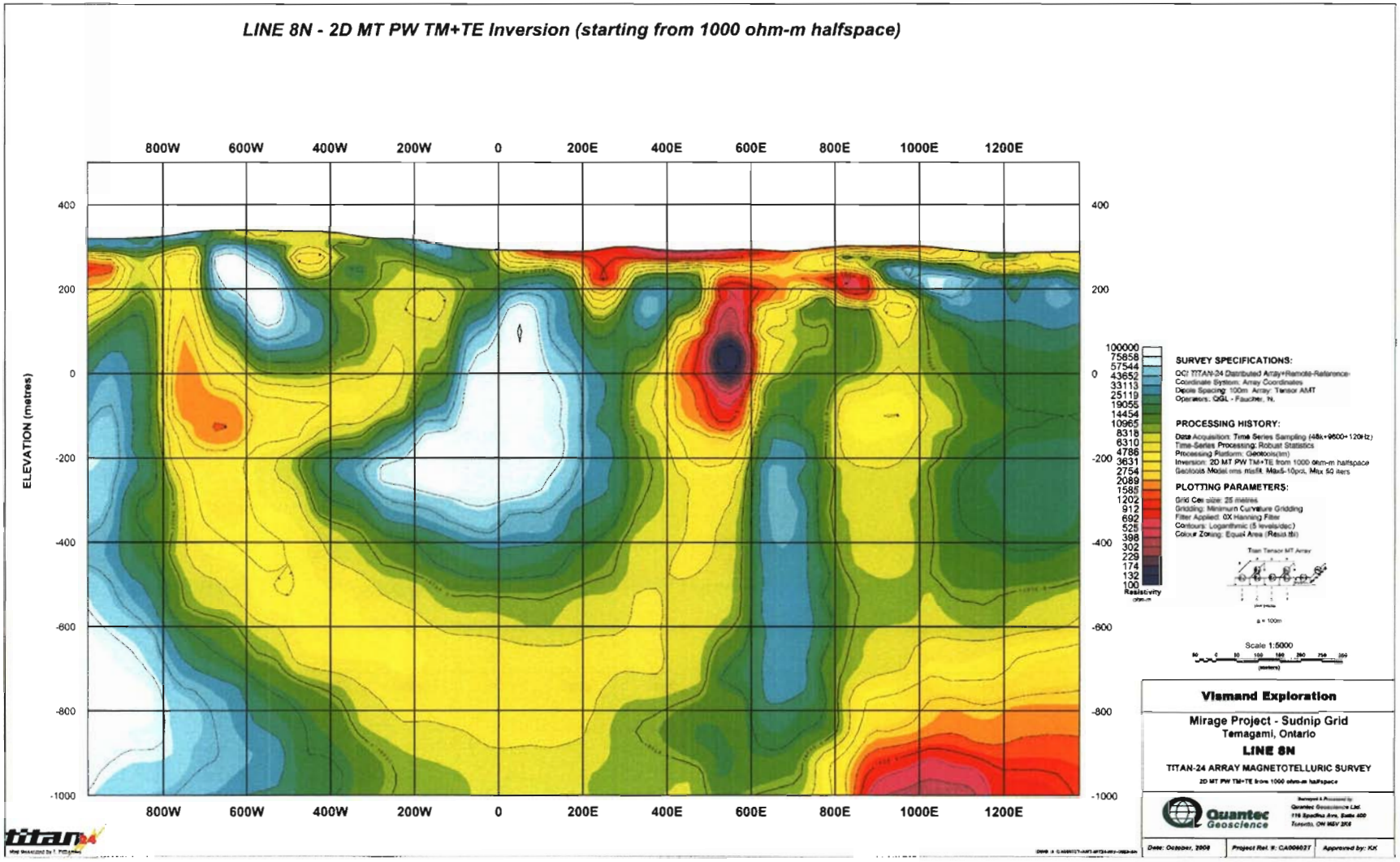

Line 800N – 2D MT RLM TM+TE(phs) Inversion (starting from 1D Det model)

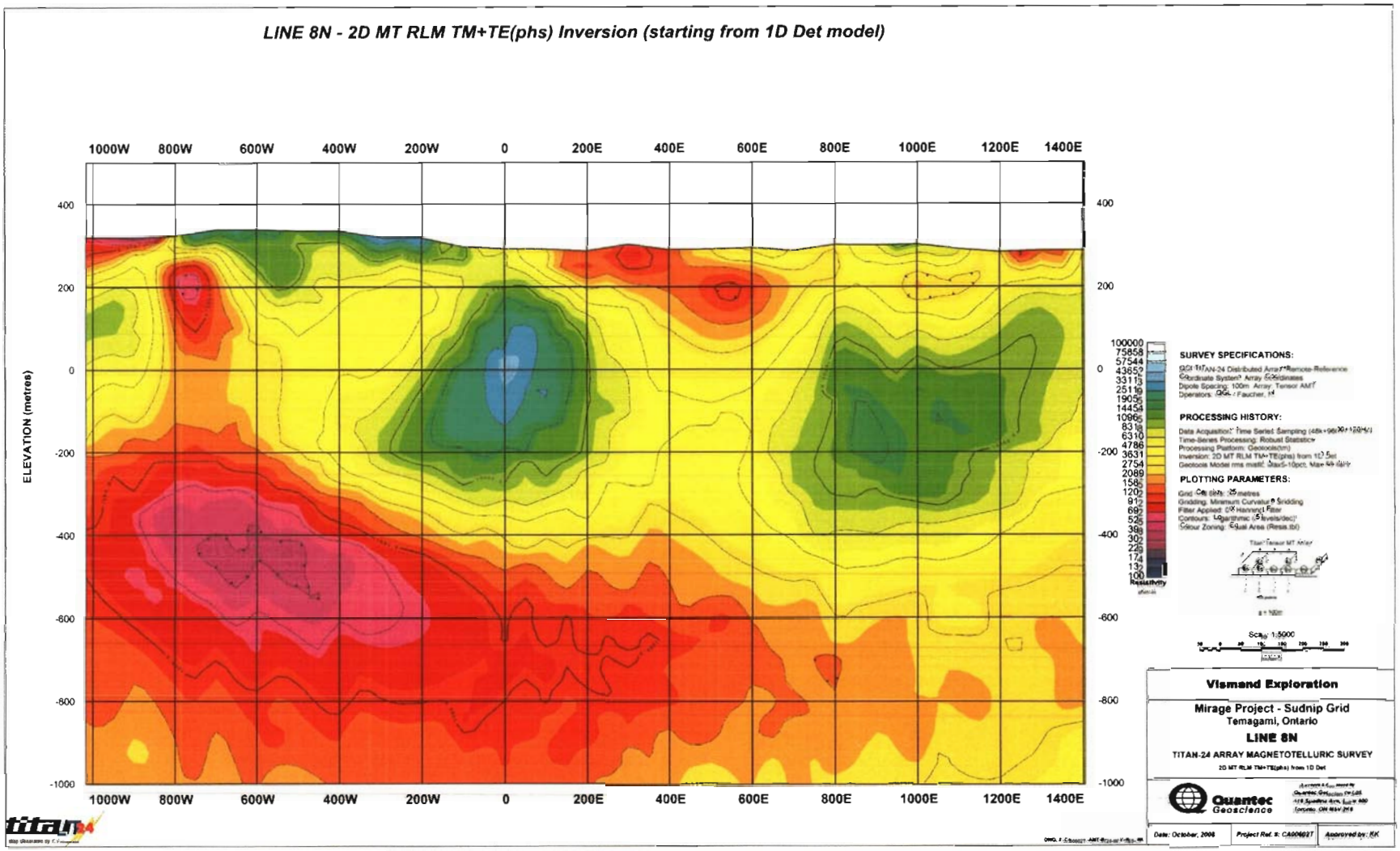

Line 800N – 2D MT RLM TM+TE Inversion (starting from 1D Det model)

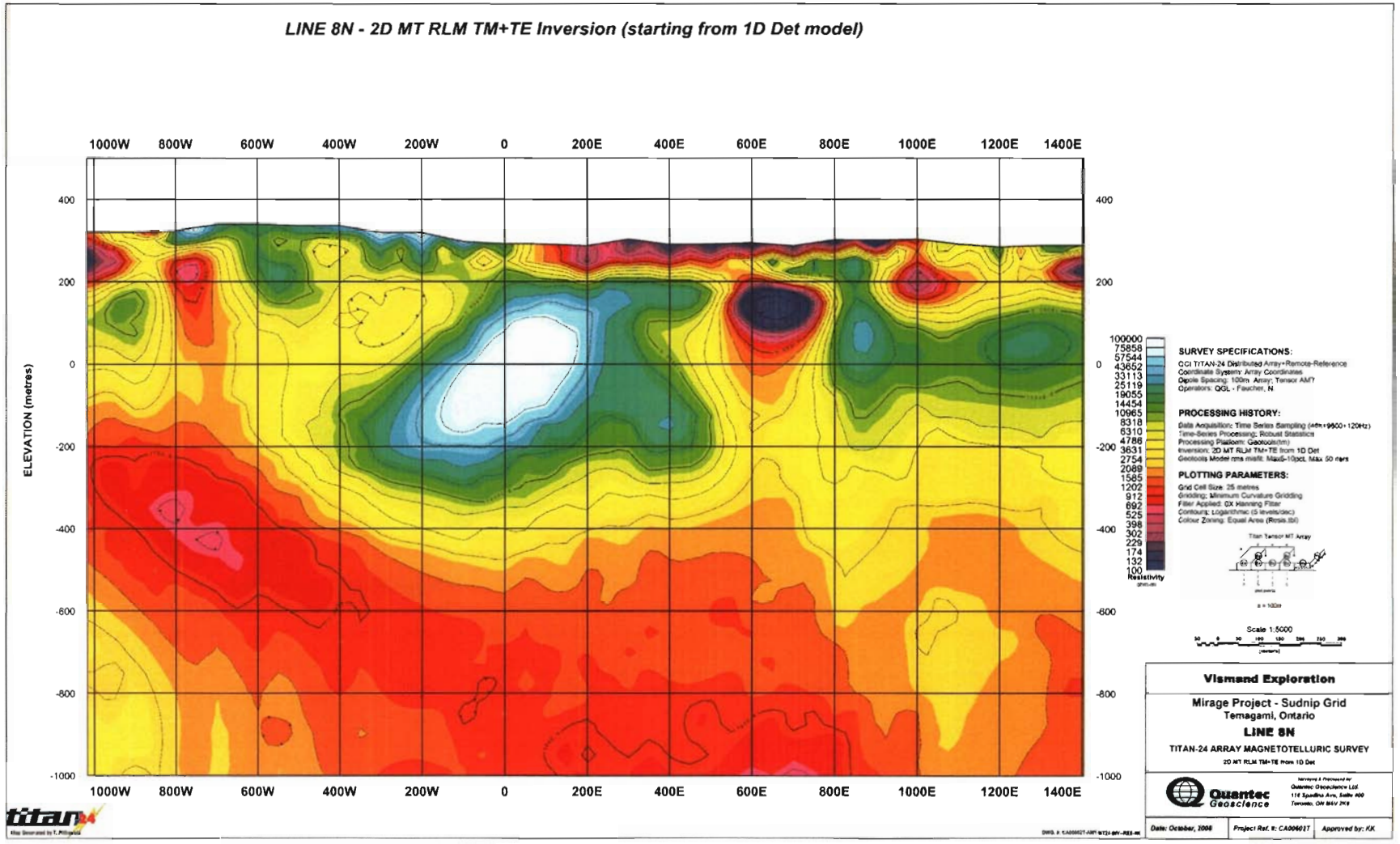

Line 800N – 2D MT RLM TM+TE(phs) Inversion (starting from 1000 ohm-m halfspace)

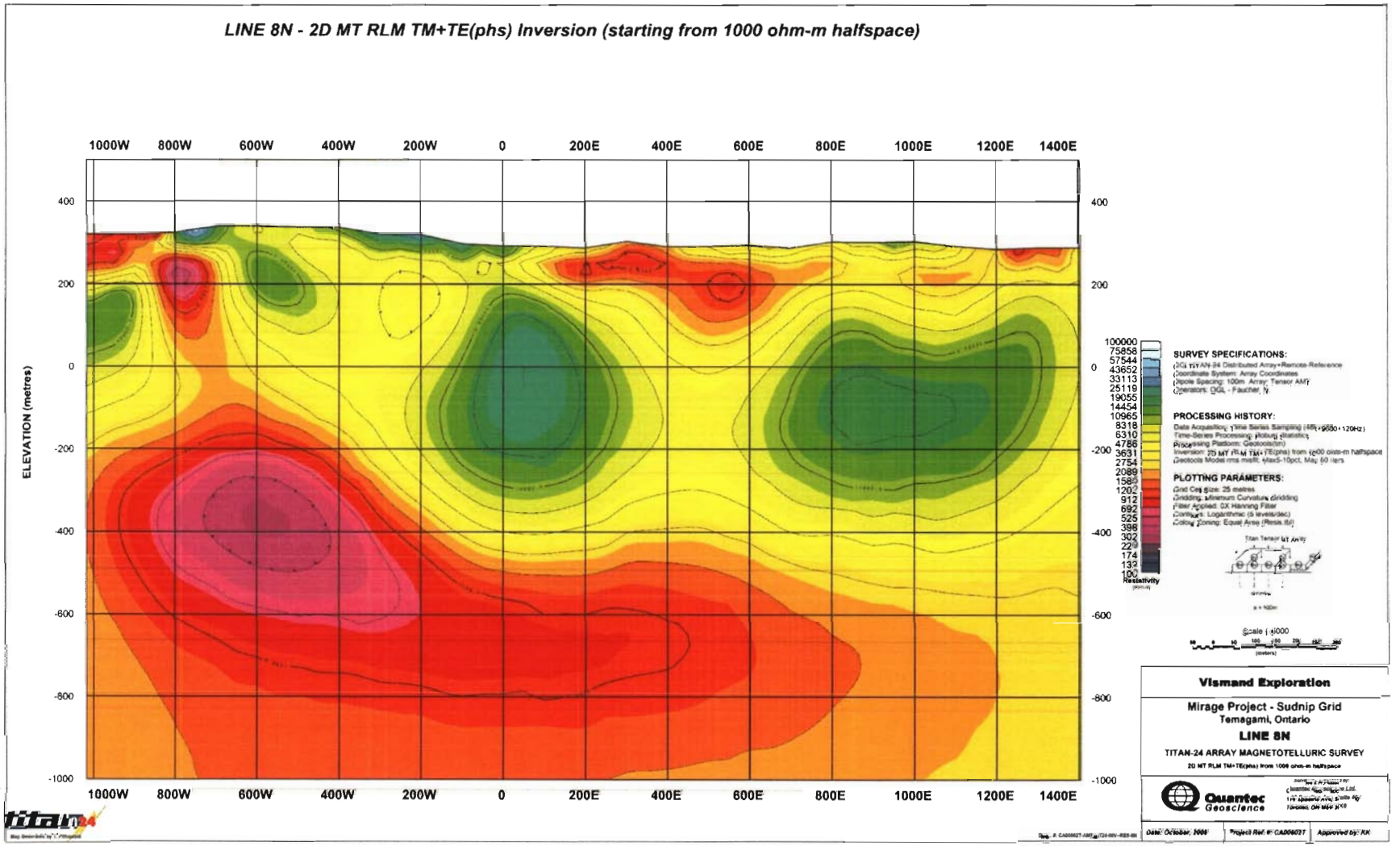

Line 800N – 2D MT RLM TM+TE Inversion (starting from 1000 ohm-m halfspace)

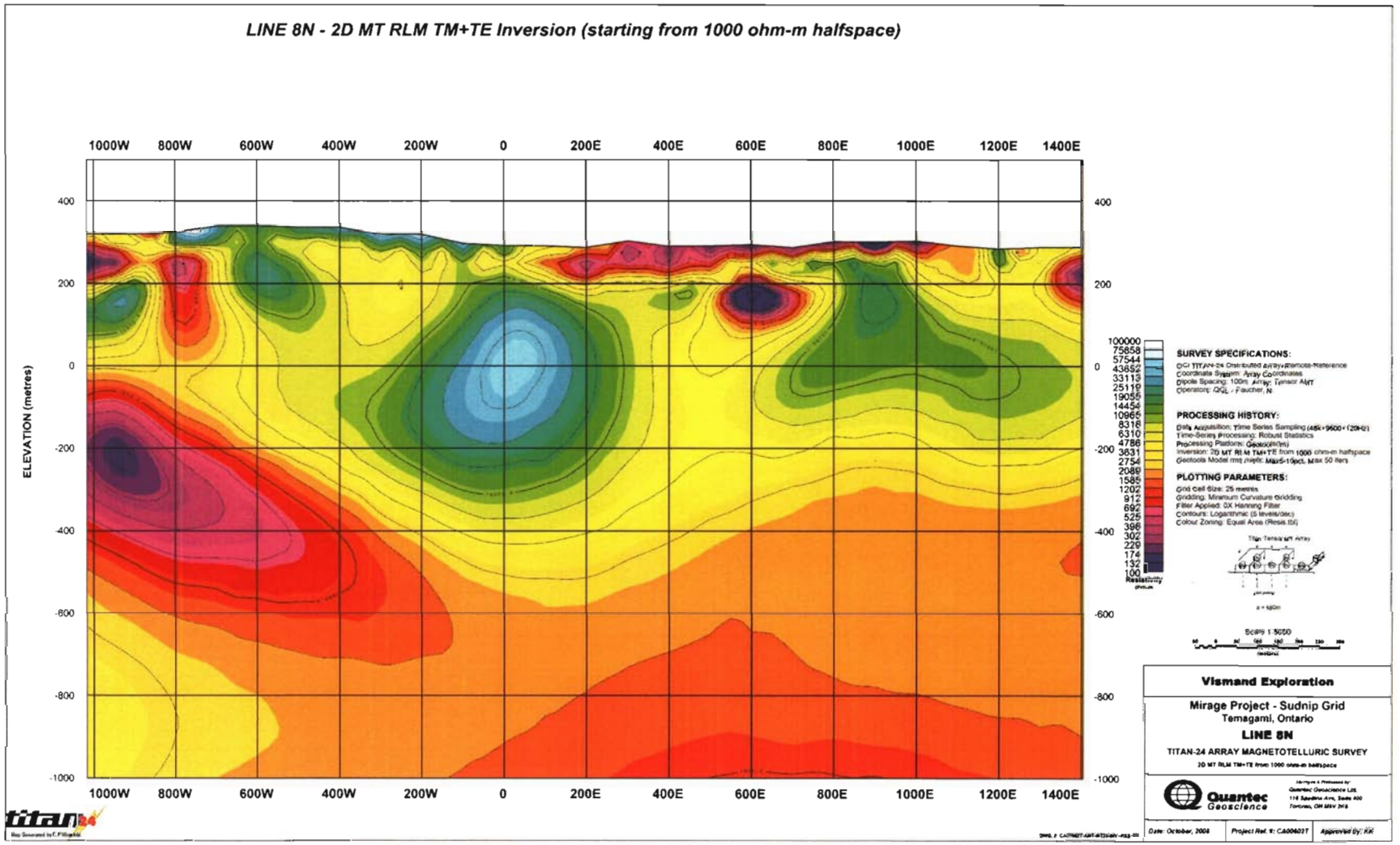

2D Resistivity (Z=50m) – 2D UBC Smooth DC Resistivity Model

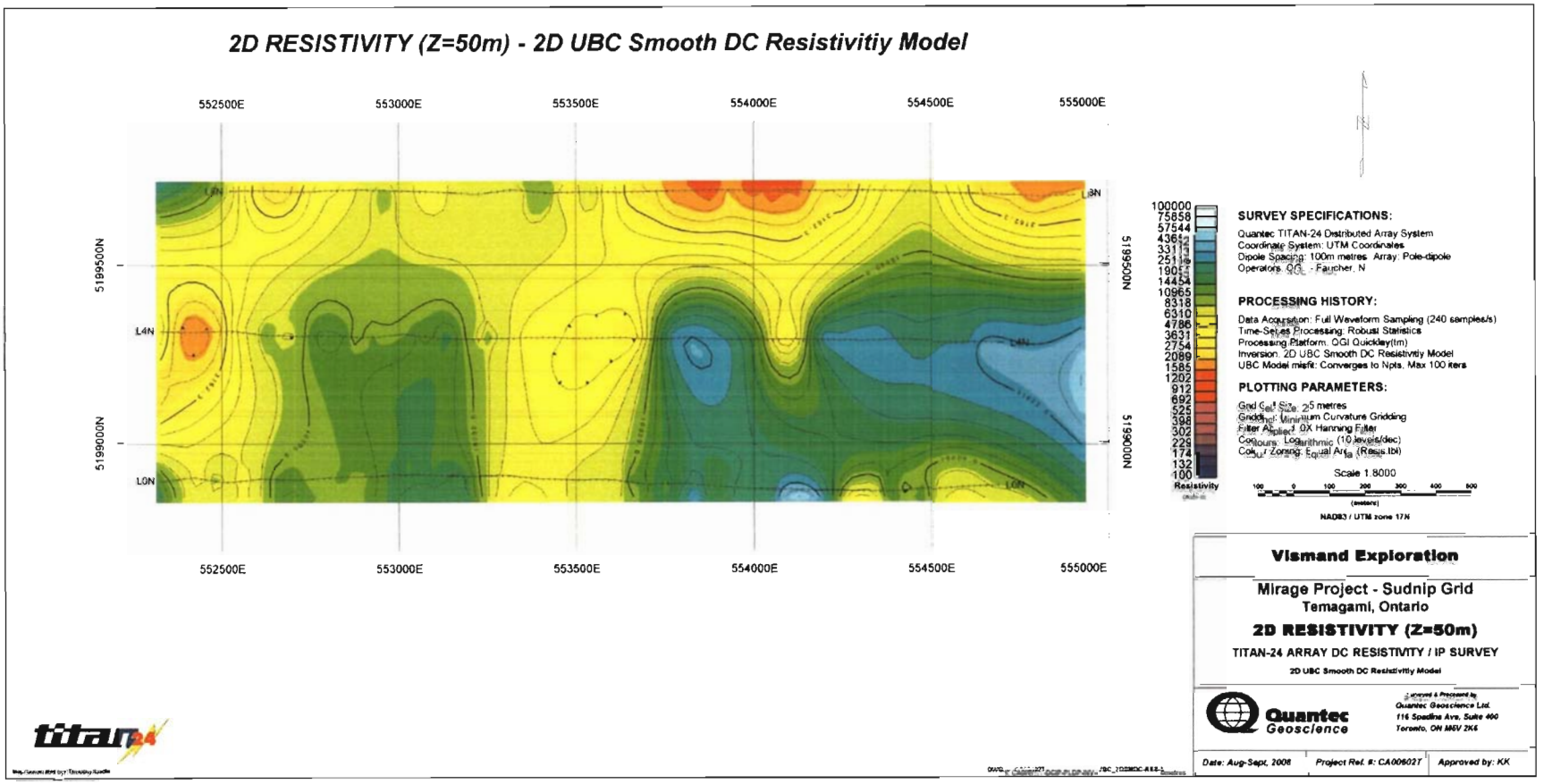

2D Resistivity (Z=100m) – 2D UBC Smooth DC Resistivity Model

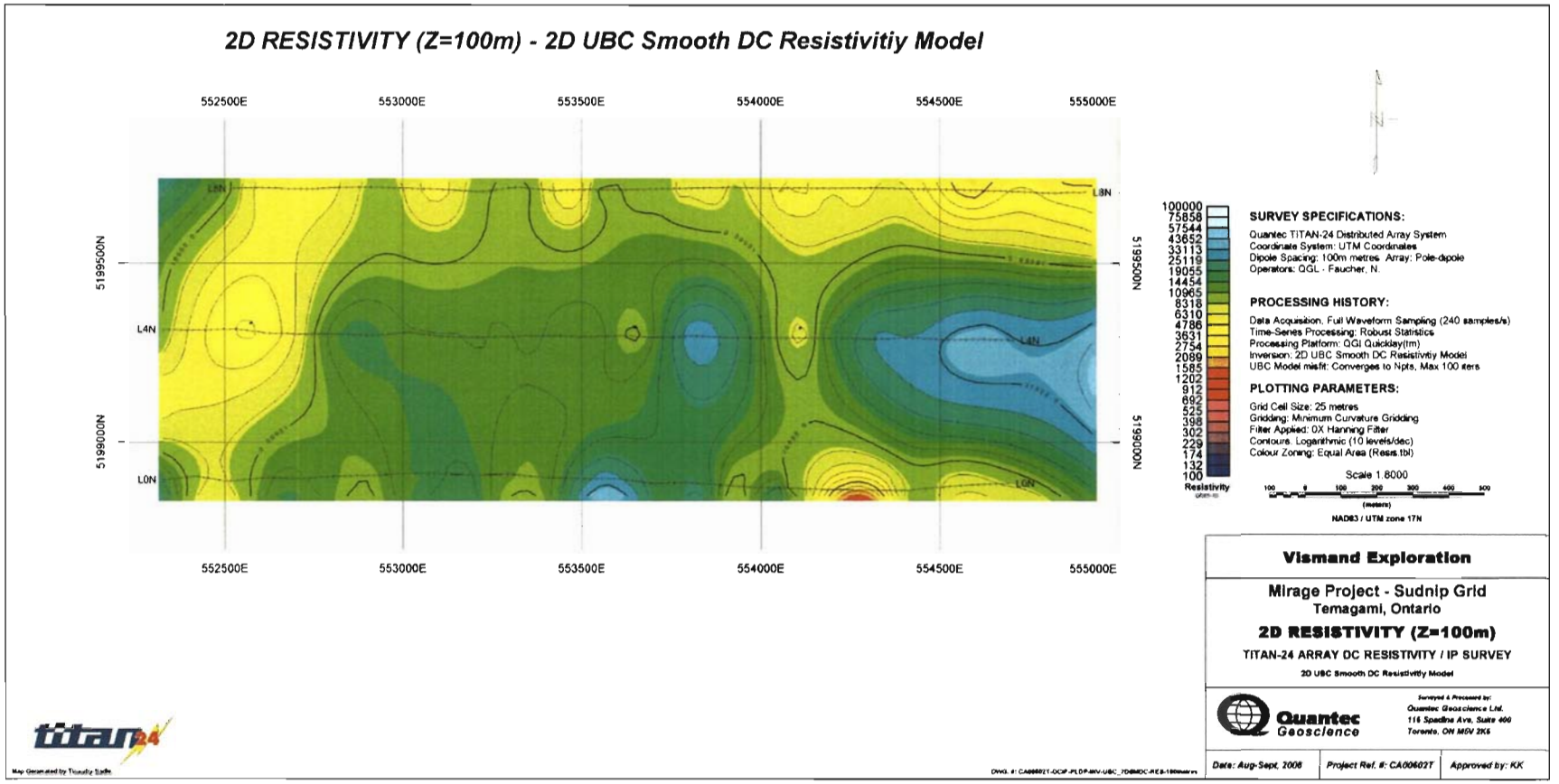

2D Resistivity (Z=200m) – 2D UBC Smooth DC Resistivity Model

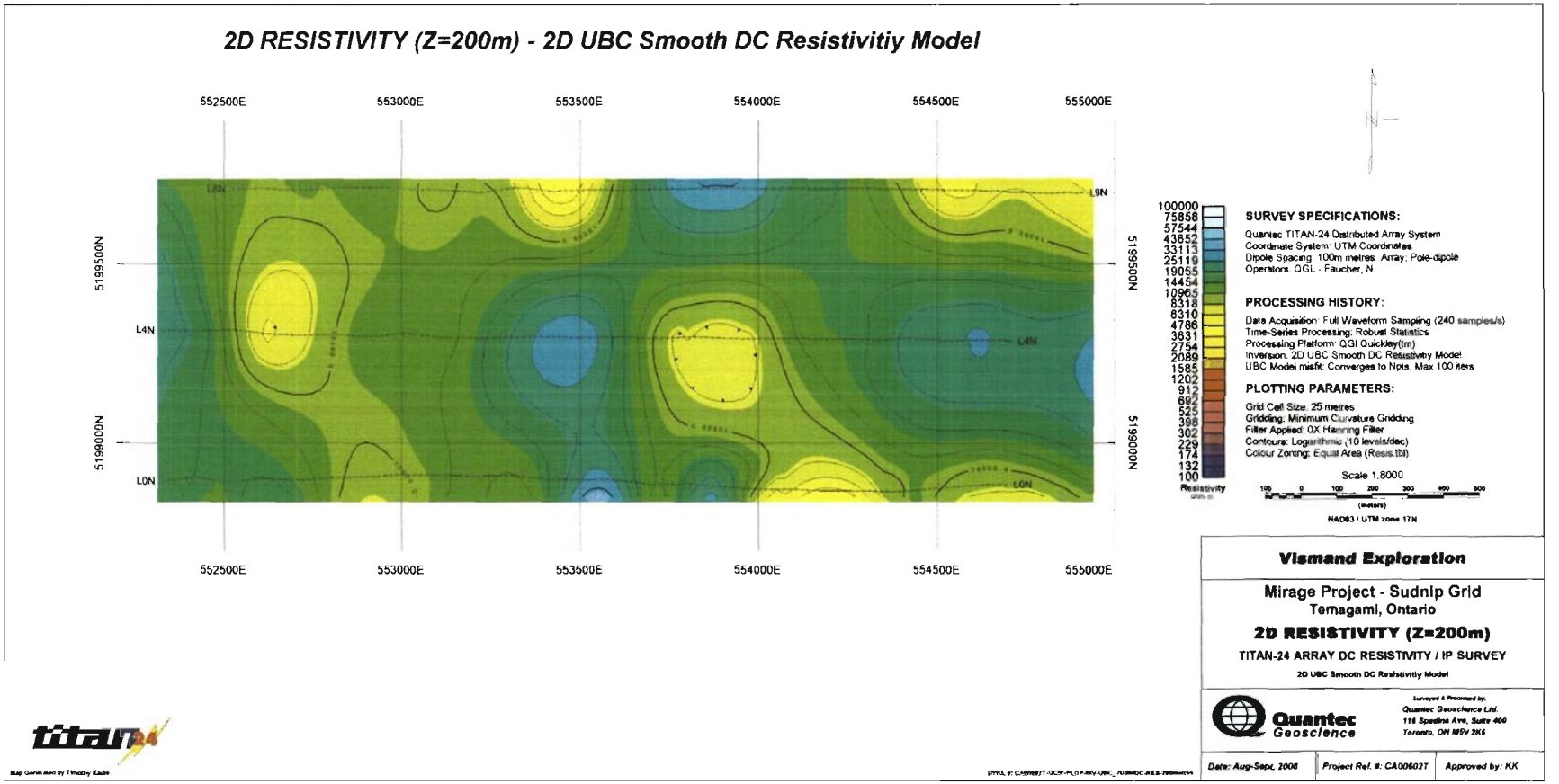

2D Resistivity (Z=400m) – 2D UBC Smooth DC Resistivity Model

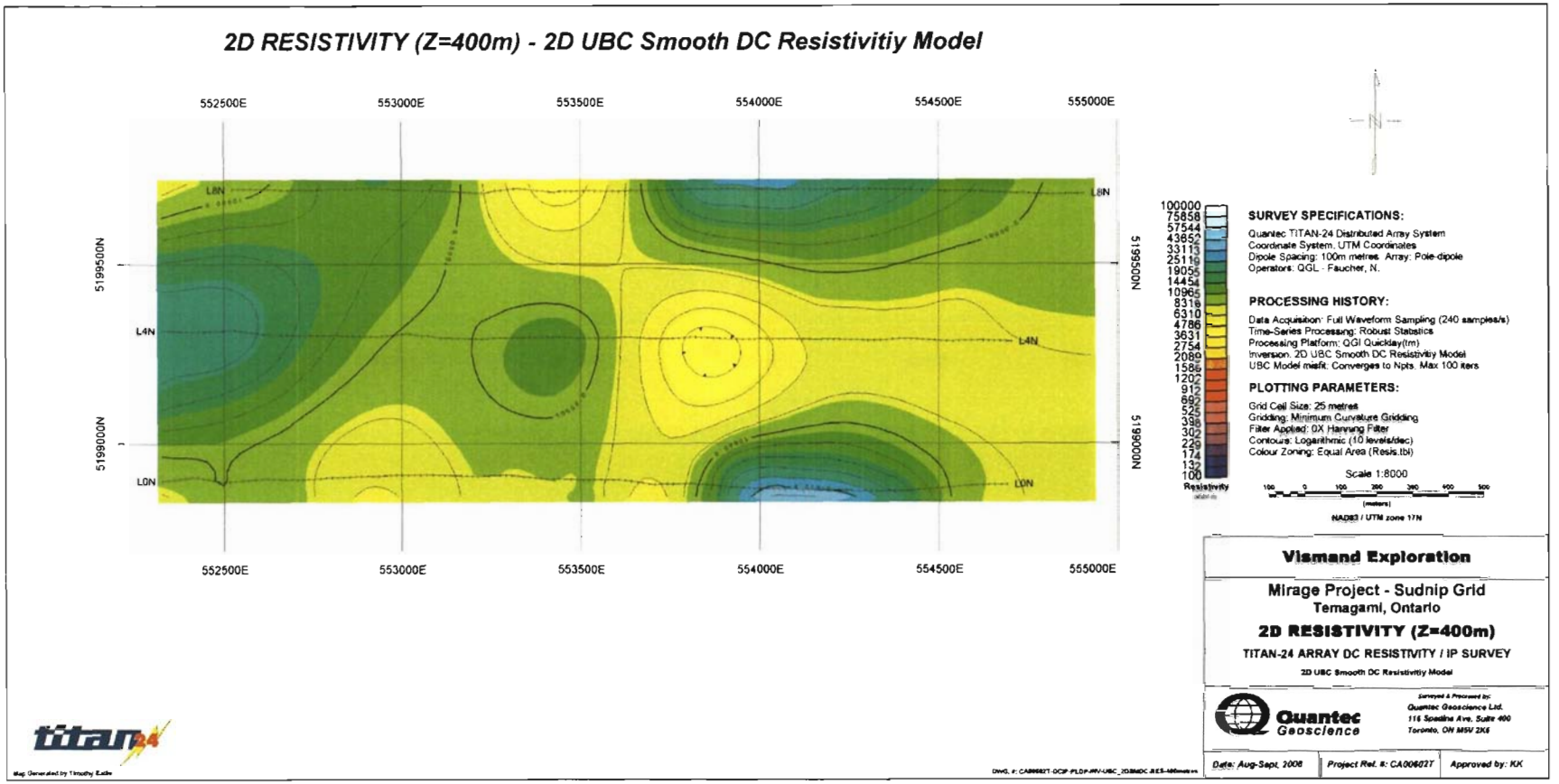

2D Chargeability (Z=50m) – 2D UBC Smooth IP Chargeability Model

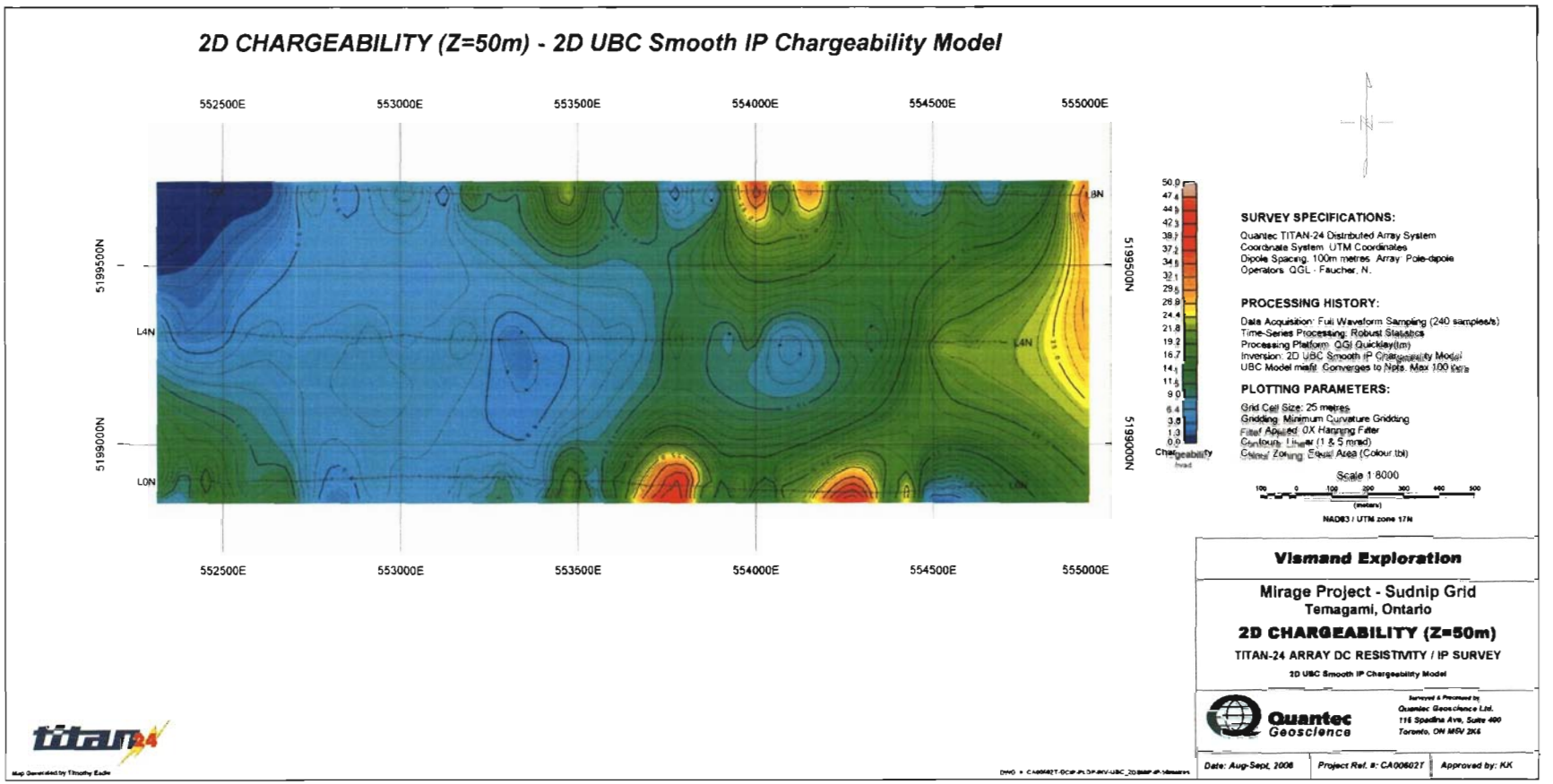

2D Chargeability (Z=100m) – 2D UBC Smooth IP Chargeability Model

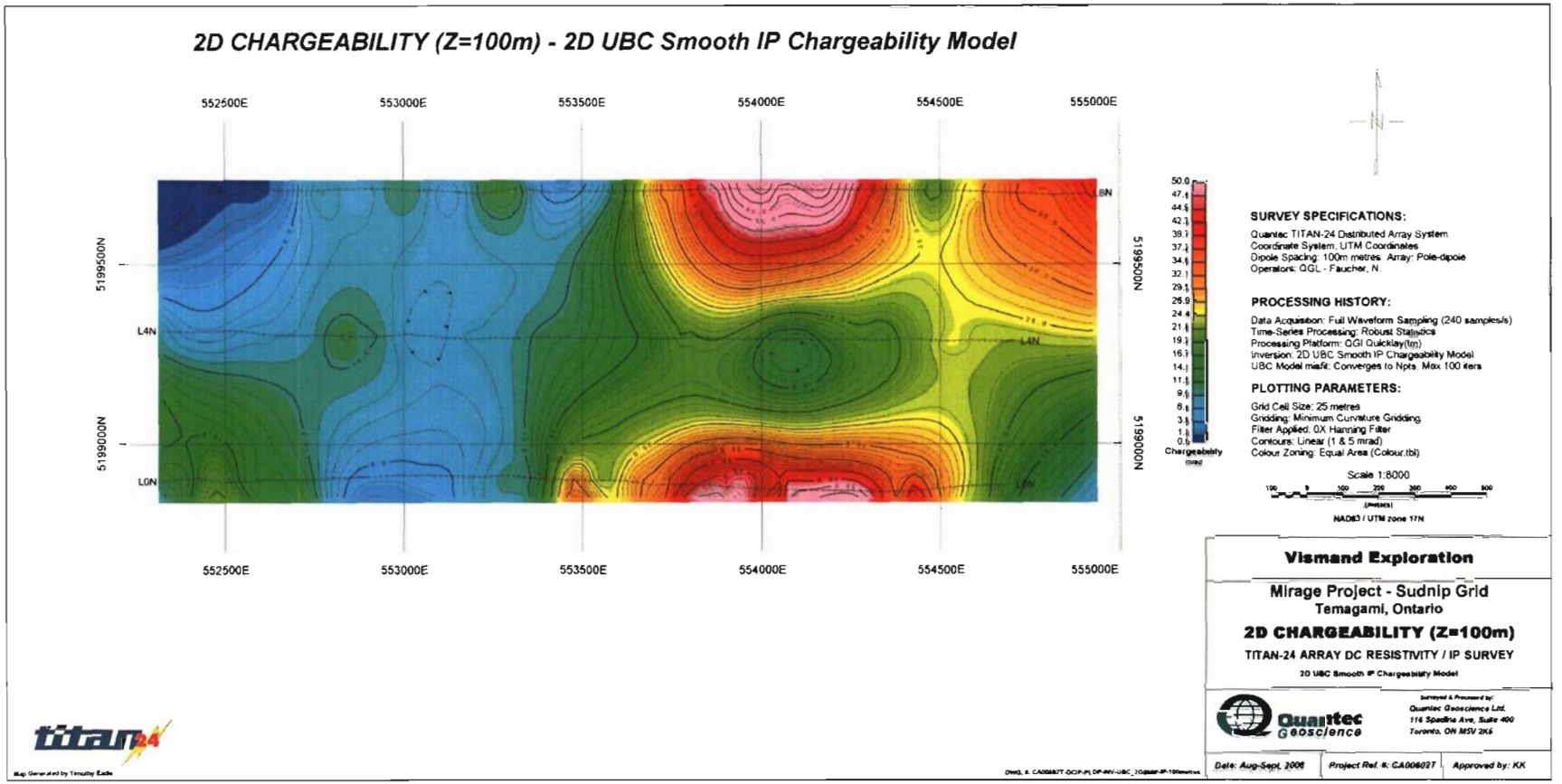

2D Chargeability (Z=200m) – 2D UBC Smooth IP Chargeability Model

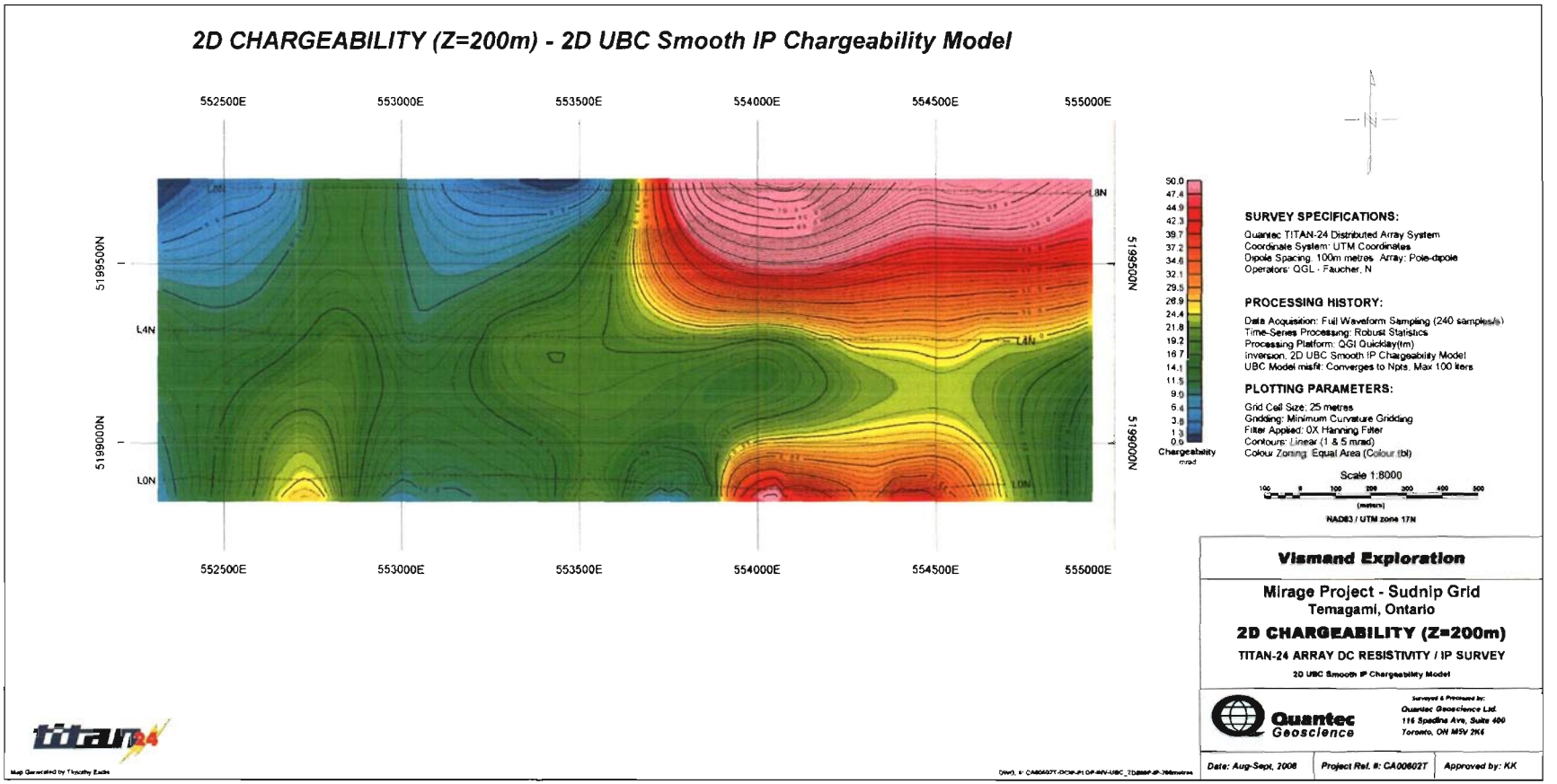

2D Chargeability (Z=400m) – 2D UBC Smooth IP Chargeability Model

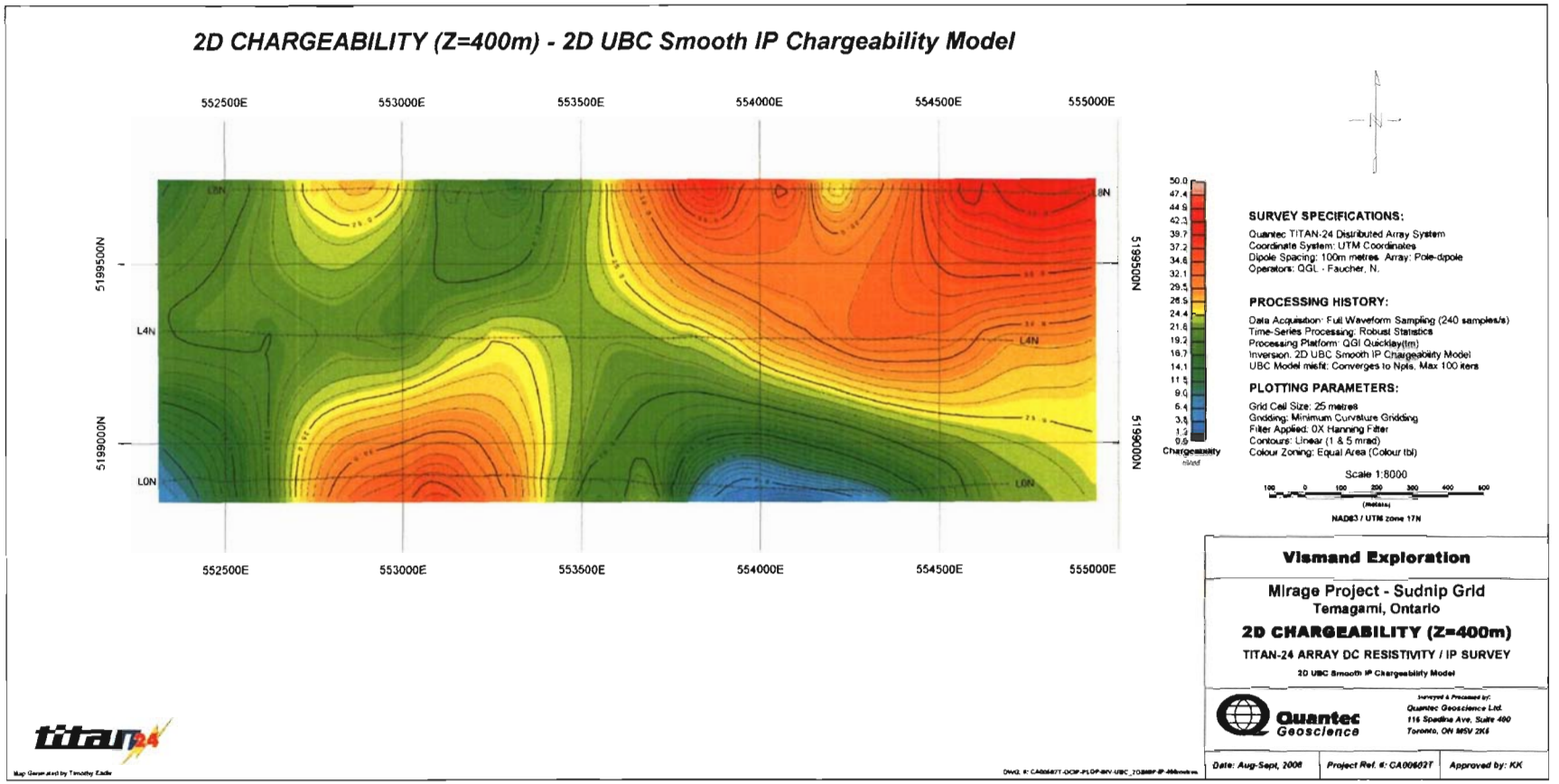

2D Chargeability (Z=50m) – 2D UBC Null Con IP Chargeability Model

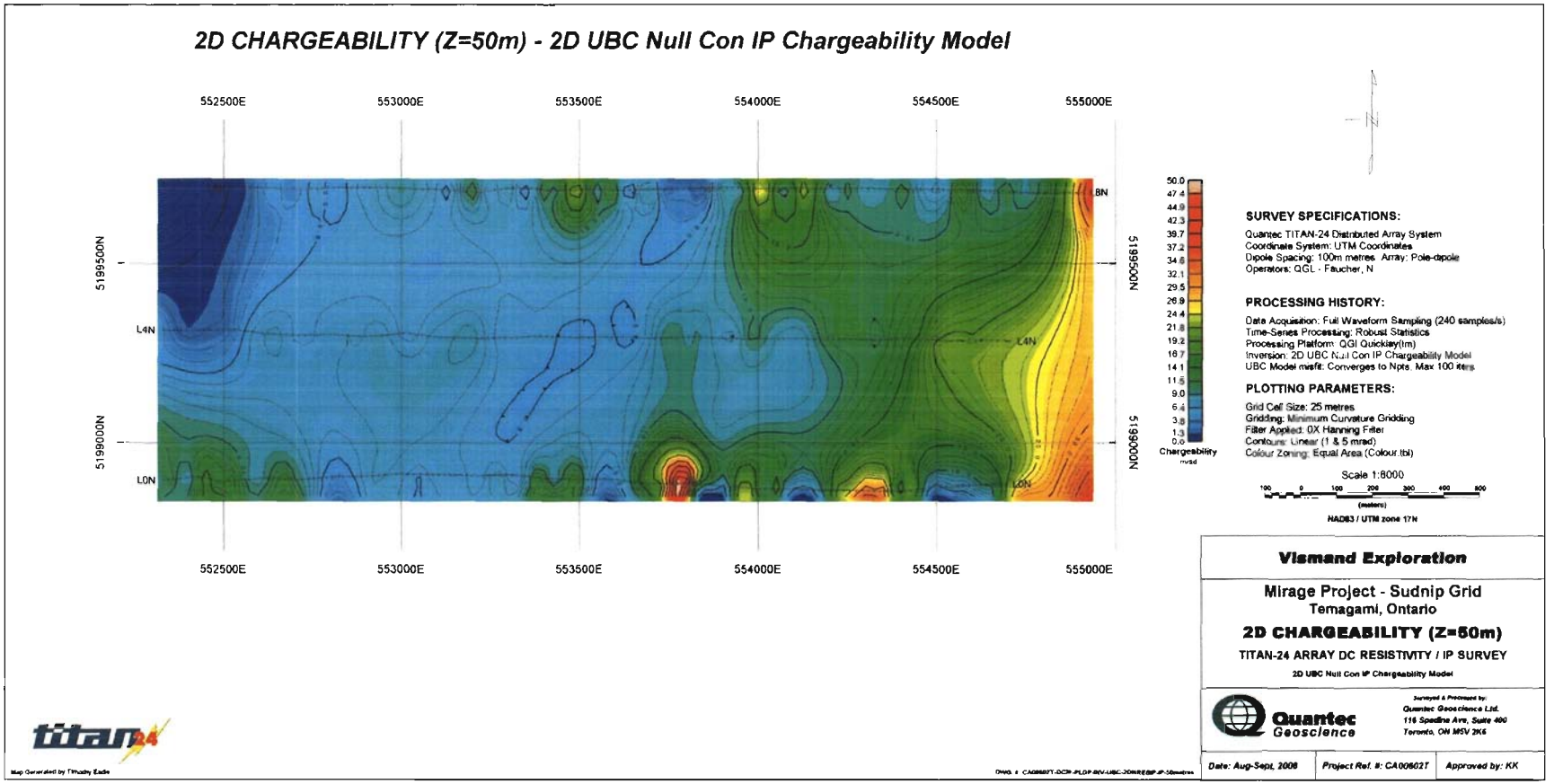

2D Chargeability (Z=100m) – 2D UBC Null Con IP Chargeability Model

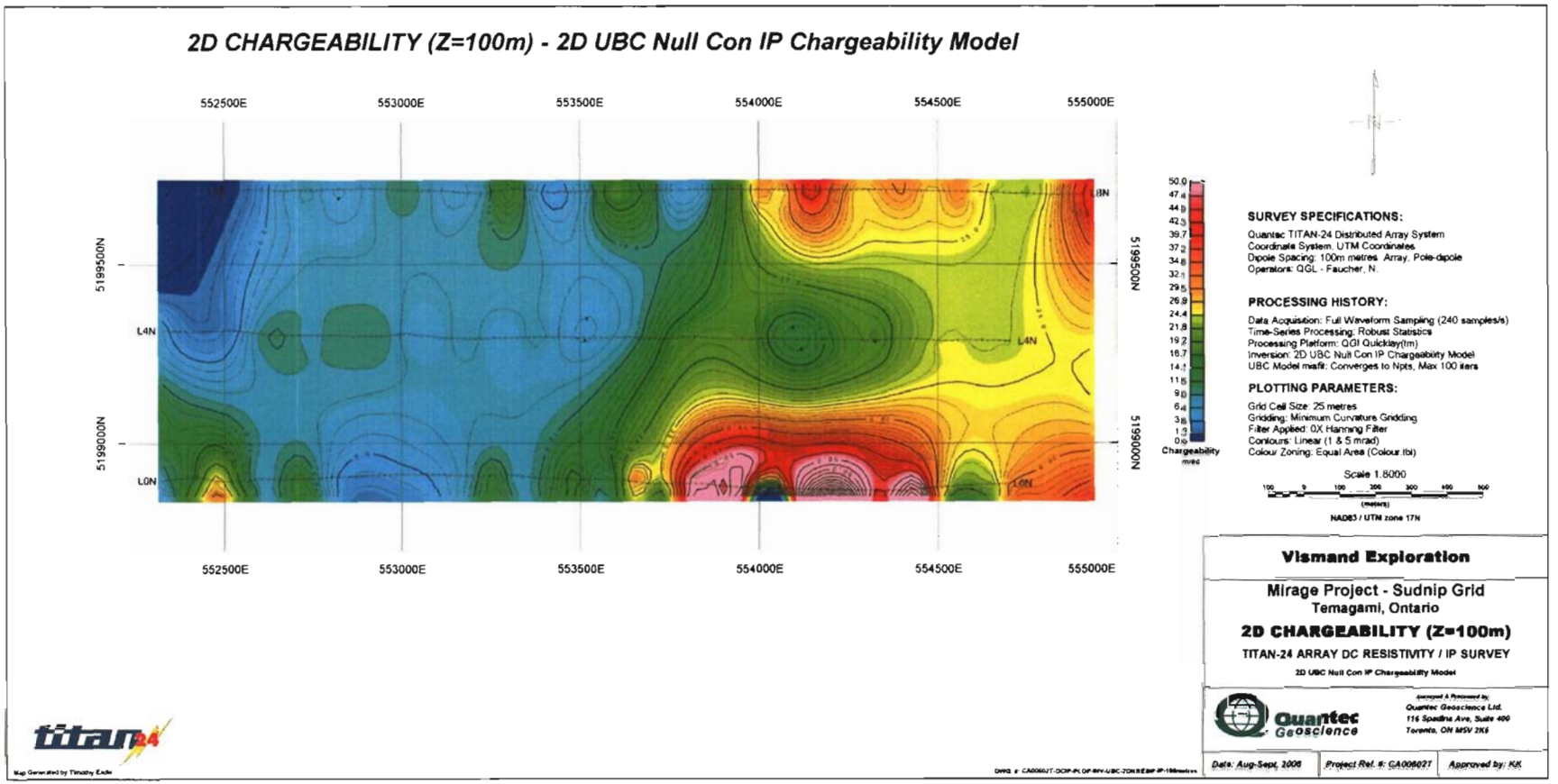

2D Chargeability (Z=200m) – 2D UBC Null Con IP Chargeability Model

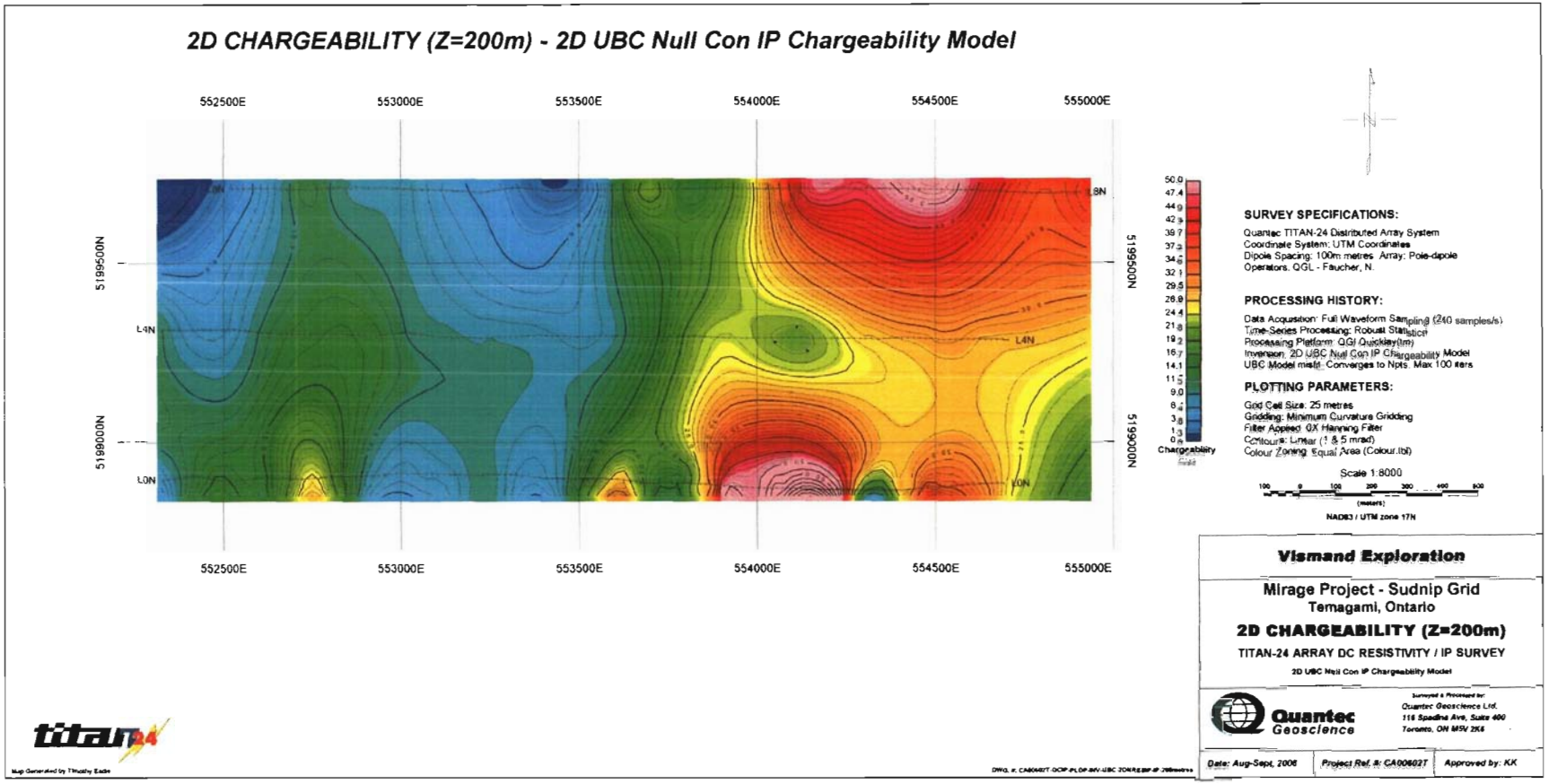

2D Chargeability (Z=400m) – 2D UBC Null Con IP Chargeability Model

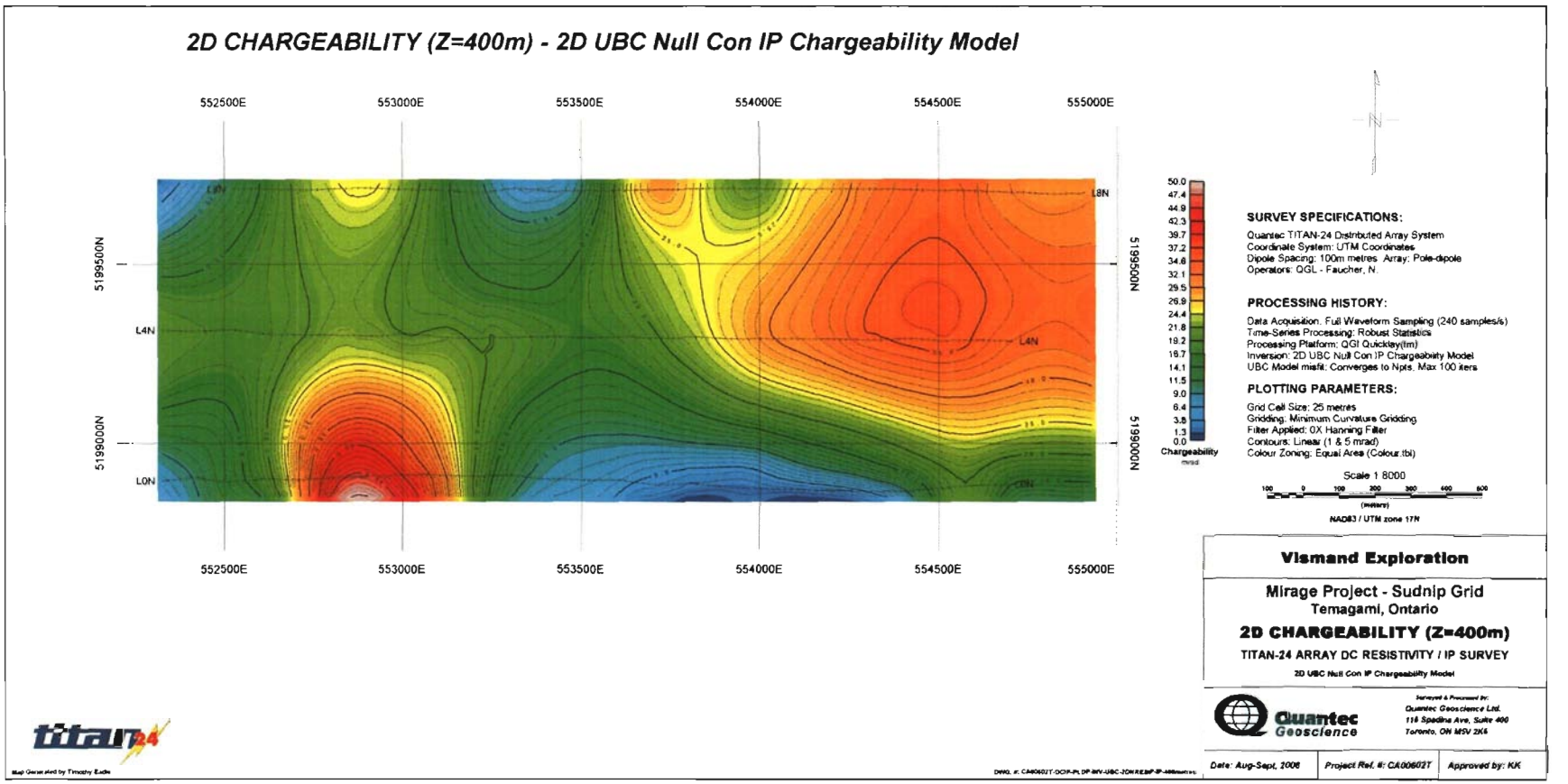

2D Resistivity (Z=50m) – 2D MT PW TM+TE(phs) Inversion (starting from 1000 ohm-m halfspace)

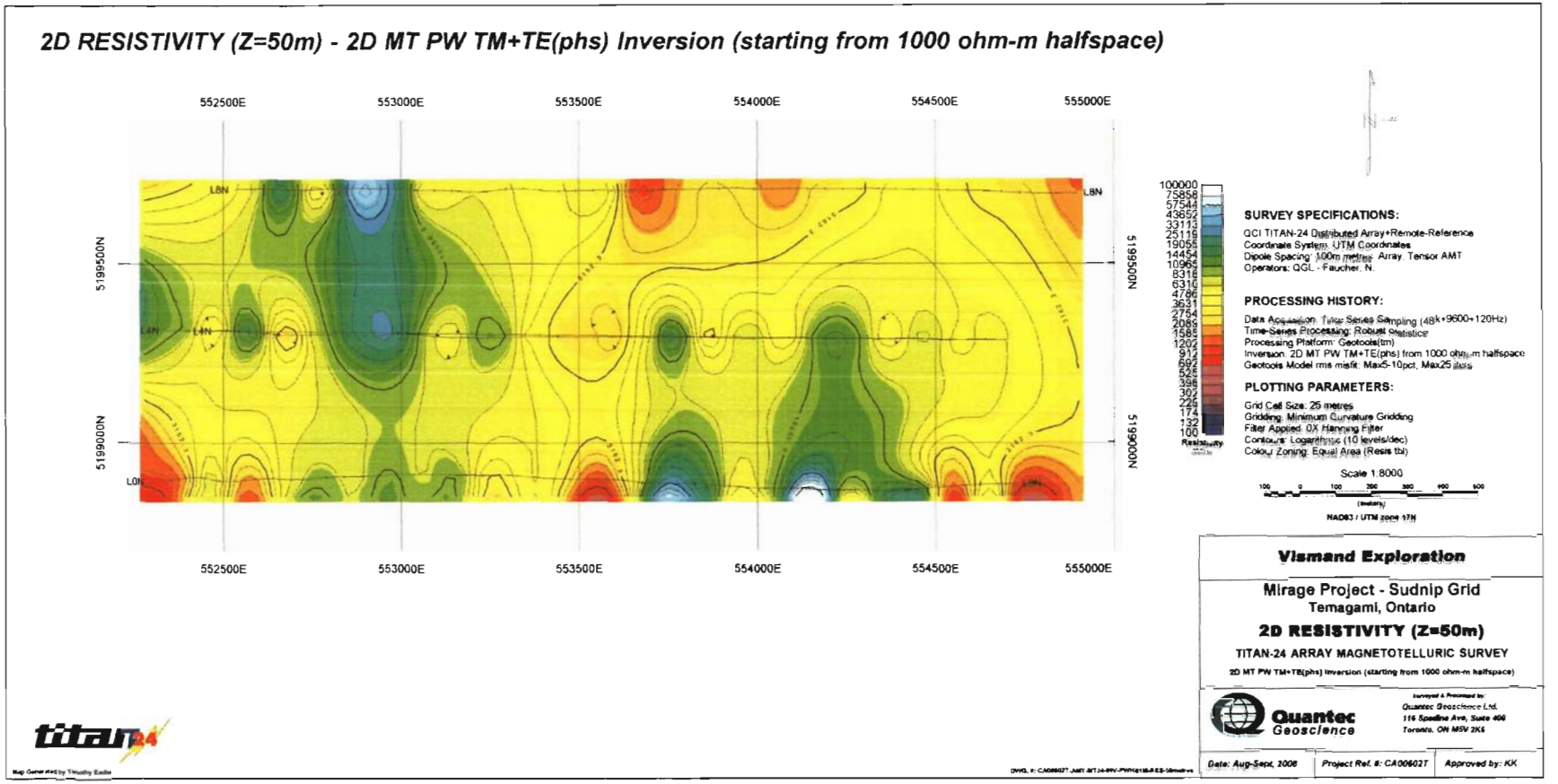

2D Resistivity (Z=100m) – 2D MT PW TM+TE(phs) Inversion (starting from 1000 ohm-m halfspace)

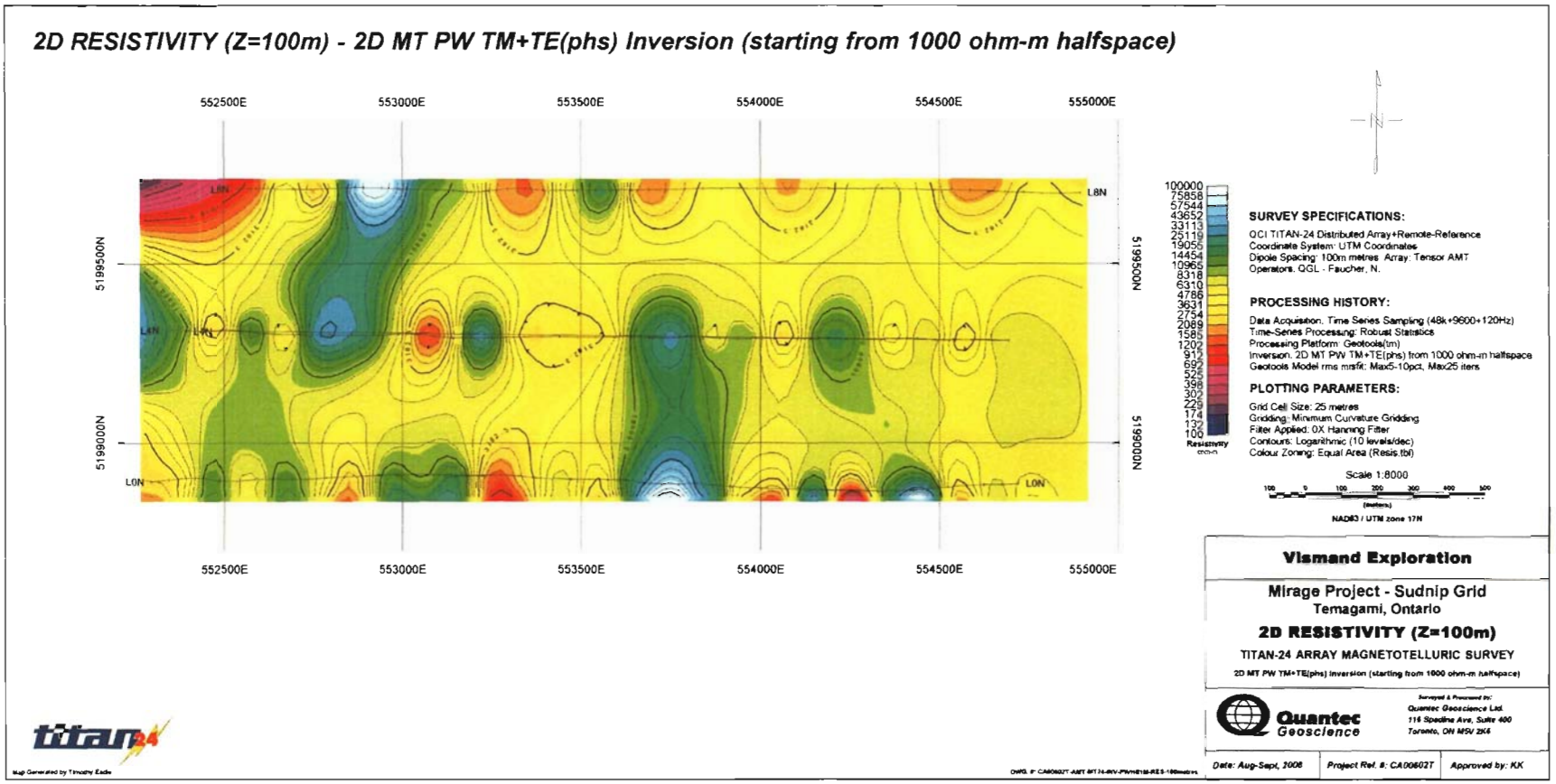

2D Resistivity (Z=200m) – 2D MT PW TM+TE(phs) Inversion (starting from 1000 ohm-m halfspace)

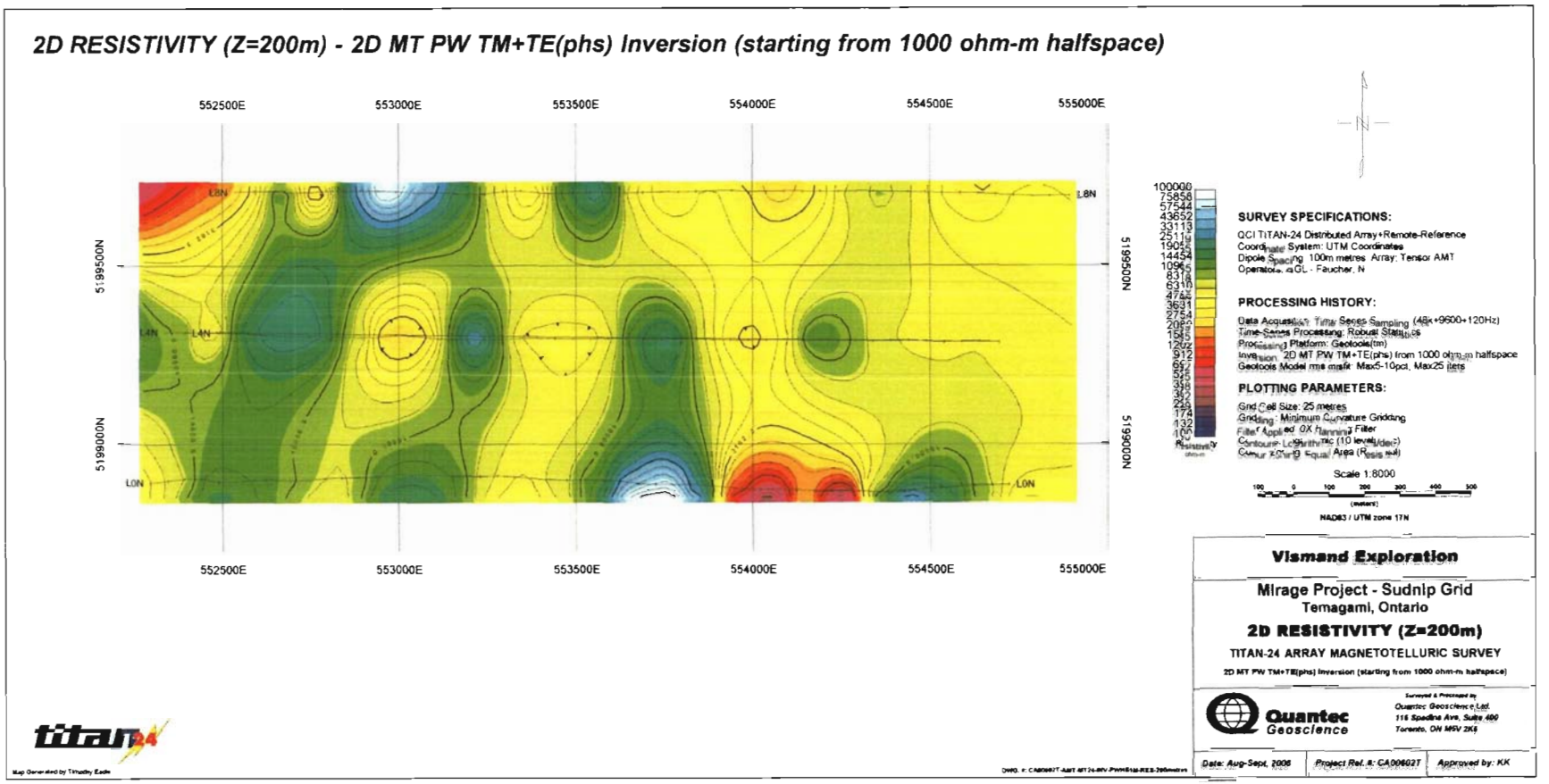

2D Resistivity (Z=400m) – 2D MT PW TM+TE(phs) Inversion (starting from 1000 ohm-m halfspace)

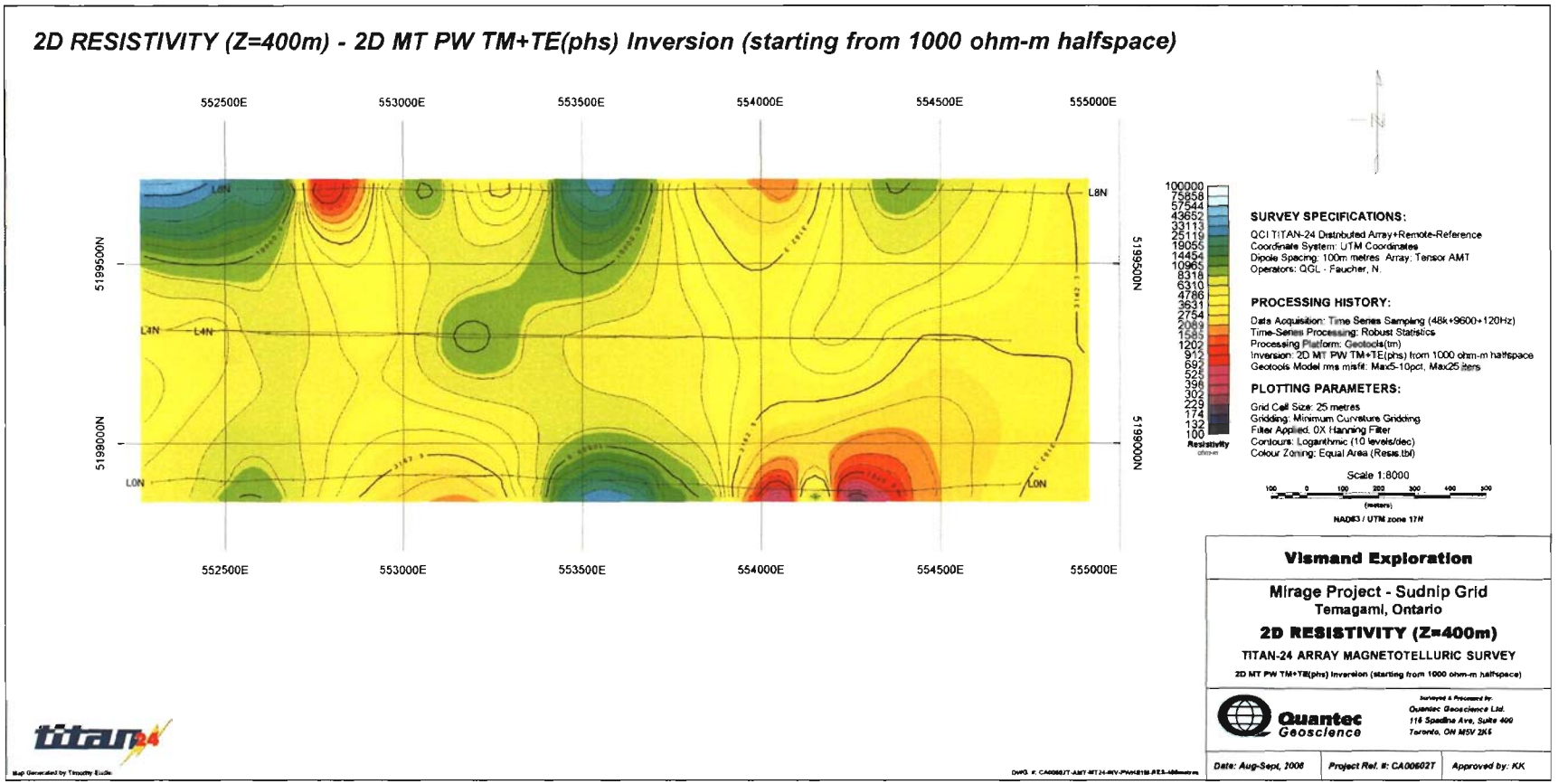

2D Resistivity (Z=1000m) – 2D MT PW TM+TE(phs) Inversion (starting from 1000 ohm-m halfspace)

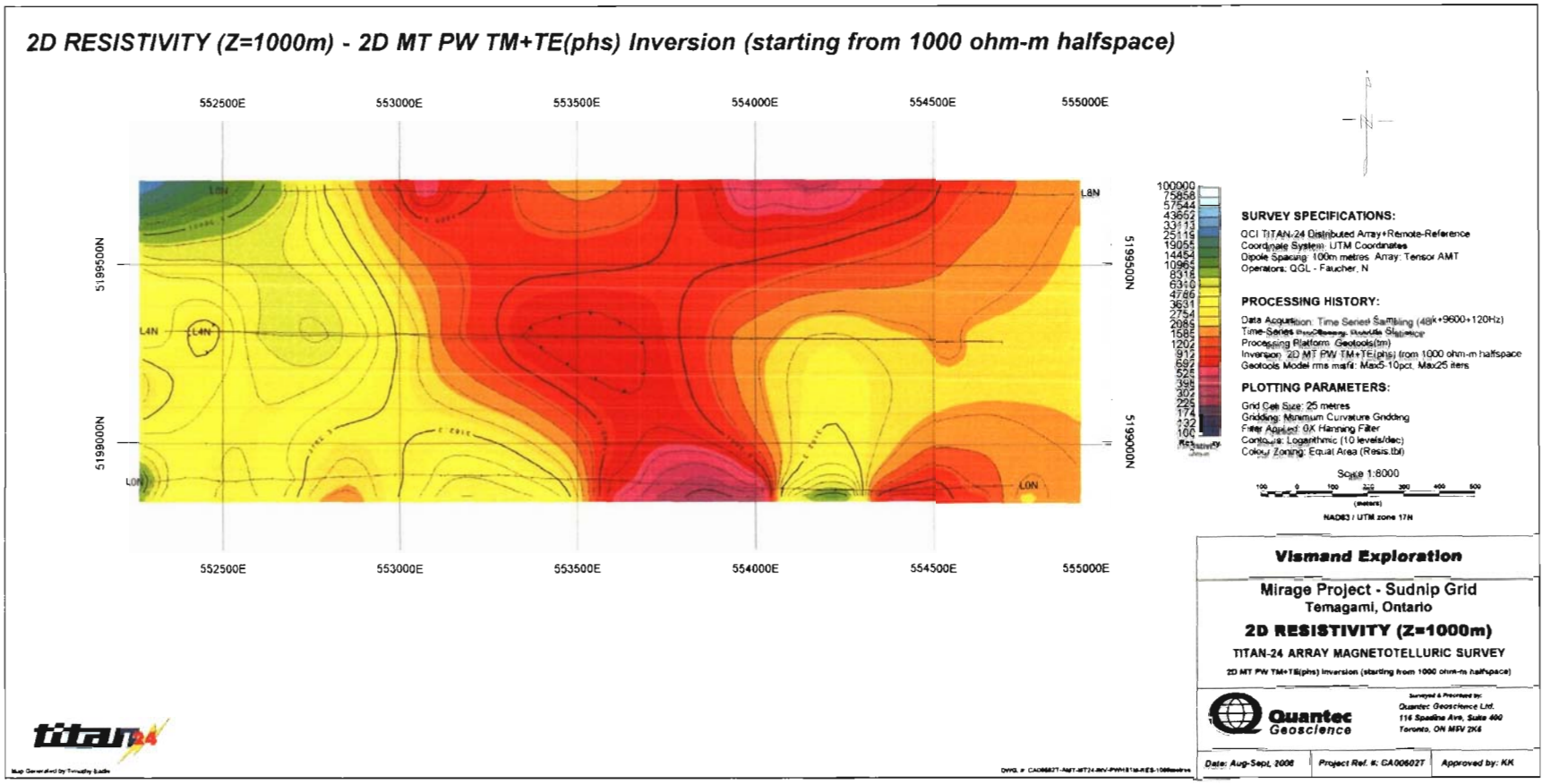

Zit Grid

Line 0E – 2D UBC Smooth DC Resistivity Model

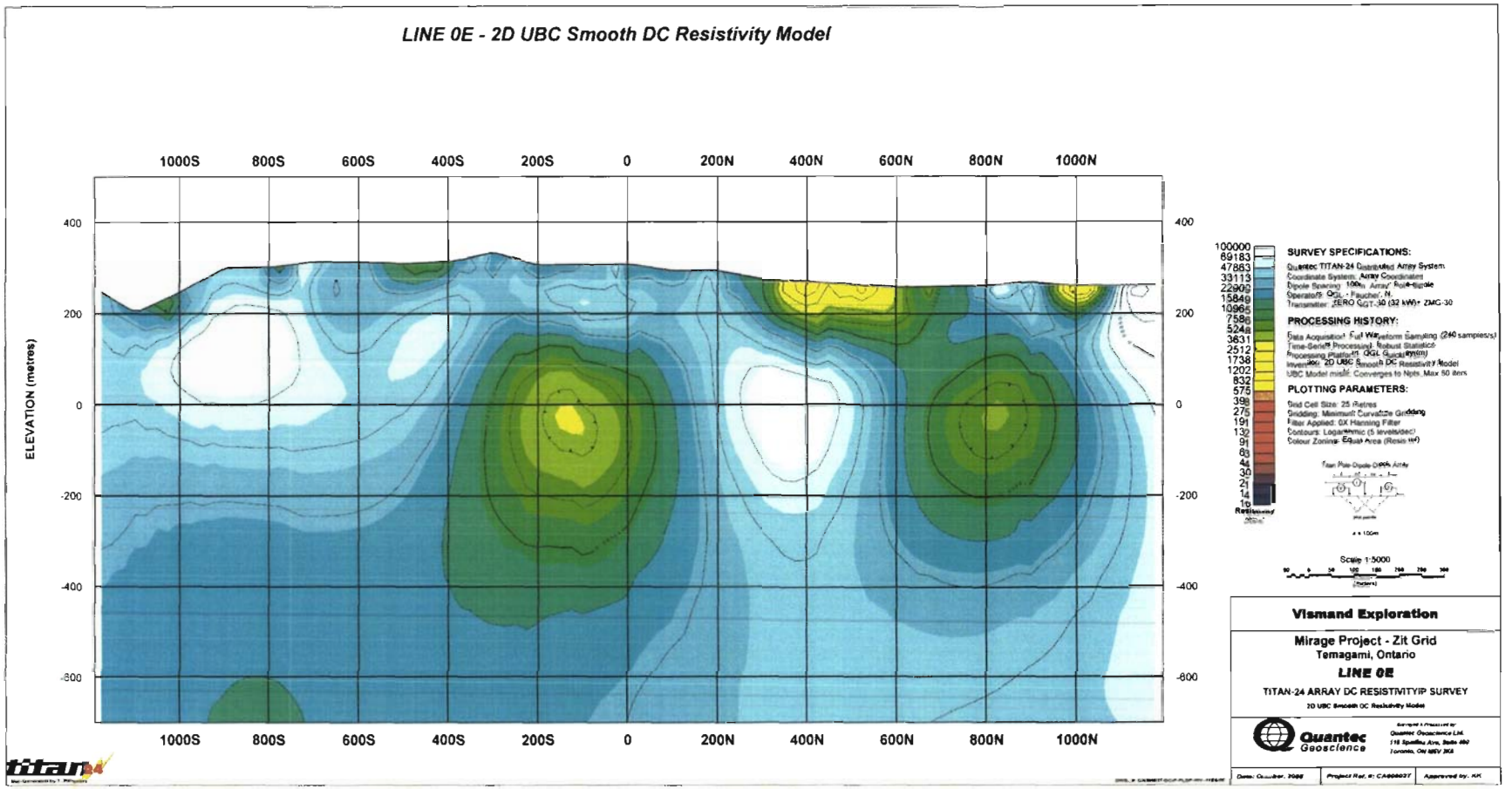

Line 0E – 2D UBC Smooth IP Chargeability Model

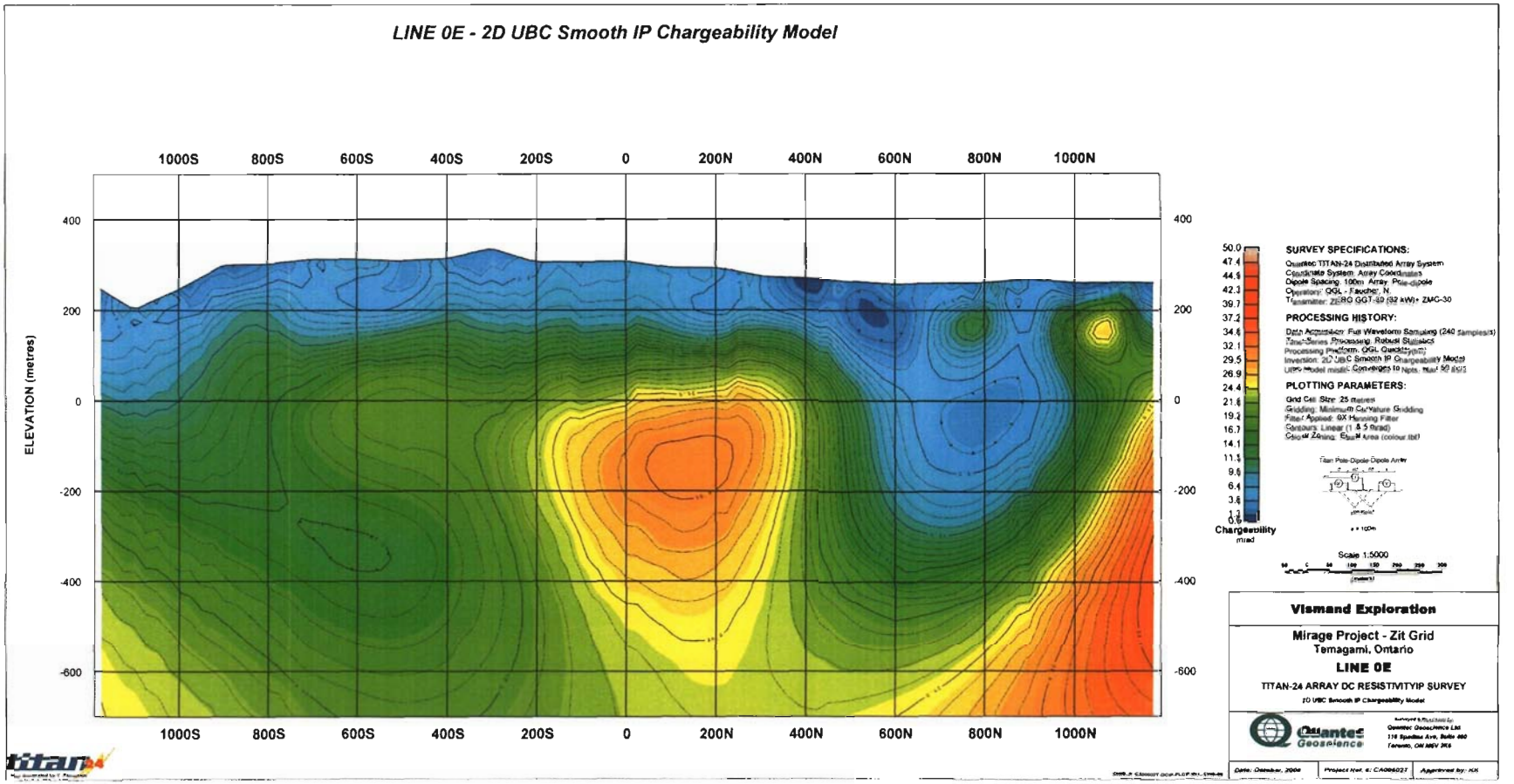

Line 0E – 2D UBC Null Con IP Chargeability Model

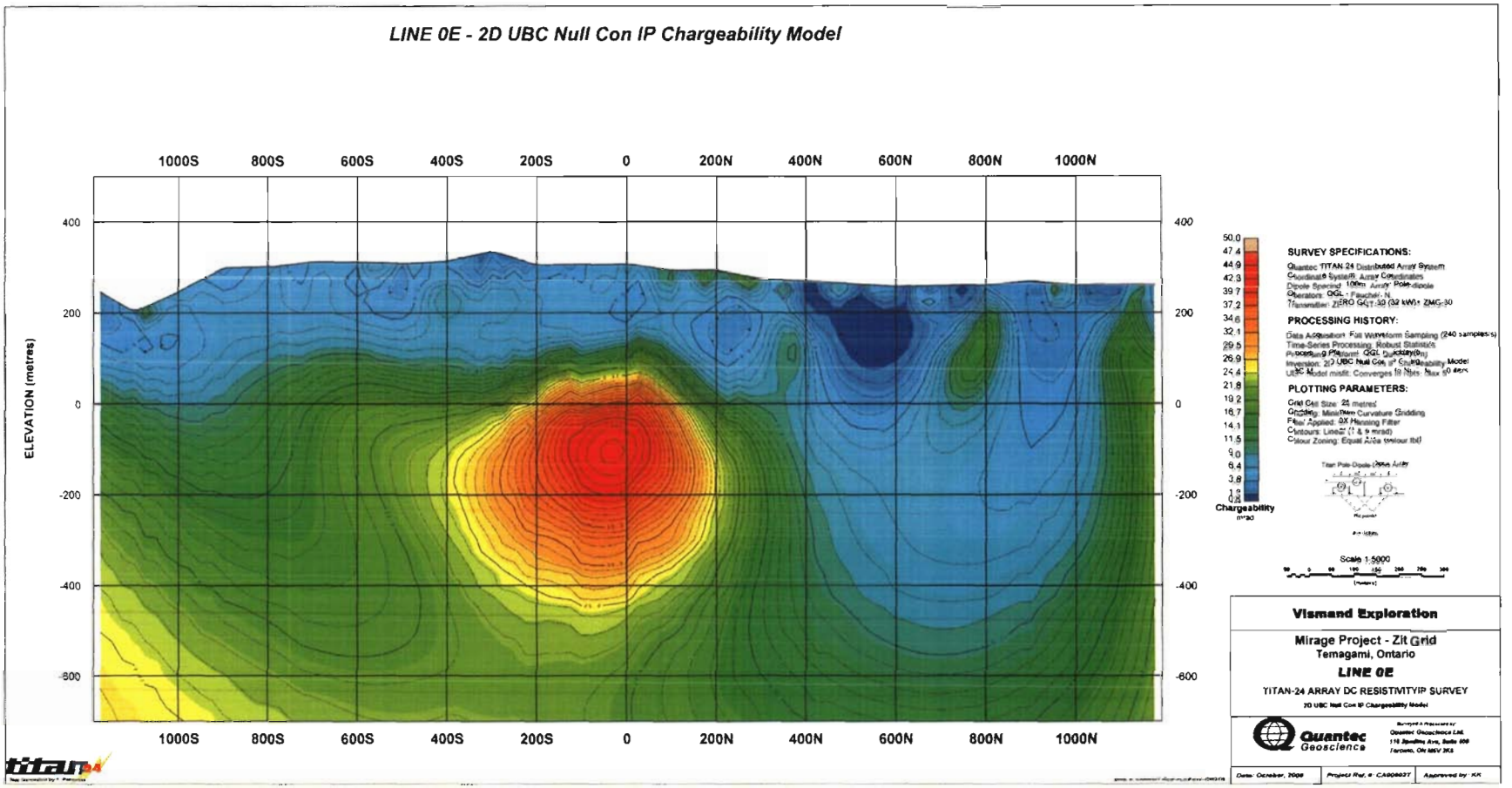

Line 0E – 2D MT PW TM+TE(phs) Sharp Inversion (starting from smooth 1D PW model)

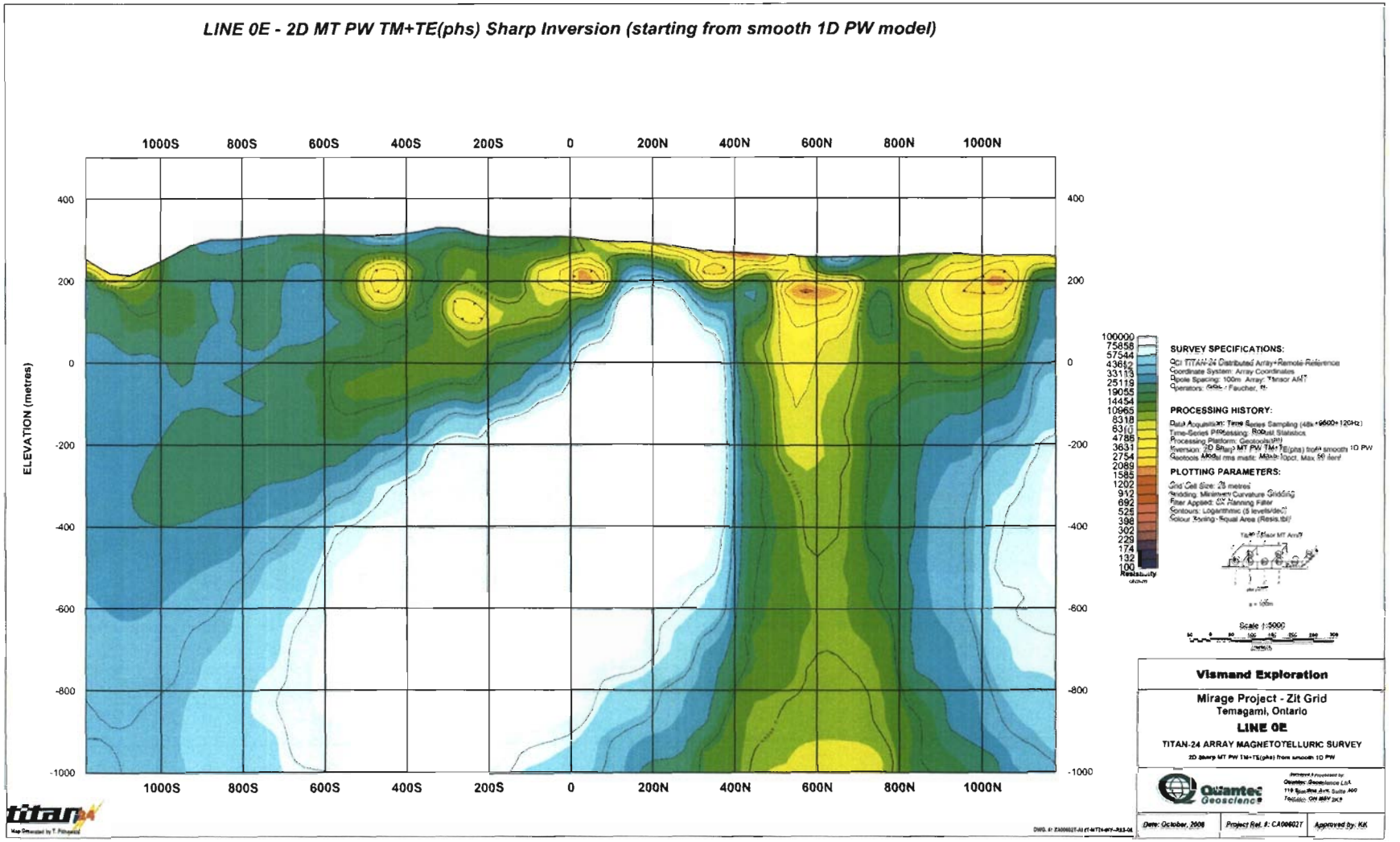

Line 0E – 2D MT PW TM+TE Sharp Inversion (starting from smooth 1D PW model)

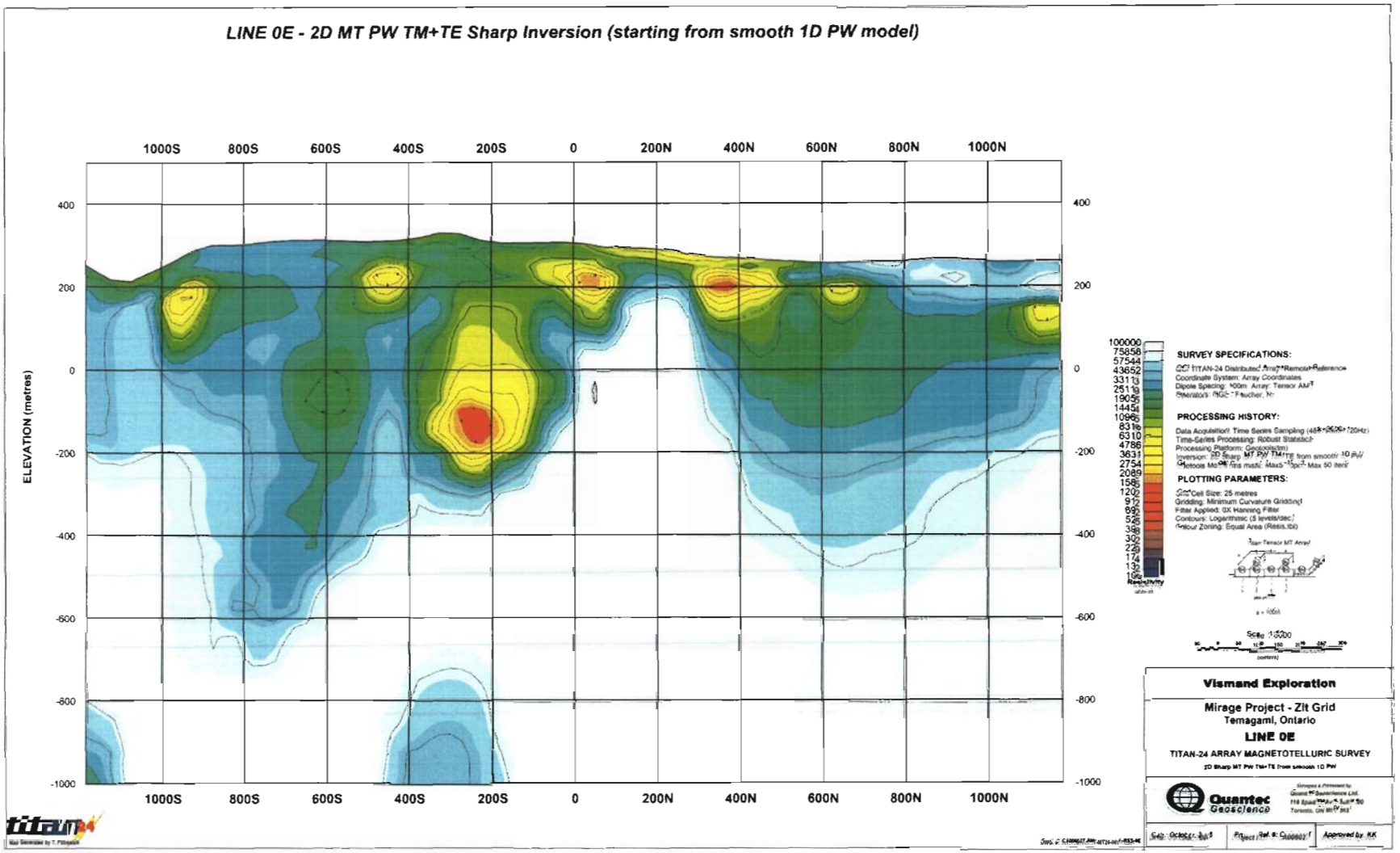

Line 0E – 2D MT PW TM+TE(phs) Inversion (starting from 1000 ohm-m halfspace)

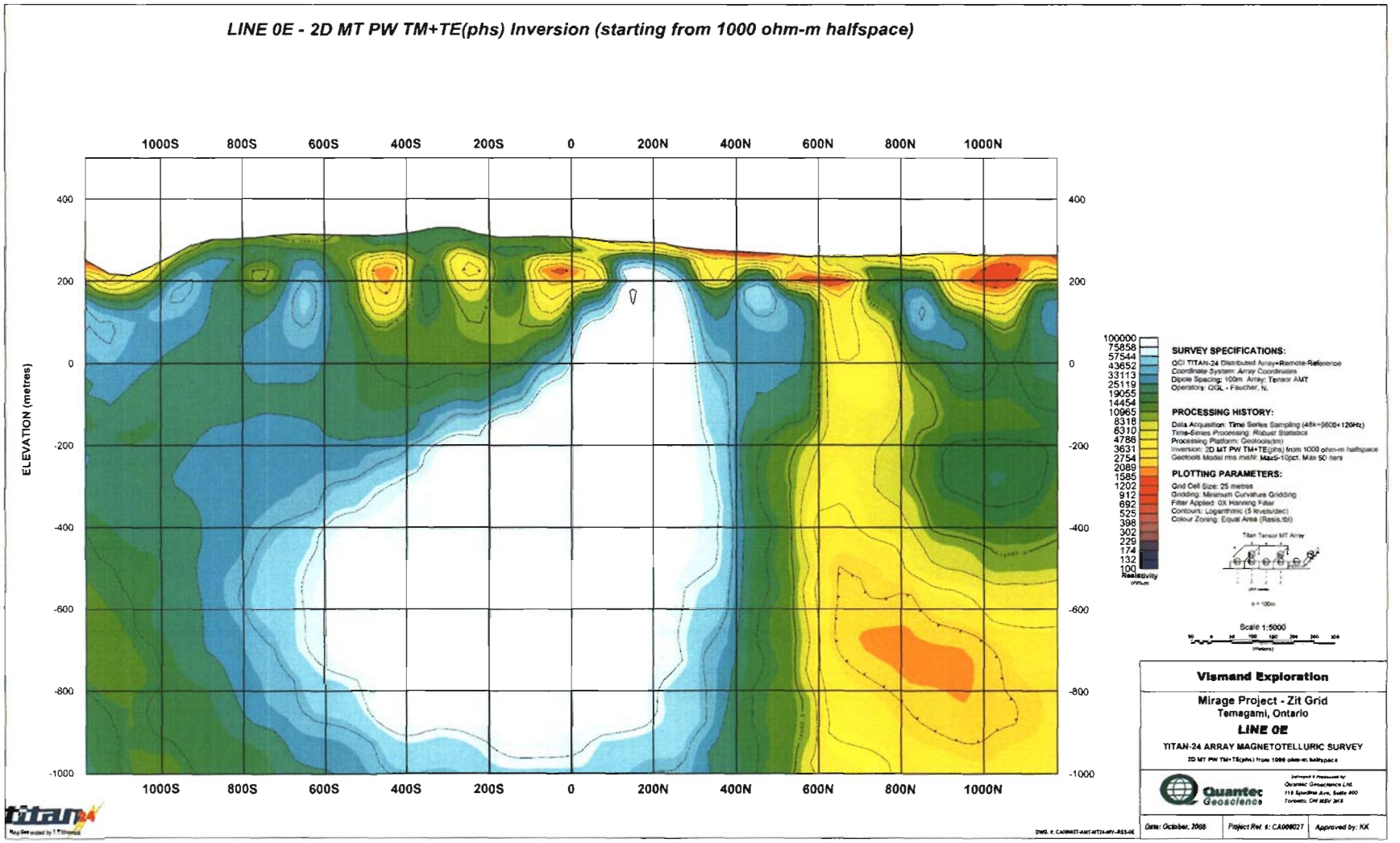

Line 0E – 2D MT PW TM+TE Inversion (starting from 1000 ohm-m halfspace)

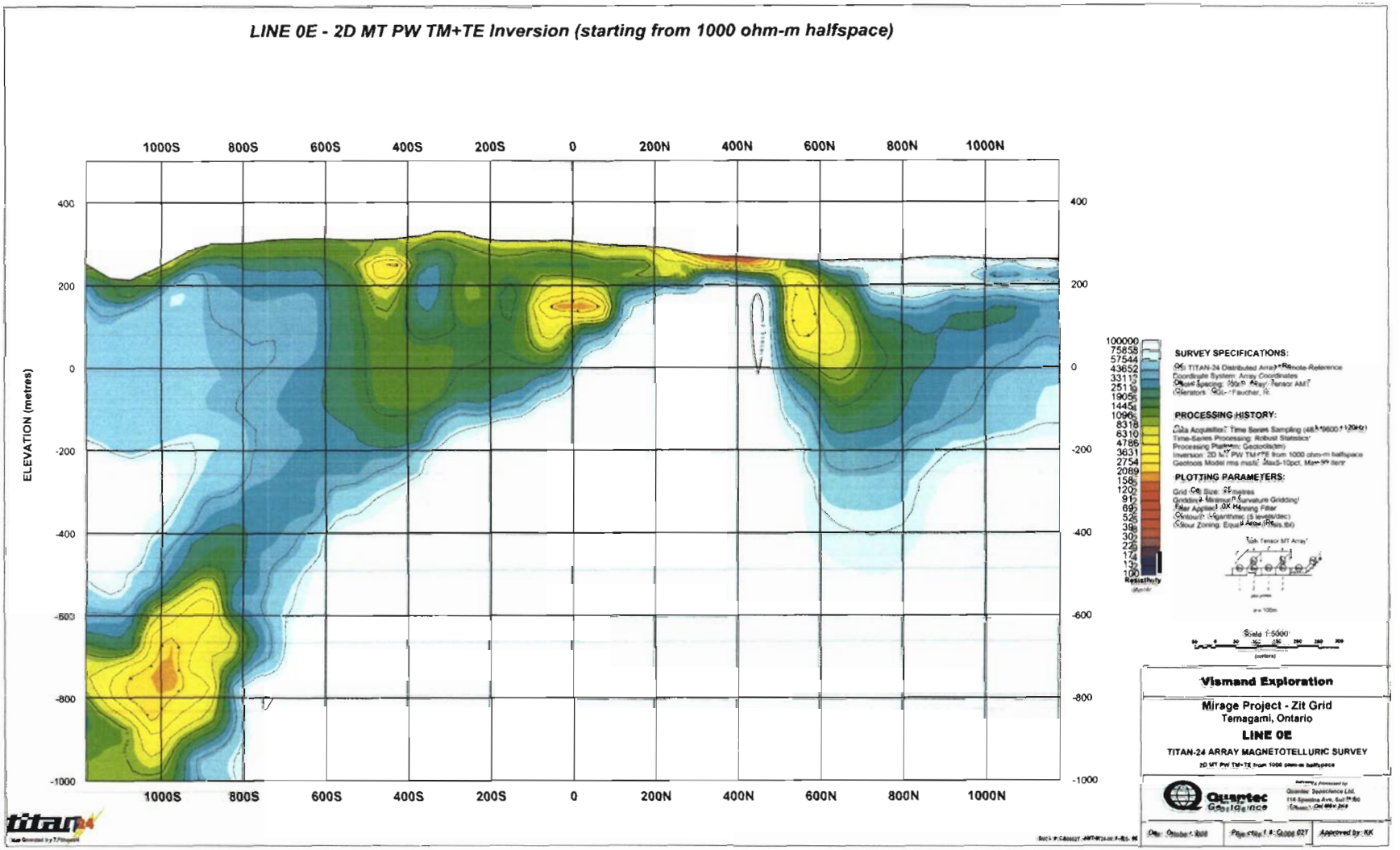

Line 0E – 2D MT RLM TM+TE(phs) Inversion (starting from 1D Det model)

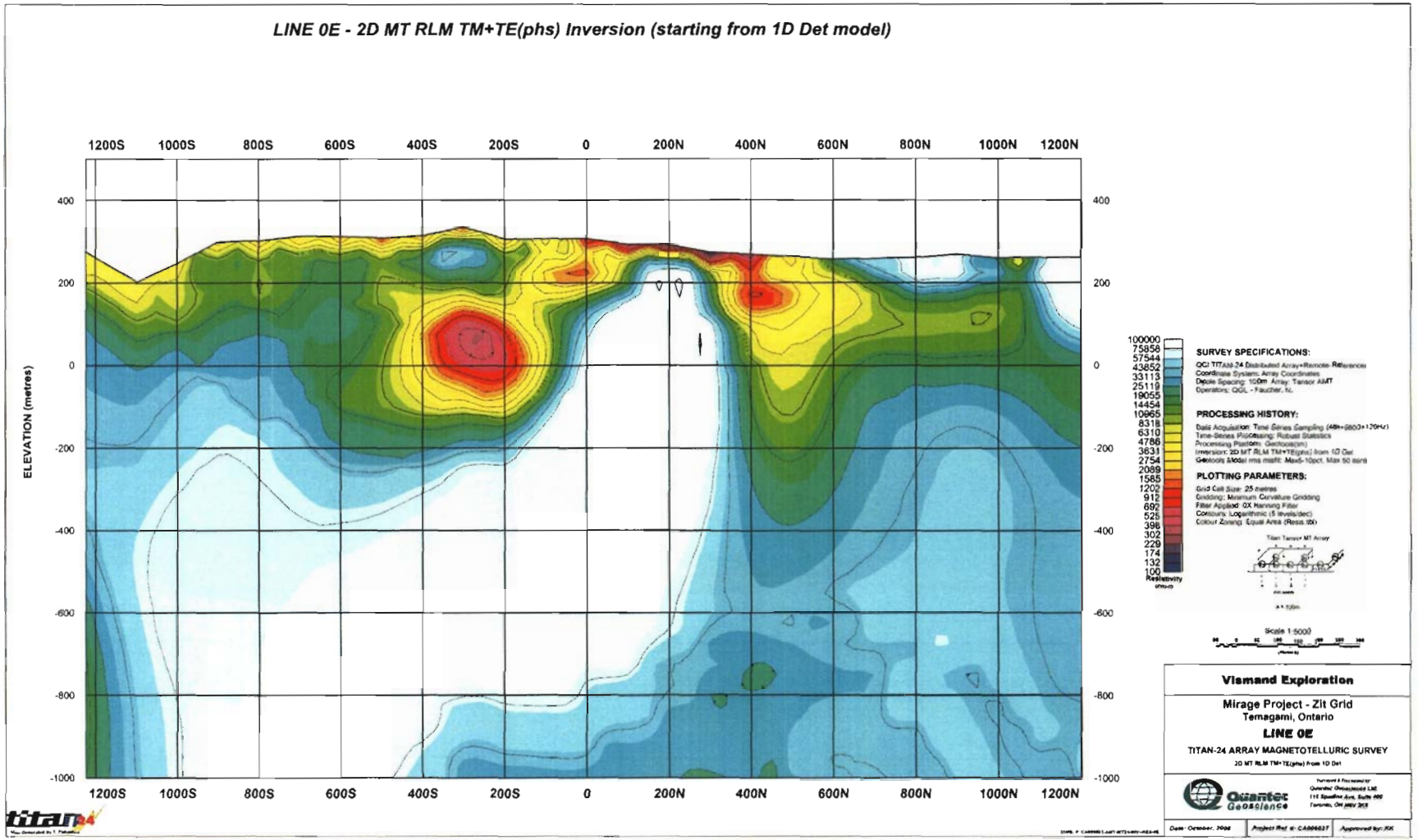

Line 0E – 2D MT RLM TM+TE Inversion (starting from 1D Det model)

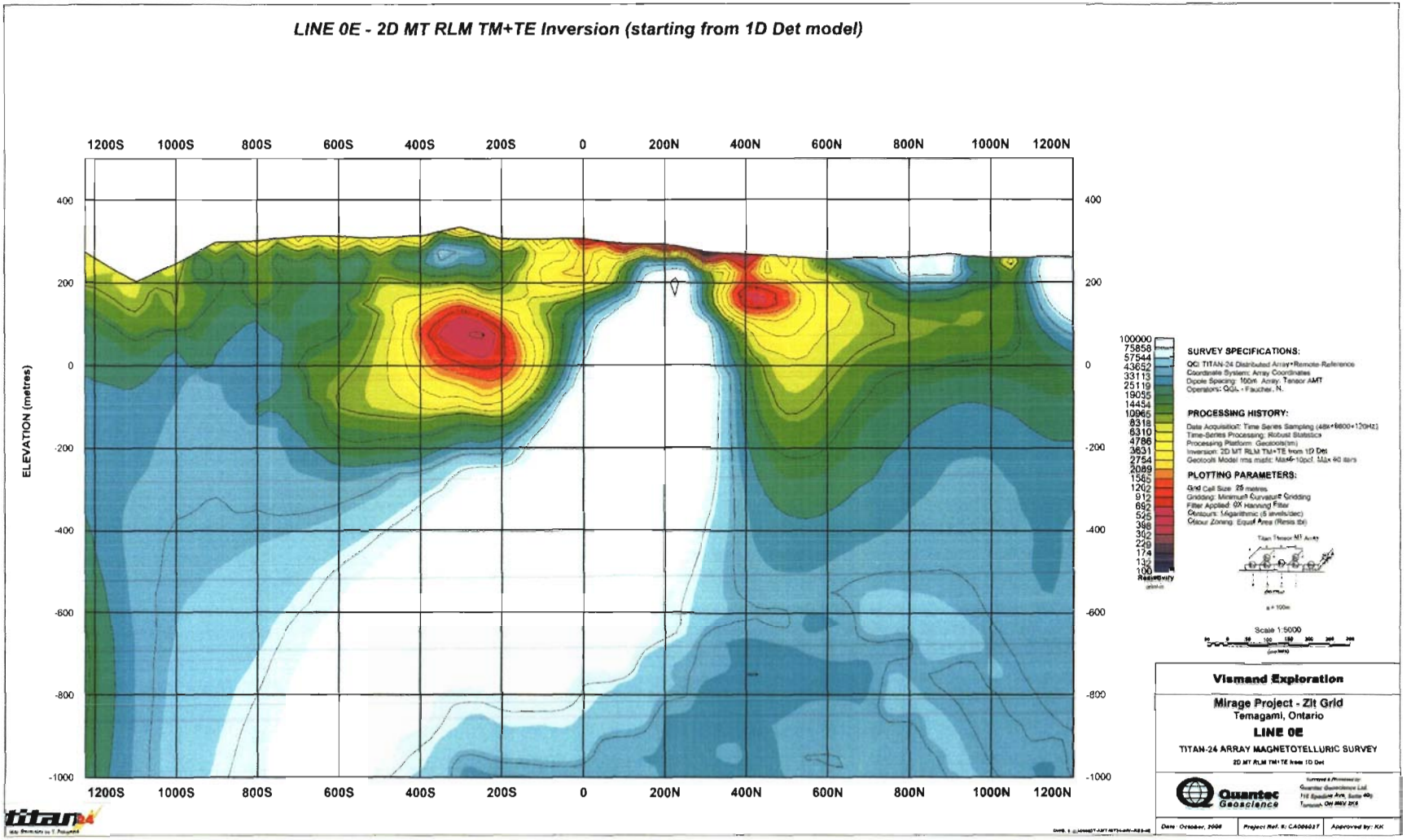

Line 0E – 2D MT RLM TM+TE(phs) Inversion (starting from 1000 ohm-m halfspace)

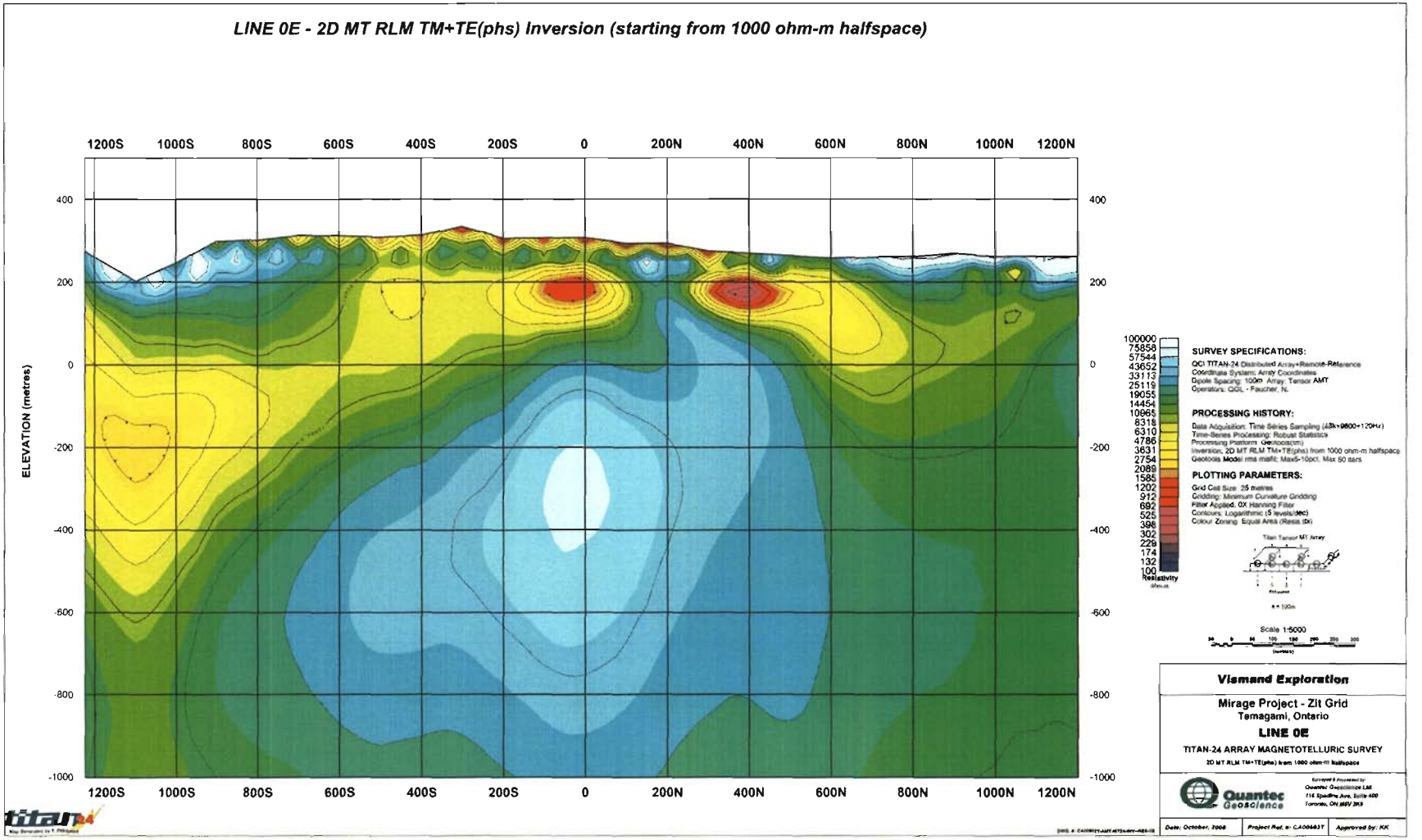

Line 0E – 2D MT RLM TM+TE Inversion (starting from 1000 ohm-m halfspace)

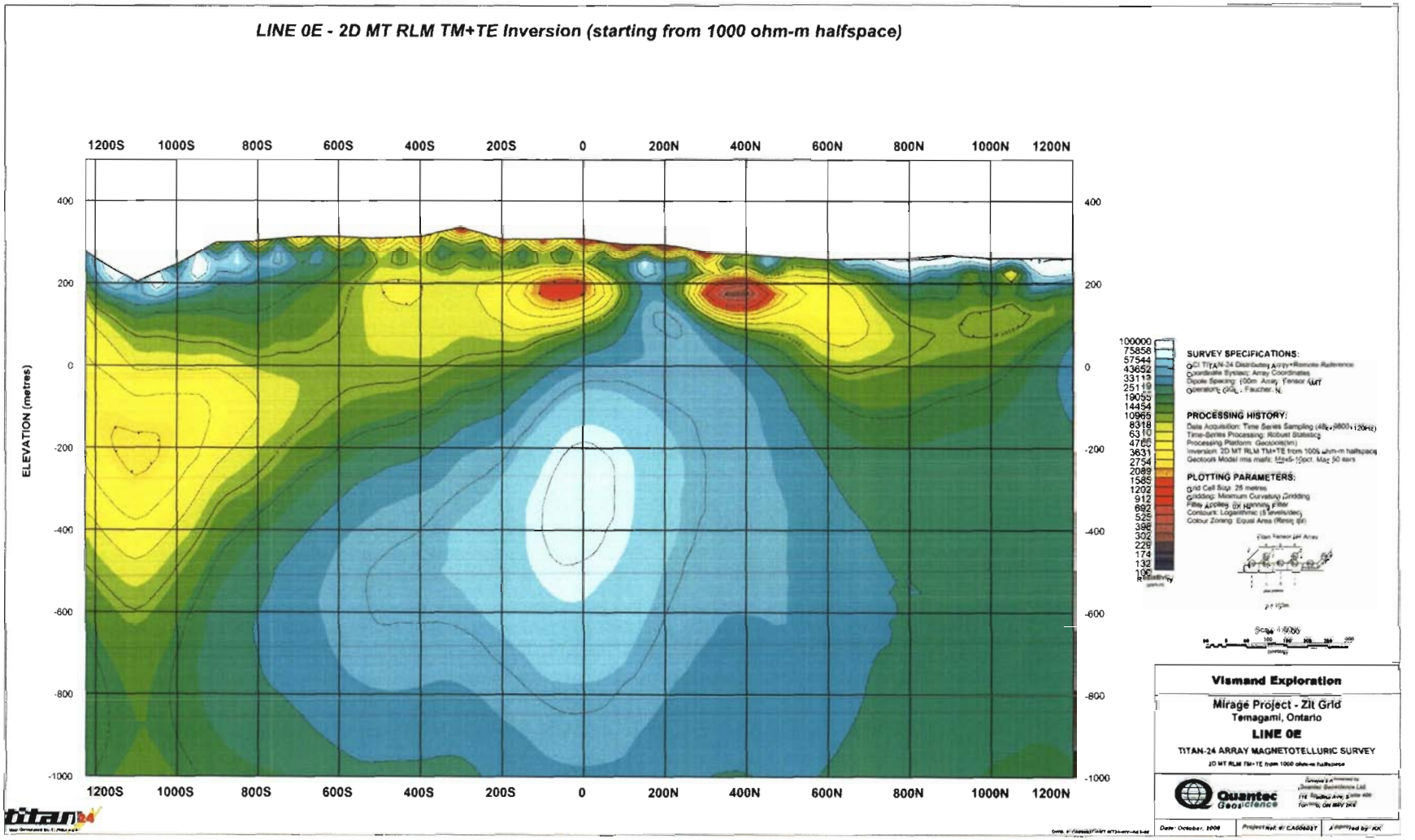

Line 375E – 2D UBC Smooth DC Resistivity Model

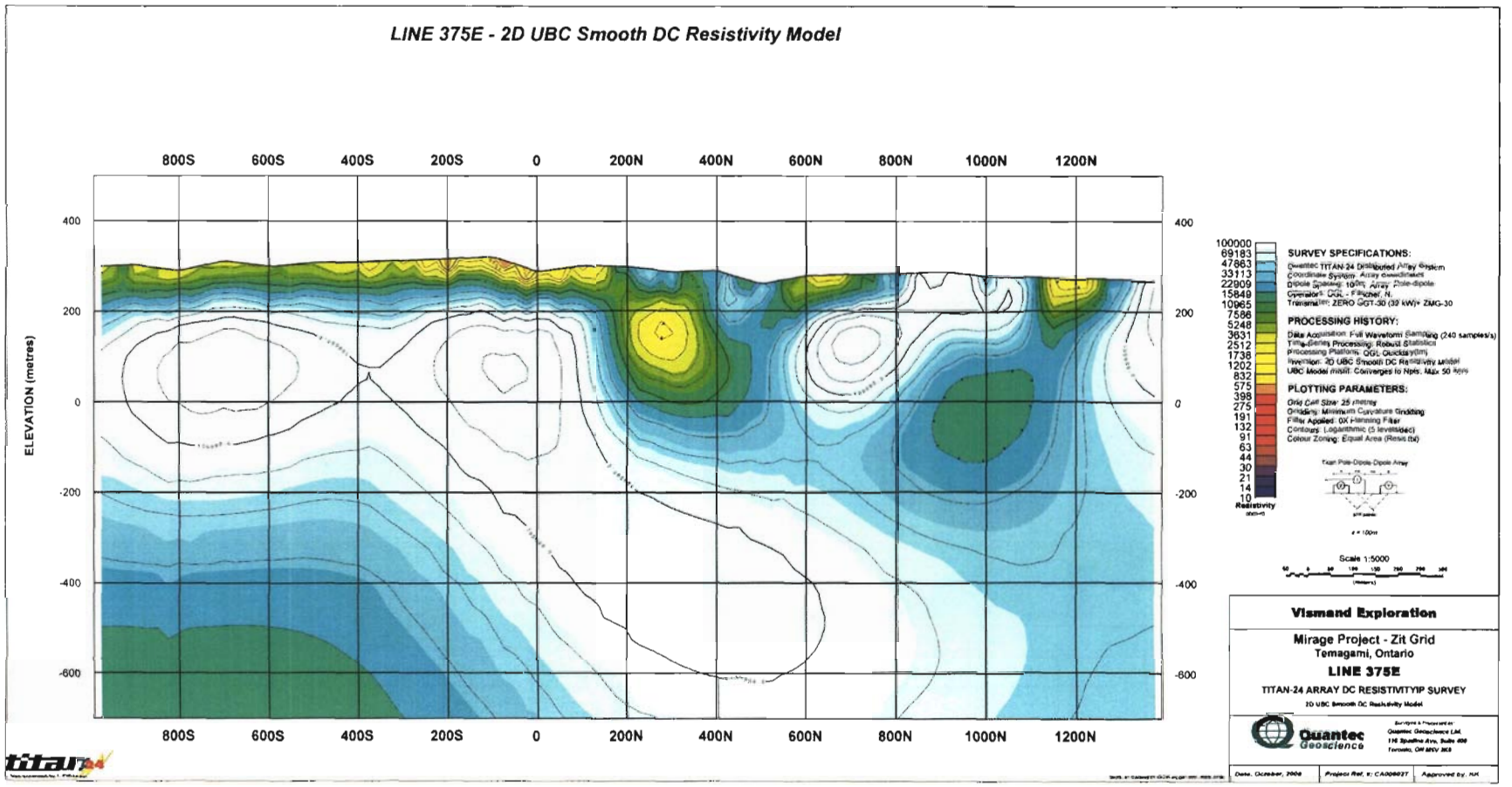

Line 375E – 2D UBC Smooth IP Chargeability Model

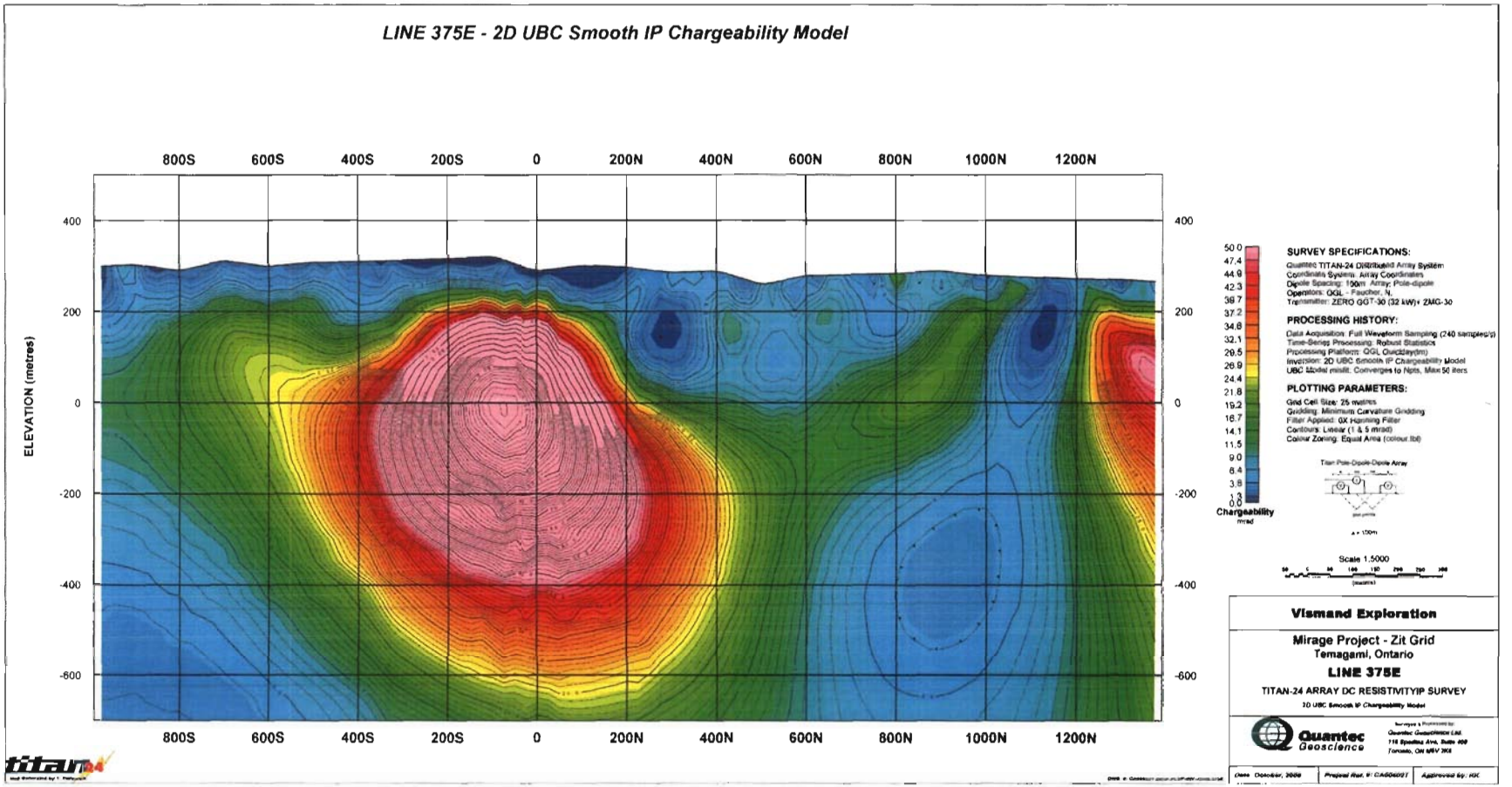

Line 375E – 2D UBC Null Con IP Chargeability Model

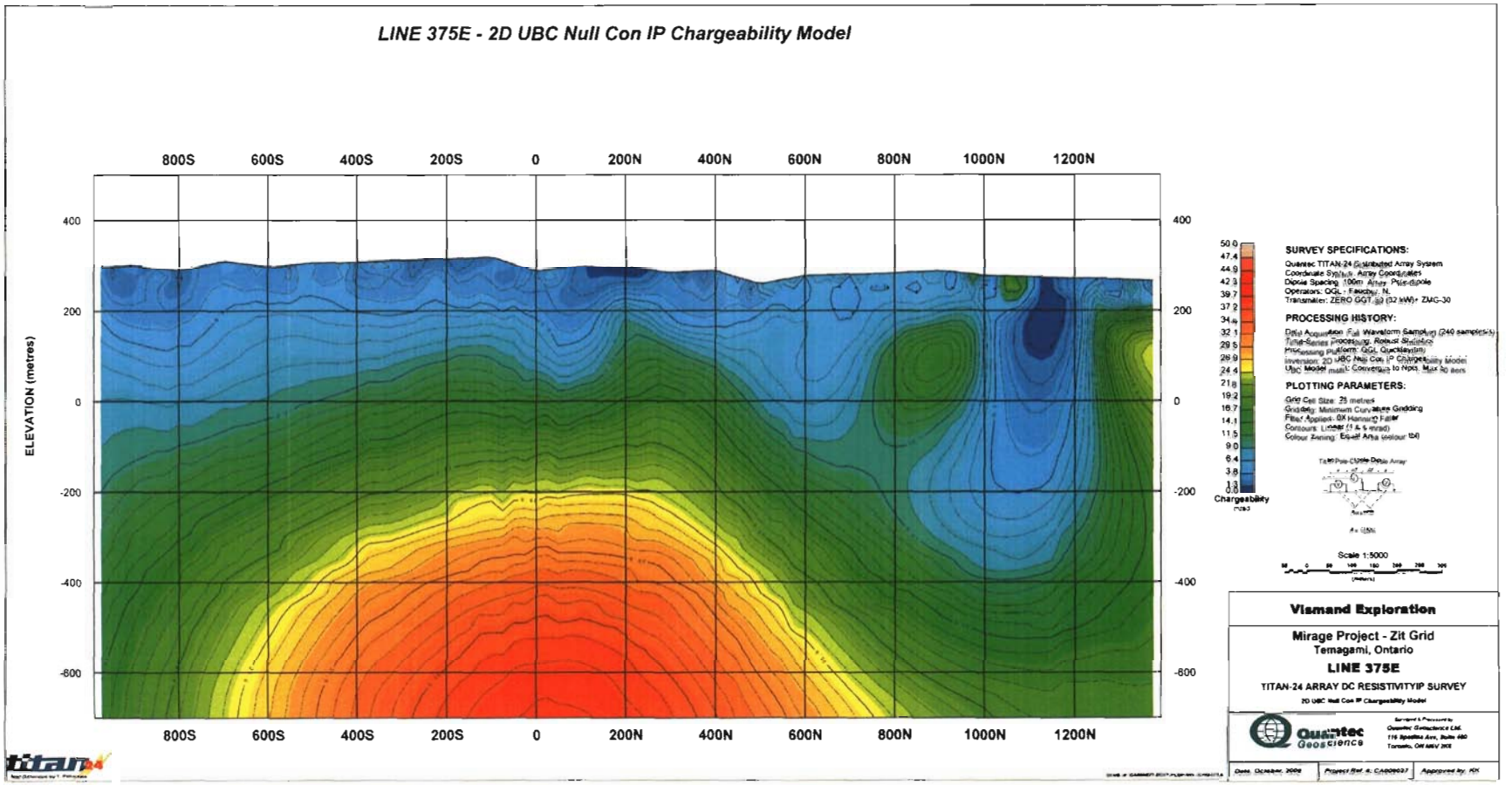

Line 375E – 2D MT PW TM+TE(phs) Sharp Inversion (starting from smooth 1D PW model)

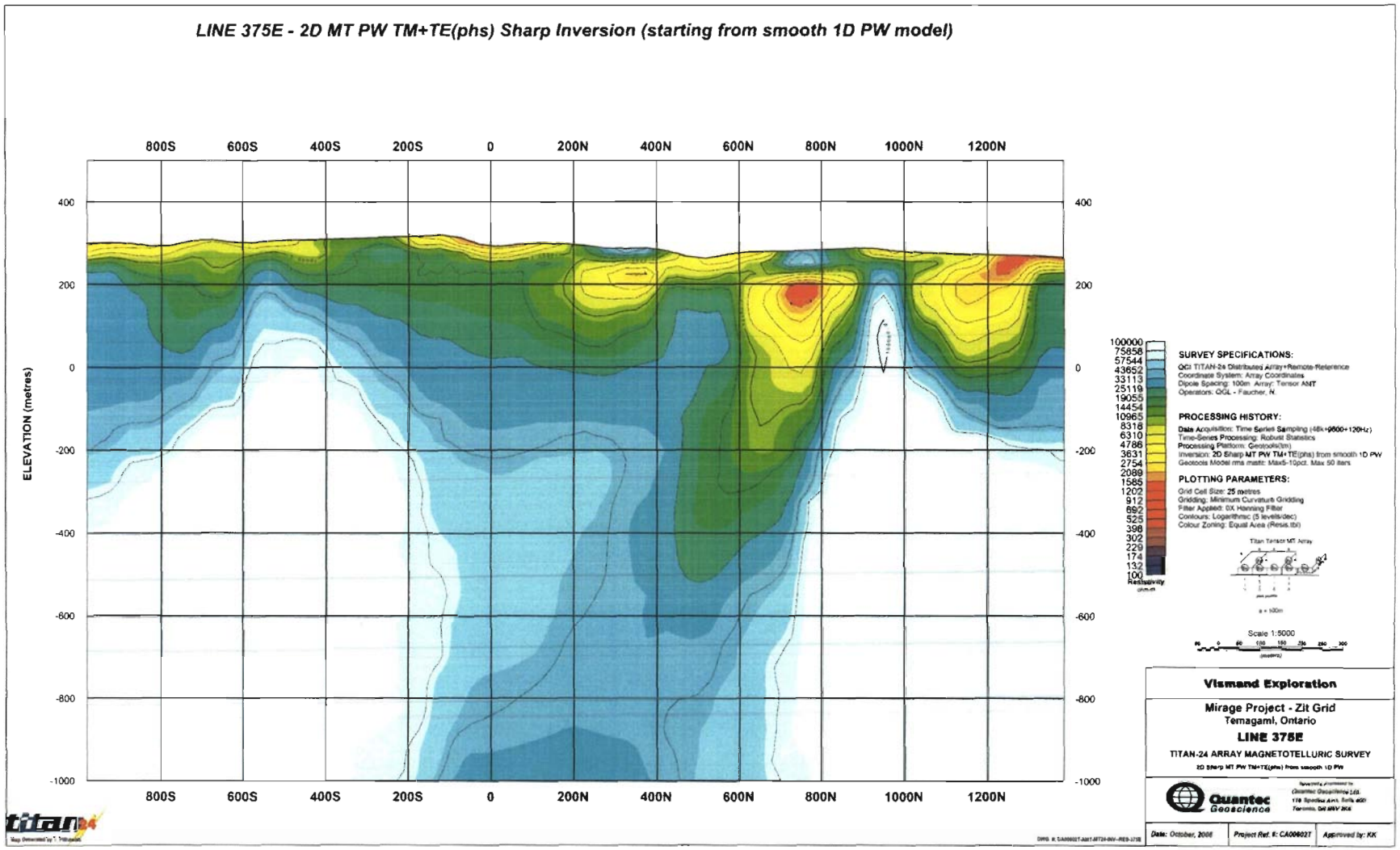

Line 375E – 2D MT PW TM+TE Sharp Inversion (starting from smooth 1D PW model)

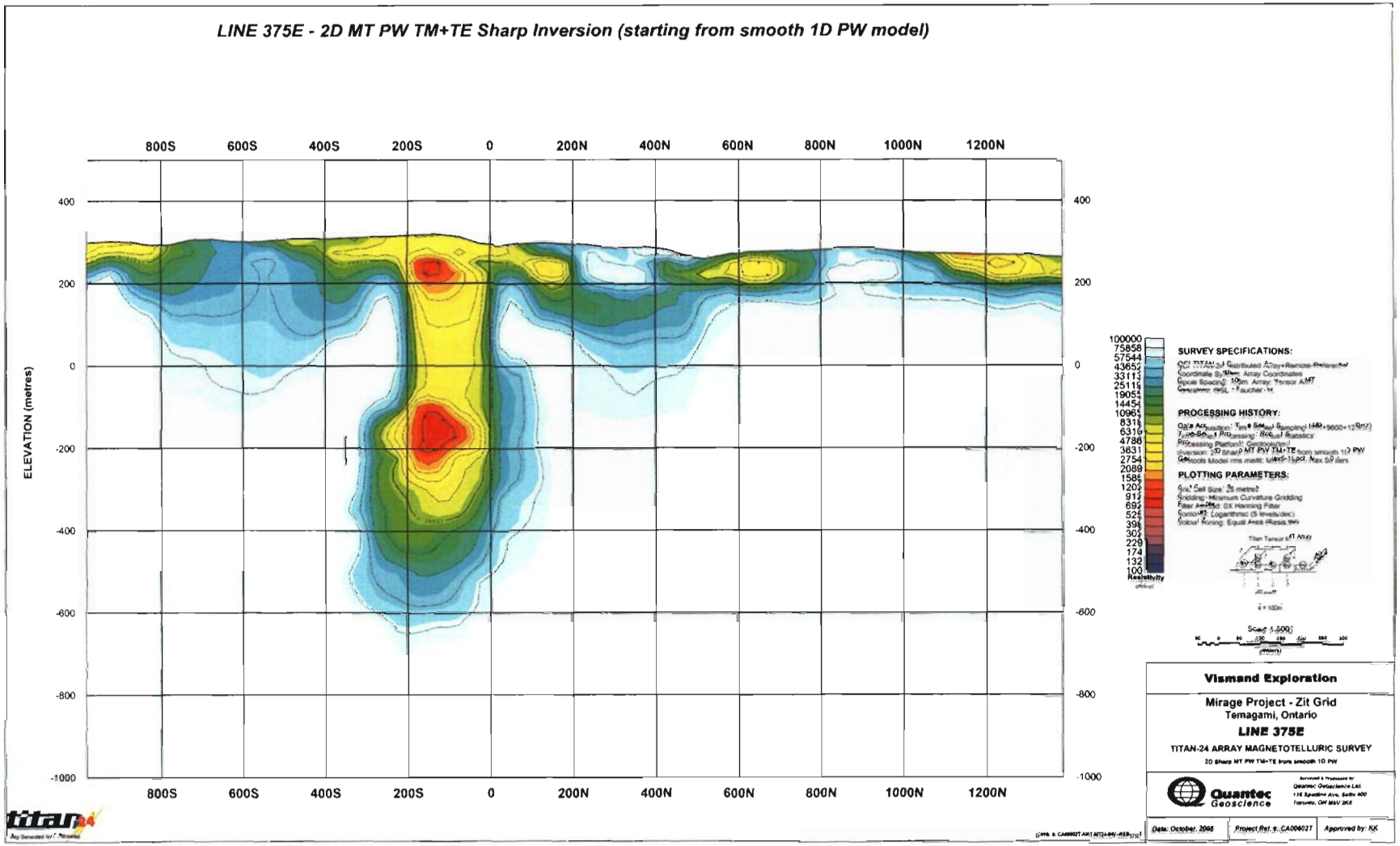

Line 375E – 2D MT PW TM+TE(phs) Inversion (starting from 1000 ohm-m halfspace)

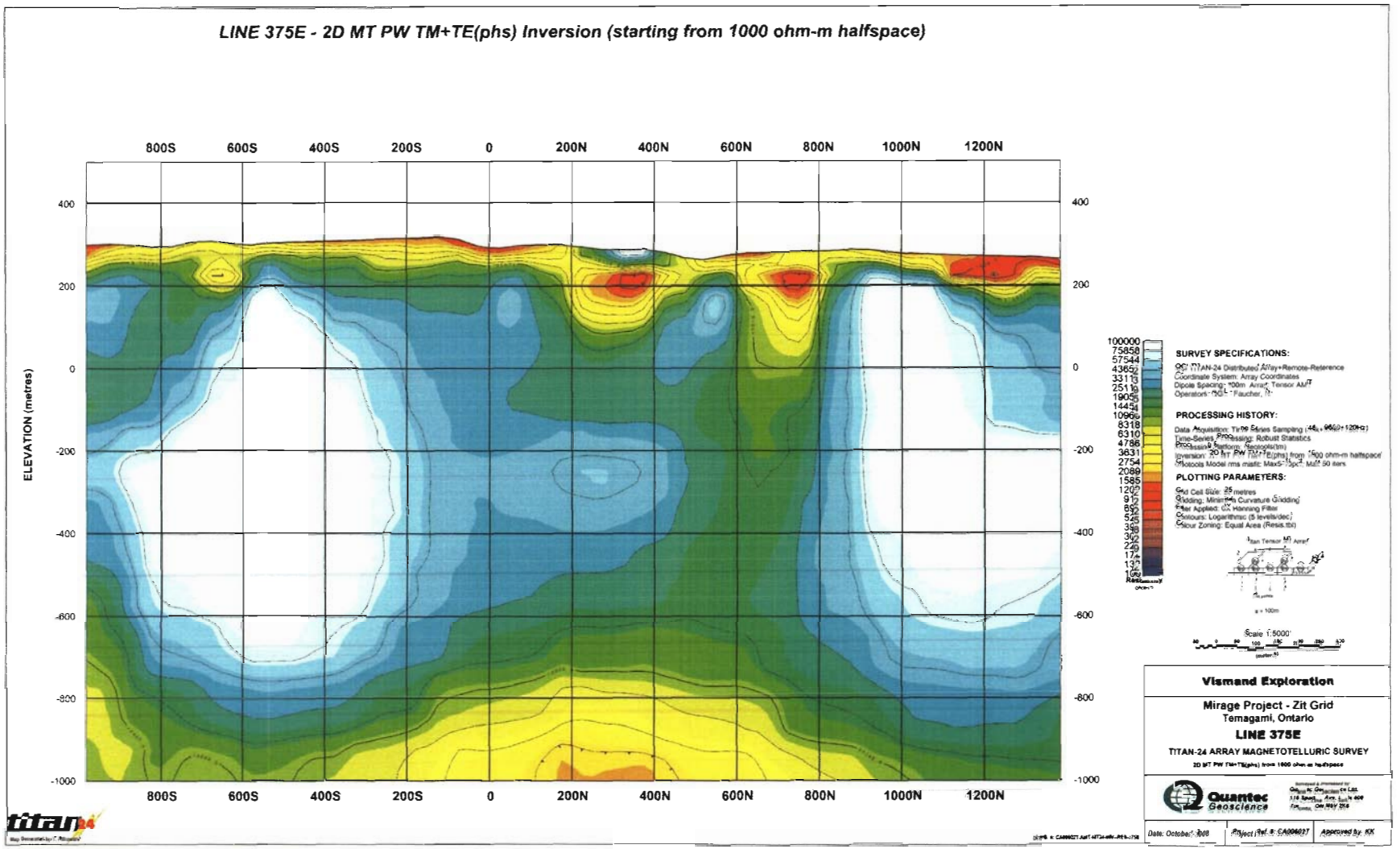

Line 375E – 2D MT PW TM+TE Inversion (starting from 1000 ohm-m halfspace)

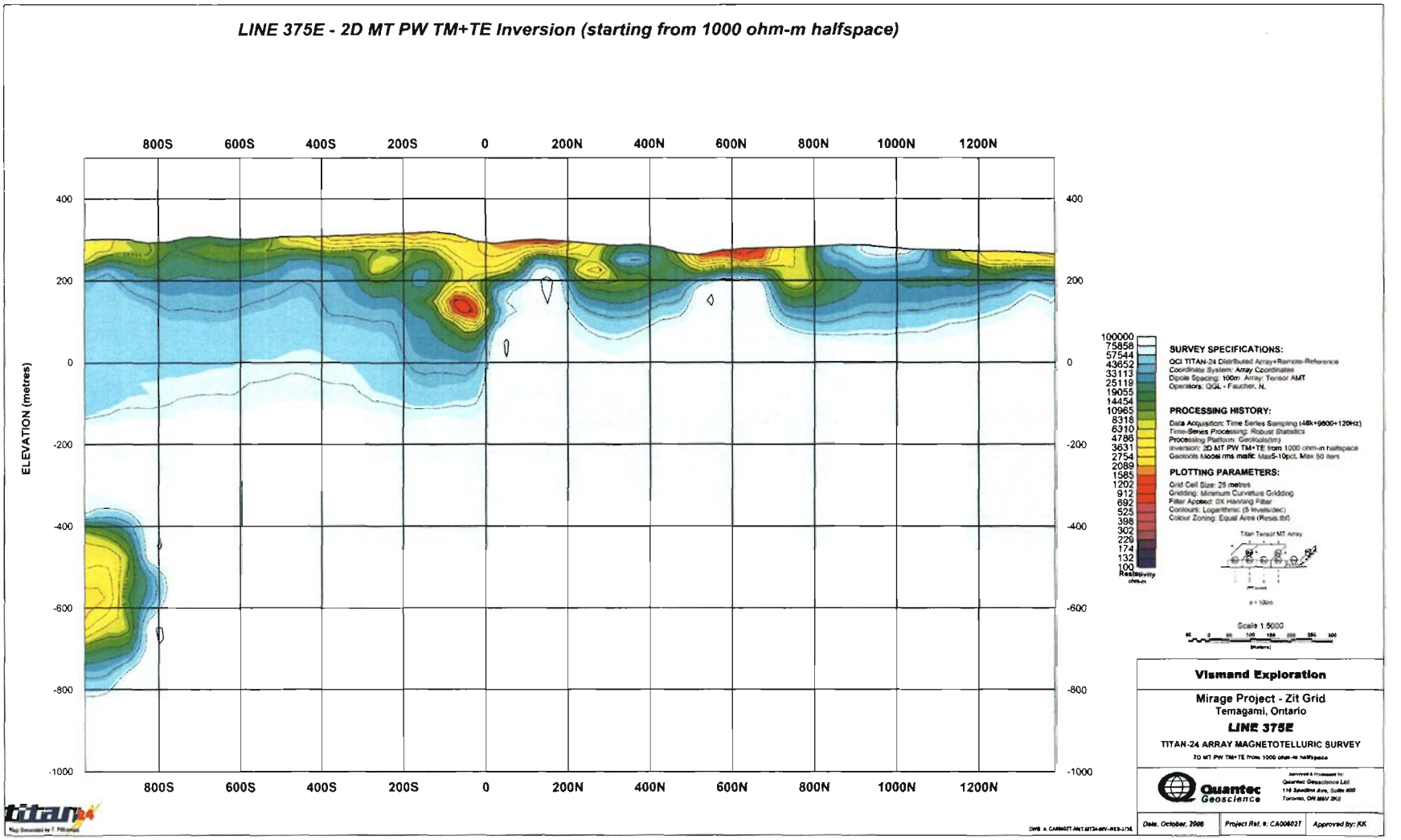

Line 375E – 2D MT RLM TM+TE(phs) Inversion (starting from 1D Det model)

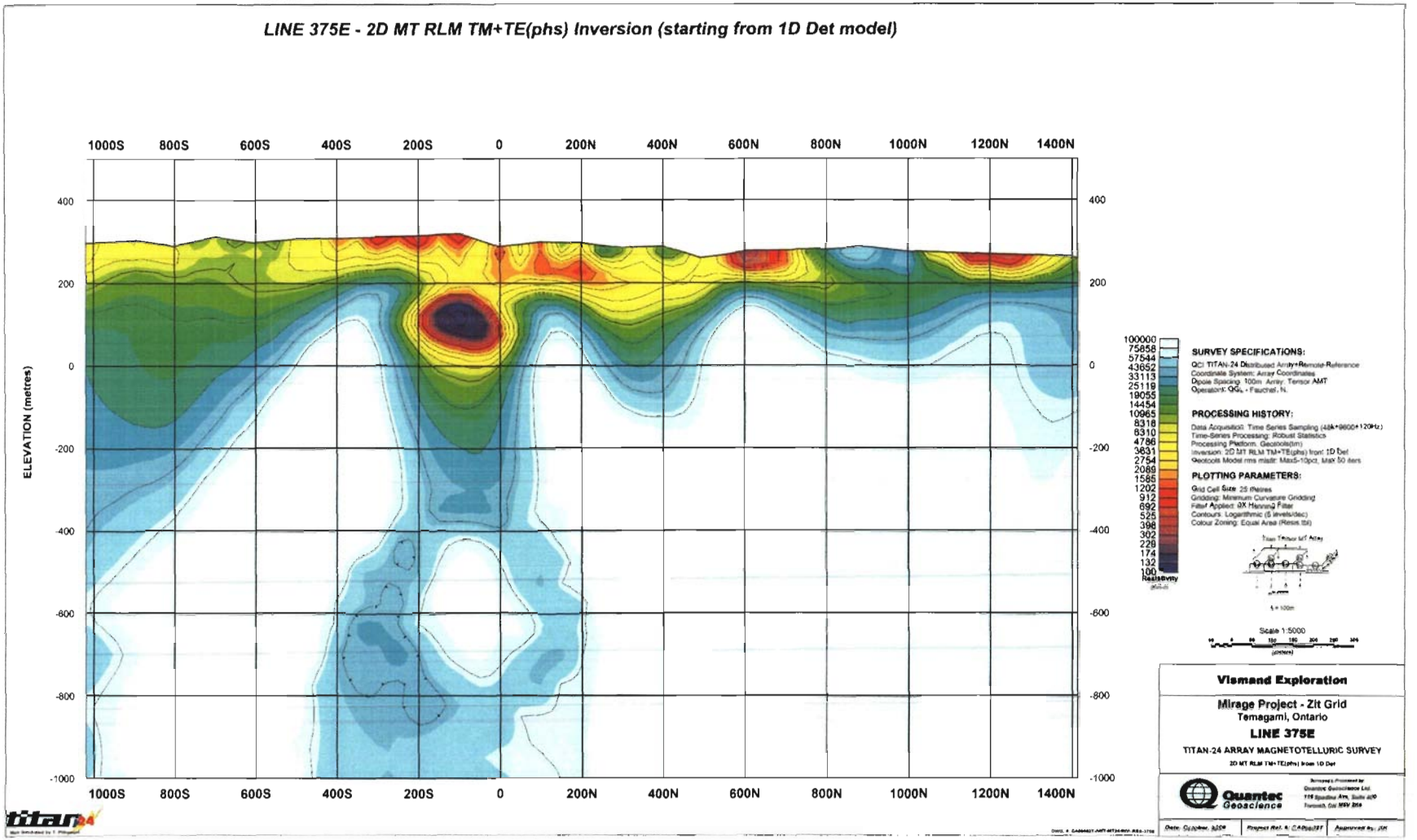

Line 375E – 2D MT RLM TM+TE Inversion (starting from 1D Det model)

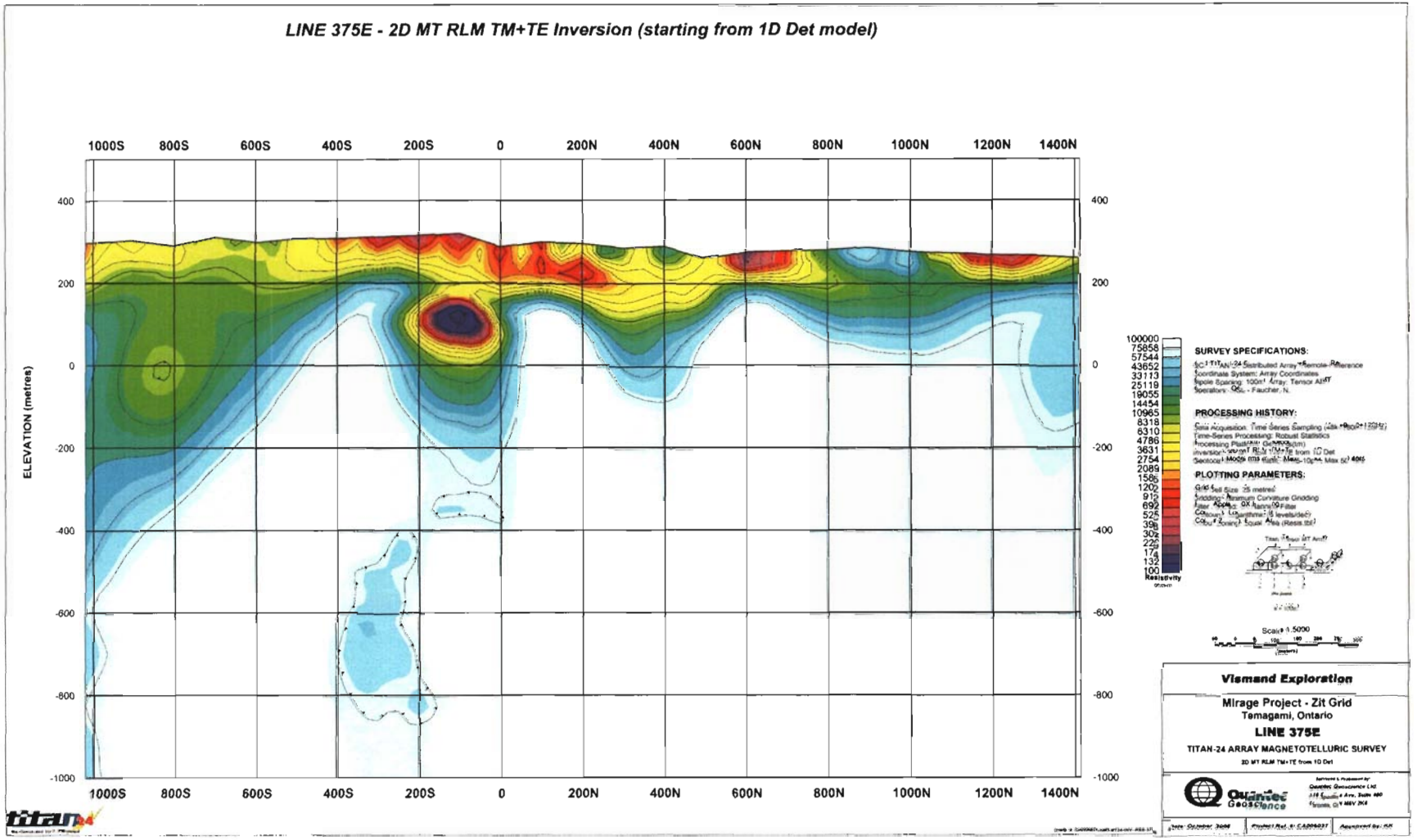

Line 375E – 2D MT RLM TM+TE(phs) Inversion (starting from 1000 ohm-m halfspace)

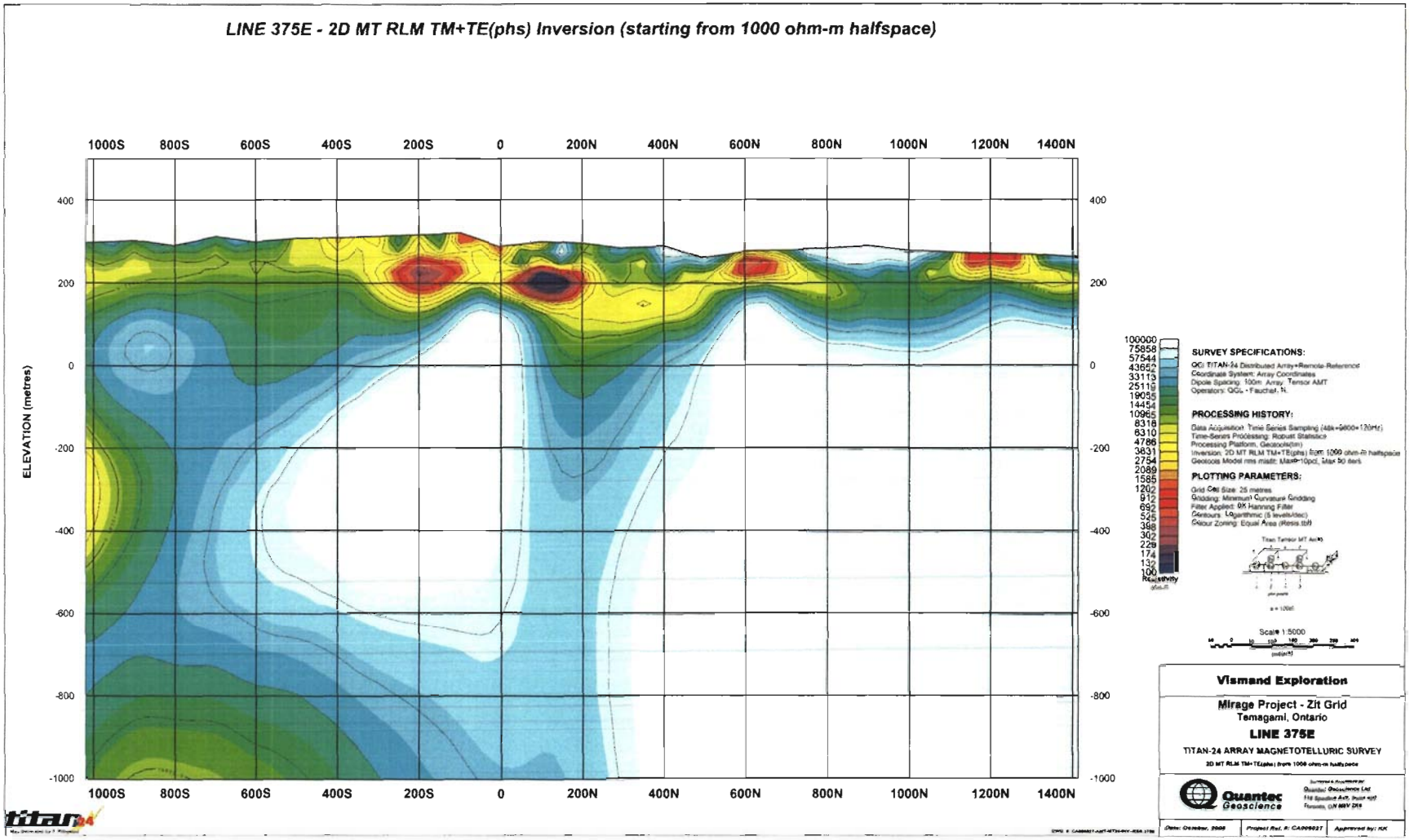

Line 375E – 2D MT RLM TM+TE Inversion (starting from 1000 ohm-m halfspace)

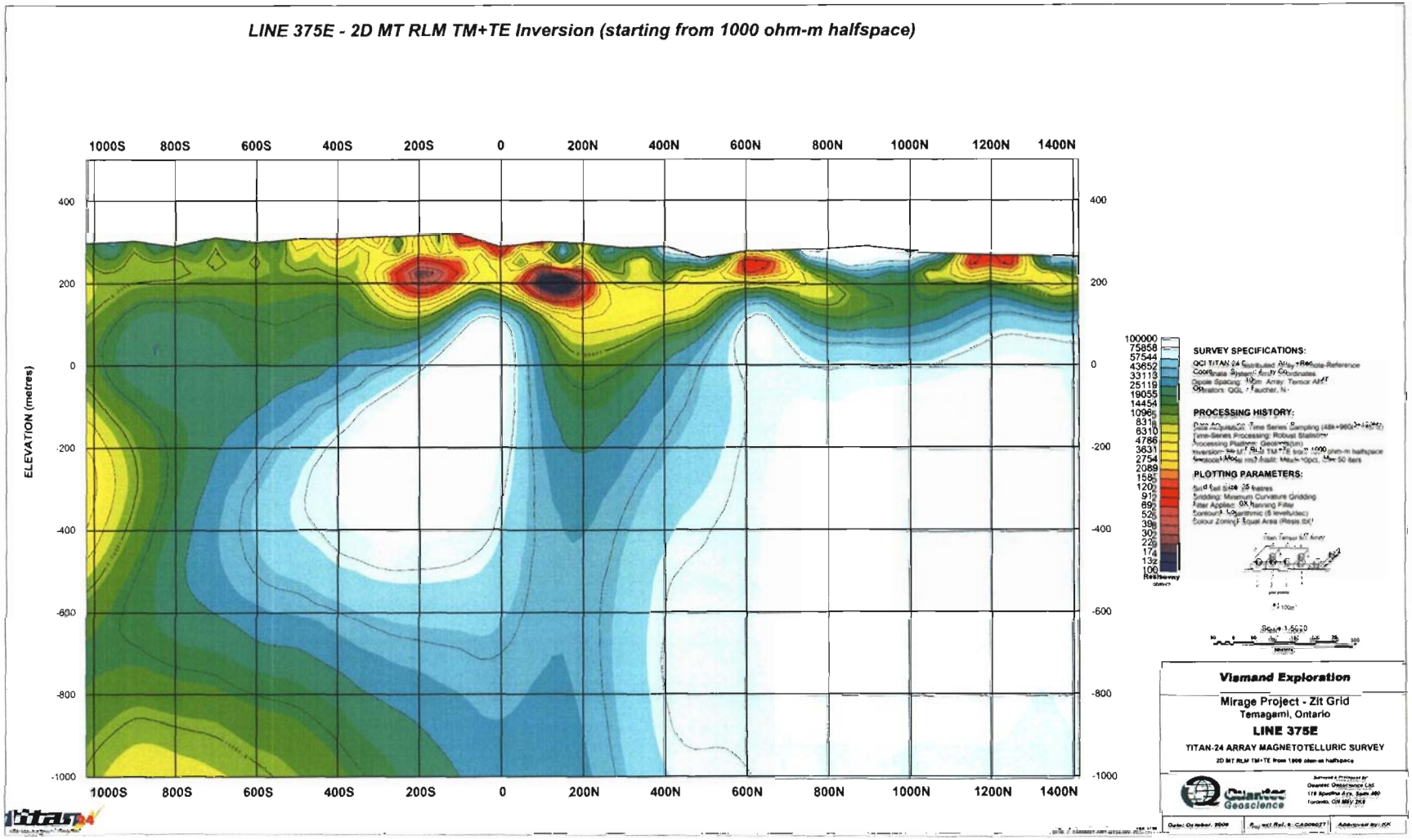

Line 925E – 2D UBC Smooth DC Resistivity Model

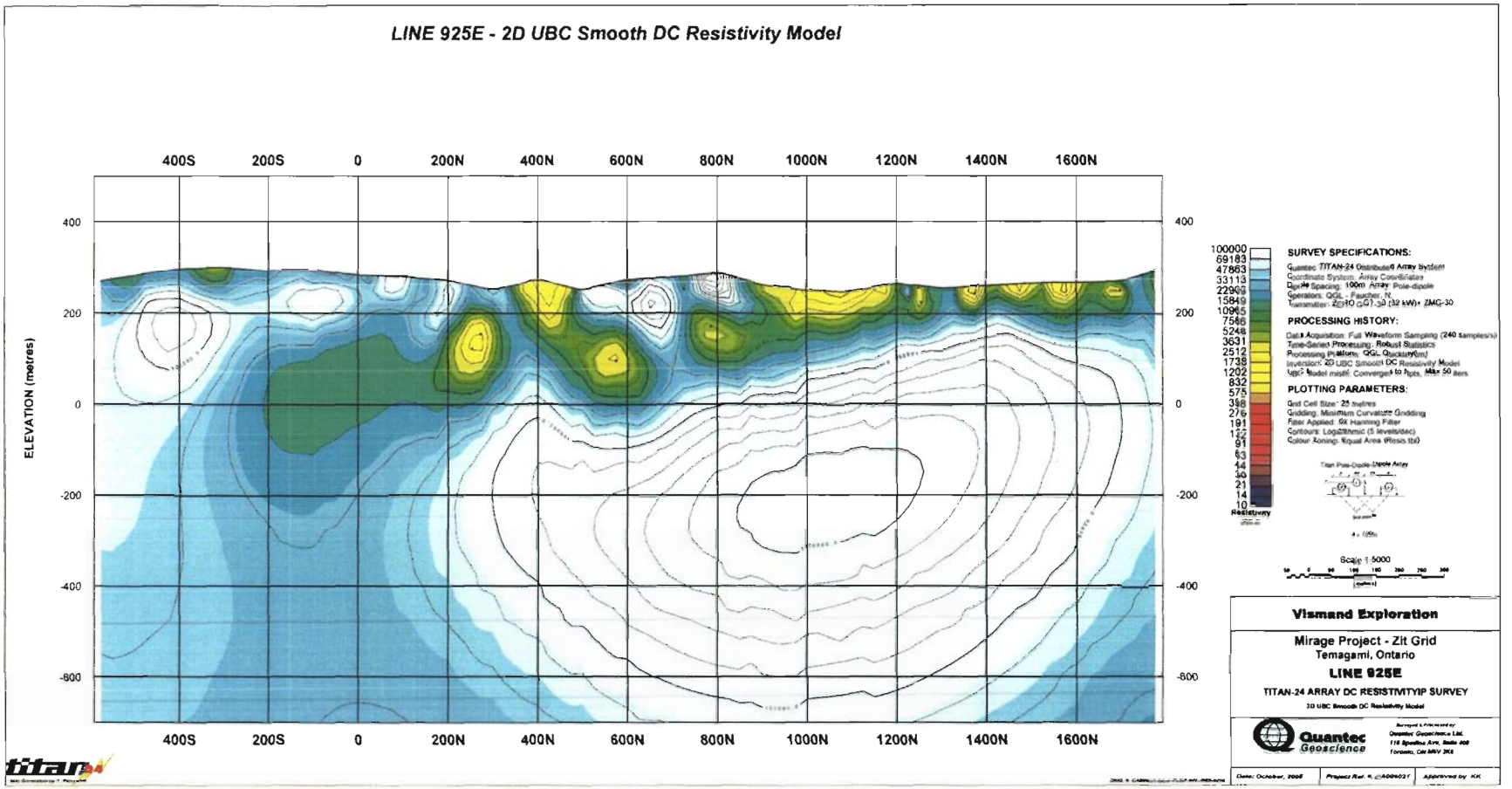

Line 925E – 2D UBC Smooth IP Chargeability Model

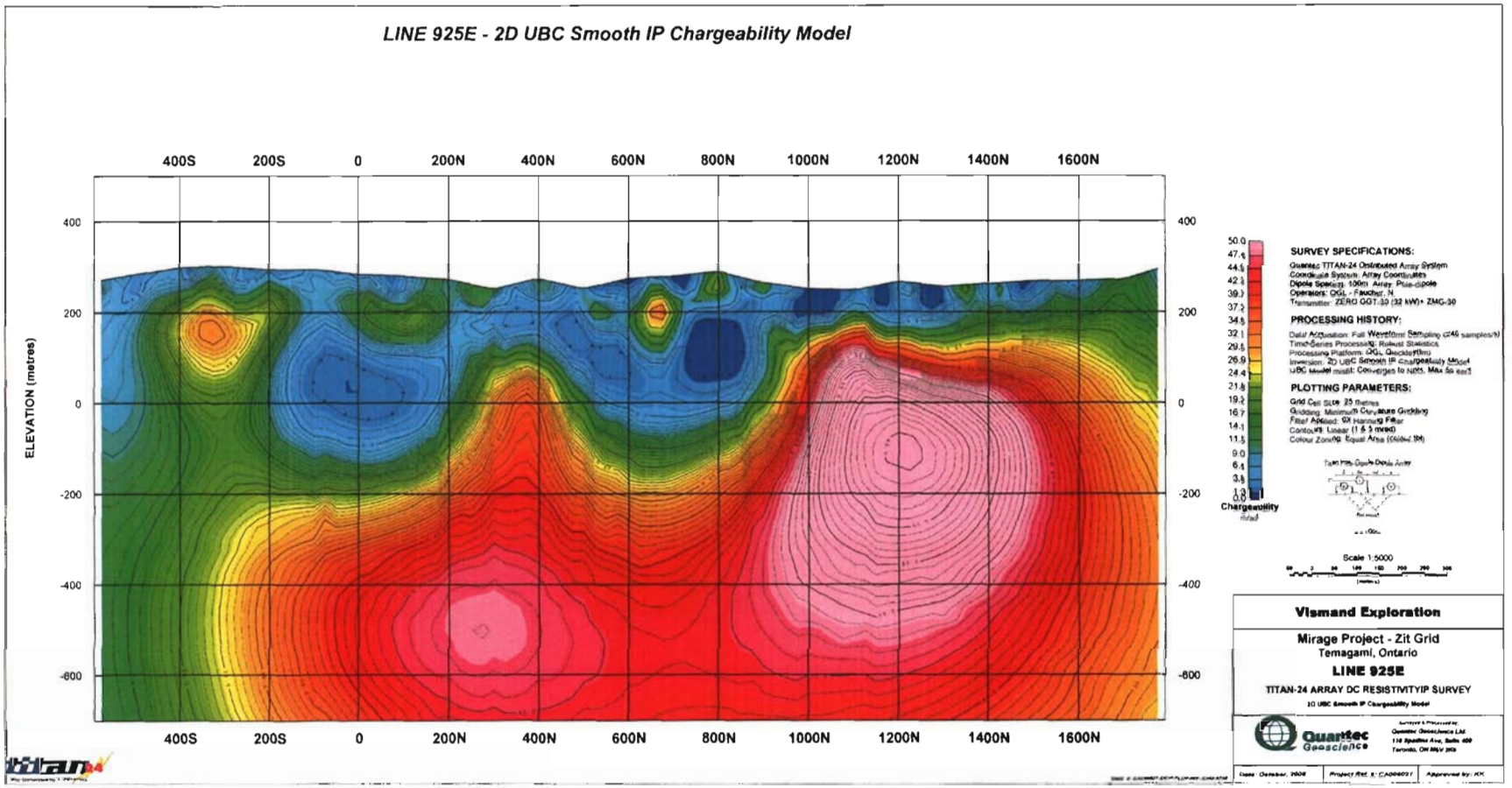

Line 925E – 2D UBC Null Con IP Chargeability Model

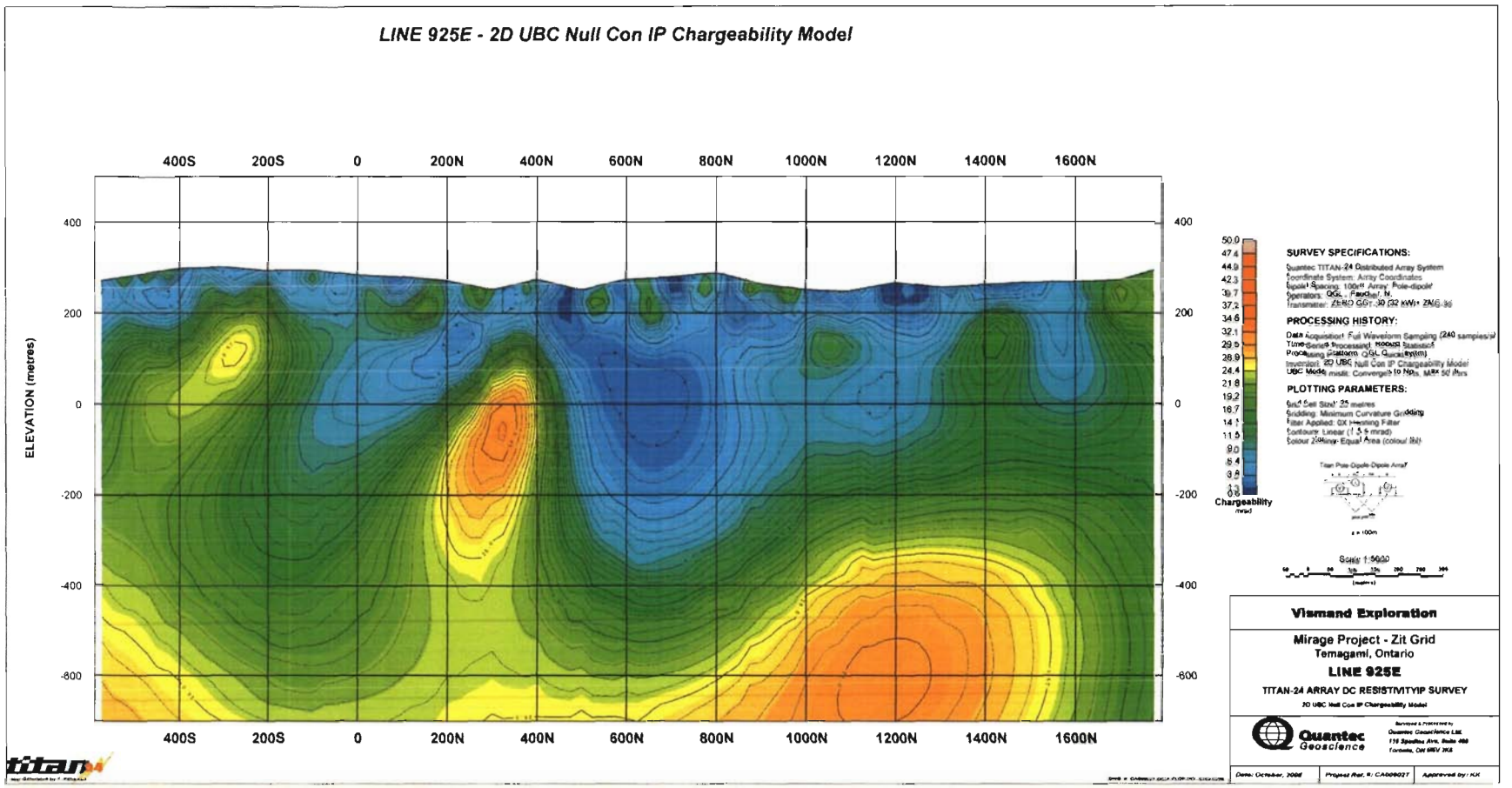

Line 925E – 2D MT PW TM+TE(phs) Sharp Inversion (starting from smooth 1D PW model)

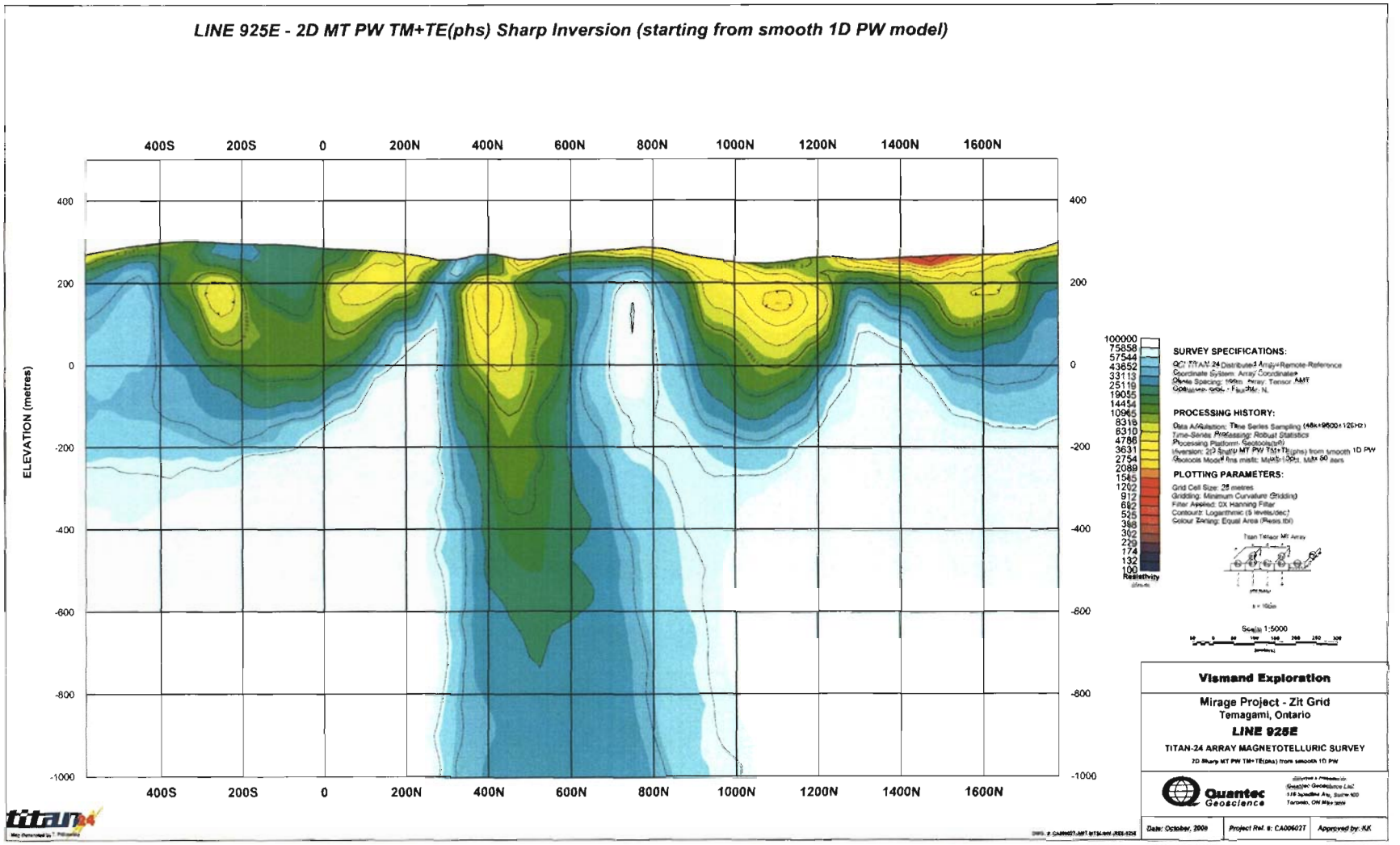

Line 925E – 2D MT PW TM+TE Sharp Inversion (starting from smooth 1D PW model)

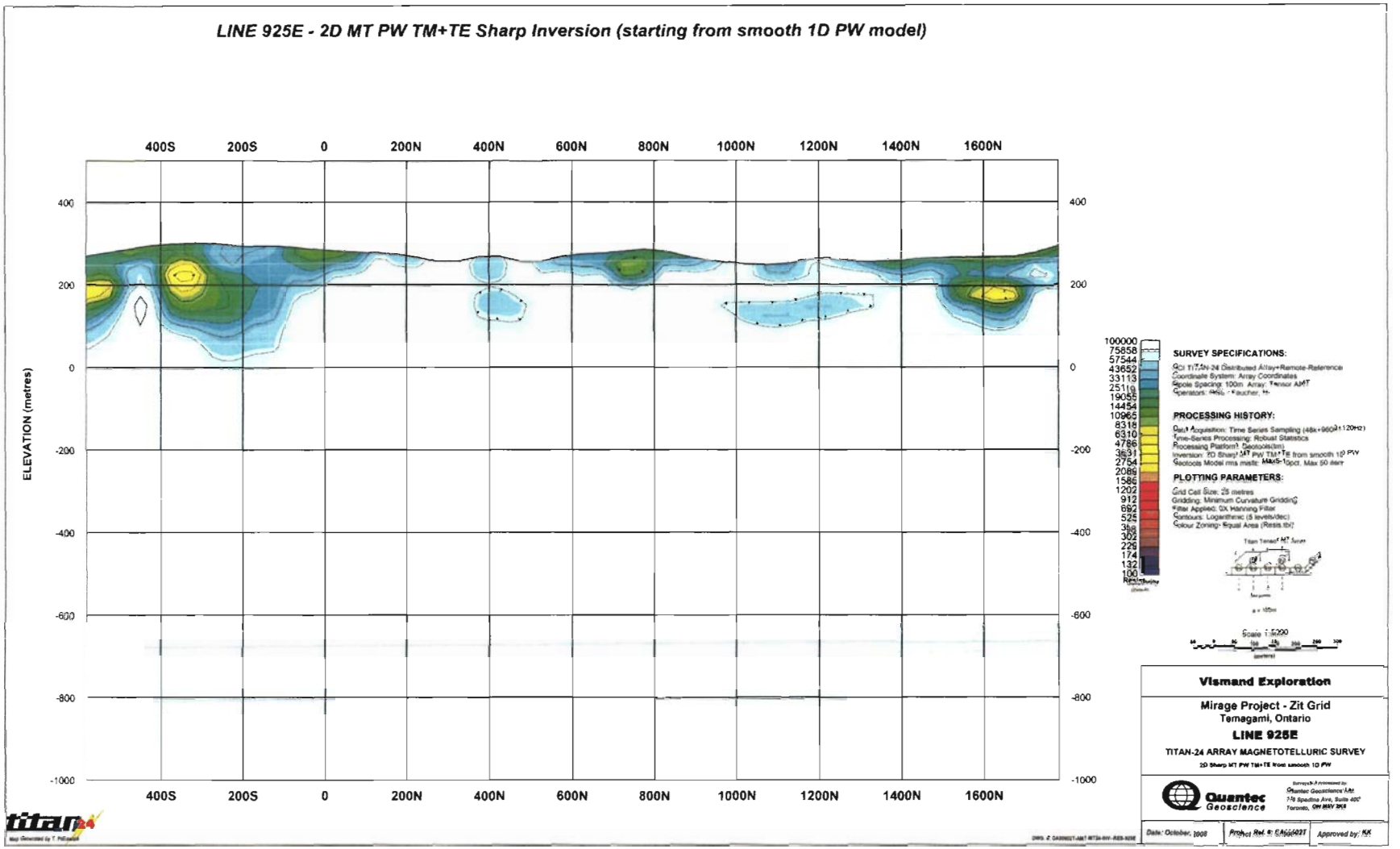

Line 925E – 2D MT PW TM+TE(phs) Inversion (starting from 1000 ohm-m halfspace)

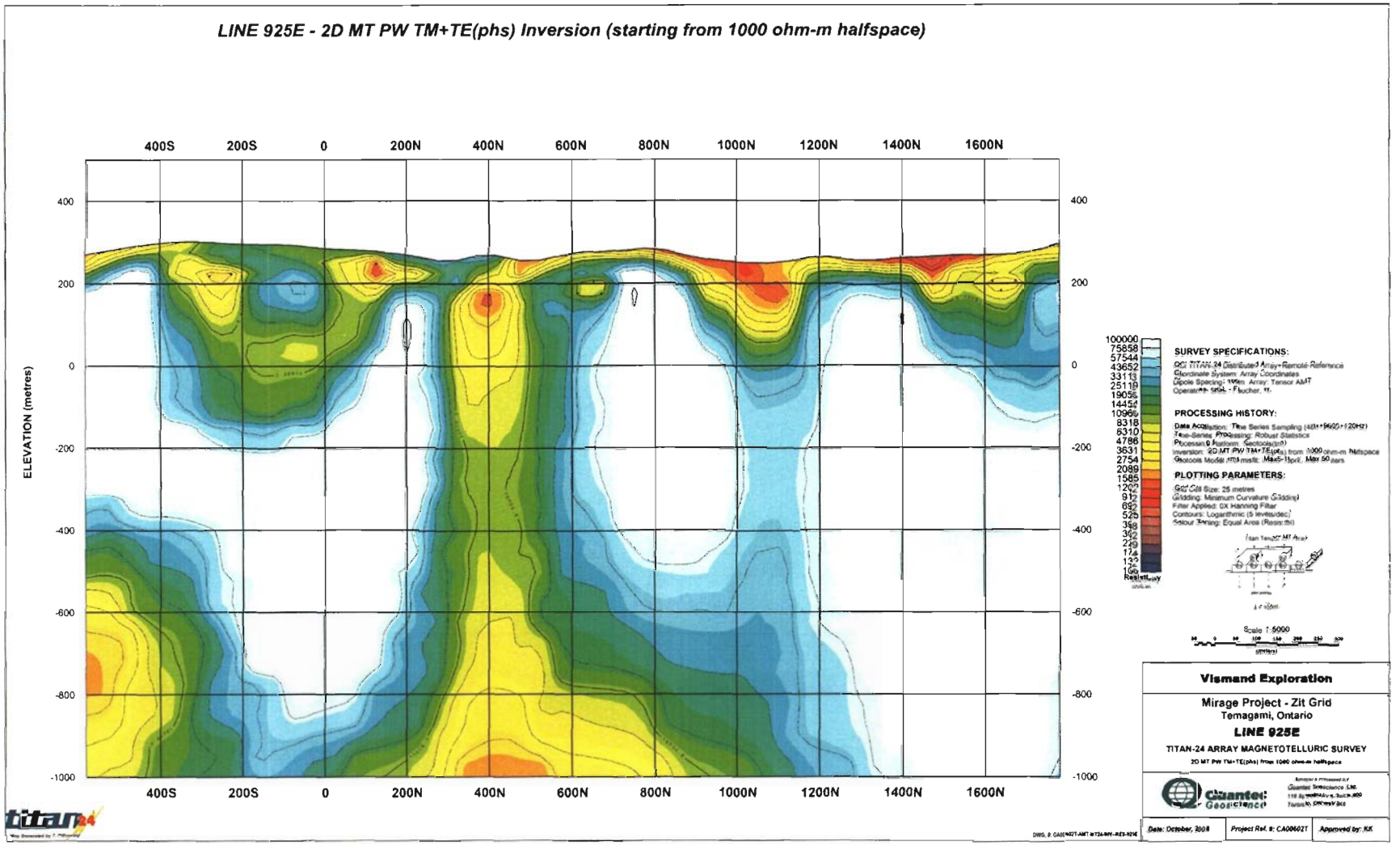

Line 925E – 2D MT PW TM+TE Inversion (starting from 1000 ohm-m halfspace)

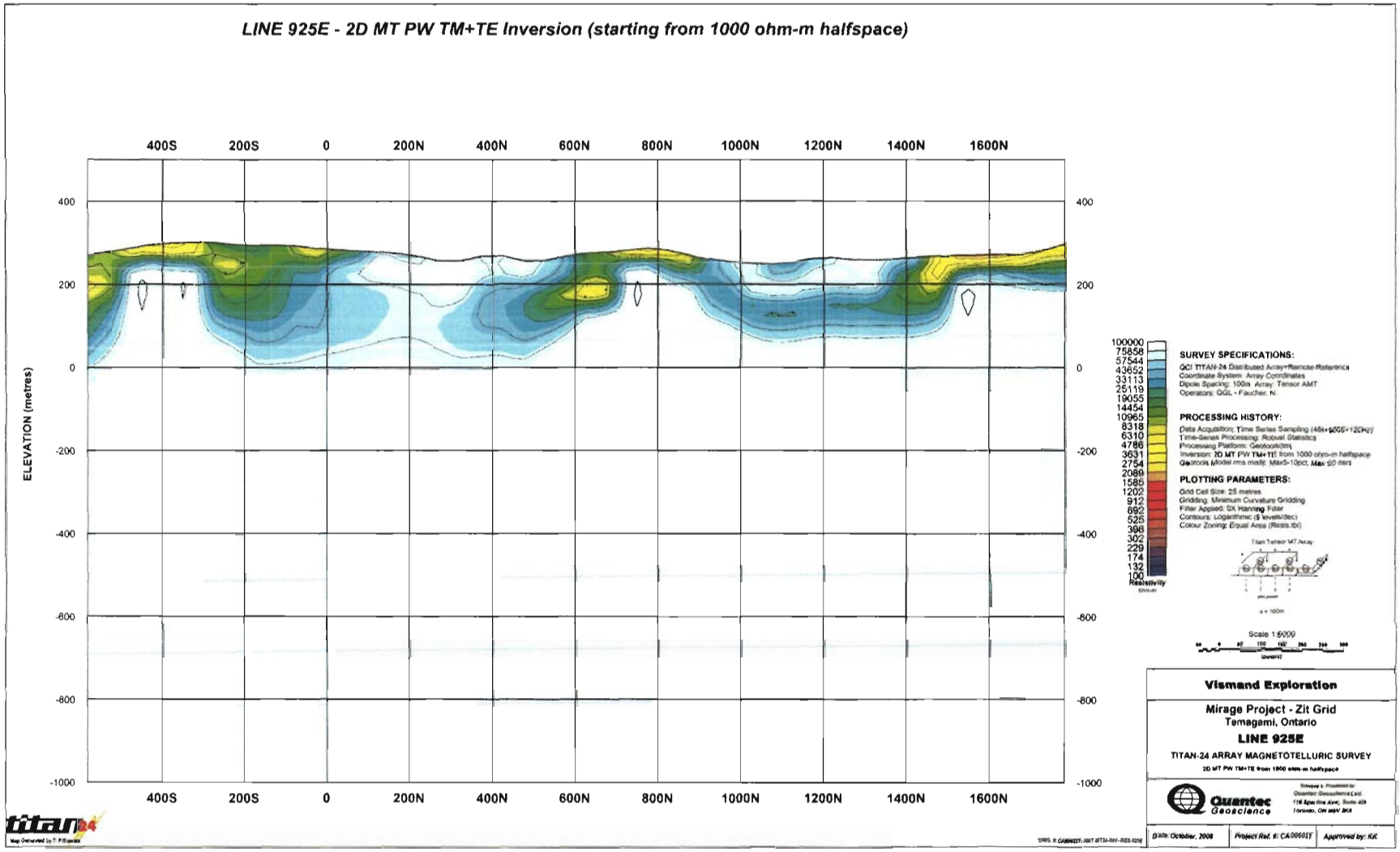

Line 925E – 2D MT RLM TM+TE(phs) Inversion (starting from 1D Det model)

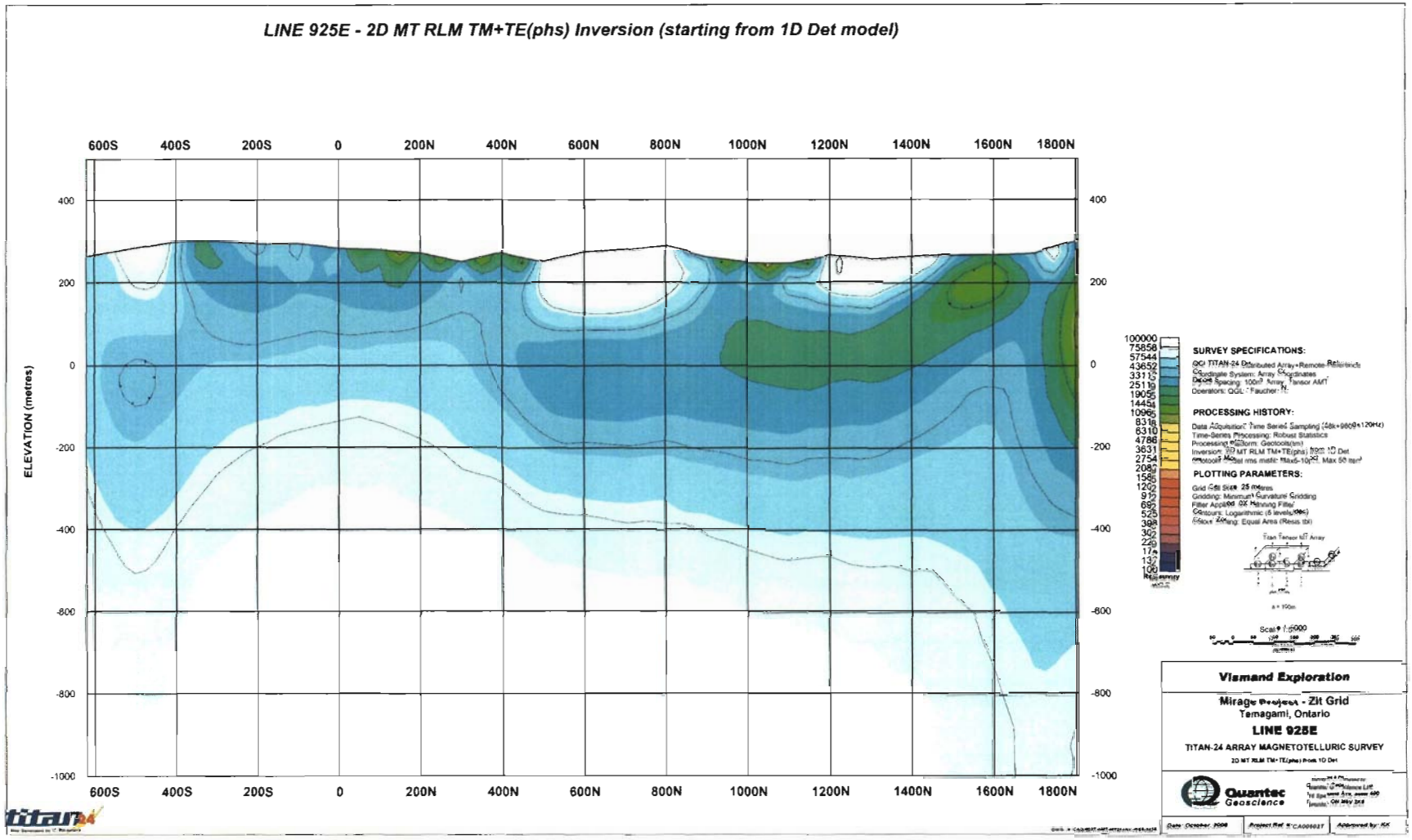

Line 925E – 2D MT RLM TM+TE Inversion (starting from 1D Det model)

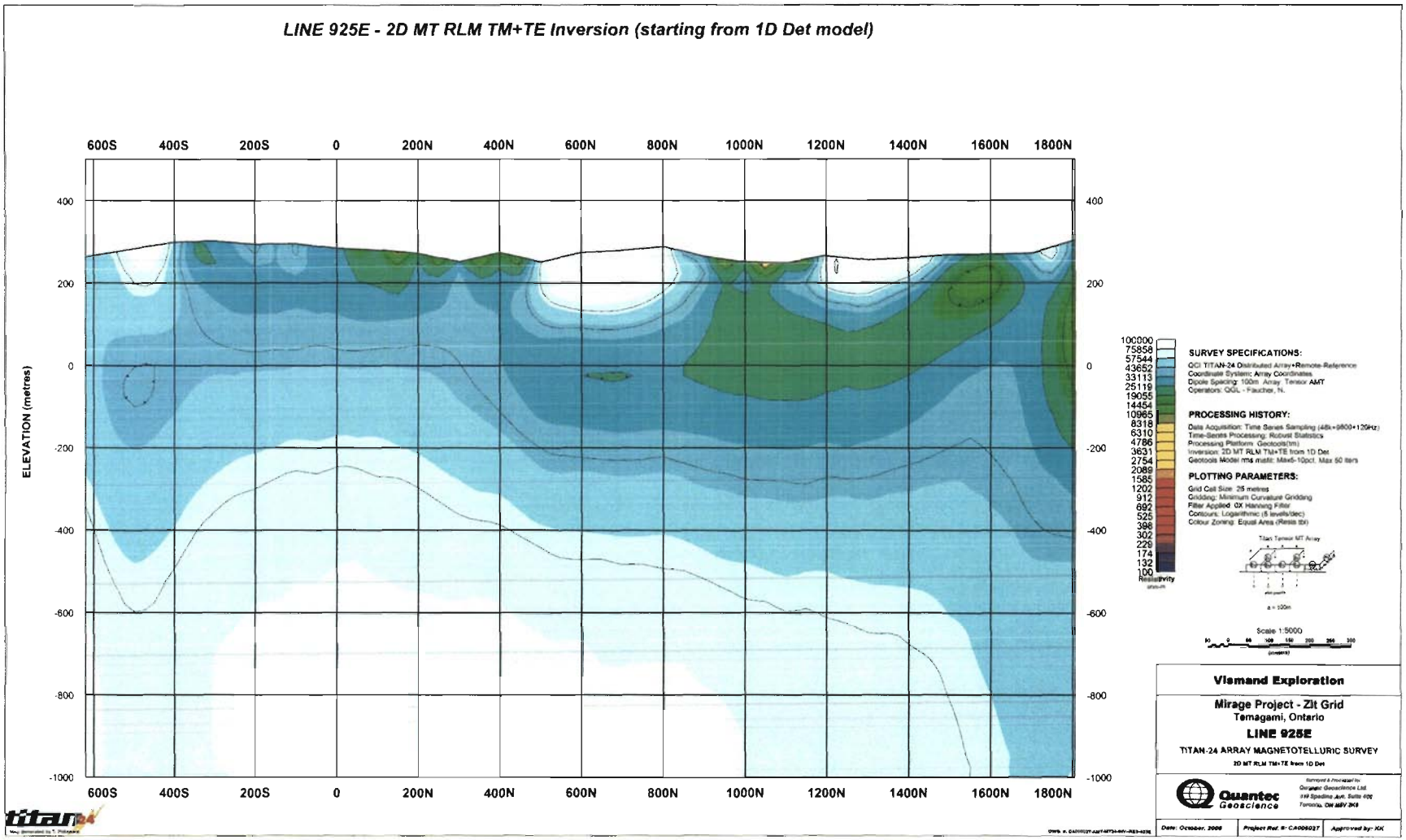

Line 925E – 2D MT RLM TM+TE(phs) Inversion (starting from 1000 ohm-m halfspace)

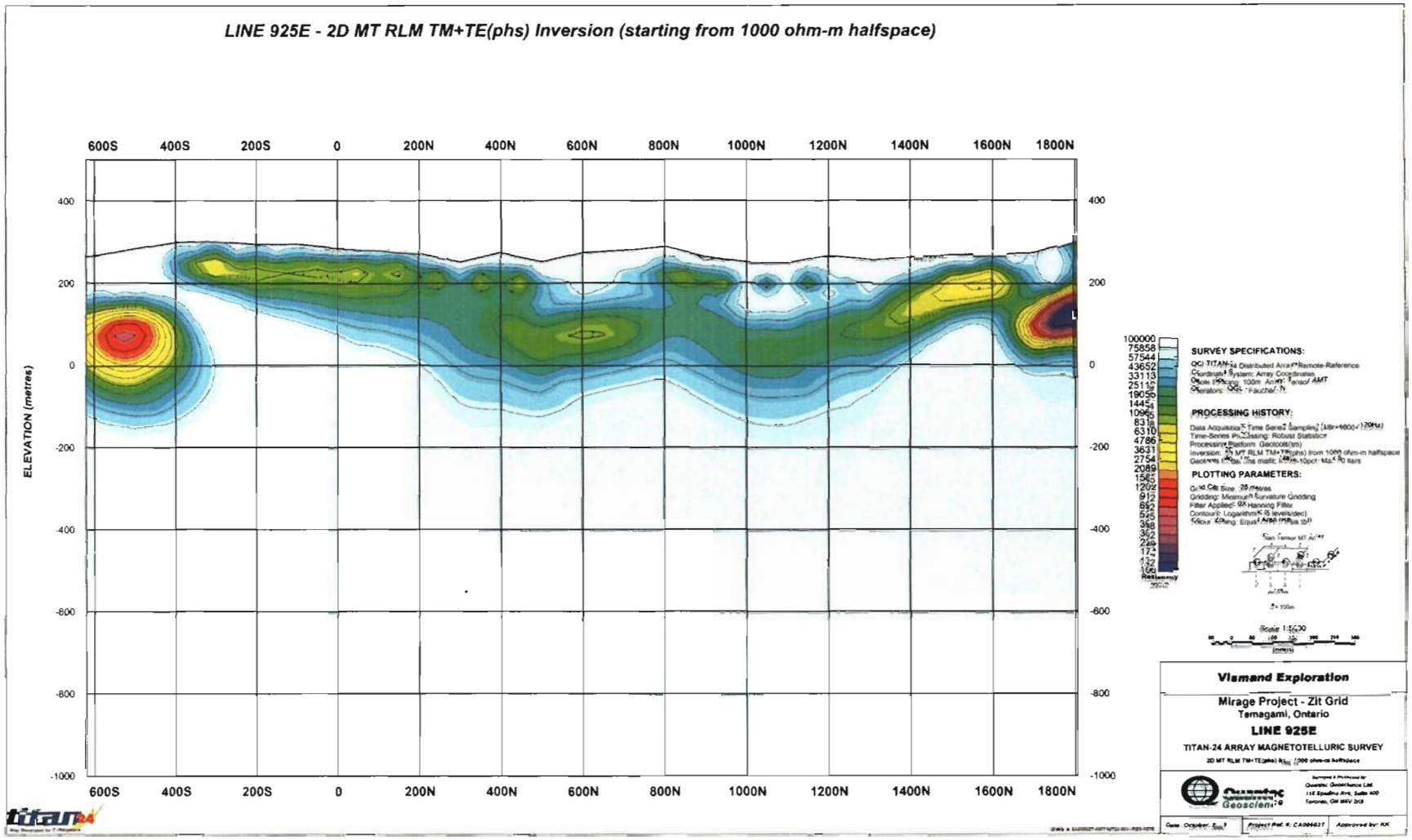

Line 925E – 2D MT RLM TM+TE Inversion (starting from 1000 ohm-m halfspace)

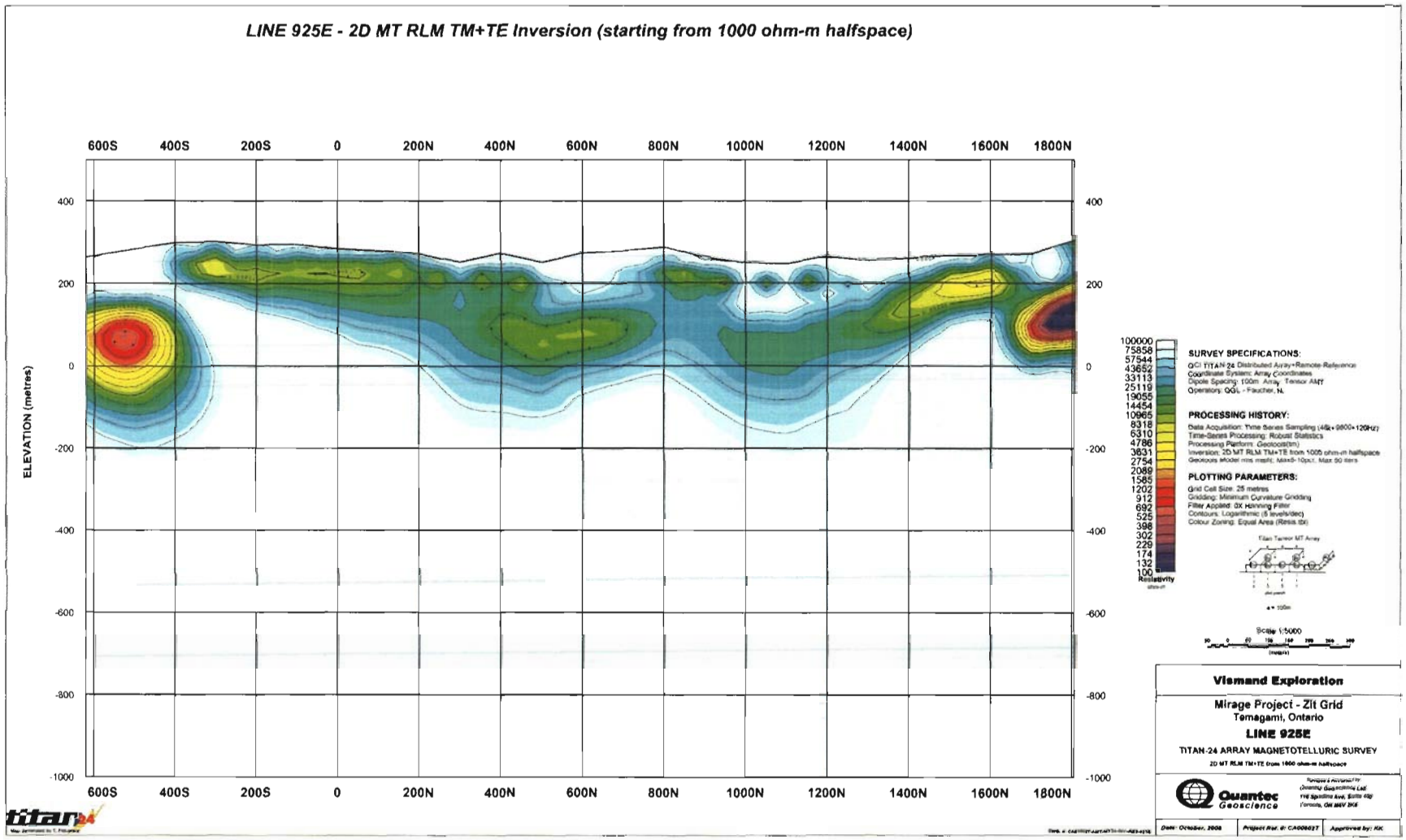

2D Resistivity (Z=50m) – 2D UBC Smooth DC Resistivity Model

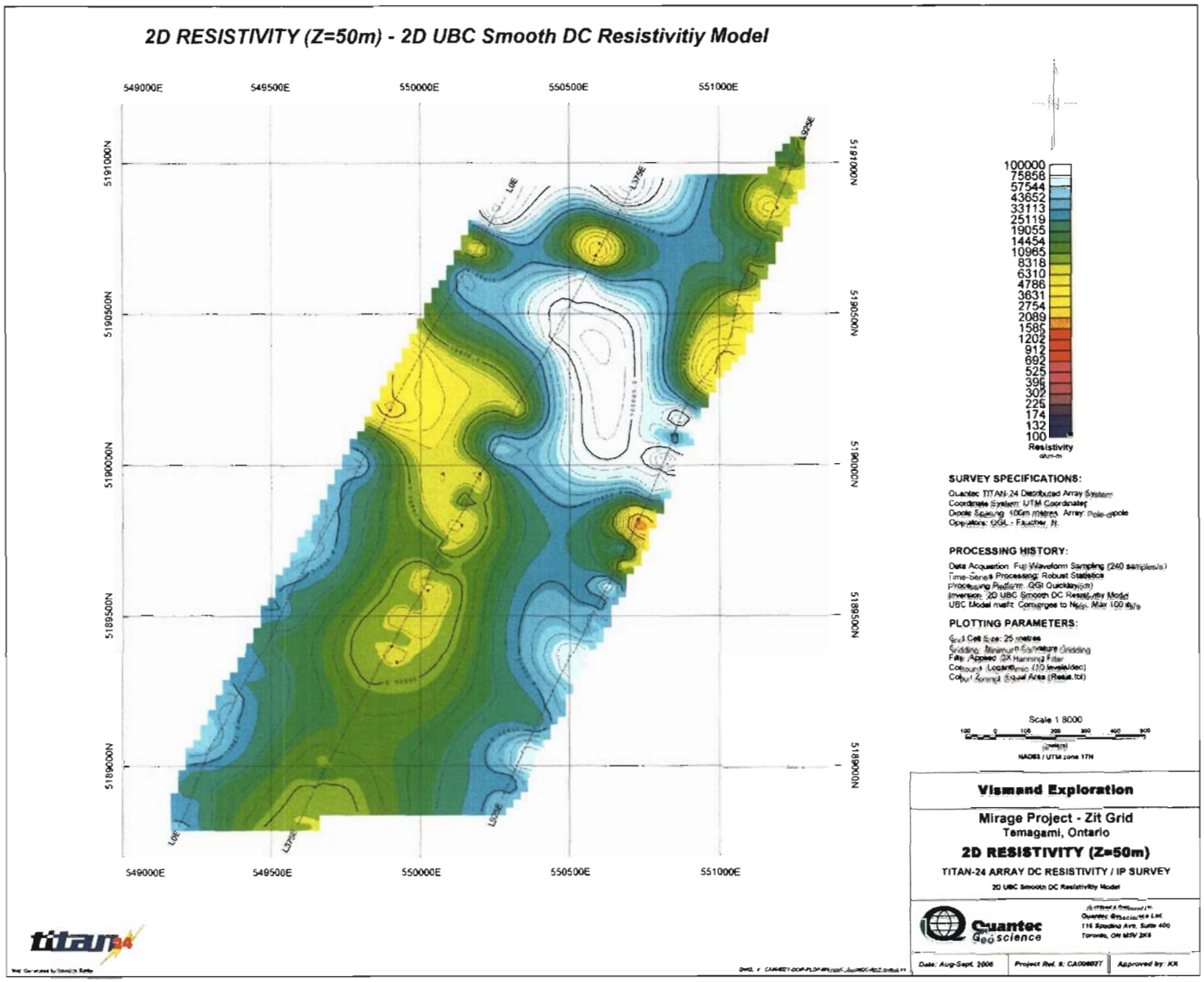

2D Resistivity (Z=100m) – 2D UBC Smooth DC Resistivity Model

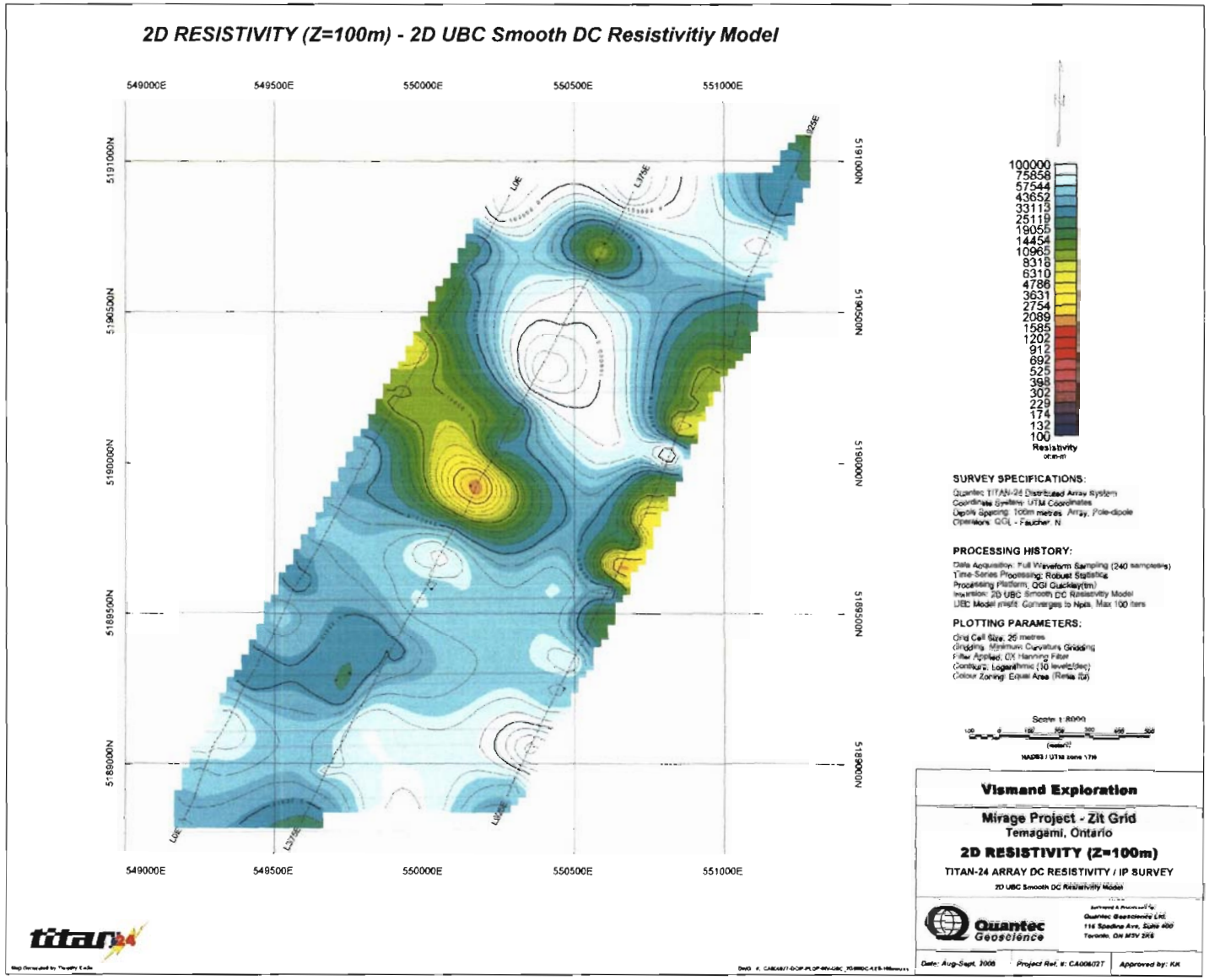

2D Resistivity (Z=200m) – 2D UBC Smooth DC Resistivity Model

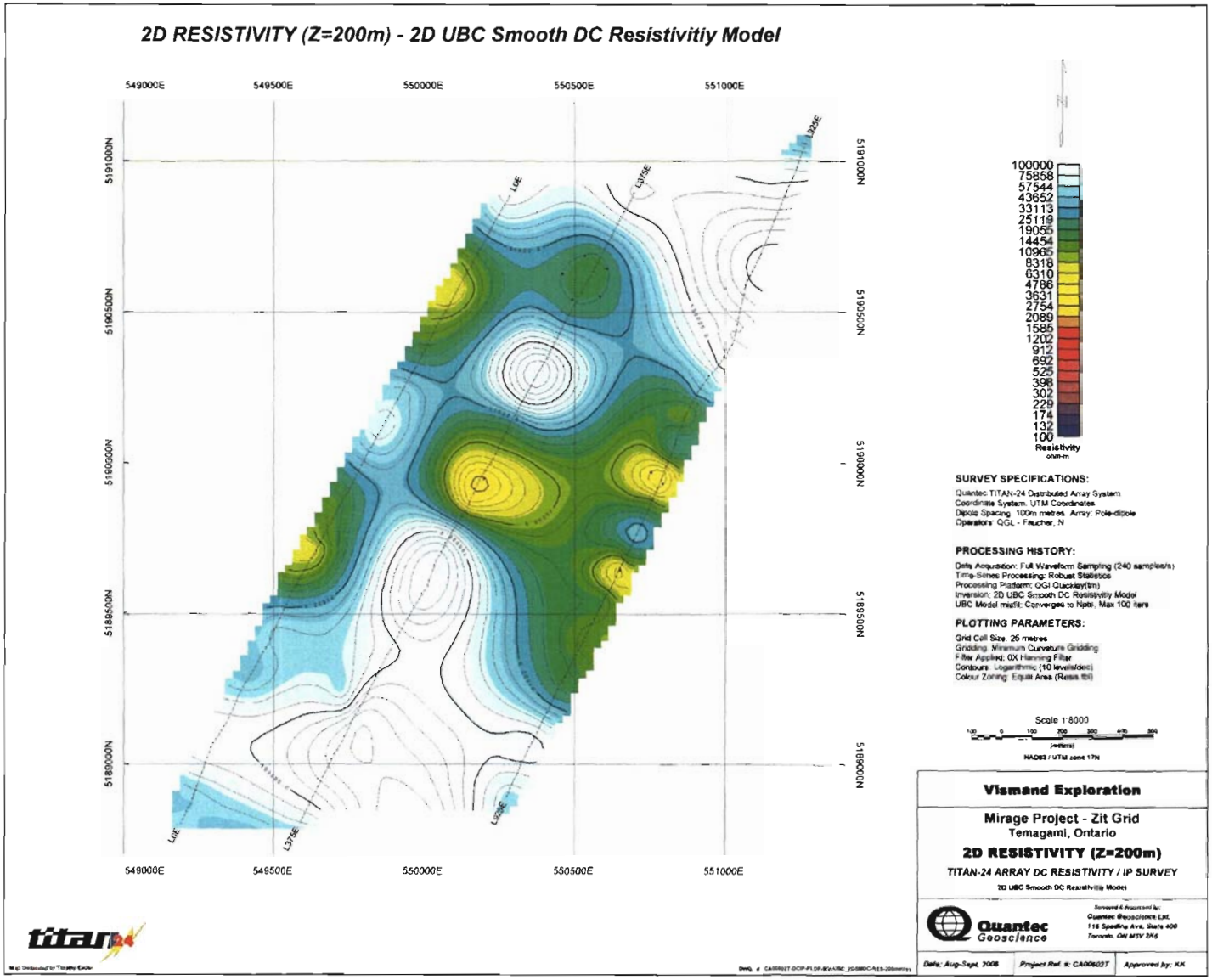

2D Resistivity (Z=400m) – 2D UBC Smooth DC Resistivity Model

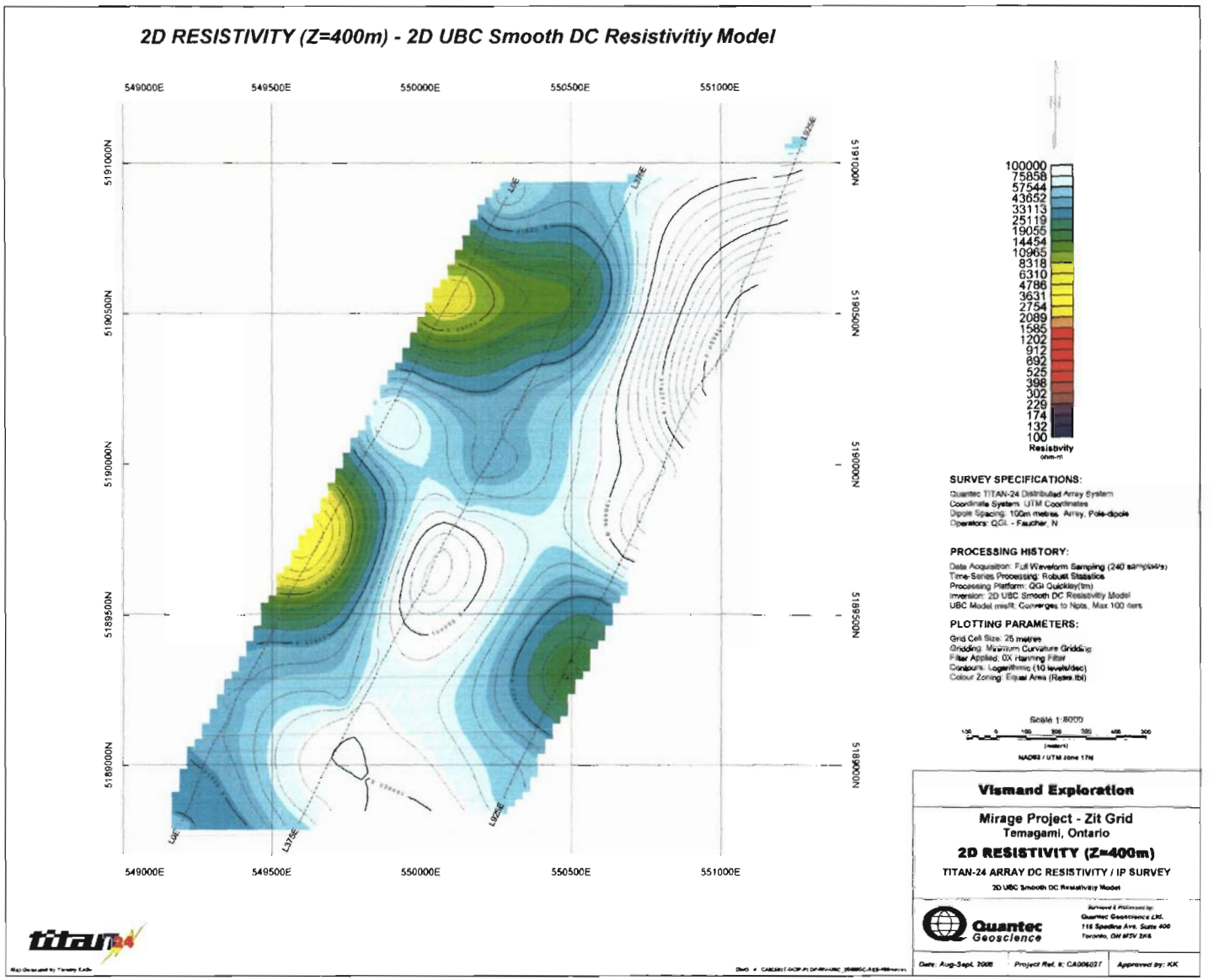

2D Chargeability (Z=50m) – 2D UBC Smooth IP Chargeability Model

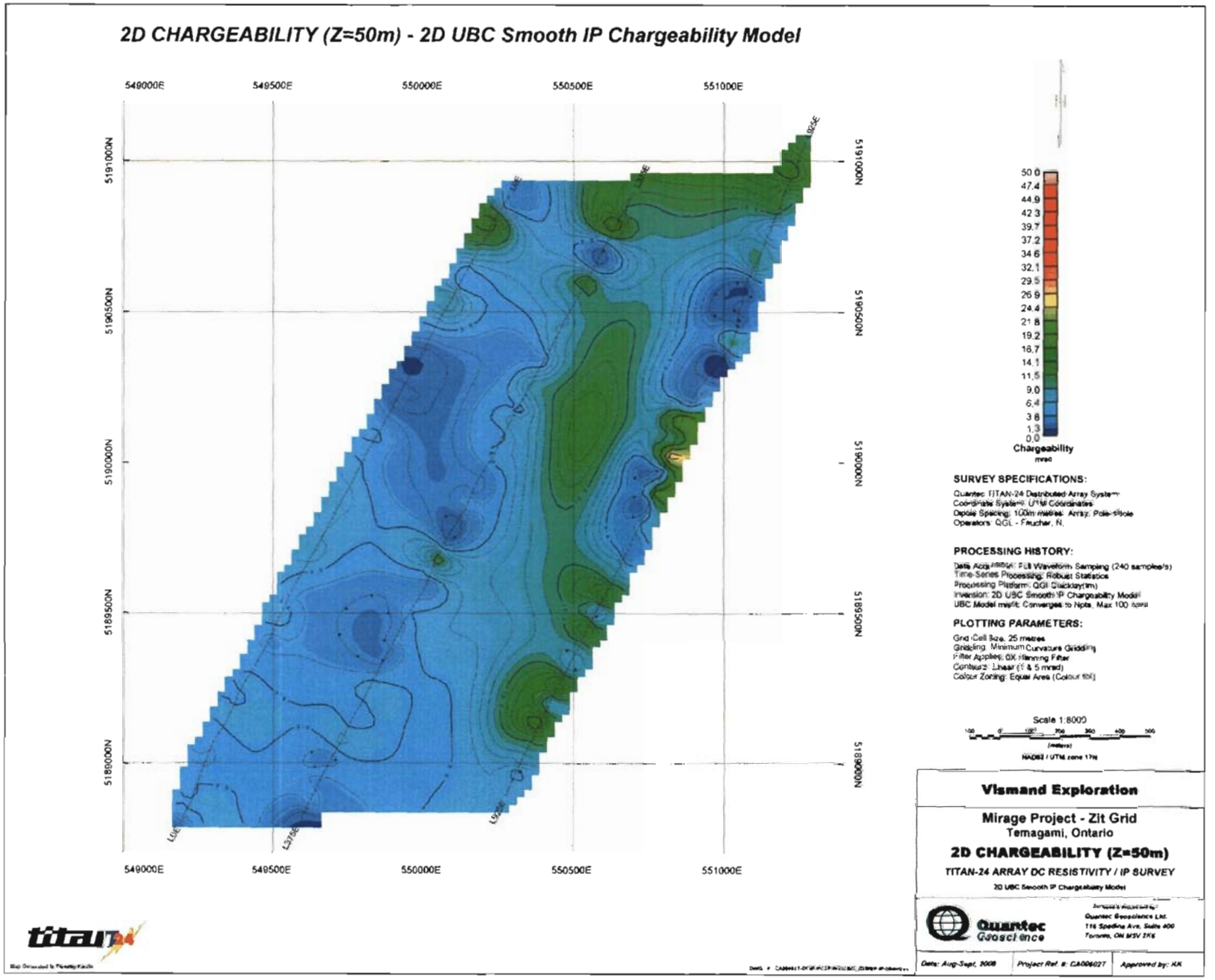

2D Chargeability (Z=100m) – 2D UBC Smooth IP Chargeability Model

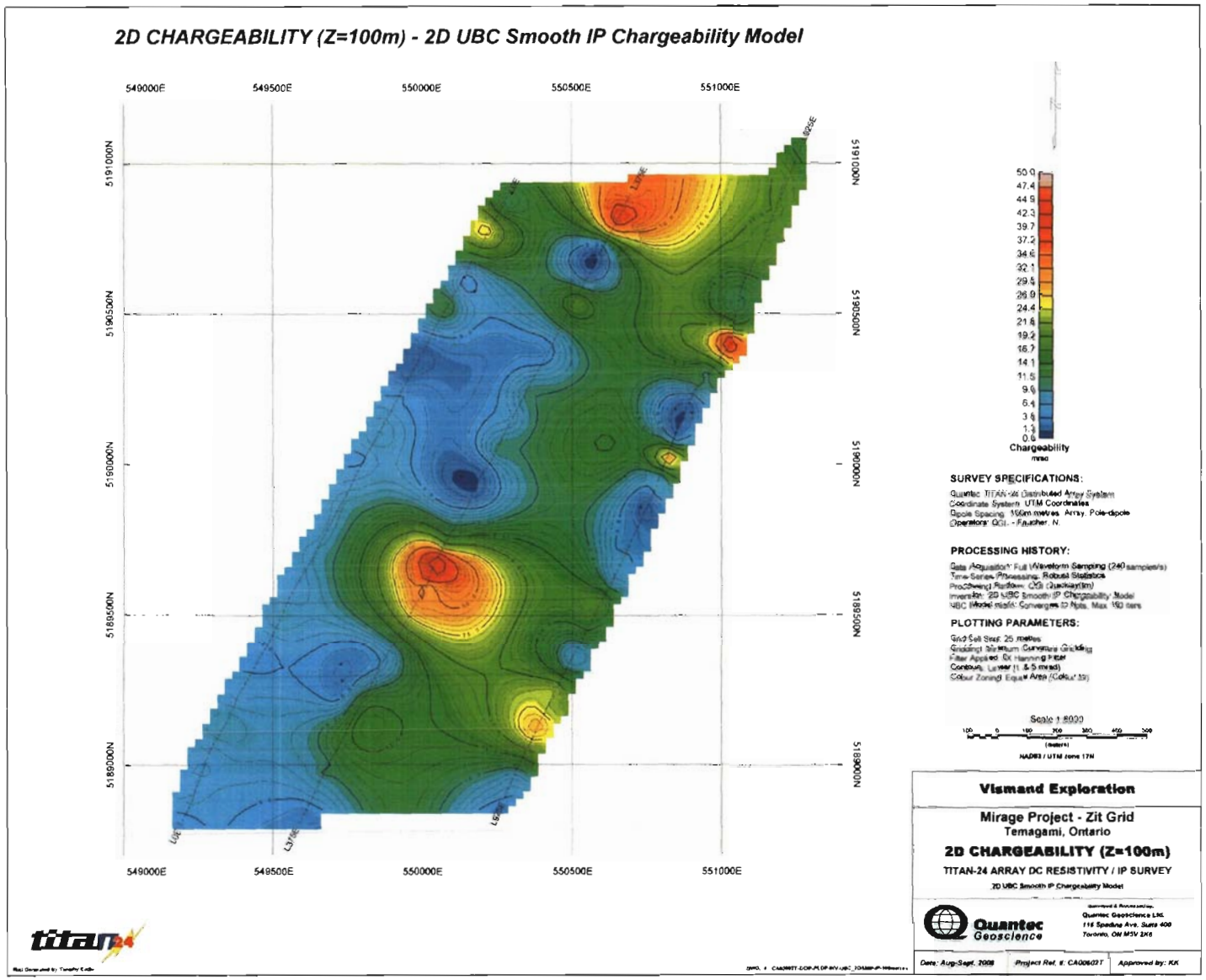

2D Chargeability (Z=200m) – 2D UBC Smooth IP Chargeability Model

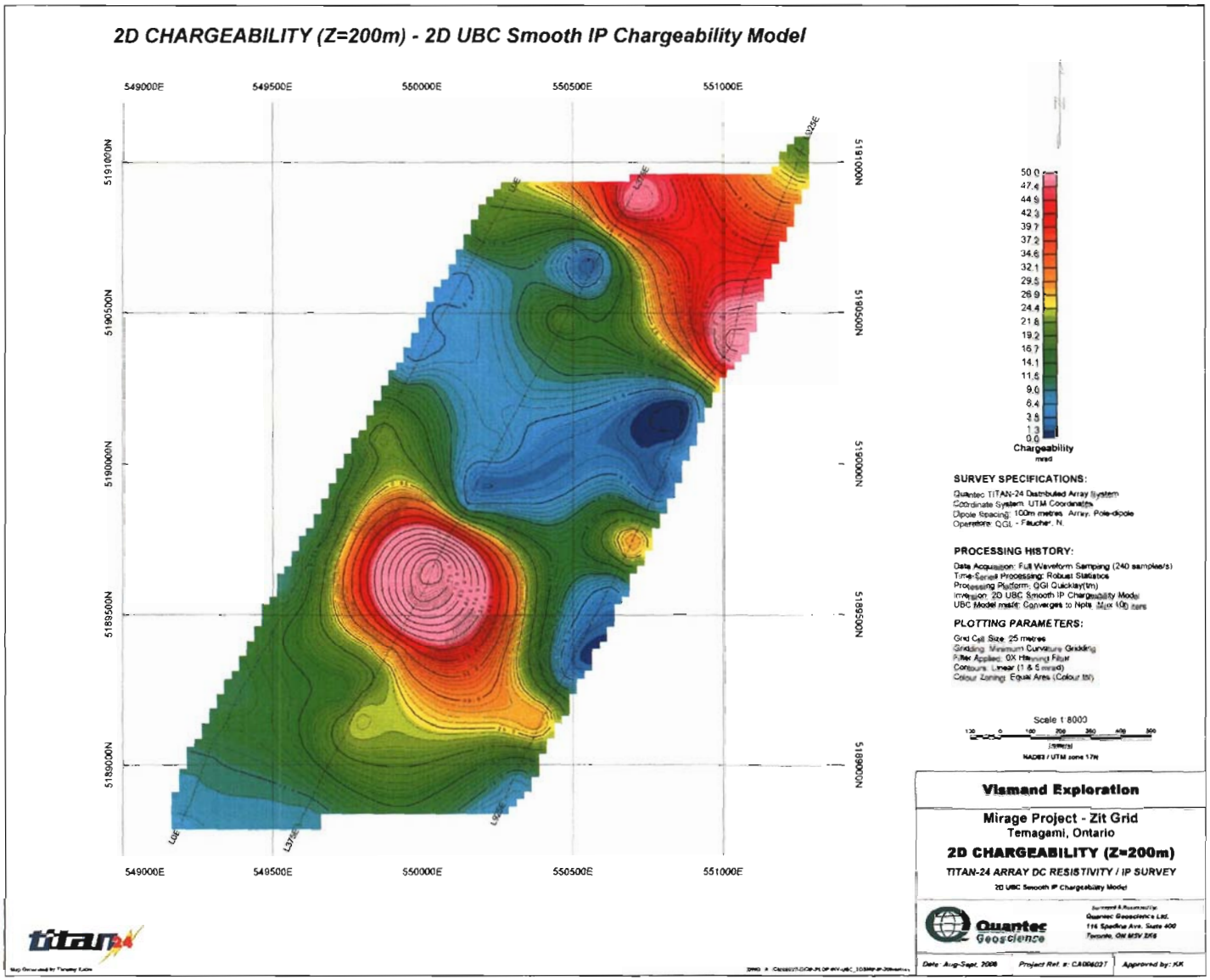

2D Chargeability (Z=400m) – 2D UBC Smooth IP Chargeability Model

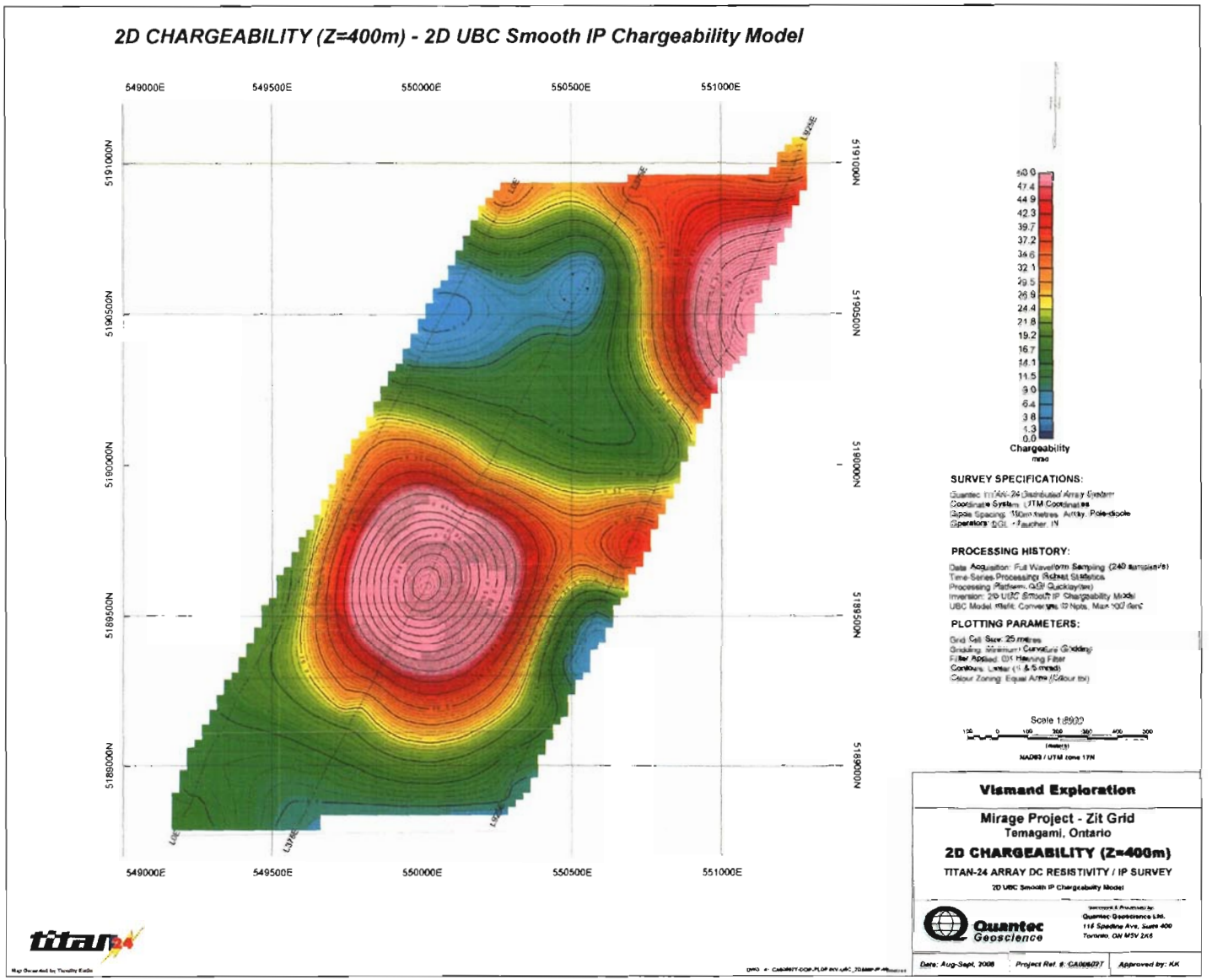

2D Chargeability (Z=50m) – 2D UBC Null Con IP Chargeability Model

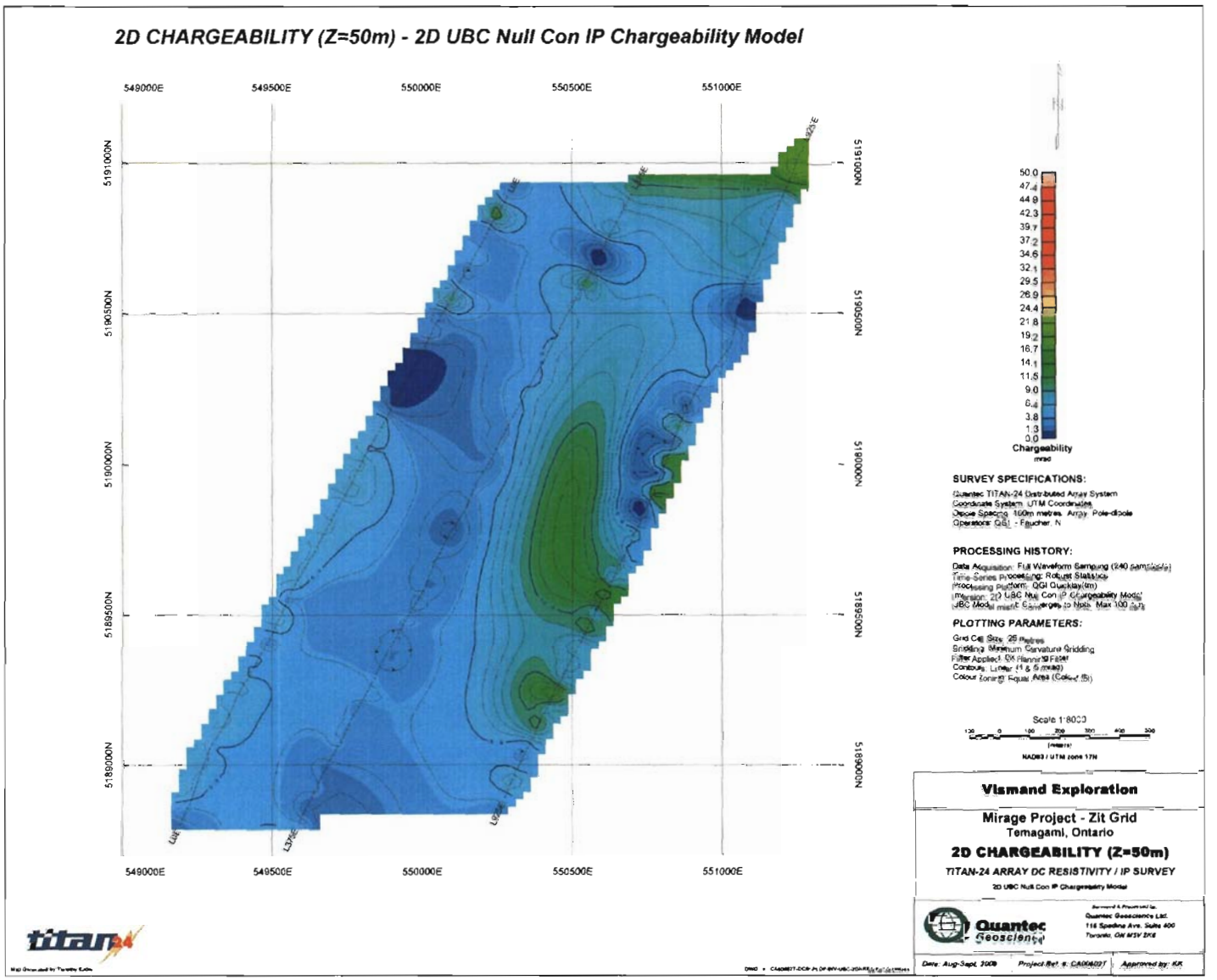

2D Chargeability (Z=100m) – 2D UBC Null Con IP Chargeability Model

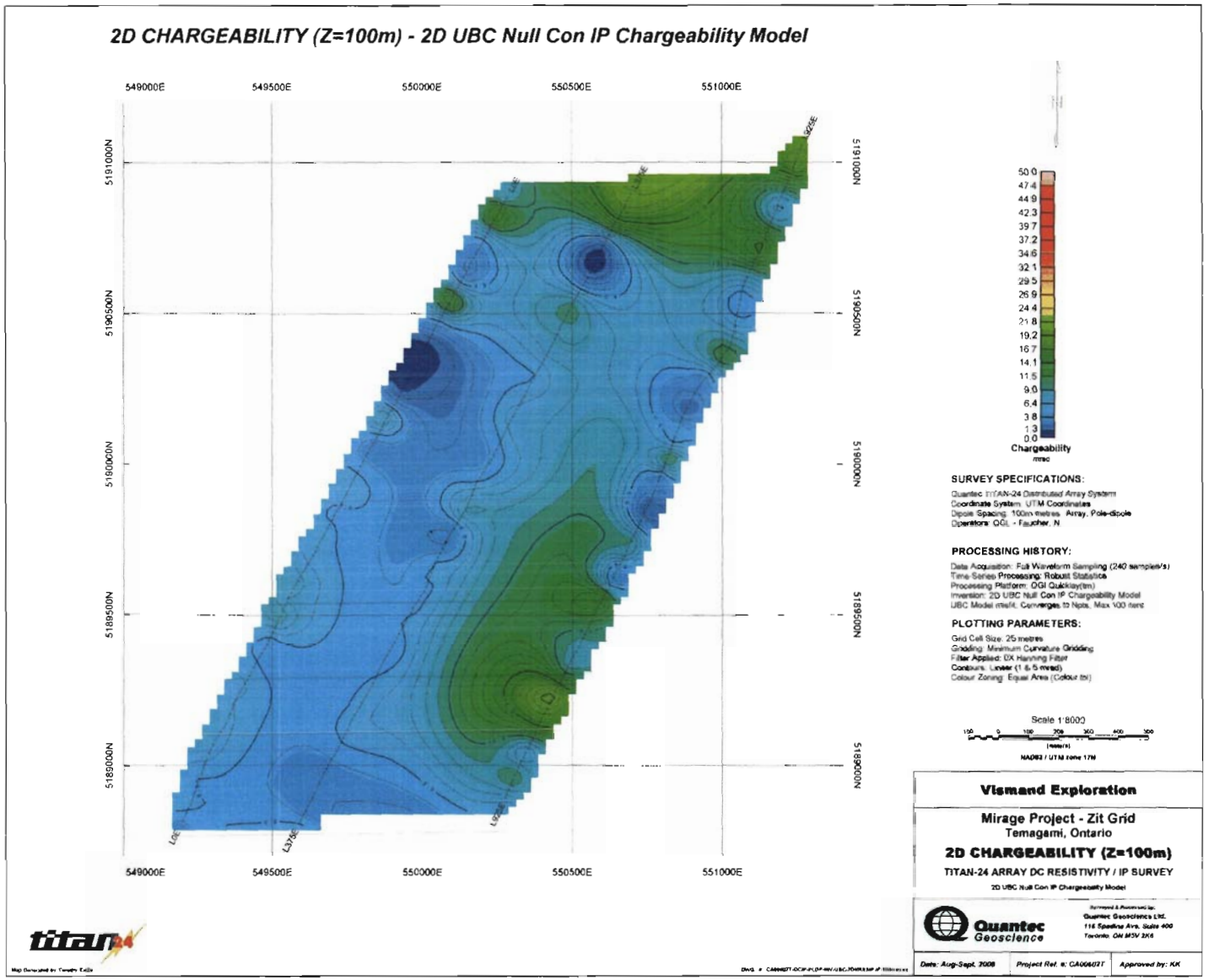

2D Chargeability (Z=200m) – 2D UBC Null Con IP Chargeability Model

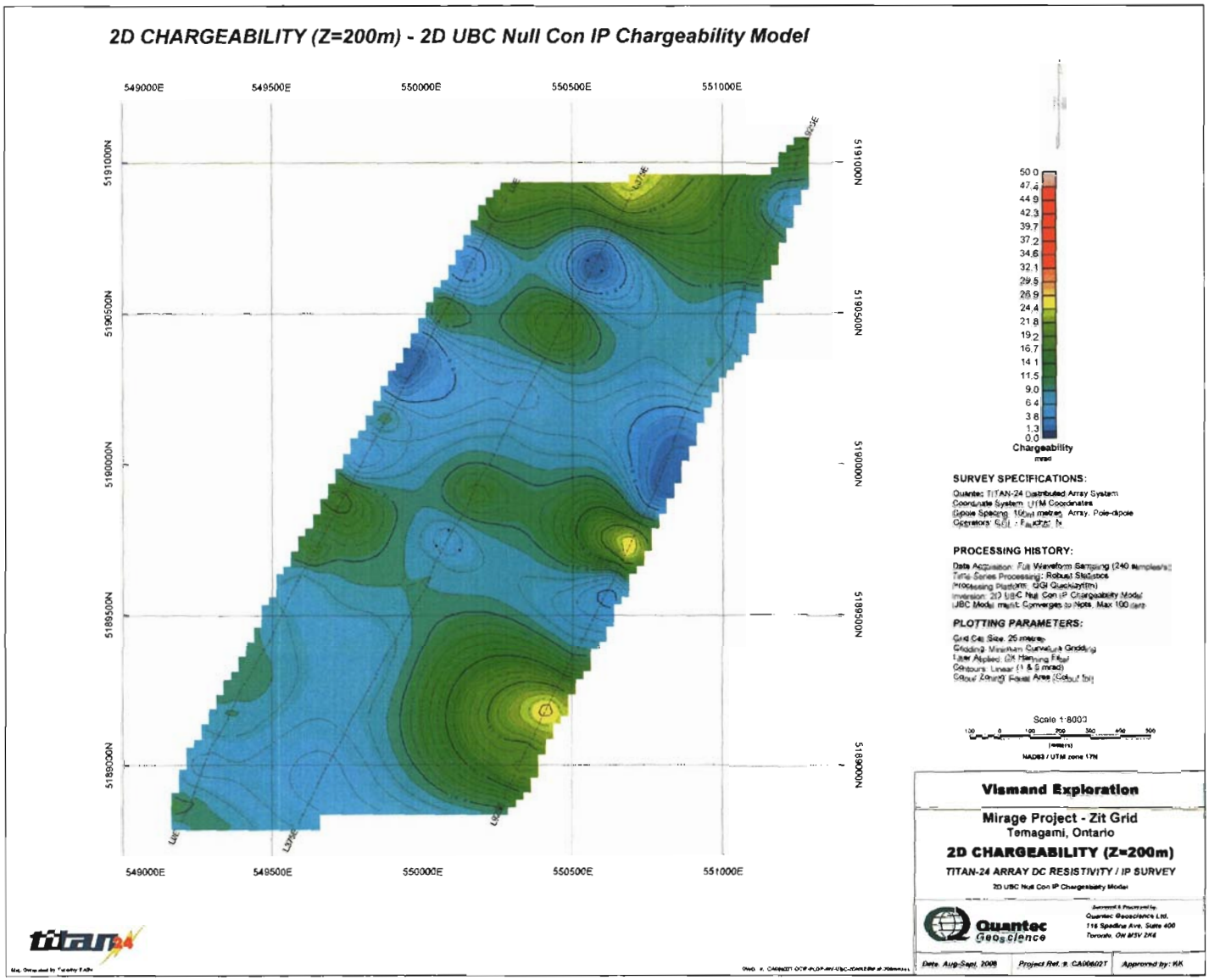

2D Chargeability (Z=400m) – 2D UBC Null Con IP Chargeability Model

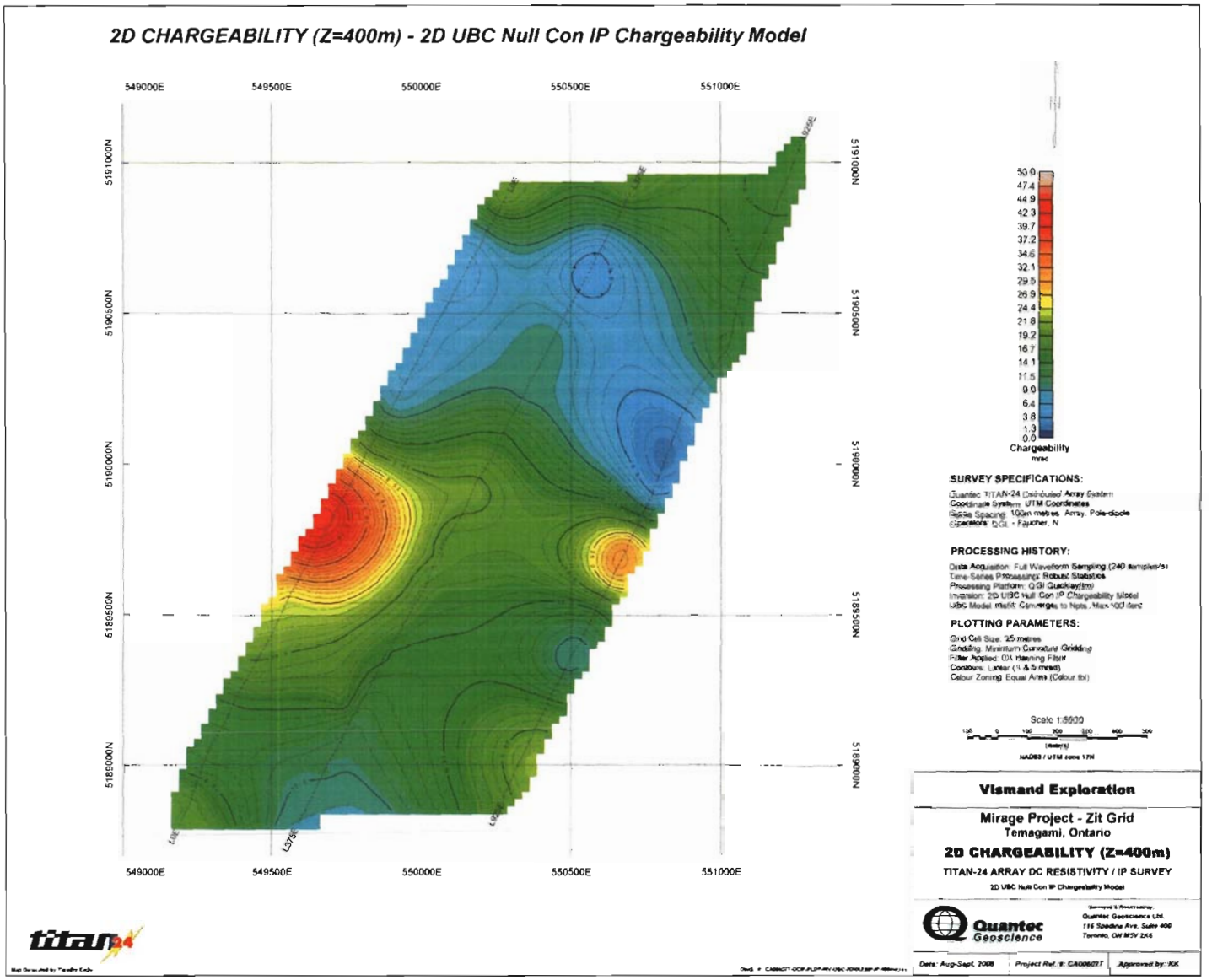

2D Resistivity (Z=50m) – 2D MT PW TM+TE(phs) Inversion (starting from 1000 ohm-m halfspace)

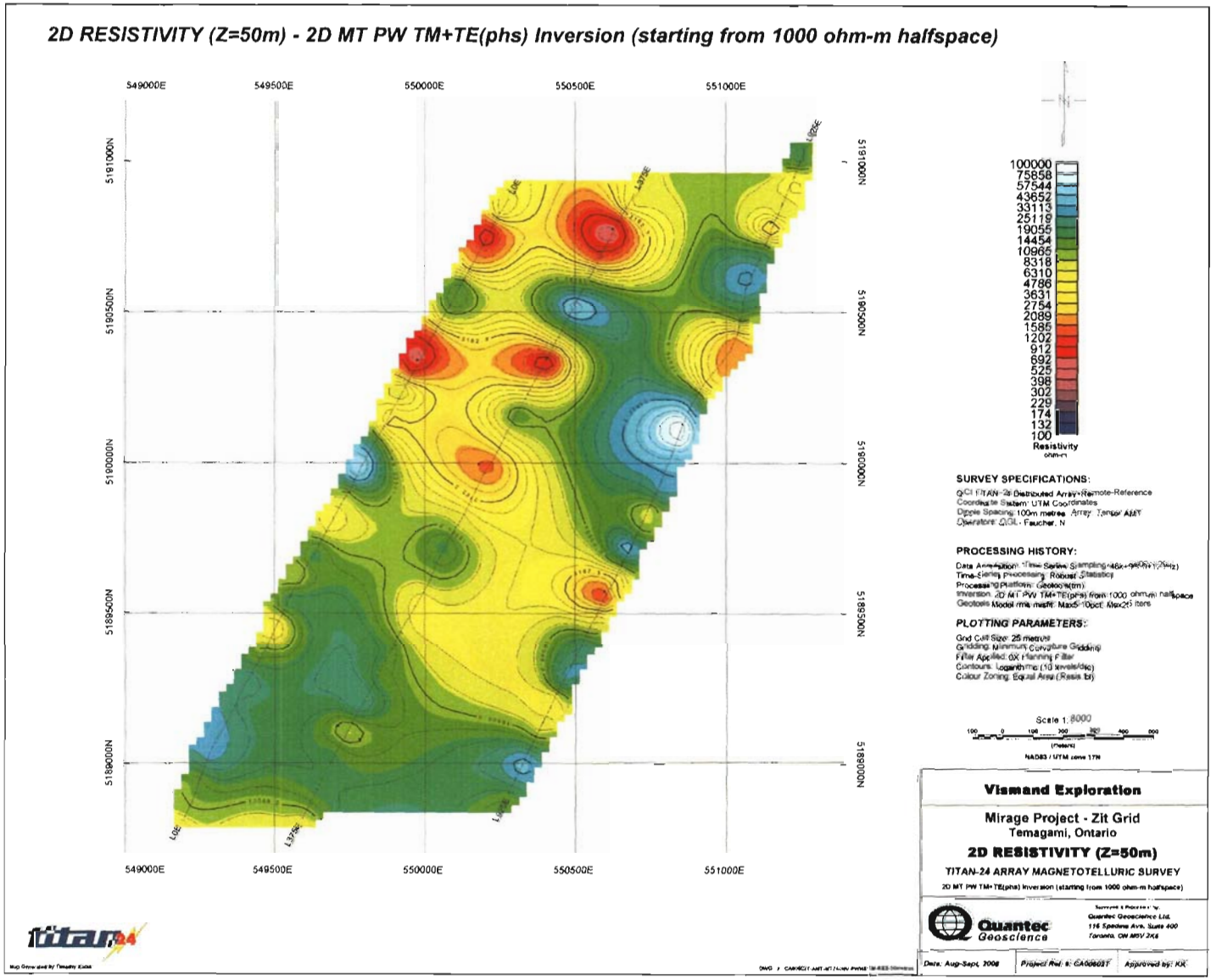

2D Resistivity (Z=100m) – 2D MT PW TM+TE(phs) Inversion (starting from 1000 ohm-m halfspace)

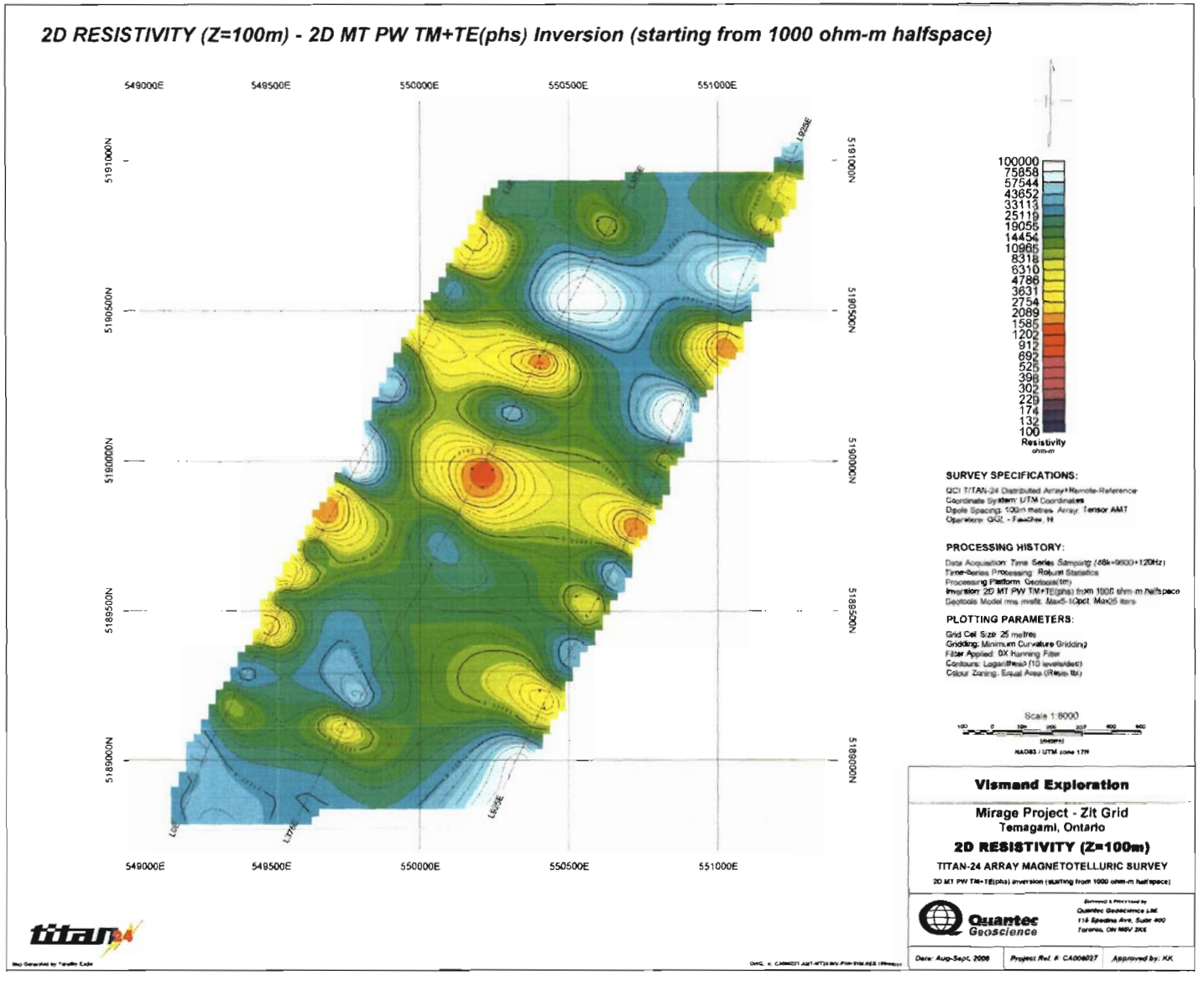

2D Resistivity (Z=200m) – 2D MT PW TM+TE(phs) Inversion (starting from 1000 ohm-m halfspace)

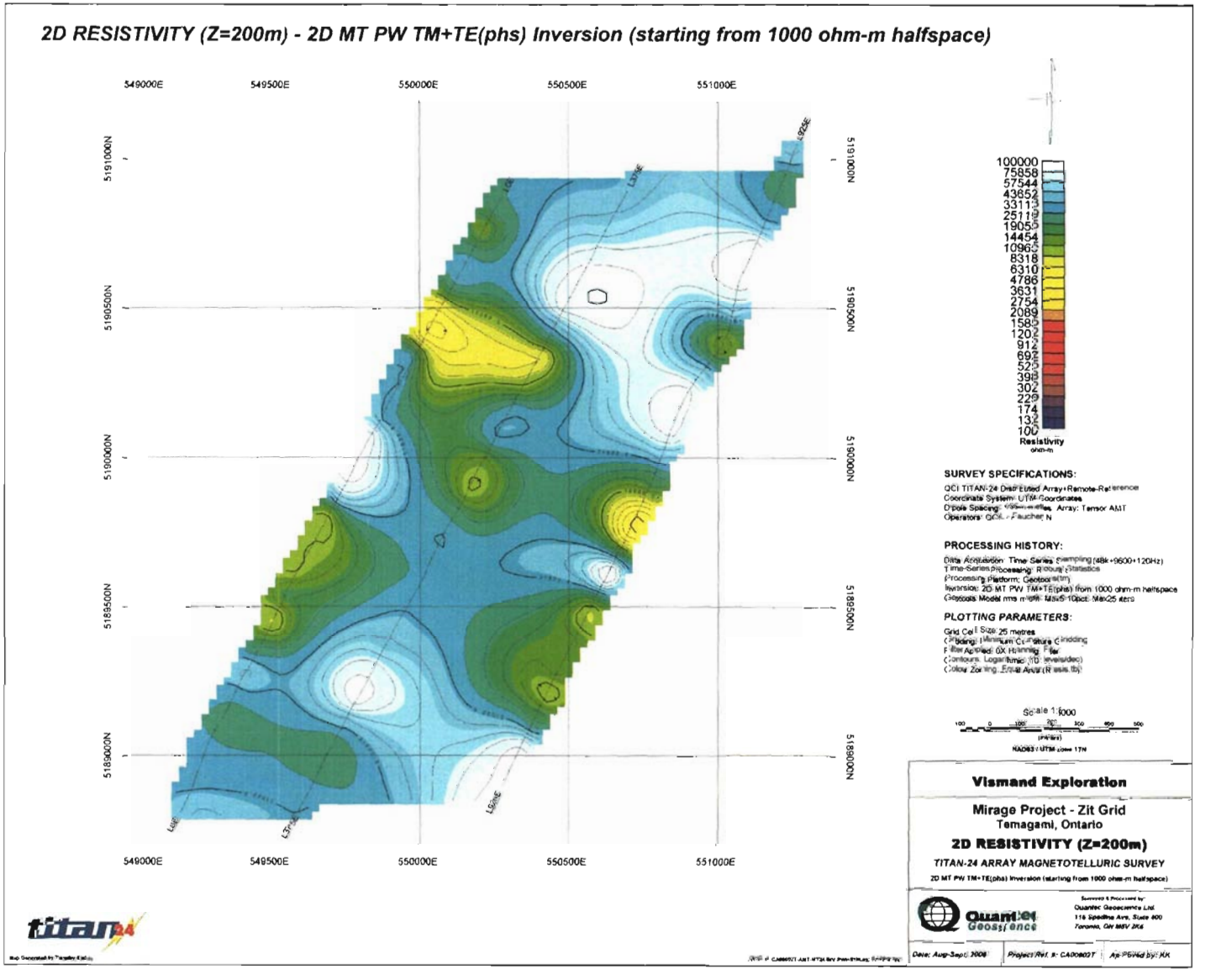

2D Resistivity (Z=400m) – 2D MT PW TM+TE(phs) Inversion (starting from 1000 ohm-m halfspace)

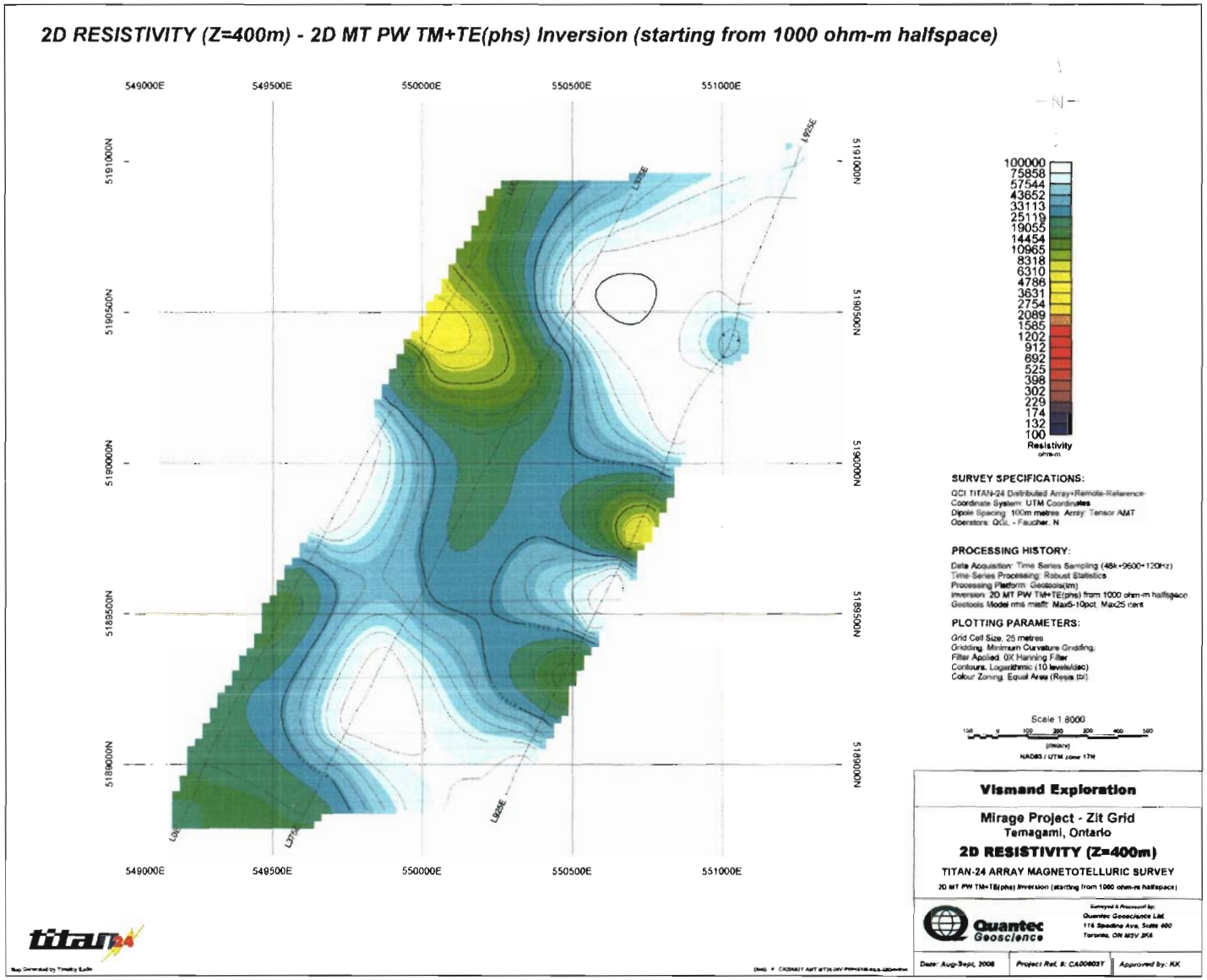

2D Resistivity (Z=1000m) – 2D MT PW TM+TE(phs) Inversion (starting from 1000 ohm-m halfspace)

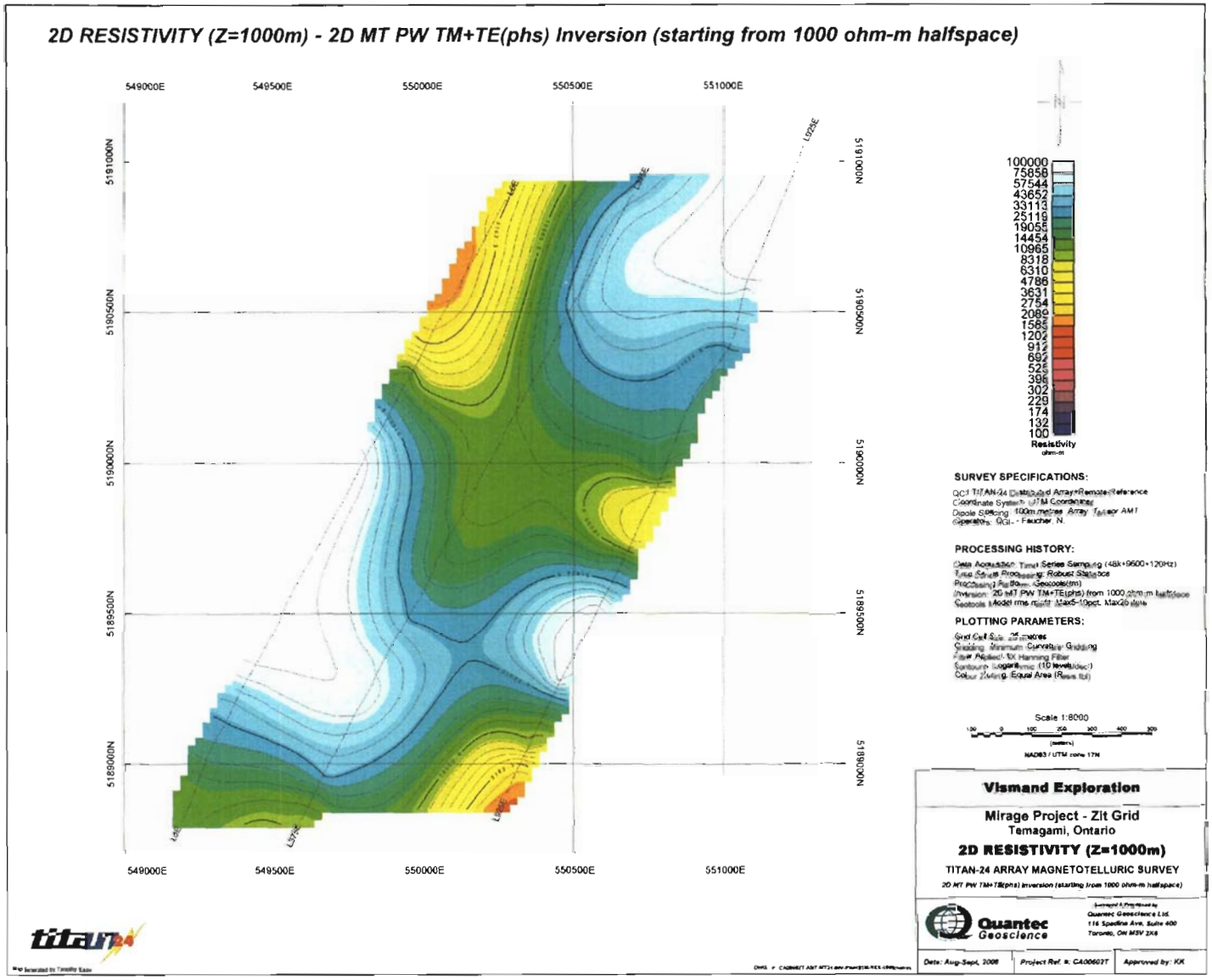

APPENDIX E: DCIP THEORY

INTRODUCTION

The resistivity is among the most variable of all geophysical parameters, with a range exceeding 10^6. Because most minerals are fundamentally insulators, with the exception of massive accumulations of metallic and submetallic ores (electronic conductors) which are rare occurrences, the resistivity of rocks depends primarily on their porosity, permeability and particularly the salinity of fluids contained (ionic conduction), according to Archie's Law. In contrast, the chargeability responds to the presence of polarizeable minerals (metals, submetallic sulphides and oxides, and graphite), in amounts as minute as parts per hundred. Both the quantity of individual chargeable grains present, and their distribution within subsurface current flow paths are significant in controlling the level of response. The relationship of chargeability to metallic content is straightforward, while the influence of mineral distribution can be understood in geologic terms by considering two similar, hypothetical volumes of rock in which fractures constitute the primary current flow paths. In one, sulphides occur predominantly along fracture surfaces. In the second, the same volume percent of sulphides are disseminated throughout the rock. The second example will, in general, have significantly lower intrinsic chargeability.

More detailed descriptions on the theory and application of the IP/Resistivity method can be found in Van Blaricom (1992) and Telford et al. (1976).

HALVERSON-WAIT CHARGEABILITY

The Titan-24 DCIP chargeability decays are described using the Halverson-Wait spectral model (Halverson et al., 1981), which is not well known, but is similar to the Cole-Cole model proposed by Pelton et al. (1978) which is a simple relaxation model that fits complex (frequency-dependant) resistivity results.

The time domain chargeability, originally proposed by Siegel (1959), is defined (Telford et al., 1976) as

$$M = \frac{1}{V_C} \int_1^2 V(t)dt$$

Where $V(t)$ is the residual or secondary voltage at a time t, that is decaying after the current is cut off, between time t_1 and t_2, with the steady voltage V_C during the current flow interval. The ratio $V(t)/V_C$ is expressed in millivolts per volt.

In the frequency domain, the "frequency effect" is defined as:

$$fe = (\rho_{DC} - \rho_{AC}) / \rho_{AC}$$

Where ρ_{DC} and ρ_{AC} are apparent resistivities measured at d.c. and "very high" frequency, usually in the 0.1 to 10 Hz range.

The Cole-Cole model for the chargeability m, as defined by Pelton et al. (1978) is given by the following:

$$Z(\omega) = R_0 \left[1 - m \left(1 - \frac{1}{1 + (i\omega\tau)^C} \right) \right]$$

Where $Z(\omega)$ is the complex impedance, R_0 is the DC resistivity, m is the chargeability in volts per volt, ω is

the angular frequency in Hz, τ is the time constant in seconds, and ***c*** is the frequency dependence (unitless). The latter two physical properties describe the shape of the decay curve in time domain or the phase spectrum in frequency domain, and commonly range between 0.01s to +100s and 0.1 to +0.5, respectively (Johnson, 1984).

The Halverson-Wait model was proposed by Halverson et al. (1981) as an extension to the Wait (1959) model of the impedance of "volume loading" of spheres, given by:

$$Z(\omega) = \frac{\rho}{G}\left[1 - 3v\left(1 - \frac{3\delta}{1+2\delta}\right)\right]$$

Where ***G*** is a geometric factor, ρ is the resistivity of the media, ***v*** is the volume loading (the volume fraction of chargeable "spheres"), δ is the sphere surface impedance. The Wait model was designed to provide an explanation of the differences in the shape of decay curves from different polarizeable targets, but does not describe very well the physical attributes of the rocks.

The Halverson-Wait model expands the Wait coated sphere IP model to include a new formulation of the sulphide-rock interface impedance, based on field studies and laboratory tests on samples. It is closely correlated to the Pelton et al. (1978) Cole-Cole model and is given by:

$$Z(\omega) = \frac{\rho}{G}\left[1 - 3v\left(1 - \frac{3/2}{1 + r[i\omega]^{K}}\right)\right]$$

Where ***r*** is the sphere radius and is equivalent to τ - the Cole-Cole time constant ($r = \tau^{K}$). The ***v*** volume loading compares well to ***m*** – the Cole-Cole chargeability (see equation below) – and the exponent ***k*** is equal to ***c*** - the Cole-Cole frequency dependence (Halverson et al., 1983). For sulphide systems, the *r*-factor reflects the size or interconnection of the sulphide grains and the *k*-factor reflects the electrical characteristics of the sulphide surfaces. An example of time domain Halverson-Wait model responses is shown in Figure G.1.

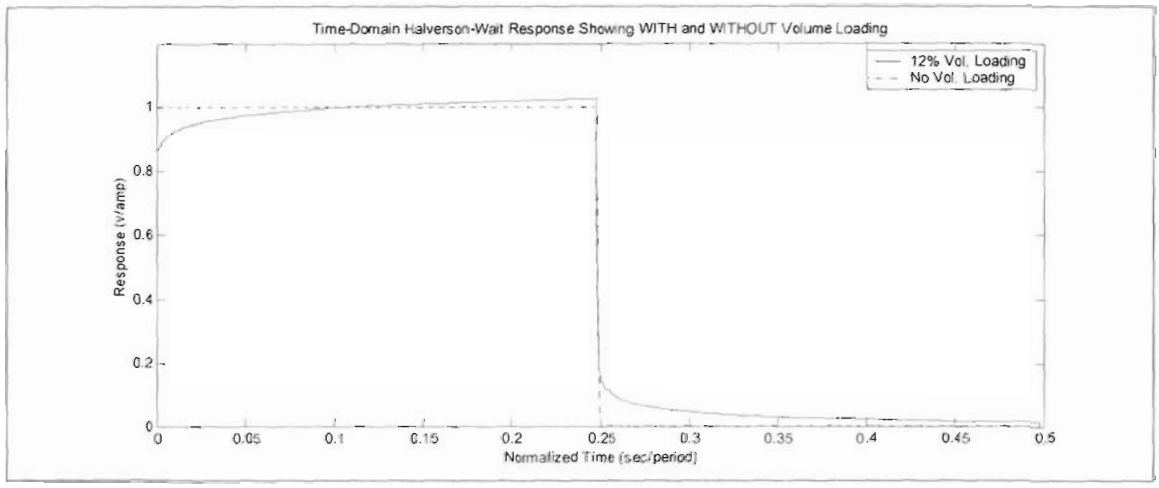

Figure G.1: Polarizeable versus Non-Polarizeable TDIP Response using Halverson-Wait Model

In practice the Titan chargeability decays are fit to a Halverson-Wait model. In order to solve for the volume loading *v*, the *r*-factor and *k*-factor are set to the standard (typical) Halverson-Wait values of 1.0 and 0.2, respectively. In the Halverson-Wait model the theoretical PFE (for infinite bandwidth), which equates to the theoretical chargeability in the Cole-Cole equation, is thereby defined by the volume loading:

$$PFE_0 = m_0 = \frac{9v}{(2+3v)}$$

and ***m*** is output in units of milliradians.

INVERSION THEORY

An excellent overview and introduction to both the philosophy and use of inversions in geophysics is available on the University of British Columbia (UBC) website (http://www.geop.ubc.ca/ubcgif/; Oldenburg et al., 1998).

Several points, detailed on the website, are crucial to understanding the Titan-24 approach to exploration:

- Inversion is a powerful 'tool', not a 'solution'
- Inversion is not normally "unique". Given noisy and incomplete data of inherently limited resolution there are usually an 'infinite' range of models that 'fit' the data equally well. Recognition of this inherent non-uniqueness is why inversion must be viewed as a tool rather than a solution. Understanding and exploration of this non-uniqueness is an important part of the interpretive process.
- Inversion finds a model that 'fits' the data. The precise definition of 'fit' can be critical in the actual model that is found.
- The inversion depends on the data, and the data errors. The importance of the data errors is often overlooked.
- Inversion depends on a "model norm" – the mathematical definition of which model the inversion should try to find. This definition is almost as important as the actual data in determining the final inversion model.

Mathematically, inversion is the process of minimizing a function. The choice of which function to minimize ultimately defines the inversion model. Schematically, this function might be expressed:

$$\phi = \phi_d + \beta \phi_m = \text{(misfit)} + \beta\,\text{(model norm)}$$

$$0 < \beta < \infty \quad \beta \text{ is a constant}$$

This defines a function to be minimized that consists of some function that minimizes the data misfit, combined with some function that finds a "smooth" model. Beta represents a relative weighting between fitting the data and smoothing the model.

Clearly, the data misfit function must be defined in more detail. One approach might be:

$$\phi_d = \sum_{i=1}^{N} \left(\frac{F_i[m] - d_i^{obs}}{\varepsilon_i} \right)^2$$

This function defines the data misfit as the sum of the individual misfits squared, normalized by the errors associated with each data point. It is a very common, and stable, definition of the data misfit.

An important point not made on the UBC website is that the errors depend on many factors. The most common measure of data errors is simply the repeatability of the voltage and current measurements in the field. This may be misleading as there are also "errors" associated with electrode positioning, geologic complexity (2D vs 3D, but also coupling of shallow and deeper structure), and errors in the numerical calculation of model responses and inversion.

Another point not sufficiently detailed on the UBC site is the importance of not overestimating the data errors and fitting the data as closely as possible. Most geophysical techniques, but particularly electrical techniques, have large responses to shallow structure. This is expressed as "pant legs" in DC/IP, or "statics" in MT. The response to deep structure is generally a very subtle component of the data, compared to the sensitivity to shallow structure. Without excellent data, and an excellent match between the data and model response, the deep structure will not be imaged to the degree necessary for commercial exploration.

The model misfit function must also be defined in more detail. One of the most flexible definitions is the one used by UBC:

$$\phi_m(m,m_0)=\alpha_s\int_{vol}(m-m_0)^2dv+\alpha_x\int_{vol}\left(\frac{\partial(m-m_0)}{\partial x}\right)^2dv+\alpha_z\int_{vol}\left(\frac{\partial(m-m_0)}{\partial z}\right)^2dv$$

In this definition there are three components to the "model norm" (or "smoothness" constraint, or "regularization"), each of which contains an α constant (α_S, α_X, α_Z) that are commonly referred to as "alpha parameters". The first component is simply an overall difference between the model and a "target" model, the second component is a horizontal smoothness, and the third component is a vertical smoothness. The three "alpha" parameters (α_S, α_X, α_Z) represent a relative weighting of each component. A fourth variable, m_0, refers to the starting or reference model – either a half-space or geophysical constraint – that also has a profound influence on the model-misfit.

The UBC website provides an excellent example of the importance of selecting an appropriate "model norm", reproduced in Figure G.2

In this example the expected response of the top figure was computed. These 'data' were then inverted six times, using different "model norms" (α_S, α_X, α_Z, m_0). The lower six figures show the range of valid inversion models that can be produced. Note that six of these models are essentially mathematically equivalent, they all "fit" the data.

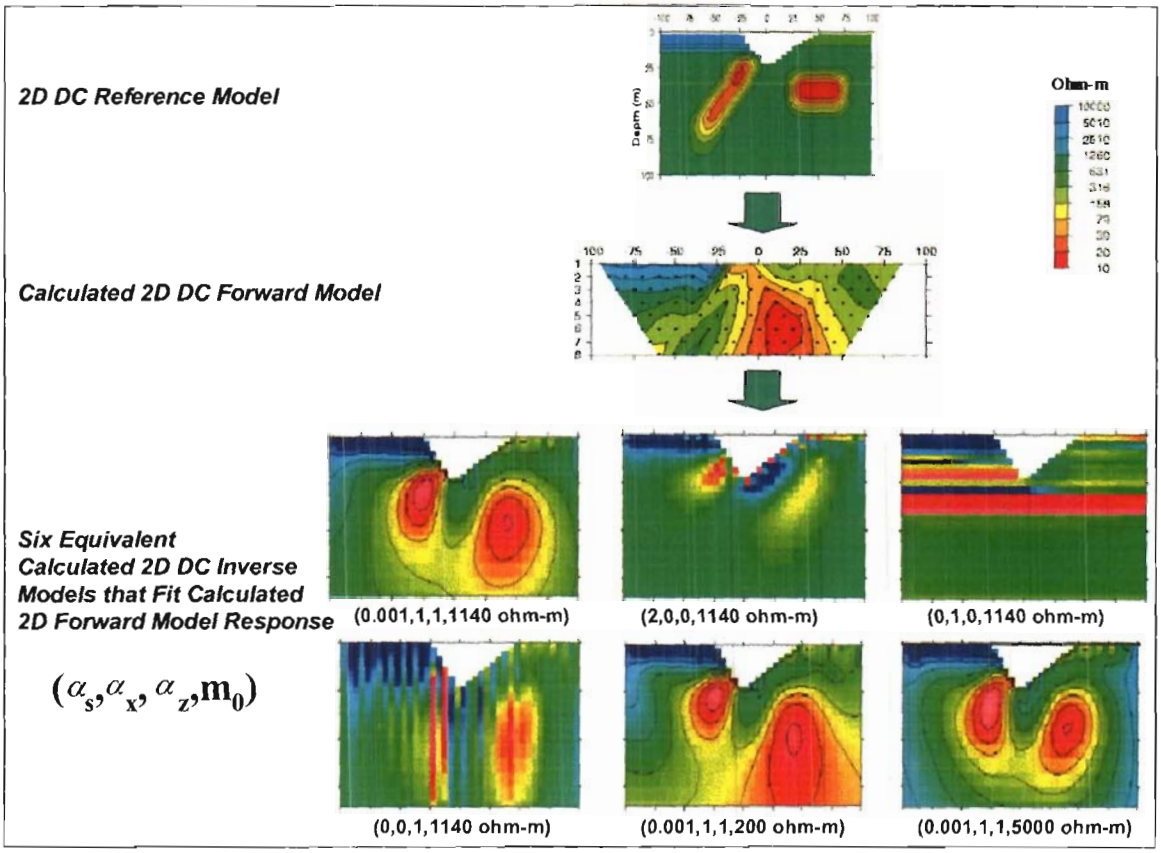

Figure G.2: Effects of Model Norm and Starting Model on Inversion Results (modified after Oldenburg, et al.,1998).

An important philosophy, driving much of the academic communities approach to inversion for the last two decades, is that the "best" model is the "smoothest" model consistent with the data. There are good reasons for taking this approach. However, from an exploration viewpoint this philosophy can be re-phrased to "find the model with the least exploration value" – perhaps not reflecting the real goal of an exploration program.

Recently, several groups have taken major steps towards developing inversion approaches more tuned to exploration needs. Instead of using "smooth" model norms, they are being replaced with "focused (minimum transition zone) inversion, or smoothing to a geologic "target" model.

For exploration smoothing to a geologic target model makes sense. It requires good geologic control, and some understanding of the rock physical properties. There are three drawbacks to the geologic target approach:

- The geologic information is incomplete or inaccurate.
- Physical property data are incomplete.
- It is difficult to determine whether the geophysical data support the geologic model, or simply provide no information.

The most sensible approach is to combine smooth model inversion with geologic target inversion. For now, we are focusing on providing inversions using both approaches. It is up to the project geologist and geophysicist to review these inversions and develop a final interpretation.

REFERENCES

1. Halverson, M., Zinn, W.G., McAlister, E., Ellis, R., and Yates, W. (1981). Assessment of results of broad-band spectral IP field tests. In: Advances in Induced Polarization and Complex Resistivity, pp. 295–346, University of Arizona.
2. Johnson, I. (1984). Spectral induced polarization parameters as determined through time-domain measurements. Geophysics, v. 49, pp. 1993-2003.
3. Oldenburg, D., and Li, Y. (1999). Estimating depth of investigation in DC and IP surveys. Geophysics, v. 64, pp. 403-416.
4. Oldenburg, D., and Li, Y. (1994). Inversion of induced polarization data. Geophysics, v. 59, pp. 1327-1341.
5. Oldenburg, D., Li, Y., and Jones, F. (1998). Tutorial: Inversion (Res/IP) Methodology. In: The UBC Geophysical Inversion Facility Tutorials. [On line]. http://www.geop.ubc.ca/ubcgif/tutorials/invtutorial/index.html.
6. Pelton, W., Ward, S., Hallof, P., Sill, W. and Nelson, P. (1978). Mineral discrimination and removal of inductive coupling with multifrequency IP. Geophysics, v. 43, pp. 588-609.
7. Seigel, H. (1959). Mathematical formulation and type curves for induced polarization. Geophysics, v. 24, pp. 547-565.
8. Telford., W.M., Geldart, L., Sheriff, R., and Keys, D. (1976). Applied Geophysics. Cambridge University Press, New York, NY, 860 pp.
9. Van Blaricom, R. (1992). Practical Geophysics for the Exploration Geologist. Nortwest Mining Association, Spokane, WA, 570 pp.
10. Wait, J. (1959). Overvoltage Research and Geophysical Applications. Pergammon Press.

APPENDIX F: MAGNETOTELLURIC THEORY

The magnetotelluric (MT) method measures time-variations in the Earth's natural electric (E) and magnetic (H) fields to image the subsurface resistivity structure. No source or transmitter is used. These natural fields penetrate much deeper than is practical with a transmitter. At the same time the natural signals are a plane-wave source. The plane-wave source is much simpler to model than complex transmitter geometries and signals.

The E and H fields are measured over a broad range of frequencies. Typically, the frequencies can range from above 10 kHz to below 0.001Hz. High frequency signals are attenuated more rapidly in the subsurface. High frequency data are indicative of shallow resistivity structure while low frequency data are indicative of deep resistivity structure.

At frequencies below 1Hz the signal source is due to oscillations of the Earth's ionosphere as it interacts with the solar wind. At frequencies above 1Hz the signal source is due to worldwide lightning activity. There is a lack of signal around 1Hz, often referred to as the "hole". Modern 24-bit recording hardware and signal processing techniques have largely eliminated the data quality problems that have been traditionally seen around the 1Hz signal hole.

Between about 8Hz and 300Hz the signal from worldwide lightning activity propagates in a "resonant" cavity (the resistive atmosphere) between the conductive ionosphere and the Earth's surface. Above 3 kHz the signal propagates as a ground wave. Between 300Hz and 3 kHz there is a "dead-band" where the signal does not propagate well. Despite hardware and signal processing improvements this dead-band remains problematic. When signal (atmospheric activity) is present within several hundreds of miles of the survey area the data is quite good. When no signal is being generated in the vicinity data quality is poor.

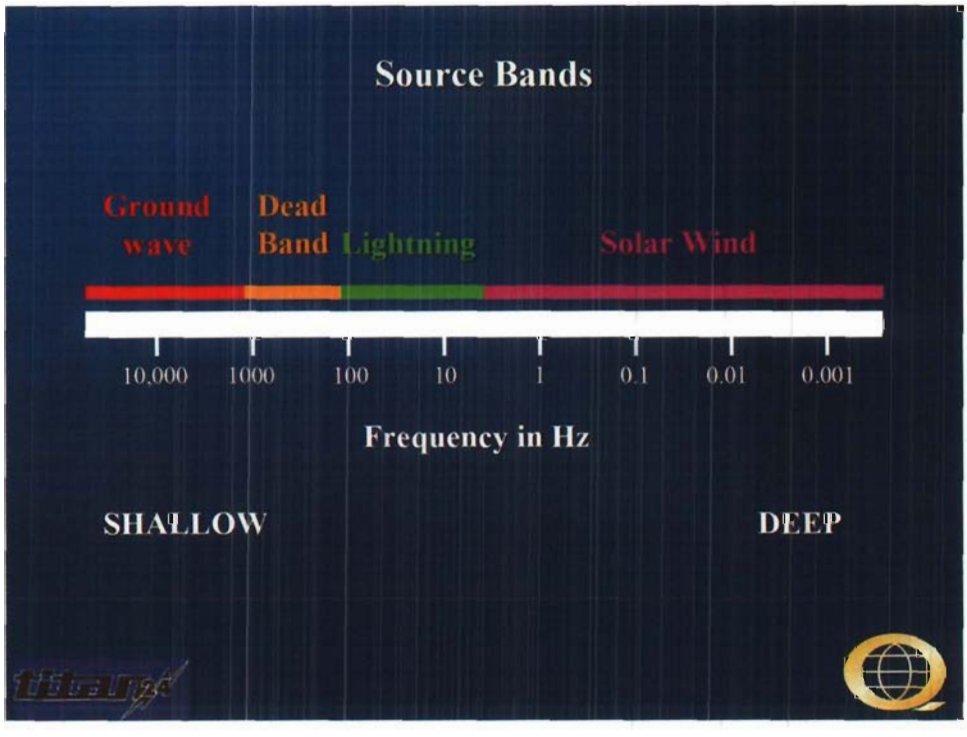

Both the electric and magnetic fields are measured. The measured fields depend on the ionosphere and lightning, and are essentially random. While the E and H fields are random the ratio of the fields depends on the subsurface resistivity structure. Note that it is primarily the orthogonal E and H fields that are related. The magnetic field must be measured perpendicular to the electric field. It is possible for complex subsurface resistivity structure to rotate the fields, and full tensor data are usually measured.

It is often useful to think of the magnetic field as the source signal and the electric field as the response. Time variations in the magnetic field induce currents to flow in the ground.

In the field the electric and magnetic fields are measured as a function of time. The electric field is measured using two orthogonal dipoles consisting of a wire connecting two grounded electrodes. In essence, the recording system consists of a voltmeter between the electrodes. The voltage measured depends on the electric field strength and the length of the dipole. The magnetic field is measured using an induction coil.

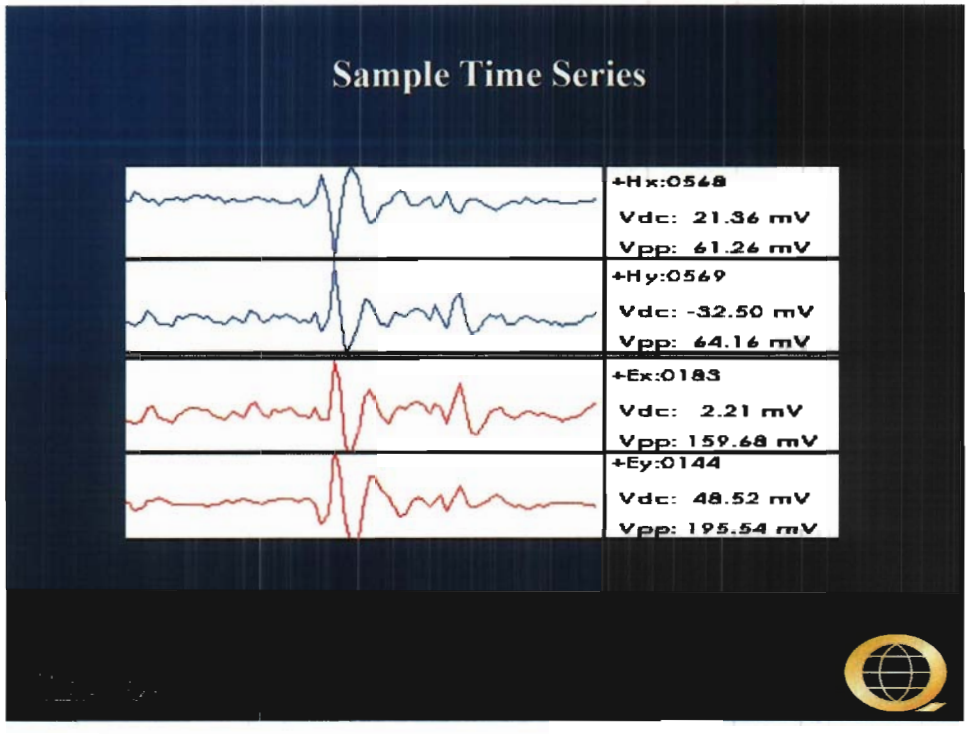

While the actual fields that are measured vary randomly (with solar and lightning activity), the relationship between the measured magnetic and electric fields is constant and depends on the subsurface resistivity structure. Extracting the subsurface resistivity structure from the measured magnetic and electric fields is a multi-step process. First time series processing techniques are used to derive geophysical parameters from the electric and magnetic fields. Then geophysical processing and inversion techniques are used to convert the geophysical parameters to a subsurface resistivity image. Finally, the resistivity image must be interpreted in terms of geologic units.

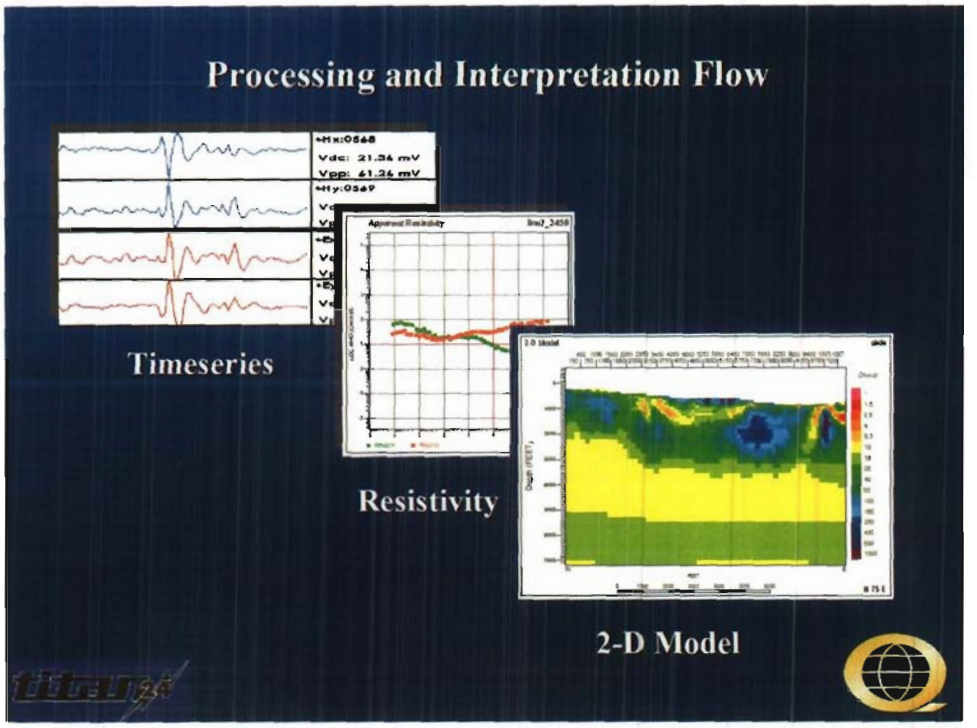

The measured magnetic and electric fields are Fourier transformed into the frequency domain. The system response is removed from the data (making the measurement independent of the hardware system). The Fourier coefficients represent the amplitude and phase of the electric and magnetic fields as a function of frequency.

A variety of signal processing techniques are used to minimize noise and bias in the estimation of geophysical parameters from the measured fields. The details are complex, but the approach is easily understood. Philosophically, the idea is to use multiple approaches to noise and bias reduction, not letting any one statistical approach have too much impact on the data, but relying on the combination of approaches to produce good estimates. The approaches include:

1. Spatial isolation of noise. A remote reference magnetic station is used to separate widely distributed signal from local noise.
2. Coherency sieves to find coherent signal. First the local and remote magnetic field measurements are compared and coherent signal kept. Then the local magnetic and electric fields are compared for coherency.
3. Frequency isolation of noise. Long Fourier transforms are used to provide extremely sharp isolation of noise in frequency.
4. Time isolation of noise. Short Fourier transforms are used to remove noise that is isolated in time (noise spikes, or noise that is randomly turning off and on).
5. Robust statistics that minimize biasing effects of a few isolated measurements.

Once the time series processing is complete geophysical parameters can be estimated. The primary geophysical parameters for MT are typically the apparent resistivity versus frequency and phase versus frequency.

The depth of penetration of the signal depends on its frequency and the resistivity of the rocks. The depth at which the signal amplitude has been attenuated to 37% (1/e) is called the skin depth and is defined:

$$\delta = \sqrt{\frac{2}{\mu\omega\sigma}} = 503\left(\sqrt{\frac{\rho}{f}}\right)(m)$$

where

δ = skin depth

μ = magnetic permeability

σ = conductivity=1/resistivity

ω = angular frequency=$2\pi f$

ρ=resistivity=1/conductivity

The ratio between the two measured components (E and H) is the electrical impedance. The impedance (denoted Z) is defined as $|Z| = |E/H|$. The impedance is a complex number because the E and H fields are out of phase. Note that Z, E, and H are all functions of frequency.

The complex impedance is used to calculate an apparent resistivity as follows:

$$\rho_a = \frac{1}{\mu\omega}|Z|^2 (ohm.m)$$

The apparent resistivity is also a function of frequency. At any frequency the fields must travel through the overlying geology. The apparent resistivity depends on the integrated (weighted) conductance of the rocks being sampled. It is a smoothly varying function of frequency because it represents the average resistivity of a progressively larger volume of the subsurface. On a log resistivity-log frequency plot the apparent resistivity generally can not exceed a slope of +/- 45 degrees.

The phrase "apparent resistivity" arises from the volume averaging. At a single frequency the electric and magnetic fields measurements can be used to calculate an impedance. This impedance depends on the resistivity of a large volume of the subsurface. The impedance can be thought of as the impedance of a half-space that would provide identical measurements to the actual subsurface.

The calculated phase or apparent phase is the difference between the measured E field phase and the measured H field phase. If the subsurface is one-dimensional (1D) or two-dimensional (2D) the phase is related to the resistivity. The Hilbert formula (minimum phase wavelet) relates the phase to the slope of the apparent resistivity curve. If the slope of the resistivity curve (on a log-log plot) is 0 the phase is 45 degrees. If the resistivity is increasing with decreasing frequency the phase is less than 45 degrees. If the resistivity is decreasing with decreasing frequency the phase is more than 45 degrees. As the apparent resistivities are constrained to a slope of no more than 45 degrees on a log-log plot, the phases are constrained to remain in a quadrant, between 0 and 90 degrees.

The phase measurement is largely independent of the apparent resistivity measurement. The Hilbert relationship provides an independent way to calculate the apparent resistivity curve from the phase data. There are effectively two independent measurements of the resistivity curve, providing a powerful check on data quality.

The apparent resistivity and phase curves are the primary parameters used in the interpretation of MT data. For a layered (1D) earth the apparent resistivity and phase data can be converted into intrinsic resistivity versus depth simply by accounting for the volume averaging nature of the method. There are a variety of algorithms for doing the conversion. The conversion is not unique. Some algorithms provide smoothly varying intrinsic resistivity versus depth functions (Occam inversion, Bostick transform). Others provide distinct layered solutions (Marquardt inversion).

1D modeling and inversion raises the following points:

- A single MT site provides information about resistivity versus depth. This is a major distinction from potential fields techniques that only provide information about relative variations along a profile.
- The conversion from apparent resistivity versus frequency to intrinsic resistivity versus depth is not unique. It is susceptible to equivalence. In particular any sharp resistivity contrast can be replaced by an equivalent transition zone.
- In a layered model the thickness of a resistive layer is well resolved. The resistivity of a resistive layer is poorly resolved.
- In a layered model the conductance (conductivity*thickness) of a layer is resolved. Neither the thickness nor the conductivity is uniquely resolved.
- Once the constraint that the subsurface is composed of distinct, resolvable, units is imposed the 1D inversion of MT data is essentially unique. Resolution is excellent (better than 5% of depth).

Apparent resistivity versus frequency is the most fundamental way of looking at the data in the interpretation phase. While the overall process is complex, with advanced processing techniques and inversions, it is important to keep in mind that the subsurface structures are apparent in the raw data – the apparent resistivity plots.

The following sequence of illustrations is intended to introduce the apparent resistivity versus frequency sounding curves. But it is also intended to highlight the relatively complex, but understandable, relationships between the observed data and subsurface structure.

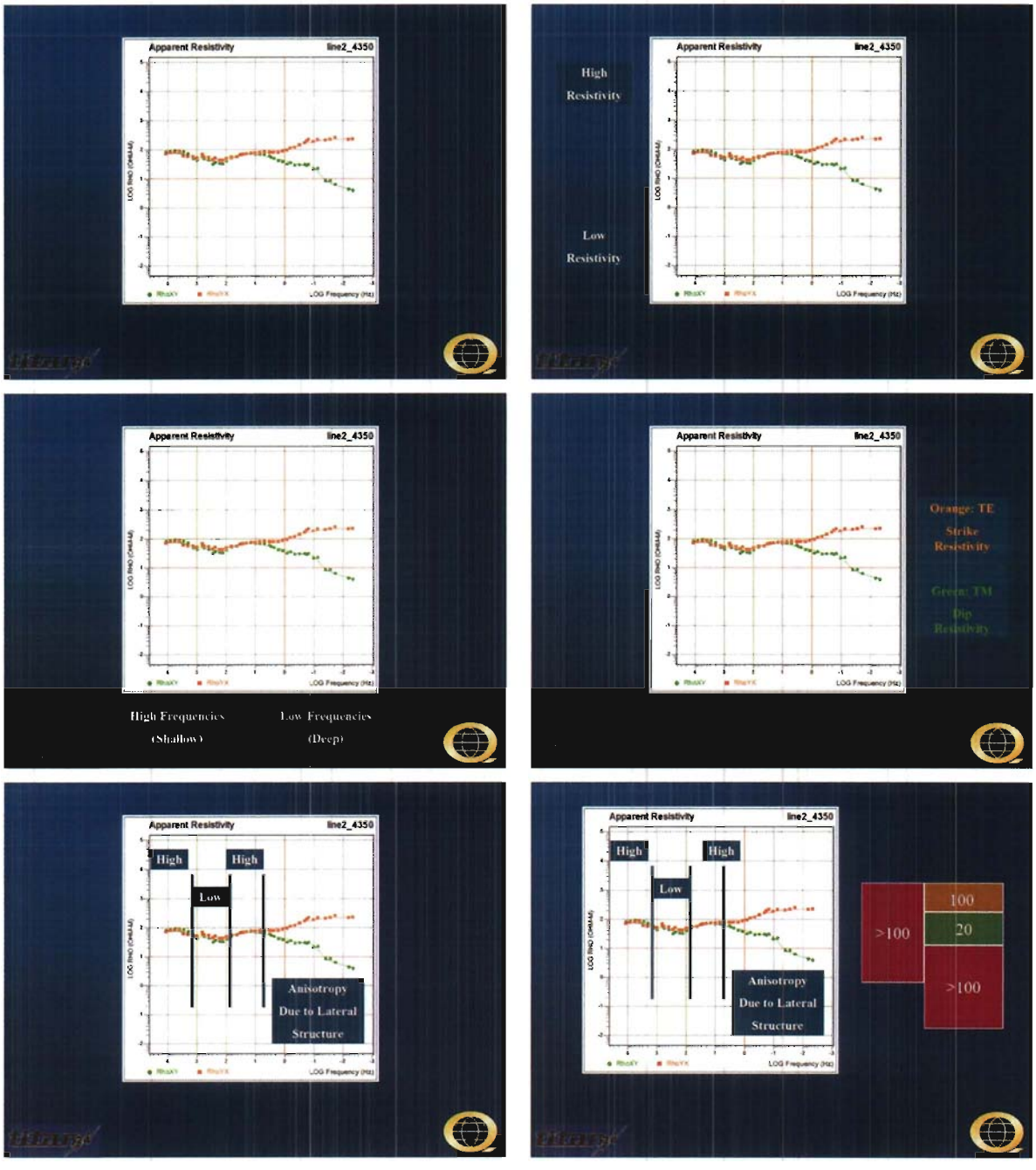

A simple layered subsurface structure is not generally the problem of immediate interest in exploration. In the case of more complex two-dimensional (2D) or three-dimensional (3D) structure the MT response will be affected by lateral resistivity variations.

The MT measurement relies on natural, plane-wave, source signals. The measured response depends on lateral resistivity variations as much as (or more than) resistivity variations below the immediate sounding site.

Full tensor measurements of the E and H fields are made at every site. For each site there are two apparent resistivity sounding curves (or modes) and phase curves. These two modes are arbitrarily labeled Rho-XY and Rho-YX. The first, Rho-XY, refers to the apparent resistivity (Rho) calculated from Ex and Hy.

Once full tensor measurements are made in the field it is possible to mathematically rotate the fields to any arbitrary coordinate system. Traditionally, the data are rotated independently at each frequency to maximize the difference between the two apparent resistivity sounding curves. This puts the data into "geologic" or "principal" coordinates.

One sounding curve will have the electric field in the geologic strike direction and is referred to as "Transverse Electric" or TE. The other mode will have the electric field in the geologic dip direction and is referred to as "Transverse Magnetic" or TM. Note that TE and TM are interpretive designations, and refer to geologic strike. XY and YX were simply geometric designation.

For a layered (1D) earth the two measurements are identical. When the structure is 2D or 3D the lateral resistivity variations will distort (often severely) the simple 1D response. The distortion of the fields by complex structure is realized in the apparent resistivity data as "anisotropy". This is a divergence between the two apparent resistivity sounding curves.

The measurement of two orthogonal apparent resistivity sounding curves provides valuable information. Both curves reflect the resistivity structure underlying the site. Both curves will show increasing or decreasing resistivity at a frequency in response to resistivity structure under a site. The two apparent resistivity curves will diverge in response to lateral resistivity variations.

If the site is located on the resistive side of a lateral resistivity contrast the TE mode will be slightly suppressed due to the contact and the TM mode will be significantly biased up by the contact. If the site is located on the conductive side of a lateral resistivity contrast the TE mode will be slightly biased up while the TM mode will be significantly biased down by the contact.

For a 2D resistivity structure the TE mode is always providing an indication of the integrated conductance of the volume being sampled. It will always be a slowly varying function of position. The TM mode is responding dramatically to the presence of charges on the lateral resistivity boundaries, and will dramatically overshoot on the resistive side of a contact and undershoot on the conductive side. The anisotropy (divergence of the two sounding curves) is diagnostic of a lateral resistivity contrast.

The following simple model demonstrates most of the critical 2D behaviours. The model consists of a 100 Ohm-m host with a 10 Ohm-m basin on the right. There is a 1 Ohm-m layer buried within the host and below the basin. The response is shown at two sites, one immediately on the resistive side of the basin contact and the other immediately on the conductive side of the contact.

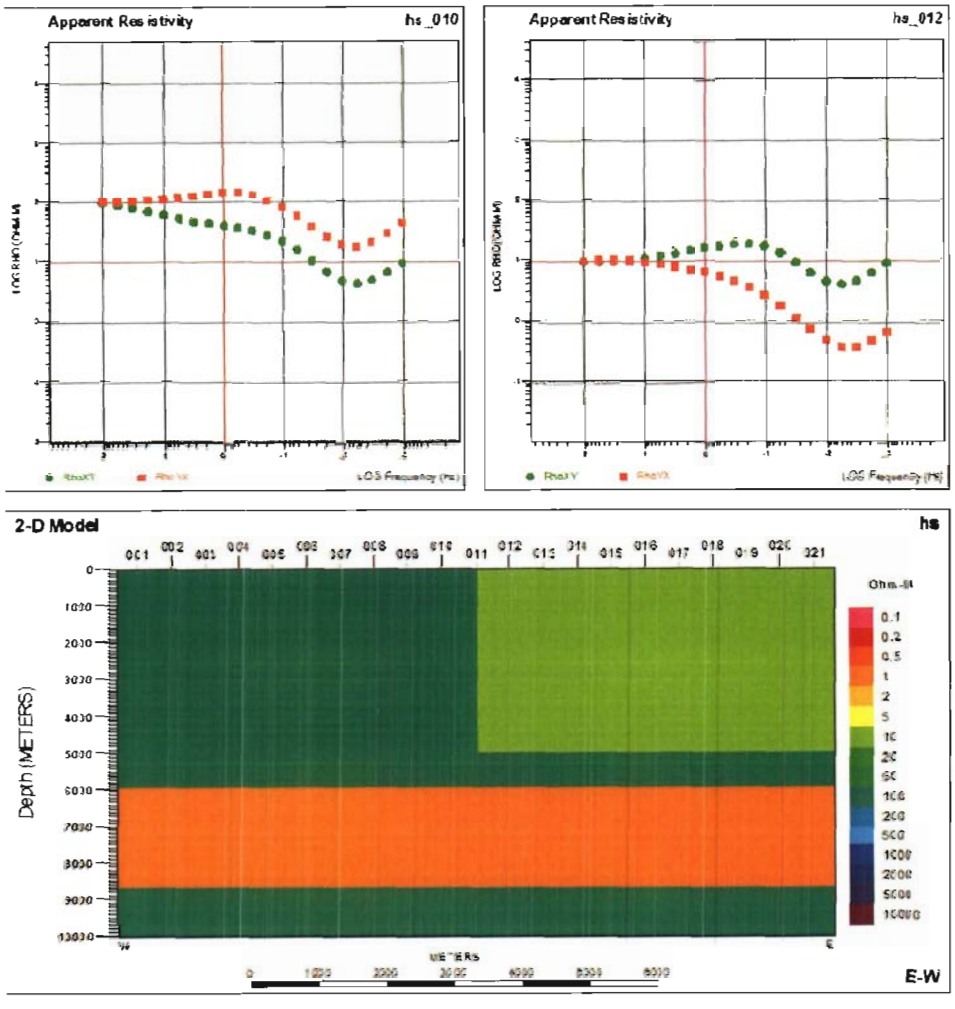

The following observations summarize the behaviour of 2D MT responses:

- The apparent resistivity at high frequencies reflects the true shallow resistivity.
- The apparent resistivities converge at high frequencies to the true shallow resistivity.
- The divergence in apparent resistivities occurs at a higher frequency for the site on the resistive side of the contact. Because the skin depth is larger in the resistive media the site on the resistive side of the contact is effectively "closer" to the contact than the site on the conductive side of the contact. The TE mode is constrained to the range of physical resistivities actually present in the model
- The TE mode "volume averages" the intrinsic resistivity. The TM mode exhibits apparent resistivities outside the range of physical resistivities in the model. Note that for the site on the right the TM mode indicates resistivities below 1 Ohm-m.
- Both the TE and TM modes respond in tandem, at the same frequency, to resistivity structure under the site. At both sites both the TE and TM modes indicate the top and bottom of the 1 Ohm-m layer. While 1D inversion of the TE and TM modes would place different apparent depths to the 1 Ohm-m layer the response is at the same frequency in both modes indicating it is the response of one layer.
- The intrinsic resistivity of the 1 Ohm-m layer is difficult or impossible to discern. Without physical property data only the conductance of the layer can be resolved.

These effects can also be clearly seen in pseudo-sections of the TE and TM apparent resistivity response of the model:

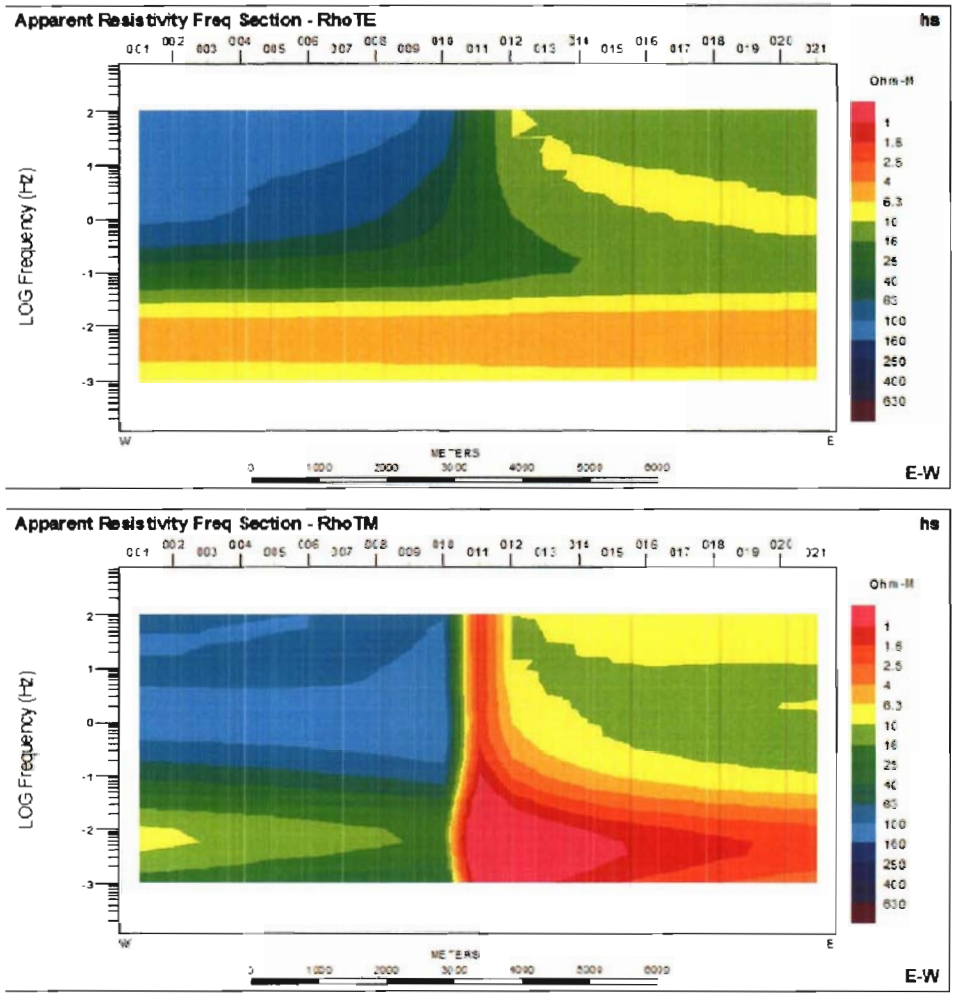

The apparent resistivity data at each site have been contoured, as a function of frequency. The inherent smoothness of the TE section can be clearly discerned. The distinctive "undershoot" of the TM response on the conductive side of the contact can be clearly seen.

One of the key factors in multidimensional MT data is "static shifts". The apparent resistivity sounding curves can be biased, up or down, by lateral resistivity contrasts too small to be resolved by the MT data. The curve is essentially DC shifted on the log-log apparent resistivity plot. This can be seen by examining the sounding curves from the previous 2D model. Assuming data had not been acquired above 1Hz the two sounding modes would be seen to be separated in the highest frequency data. Note that there are no static shift effects in the phase data.

Inversions and forward modeling are used to derive the subsurface resistivity structure from the data. The primary interpretation tools are 2D inversions. Problems emerge when the real world, complex, data are not consistent with the simplistic 2D assumptions. In a perfect world we would use modeling and inversion programs capable of reflecting the full complexity of the subsurface. However, in practice incorporating too much complexity in the modeling and inversion programs results in very coarse models which are incapable of resolving exploration targets. Instead, we must find ways to remove some of the complexity from the actual data. To this end, we have developed the Titan "EVA" data processing stream:

- Rotation to principal coordinates. The inversion algorithms presume that we have acquired a true geologic dip profile. In reality, geologic dip is often difficult to define, and seldom known prior to acquisition. However, because we have acquired full tensor data we

can rotate our data to the geologic dip direction after acquisition.

- Eigenvector processing. 3D structures can introduce complex "rotations" of the electrical currents. These rotations produce effects, such as excessively steep resistivity curves and out-of-range phases, which would be impossible to fit with 2D modeling programs. By relaxing the assumption that the electric and magnetic fields are orthogonal, eigenvector analysis provides a unique and trivial methodology for simplifying complex 3D data.
- 1D inversion for curve fitting. Real data are often noisy, and inconsistent. Out-of-range phases are a typical example of features seen in real data that can not be fit using 2D inversion. It is often best to make use 1D inversion to make interpretative decisions about how to "best" fit the data, rather than letting the 2D inversion thrash trying to fit inconsistent data.

Once these data processing techniques have been completed the data are inverted. Generally, two inversions of the MT data are done. The first inversion uses an approach (a model norm) that explicitly looks for the "smoothest" model consistent with the data. This approach essentially finds the minimal subsurface structure consistent with the data. The second inversion uses an approach (a model norm) that looks for a model most consistent with the known geology.

For the geologically constrained inversion we use a proprietary approach developed by Dr. Phil Wannamaker. This approach uses the geologic constraints as a target, while not imposing any intrinsic smoothing on the inversion. The approach finds the maximum structural information, at the risk of sometimes including structure not required by the data. It represents an effort to extract the maximum exploration information from the data.

Both approaches are valid, and important. A smooth model approach to inversion can be viewed as finding the least possible useful exploration information. However, it does provide an independent assessment of what the data actually require. The geologically constrained inversion will provide a much sharper subsurface image. But it will also reproduce the known geology where the data does not require a change to the model. Without an independent smooth model inversion it can be hard to determine whether a geologically constrained inversion has confirmed the geologic interpretation, or simply doesn't have any information either way.

REFERENCES

Orange, A. S, 1989. Magnetotelluric exploration for hydrocarbons: Proceedings of the IEEE, 77, 287–317.

Vozoff, K., 1972. The Magnetotelluric method in the Exploration of Sedimentary basins. Geophysics, 37, 98-141.

APPENDIX G: INSTRUMENT SPECIFICATIONS

REF TEK – 120 DATA ACQUISITION SYSTEM

REFRACTION TECHNOLOGY INC. – PLANO, TEXAS
(WWW.REFTEK.COM)

SPECIFICATIONS:

Specification	Description
Physical	
Size:	267 x 248 x 184 mm 10.5 x 9.75 x 7.25 in.
Weight:	3.7kg 305 g 8 lbs (2-Channels maximum weight))
Temperature:	-40°C to 60°C operating range.
Environmental:	Operates in 1m of water without leaking for 48 hours. Airtight to 1.0 psi.
Shock:	Remains operational after 1m drop (any corner) onto cement floor.
Connectors	
Line A & Line B:	A pair of identical 10 pin U77/U style connectors. Each connector provides 3 pairs of lines (+): • A (+)/B (-) Receive telemetry data and/or commands • C (+)/D (-) Transmit telemetry data and/or commands • E (+)/F (-) Sync
Power:	PTO7A12-8S style connector. Provides input +12 VDC supplied from battery.
Sensor:	PU283/U style connector. Provides for a direct connection from the AM to the sensor.
Power Requirements	
Battery:	Two 12 volt lead acid battery (7 Ah).
Signal Input	
Input Impedance:	10 megohms, 330pF, differential
Broadband Dynamic Range:	130dB (noise power ratio test @ 125 sample per second [sps])
ADC Type:	Delta-sigma modulation
Sample Rage:	Multiple 50 to 48,000
Gain Settings:	Four – programmable for 1, 4, 16 and 64.

Sensor Input Signal Range:

Gain	24-Bit High Speed A/D		24-Bit Low Speed A/D	
	Actual	Reported	Actual	Reported
1	1.192µV	78.12mV	1.907µV	125.0mV
4	298.0nV	19.53mV	476.8nV	31.25mV
16	74.51nV	4.883mV	119.2nV	7.812mV
64	18.63nV	1.221mV	29.80nV	1.953mV

Data Storage	
Data Size:	32-bit two's compliment.
Base Memory:	128K EPROM 6.5Mb SRAM
Base Capacity:	Better than 1.5 million samples or approximately 3 hours 10 minutes continuous data @ 125 sps.

Specification	Description
AM Telemetry	
Protocol:	Full duplex synchronous data link control (SDLC).
Error Correction:	Packet acknowledge with modulo 8 sliding window.
Speed	3.072Mb/second
Encoding:	Bi-phase pulse = 1, missing pulse = 0
Line Impedance:	100 Ohm
Synchronization	
Timing:	Each AM on-line is timed and synchronized for simultaneous sampling within + 1.50 µsecond.
Protection	
Electrical Protection:	Line A and Line B signals circuits are protect by: • A surge arrestor located on the RT514 board (SS1-14). • A line isolation transformer located on the RT514 board (T1-6) with over-voltage diodes (D1-4) on both sides of each secondary windings.
State-of-Health	
Information Provided:	The AM reports information on battery status, clock setting, gain setting, calibration mode and the communications link.

ACQUISITION PARAMETERS

Acquisition parameters include the sample rate, transmitter frequency and number of samples desired. The operator can also determine whether the AMs calibration signal is activated during data collection. In typical use, the acquisition parameters are set according to the specific application configuration and event type. For each event type, several recording sessions are made, each at a different transmitter frequency and sample rate. The recording period is set based on event type and transmitter frequency. The listing below shows several examples of event type, typical transmitter frequency (Hz), sample rates (with applicable ADC resolution) and the corresponding number of samples (record period).

Event Type	Transmit Frequency	Sample Rate	ADC Resolution	Number of Sample
Geophysical Response	375 Hz	48,000	24	124,032
Gain Test	375	48,000	24	65,536
Geophysical Response	75	9,600	24	130,176
Gain Test	75	9,600	24	65,536
Geophysical Response	25/8	3,200	24	139,264
Gain Test	25/8	3,200	24	32,768
Sensor Impedance	N/A	1,600	24	8,704
Ambient Noise	N/A	1,600	24	8,192
Geophysical Response	25/128	800	24	147,456
Gain Test	25/128	800	24	16,384
Geophysical Response	25/2048	100	24	212,992
Gain Test	25/256	100	24	4,096
Gain Test	N/A	50	24	4,096
Geophysical Response	N/A	50	24	65,536

SENSOR CALIBRATION

The AM can source a 12.5Hz, 50μA signal to the sensor input for measuring the source impedance of the attached sensor. The user can also specify frequency in amplitude of calibration signal.

TELEMETRY CABLE

The telemetry cable is a *Category V* specification cable and is supplied by the customer.

SAMPLE RATES

The following table shows all available sample rates, based on a 12.288 Mhz oscillator. A 24-bit resolution ADC is used for sample rates 48000 through 4800 and a 24-bit resolution ADC is used for sample rates 3200 and below. The correct ADC is selected automatically by the AM, based on the sample rate.

Typically, different sample rates and transmitter frequencies are used in 50 Hz and 60 Hz power environments to minimize AC power effects on the data. In the table, the shaded areas indicate the sample rates typically used in a 60 Hz power environment. A few rates are typically used in both environments.

Sample Rate	Power Line
48000	50 & 60
24000	50 & 60
19200	60
16000	50
12000	50 & 60
9600	50 & 60
6400	50
4800	60
3200	50
1920	60
1600	50
960	60
800	50
480	60
400	50
240	60
200	50
120	60
100	50
60	60
50	50
60/2	60
50/2	50
60/4	60
50/4	50
60/8	60
50/8	50
60/16	60
50/16	50
60/32	60
50/32	50

APPENDIX F: INSTRUMENT SPECIFICATIONS

EMI – ELECTROMAGNETIC INSTRUMENTS INC

NOW EMI TECHNOLOGY CENTER – SCHLUMBERGER – BERKELEY, CA –
(WWW.EMIINC.COM)

BF-4 Series Magnetic Sensors

SPECIFICATIONS:

BF-4 Magnetic Field Induction Sensor

The BF-4 sensor utilizes a magnetic feedback design to provide a stable flat response over several decades of frequency. The sensors respond as a B field detector over the flat band regions. Both the amplitude and phase responses are highly stable with variations of less than 0.1dB in amplitude and +/- one degree in phase between sensors. For the frequencies below the flat response region, the sensor response is proportional to signal frequency so that the sensor acts as a dB/dt detector. The coil is potted with epoxy and housed inside a rugged impact-resistant Nema G-10 fiberglass tube. A matched low noise preamplifier is connected to the coil in a waterproof case and powered by an external +/- 12V power supply.

BF-4 Frequency Response

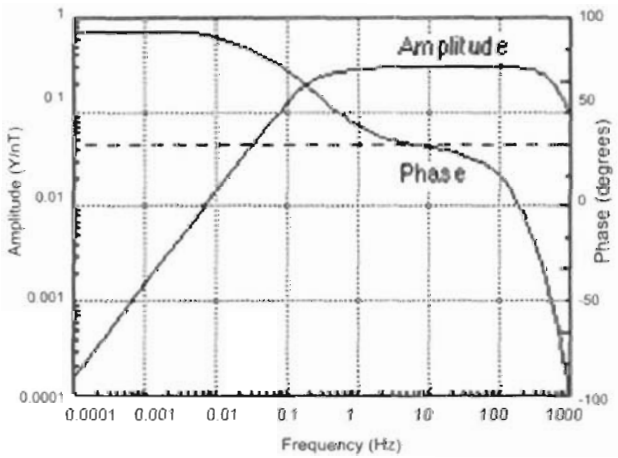

BF-4 Sensor Noise

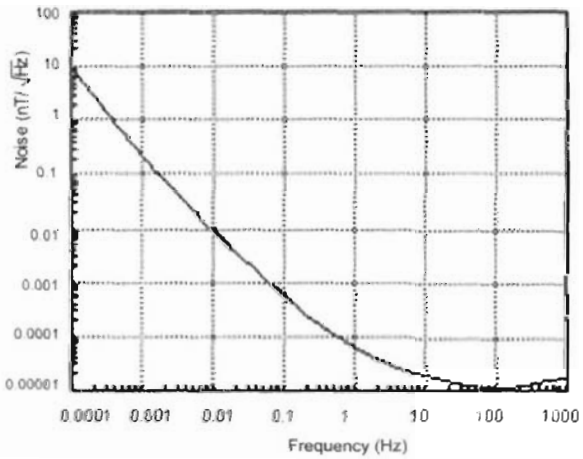

Features

- High sensitivity
- Very low noise
- Magnetic feedback design
- Chopper stabilized amplifier for best low frequency performance
- Ruggedized and waterproof
- Light weight and compact
- Low power consumption
- Stable phase response

Applications

- Magnetotellurics
- Audiomagnetotellurics
- Controlled-source electromagnetics
- Magnetometric resistivity

Technical Specifications

Performance

- Frequency Range: 0.0001 to 1000 Hz
- 3 dB frequency corners: 0.2 Hz, 500 kHz
- Sensitivity (flat region): 0.3 V/nT (standard)
- Power consumption: 12mA at +/-12V

Physical

- Housing: Nema G-10 straight tube
- Length: 142 cm (56 inches)
- Diameter: 6 cm (2.4 inches)
- Weight: 7 kg (15 lbs)
- Connector: 8-pin Tajimi

APPENDIX F: INSTRUMENT SPECIFICATIONS

EMI – ELECTROMAGNETIC INSTRUMENTS INC

NOW EMI TECHNOLOGY CENTER – SCHLUMBERGER – BERKELEY, CA –
(WWW.EMIINC.COM)

BF-6 Series Magnetic Sensors

SPECIFICATIONS:

BF-6 Magnetic Field Induction Sensor

The BF-6 sensor utilizes a magnetic feedback design to provide a stable flat response over several decades of frequency. The sensors respond as a B field detector over the flat band regions. Both the amplitude and phase responses are highly stable with variations of less than 0.1dB in amplitude and +/- one degree in phase between sensors. For the frequencies below the flat response region, the sensor response is proportional to signal frequency so that the sensor acts as a dB/dt detector. The coil is potted with epoxy and housed inside a rugged impact-resistant ABS tube. A matched low noise preamplifier is connected to the coil in a waterproof case and powered by an external +/- 12V power supply.

BF-6 Frequency Response

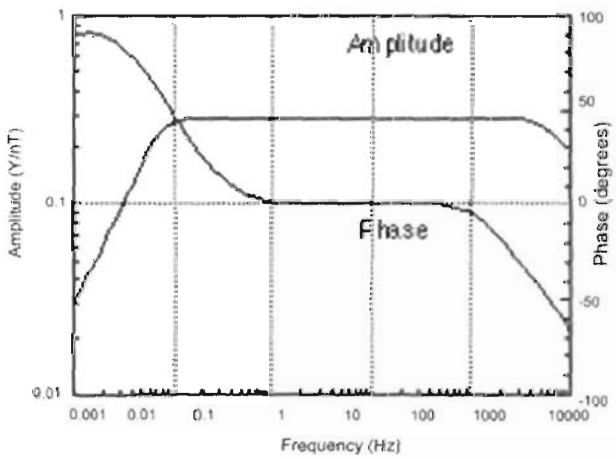

BF-6 Sensor Noise

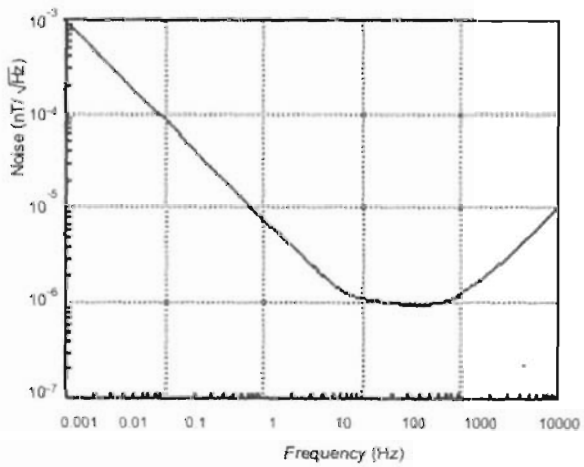

Features

- High sensitivity
- Very low noise
- Magnetic feedback design
- Ruggedized and waterproof
- Light weight and compact
- Low power consumption (210 mW)
- Stable phase response

Applications

- Magnetotellurics
- Audiomagnetotellurics
- Controlled-source electromagnetics
- Magnetometric resistivity
- Time domain electromagnetics

Technical Specifications

Performance

- Frequency Range: 1 Hz to -100 kHz or 1 Hz to 25 kHz
- 3 dB frequency corners: 10 Hz, 25 kHz or 10 Hz, 100 kHz
- Sensitivity (flat region): 0.3 V/nT (standard)
- Power consumption: 9mA at +/-12V

Physical

- Housing: High Impact ABS Straight Tube
- Length: 73 cm (29 inches)
- Diameter: 5 cm (2 inches)
- Weight: 1.7 kg (3.7 lbs)
- Connector: 8-pin Tajimi

APPENDIX F: INSTRUMENT SPECIFICATIONS

PHOENIX GEOPHYSICS LTD
(WWW.PHOENIX-GEOPHYSICS.COM)

MTC 50 (P50) Serie Magnetic Sensors

SPECIFICATIONS:

MTC-50 *magnetic sensor coils weigh just over 10 kg, and measure only 141 cm. They provide magnetotelluric data at frequencies between 400 Hz to 0.0002 Hz.*

AMPLITUDE AND PHASE RESPONSE MTC-50 SENSOR

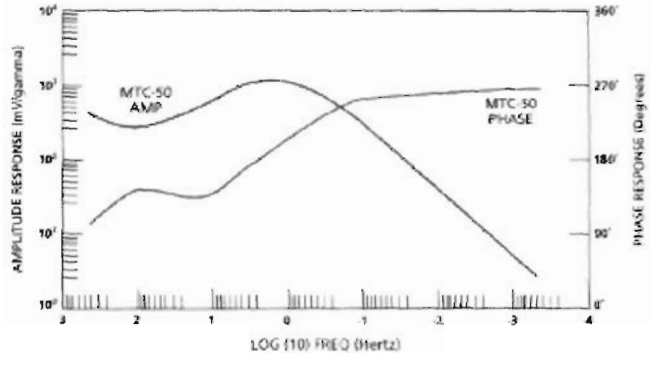

Coil model MTC-50	
Overall Length	141 cm
Outside Diameter	6.0 cm
Weight	10.5 kg
Frequency Range (for MT)	400 Hz to 0.00002 Hz

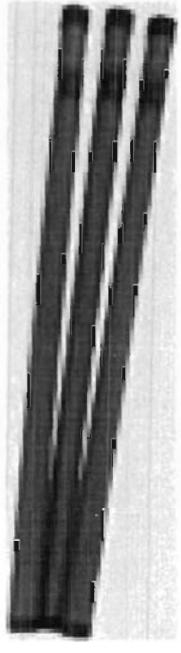

TYPICAL SPECTRAL PLOT OF SENSOR NOISE

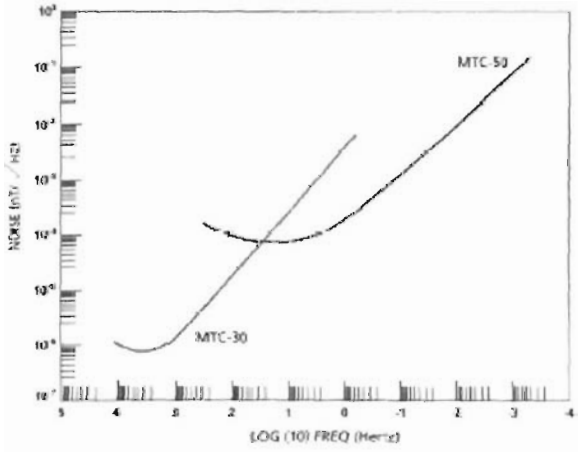

Technical Specifications

- Overall Length : 141 cm
- Outside Diameter : 6.0 cm
- Weight : 10.5 kg
- Frequency Range (for MT) : 400 Hz to 0.00002 Hz